Multi-Terminal HVDC (MTHVDC) Interaction Studies Using Small Signal Stability Assessment

By

Shaohua Ma

A thesis submitted to the Faculty of Graduate Studies in partial fulfillment of the requirements for the degree of Doctor of Philosophy

The Department of Electrical and Computer Engineering

The University of Manitoba

Winnipeg, Manitoba, Canada

ACKNOWLEDGEMENTS

First of all, my sincere thanks must go to my advisor, Dr. Udaya Annakkage, and the examiner, Dr. Chandana Karawita, for their continuous advice, guidance, and encouragement throughout this research. It has been a privilege for me to have the opportunity to work with them. Secondly, I would like to thank my supervisor for his encouragement and support. I would also like to thank my friends and colleagues for their encouragement and support. Lastly, I would like to thank Manitoba Hydro for supporting my continuing education.

This acknowledgment would not be complete without thanking my family. I would like to thank my wife and my daughters for their understanding and support throughout my studies. Last but not least, I would to also thank my parents and my parents-in-law for all the love and support.

ABSTRACT

With the development of HVDC technology, HVDC system has become more and more attractive in modern power systems. Tapping on the existing HVDC line becomes a practical option to deliver reliable power to the customer. The interaction among each terminal DC controller as well as the AC network and HVDC links is one of the major concerns in an integrated AC/DC power system. To investigate the potential interactions in the MTHVDC systems, a detailed linearized LCC-based MTHVDC system model is developed. To accurately capture the effect of controller interactions, the entire AC network, including AC transmission lines, transformers, switching capacitors, and loads are all modeled using dynamic phasor, generators are modeled including stator dynamics. This developed MTHVDC system model is then benchmarked with the corresponding PSCAD/EMTDC model and shows a good agreement.

This thesis proposes a comprehensive procedure to perform the MTHVDC system interaction study. Using the proposed study procedure, the complex oscillation modes including DC network resonance, AC-DC network interaction, HVDC controller interaction, and electromechanical oscillation of the two proposed three-terminal HVDC test systems have been evaluated. The results show that machines at different terminals interact with each other through the three-terminal HVDC systems. It proves that the MTHVDC system cannot isolate the oscillation and prevent oscillation propagation from one side of the HVDC system to the other systems. The results also demonstrate that the damping ratio for electromechanical oscillations can be improved by changing the HVDC controller parameter. In addition, the results also show that different controller arrangements have an impact on each oscillation mode. By comparing each oscillation

mode of these two control schemes, it is concluded that control scheme one is more robust than control scheme two and has a lower chance of having small signal stability concerns.

This thesis also investigates the impact of the system strength on MTHVDC controller interactions. Two MTHVDC control schemes with various system configurations, including a different HVDC line tap point, different control parameters, and different operating points, have been studied with various AC system strength conditions. The results indicate that the participation factor and mode shape angle of the oscillation mode change due to AC system strength change. As a result, both the oscillation frequency and damping ratio are impacted by AC system strength. The results also show that AC system strength has a significant impact on its own terminal controller state variable dominated oscillation mode. Most importantly, the AC system strength has a significant impact on the DC voltage controller state variable dominated oscillation mode. Other parameters, such as system configuration, controller parameter as well as the system operating point also impact the controller interaction oscillation. The results show that higher system strength does not always positively improve the oscillation damping ratio. The participation factor analysis and mode shape analysis results prove that the proposed three-terminal HVDC system scheme one, with current control at the rectifier, current control at one inverter and voltage control at the other inverter, is more robust than control scheme two and has a lower chance of having small signal stability concern. This scheme is less impacted by the operating point change. It is recommended to perform a system small signal study to cover all possible operating scenarios to ensure that the MTHVDC system has no small signal stability issues.

In general, the developed model, analytical techniques, and the study procedure proposed in this thesis can be used to analyze power system high-frequency interactions of HVDC systems, controller interactions of the MTHVDC system, and FACTS devices.

DECLARATION

I certify that research work titled “Multi-Terminal HVDC (MTHVDC) Interaction Studies Using Small Signal Stability Assessment” is my own work. The work has not been presented elsewhere for assessment. Where material has been used from other sources has been properly acknowledged.

List of Principal Symbols

t	Time
ω_0	Fundamental angular frequency of power system
V_l	Line-to-line RMS voltage
δ	Generator rotor angle or bus voltage angle
V_R, V_I	Real and imaginary components of AC bus voltage
I_R, I_I	Real and imaginary components of AC current injected to a bus
X_c	Converter transformer reactance referred to DC side
T	Converter transformer turns ratio (AC/DC)
B	Number of 6-pulse bridges in a converter
α, μ, γ	Converter firing angle, commutation angle and extinction angle
L_1, L_2, L_3	DC line inductance
R_1, R_2, R_3	DC line resistance
C_{11}, C_{12}, C_{21}, C_{22}, C_{31}, C_{32}	DC line capacitance
L_{eff1}, L_{eff2}, L_{eff3}	Effective inductance of an HVDC terminal
K_{pr} , K_{Ir}	Proportional and integral gains of rectifier side DC controller
I_{dc_order}	Current reference of DC current controller
$X_{\alpha r}$	State variable of rectifier side DC controller
K_{pi} , K_{Ii}	Proportional and integral gains of inverter side DC controller
K_{pi_t2} , K_{Ii_t2}	Proportional and integral gains of inverter side DC controller
V_{dc_order}	DC voltage reference for the DC voltage controller
$X_{\alpha i}$, $X_{\alpha i\_t2}$	State variable of inverter side DC controller
K_{PP} , K_{IP}	Proportional and integral gains of phase lock oscillator
$[A]$, $[B]$	System matrix and input matrix of a state space model
$[\Lambda]$	Eigenvalue matrix
λ	An eigenvalue
f, ζ	Frequency and damping ratio (D) of an eigenvalue
$[\Phi]$, $[\Psi]$	Right and left eigenvector matrix
Φ_i, Ψ_i	Right and left eigenvectors of i^{th} eigenvalue
p_i	Participation vector of i^{th} eigenvalue

Table of Contents

LIST OF FIGURES

LIST OF TABLES

Chapter 1:Introduction

1.1 Background

High Voltage Direct Current (HVDC) systems have been in commercial use since the 1950s. They have significant technical and economic advantages over High Voltage Alternative Current (HVAC) technology in medium-to-long distance power transmission applications. Such as precise power control, the flexibility of asynchronous grid connections, and lower transmission losses. Therefore, HVDC technology can be applied to connect grids with different system frequencies and for long-distance power transmission due to less active power losses compared to HVAC technology. In terms of applications, Multi-Terminal HVDC(MTHVDC) is gaining interest among utilities. This research will investigate the controller interactions of the Line-Commutated Converter (LCC) MTHVDC systems, specifically the three-terminal system.

Since the first HVDC commercial project went into service in the 1950s, HVDC power transmission technology has undergone continuous improvements and is currently widely used in modern power systems [1].

In recent years, several factors have contributed to the high interest in HVDC applications. One important factor is the deregulation of electrical markets around the world. Utilities are no longer monolithic entities that consist of generation, transmission, and distribution areas, but rather each area is separated into individual entities: such as generation entity, transmission entity, and distribution entity. In such a system, decisions can be made by individual entities benefiting their own rather than making decisions benefiting the entire entity made up of generation, transmission, and distribution. Because

of deregulation, there now exists multiple individual generation, transmission, and distribution entities that compete against each other in the electrical market. In this scenario, MTHVDC becomes a valuable technology. It can provide a tremendous economic advantage in the competitive electricity markets by providing the same service to multiple competing entities that were not required for monolithic entities.

The second factor is the advancement of LCC HVDC technology. In high power applications, the LCC is the dominant technology used worldwide [2]. It has gone through tremendous improvements in the past years. The technology has become more mature in valve development, filter development, and current measurement area [3-6]. In terms of cost, it has gone down significantly compared to the 1950s. These improvements along with precise active power control advantage have made HVDC, particularly the LCC a very attractive application. One of the ultra-high voltage direct current (UHVDC) applications is the Xiluodu-Zhejiang project in China. It has a rating of +/-800kV, 8,000MW/5000A, and was completed in 2014. There are also more UHVDC projects planned for the future [7]. Furthermore, with the development of thyristor technology and semi-conductor technology, the application of the HVDC power transmission systems is more convenient [8-11].

Finally, since the HVDC technology is capable of high transfer capacity and is suitable for long-distance transmission due to less active power loss over HVAC technology. HVDC technology can, therefore, be utilized to meet the rapidly growing electrical demand in developing countries. For instance, countries in the Middle-East, China, India, and South American have adapted HVDC technology to meet their rapidly growing load demand [12-16]. Today, there are more than 92 HVDC projects worldwide transmitting

more than 75GW of power [3]. By the end of 2015, there were approximately 30,000 km or 50 HVDC lines in service in China alone. Countries with areas of high population density are starting to implement multiple HVDC links that terminate in close electrical proximity to the load center. In China, a multi-terminal topology was implemented for the Zhoushan project in 2014 at the +/-200kV voltage level. The same topology was used for the Zhang-Bei project in 2018, but with a voltage rating of +/- 500kV [17]. In India, the Bishwanath-Agra multi-terminal project at +/- 800kV voltage went into service in 2015 [18].

In Canada, the Manitoba Hydro Nelson River HVDC system consists of three point-to-point Bipoles with a total capacity of 5854MW [19-20]. Bipole I was completed in 1971-1976 with a rating of 1854MW. Bipole II was commissioned in stages in 1978-1985 and is capable of transmitting 2000MW of power. Both Bipole I and II share the same corridor and are approximately 900km in length. They connect the Radisson and Henday converter stations in the Northern Collector System (NCS) in Manitoba and the Dorsey converter station in Southern Manitoba. The third +/-500kV 2000MW Bipole (Bipole III) was completed in 2018 and is located on a separate corridor on the west side of Manitoba with a line length of approximately 1350km. The new HVDC line connects the converter station of Keewatinohk (rectifier) in the north and the Riel (inverter) in the south. All three Bipoles utilize LCC technology as it gives the best technical and economical solution with the specified requirements [20].

Up to now, the majority of HVDC schemes in commercial operation are point-to-point transmissions. However, with the advancement of HVDC technology, especially semi-conductor technology, there are growing interest in multi-terminal HVDC (MTHVDC)

systems. In an MTHVDC system, three or more HVDC terminals are connected to the AC network. There are several specific areas of applications for MTHVDC systems. These are:

1. Power transmission from several different remote generating stations to several different load centers. Each generating station is connected directly to a rectifier station, thereby eliminating the need for the AC collector system. Similarly, a converter station is directly connected at each load center, which eliminates the need to build additional AC lines from the converter station to load centers.

This type of system has several advantages over the alternative of the traditional point-to-point system. For example, consider a system of two generating stations and two loads as shown in Figure. 1.1.

This is a radial system with two rectifiers and two inverters. A traditional point-to-point system would require three two-terminal DC links in addition to a link connecting the two receiving systems to ensure the same level of flexibility in energy exchange, which could be AC or DC (see Figure. 1.2). This would result in extra costs for the converter stations, extra transmission lines, and additional power losses.

The elimination of AC collector systems at remote hydro generating stations can result in better efficiency in the operation of hydraulic turbines, which are free to run at speeds independent of the nominal system frequency [21].

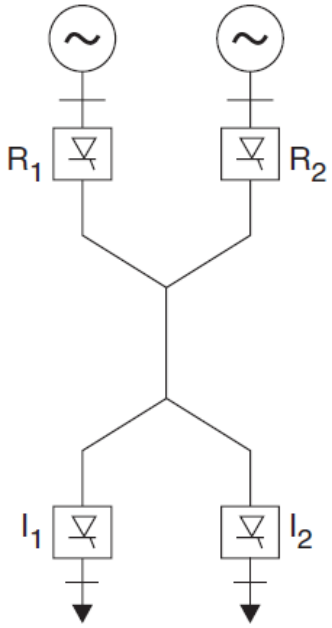

Figure 1.1 MTHVDC system configuration for bulk power transmission

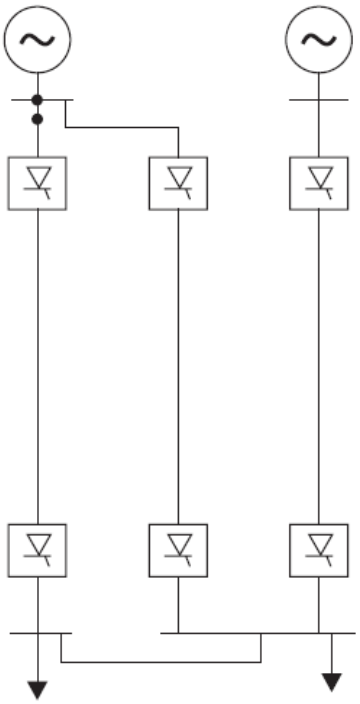

Figure 1.2 Point-to-point bulk power transmission using two-terminal HVDC links

2. Asynchronous interconnection between adjacent power systems when two AC systems have different frequencies. It can also be used to provide a controlled power flow between utilities. When more than two systems are involved, an MTHVDC system for interconnection is more flexible and economical than employing several two-terminal point-to-point DC links.

3. Reinforcing an AC network that is heavily loaded. Consider an urban power system that is fed by a distant power station. It would be advantageous to arrange the power injection at more than one point so that the underlying AC network is not overloaded. This is easily achieved using an MTHVDC system with one rectifier station and several inverter stations (see Figure. 1.3).

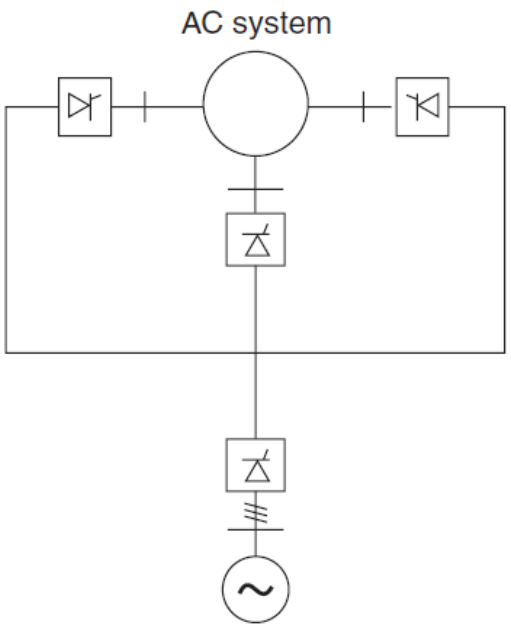

Figure 1.3 Reinforcing of AC Network using MTHVDC Link

Currently, there are only three multi-terminal LCC based HVDC systems in operation: the Quebec-New England between Canada and the United States, the SACOI system

between Italy mainland and islands of Sardinia and Corsica, and the North-East Agra link in India [17,22]. The Quebec-New England system was originally designed with five terminals but is currently operating as a three-terminal system. The SACOI multi-terminal HVDC system was refurbished and re-commissioned in 1992 [17]. It is operating as a three-terminal HVDC system with the new name of SACIO2 [23]. The latest three-terminal HVDC system is the North-East Agra scheme in India, which is the first +/- 800kV MTHVDC system with the capability of 6000MW [24].

In China, the newly in serviced Zhoushan VSC-HVDC pilot project is the first five-terminal VSC-HVDC project in the world, which operates at +/- 200kV level and has the capacity of 1000MW. The Zhangbei HVDC power transmission project in China is another world's first HVDC power transmission system to utilize VSC technology at a rated voltage of +/-500kV. It has a design capability of 4500MW [17].

In light of the significant progress of power electronics technology, HVDC transmission is becoming increasingly attractive in modern power systems. Whether in transferring bulk power over long distances or interconnecting two larger systems with weak damping, HVDC transmission offers significant advantages. The behaviors of HVDC systems are playing a greater role in the performance of the entire AC/DC power systems. Therefore, it is important to thoroughly understand the mechanisms of interactions between the HVDC system and AC network, so that the HVDC can be operated in an optimal way to enhance the stability and reliability of the entire power grid.

The interaction between the AC network and HVDC link is one of the major concerns in an integrated AC/DC power systems. The purpose of this research is to investigate the interaction in the LCC MTHVDC systems. In an MTHVDC system, each terminal

controller may interact with other terminal controllers, creating unwanted oscillations. In addition, the MTHVDC may interact with other dynamic devices in the power systems, such as the series compensated transmission line and the Static Var Compensator (SVC) [25]. Furthermore, the controller of the MTHVDC system may affect the damping of the electromechanical oscillations [26], which will impact the stable system operation. Finally, the MTHVDC systems may also interact with tightly coupled generator-turbine systems, which cause torsional oscillations [27, 28, 29] and may damage the generators. Therefore, it is very important to understand the characteristics of the MTHVDC system and establish a guideline to design the controller to avoid unnecessary control interactions.

For the purpose of identifying the interactions caused by the MTHVDC system, three types of simulation programs can be used to assess system stability. They are the Electro-Magnetic Transient (EMT) type time-domain simulations, transient stability analysis techniques, and small-signal stability techniques. For the EMT type time-domain simulation technique, the simulation results are accurate due to the very detailed models being used in the program. However, the size of the system is a major limitation. Only small power systems can be modeled in this type of program and the simulation time increases significantly as the size of the system increases.

The interactions in HVDC systems can be analyzed qualitatively, using the time domain responses obtained from EMT and transient stability simulation techniques. However, some of the oscillation modes (a mode of an oscillating system is a pattern of motion in which all parts of the system move sinusoidally with the same frequency and with a fixed phase relation) may not be observable in the time domain response. Furthermore, even if the modes are observable, the contributions of these modes cannot be identified accurately

using the responses. The interactions at a particular power system operating point can be analyzed in the frequency domain using small-signal stability assessment techniques. The contributions towards the interactions are identified accurately using eigenvalue analysis techniques [30]. Moreover, this technique can be applied to large systems efficiently [31, 32].

Small signal stability measures the ability of power systems to maintain synchronism under small disturbances [33]. Therefore, the disturbances are considered to be sufficiently small so that the linearization of the system's nonlinear behavior is possible. The nonlinear behavior of the dynamic devices of the power system is first linearized at a particular steady-state operating point. The linear state-space model of the power system is then obtained by combining the linearized models of the dynamic devices. The small-signal stability of the power system is determined from the eigenvalues of the system matrix of the state space model using Lyapunov's stability criteria [34].

The conventional small-signal stability programs are designed to analyze the low-frequency electromechanical oscillation (<5Hz) of the power system. Some simplification techniques are used in these programs. For example, the electrical network is modeled using algebraic equations (admittance matrix), ignoring high-frequency network transients. The admittance matrix representation of the AC network helps to reduce the size of the system matrix dramatically. The generator stator dynamics are also ignored to be consistent with the algebraic network model [30].

For the HVDC interaction as well as the torsional interaction analysis, the interactions may contain frequencies up to 200Hz. Therefore, the conventional small-signal stability assessment technique must be modified [35]. The AC network dynamics and the generator

stator winding dynamics must be included in the model. The network components will be modeled using the dynamic phasor model [36, 37, 38]. The lowest AC side harmonic for a 60 Hz, 12 pulse HVDC converters is 660Hz, which is well above our interested frequency (up to 200Hz). Therefore, the higher-order harmonics in the HVDC systems will be ignored.

In summary, this research will prove that the MTHVDC systems controller will interact with each other and with other dynamic devices of power systems. The modified small-signal stability assessment tool – Power System Dynamic Phasor representation can be used to analyze the interactions below 200Hz oscillations in the power system with acceptable accuracy.

1.2 Thesis Objective

The main objective of this thesis is to investigate the risk of controller interactions in an MTHVDC system. This will be achieved by developing the small-signal assessment tool and analyzing the MTHVDC interactions in power systems. The following goals will be set to achieve the main objective.

In small signal stability analysis, the nonlinear devices in power systems such as HVDC systems, generators, and the AC networks are linearized at a particular steady-state operating point such that the linear models are accurate for the desired frequency range. A linearized model of an MTHVDC system including converter models, rectifier and inverter controller models, MTHVDC transmission line systems, and Phase-Locked Loops (PLLs) [39, 40, 41] are developed. The dynamic phasor models are used to model the entire AC network, which includes transmission lines, transformers, static loads, and AC filters. The generators are modeled with an 8^{th} order model, which includes stator winding dynamics.

The overall developed MTHVDC system responses are benchmarked with EMT type time-domain simulation results. The ultimate goal of this research is to develop a study procedure and provide recommendations on how to perform an interaction study for the MTHVDC system. Particularly, the controller interactions between each terminal in the MTHVDC system will be investigated.

1.3 Thesis Outline

The outline of this thesis is summarized as follows.

The linearized model of an MTHVDC system, including the HVDC converter model, MTHVDC transmission line model, and DC controller models, are discussed in Chapter 2. The linearized models of generators with stator dynamics are briefly discussed in this chapter and the models are given in Appendix B. The concept of dynamic phasor based on the Shift Frequency Analysis (SFA) [42, 43] is introduced and the model of the AC network is also discussed. The overall modified small-signal stability assessment tool package is provided in this chapter. The purpose of this chapter is to explain how the MTHVDC small-signal model is being developed for this research work.

In Chapter 3, PSCAD/EMTDC [44] simulation is used for benchmark purposes. Simple test systems with infinity AC buses as well as a modified IEEE New England 39 bus system, including the proposed MTHVDC systems, are developed for benchmarking purposes.

In Chapter 4, the small-signal stability assessment of the power system is briefly summarized. The modes in the power systems are identified using eigenvalues of the linearized model and the modal characteristics are given by the properties of the eigenvalues and eigenvectors.

In Chapter 5, a detailed study procedure for the small-signal stability analysis of a three-terminal HVDC system is provided. The study is based on a simple test system with two control schemes for the three-terminal HVDC schemes. In scheme one, the DC voltage controller is equipped at one of the inverter stations. The other two terminals are controlled by the DC current controllers. In scheme two, the rectifier is controlled by the DC voltage controller and the DC current controllers control the other two DC inverter terminals. Detailed small-signal analysis results as well as the time domain analysis results are provided. The results demonstrate that there are controller interactions in the MTHVDC systems. By selecting proper controller parameters, all oscillation modes have enough damping ratios, and both systems can be operated with no small signal stability concerns.

In Chapter 6, further discussions on the system strength change impact on the controller interactions are given. The results indicate that with system strength changes, both the oscillation frequency and damping ratio for all controller interaction modes change. HVDC line length, system configuration, controller parameter selection, and operating point change all impact the MTHVDC system small signal stability. As a result, it is very important to perform a system small signal study to cover all possible operating scenarios to ensure that the system has no small signal stability issues.

In Chapter 7, the conclusions, contributions, and recommendations of this research are presented. A number of directions for future work are proposed for further investigation on this subject.

Chapter 2:Modeling of Power Systems

2.1 Introduction

In small signal stability analysis, the nonlinear behavior of dynamic devices is linearized at a steady-state operating point. It is assumed that the power system is a balanced system and only the positive sequence components are considered. By doing so, the size of the equivalent linear model will be reduced significantly.

In general, the nonlinear equations are linearized around an equilibrium point by expressing the nonlinear system using the Taylor series. Only the first-order terms of the expansion are considered as the higher-order changes are assumed to be negligible.

Consider the nonlinear function given in Equation (2.1). The variables $x_1, x_2, ..., x_n$ can be state variables, inputs, outputs, or their derivatives.

$$y = f(x_1, x_2, ..., x_n) \tag{2.1}$$

At a certain steady-state operating point, the value of the linearized function is given by,

$$y^0 = f(x_1^0, x_2^0, ..., x_n^0) \tag{2.2}$$

$x_1^0, x_2^0, ..., x_n^0$ are the values of variables at the operating point.

The change in the value of the function from the steady-state, i.e. $y - y^0$, can be obtained using the first-order Taylor series expansion as given in Equation 2.3.

$$\Delta y = \sum_{i=1:n} \left(\frac{\partial f}{\partial x_i}\right)^0 \Delta x_i \tag{2.3}$$

Where $(\frac{\partial f}{\partial x_i})^0$ is the steady-state value of the partial derivative of the function with respect to the i^{th} variable. Δx_i is the change in the i^{th} variable from the steady-state operating point $(x_i - x_i^0)$.

The linearized models of dynamic devices such as MTHVDC converter, FACT devices, and generator are combined to obtain the linear state-space model of the power system. It is important to evaluate the accuracy of the linearized models since there are approximations associated with each model. In this chapter, the linearization of some dynamic devices, including MTHVDC systems, a synchronous generator and its controllers (exciter and governor), and AC network models are discussed. The linear models are tested by comparing with the detailed electromagnetic transient (EMT) simulations obtained using PSCAD/EMTDC [44].

2.2 Linearized Model of MTHVDC System

It is always challenging to linearize the HVDC converter model due to the non-linear switching and self-commutation of the converter valves. Therefore, assumptions must be made to linearize the HVDC model. The higher-order harmonics generated in the conversion process are ignored and the fundamental AC components are assumed to be balanced. Some linearized models based on these assumptions can be found in [35, 39]. In [45] and [46], the HVDC converter model has been developed based on the frequency-dependent model. The changes in the DC component on the DC side and the fundamental frequency component on the AC side have been considered. The AC side equations are frequency shifted by ± fundamental frequency to combine the AC side and DC side

equations. The studies done on the CIGRE benchmark HVDC system [47] have shown that the above two methods give similar results regarding the converter operation. Neither of the above references includes the inverter firing controllers in the models.

In this research, a current injection model, which can be easily combined with the other devices in power systems is used as the linearized model of the HVDC system. The converter linearized model is obtained using the fundamental frequency relationships derived from the converter switching waveforms [32]. The HVDC system consists of the converter model, voltage controller (VC), current controller (CC), and the DC transmission line systems.

2.2.1 Converter Model

In this research, the converter model developed in [39] is used. A detailed explanation of the converter model is provided in Appendix B. Equation 2.4 represents the linearized converter model. It has four inputs (real component and imaginary component of AC side voltage, DC side current, and firing angle) and three outputs (real component and imaginary component of AC side current and DC side voltage). The changes in the outputs for small changes in the inputs are given by Equation (2.4).

$$\begin{bmatrix} \Delta I_R \\ \Delta I_I \\ \Delta V_{dc} \end{bmatrix} = \begin{bmatrix} K_a & K_b & K_c & K_d \\ K_e & K_f & K_g & K_h \\ K_i & K_j & K_k & K_l \end{bmatrix} \begin{bmatrix} \Delta V_R \\ \Delta V_I \\ \Delta I_{dc} \\ \Delta \alpha \end{bmatrix} \tag{2.4}$$

Where

$$K_a = -\frac{\sqrt{3}BX_c I_{dc}^2}{\pi V_l^2} - \frac{\sqrt{6}BI_{dc}V_I \sin(\delta - \alpha - \mu)}{\pi I V_l^2}$$

$$K_b = -\frac{\sqrt{3}BM_1}{2\pi X_c T^2} + \frac{\sqrt{6}BI_{dc}V_R \sin(\delta - \alpha - \mu)}{\pi T V_l^2}$$

$$K_c = -\frac{\sqrt{6}B\cos(\delta - \alpha - \mu)}{\pi T}$$

$$K_d = -\frac{\sqrt{6}BI_{dc}\sin(\alpha)\sin(\delta - \alpha - \mu/2)}{\pi T \sin(\alpha + \mu/2)}$$

$$K_e = -\frac{\sqrt{3}BM_1}{2\pi X_c T^2} + \frac{\sqrt{6}BI_{dc}V_I \cos(\delta - \alpha - \mu)}{\pi T V_l^2}$$

$$K_f = -\frac{\sqrt{3}BX_c I_{dc}^2}{\pi V_l^2} - \frac{\sqrt{6}BI_{dc}V_R \cos(\delta - \alpha - \mu)}{\pi T V_l^2}$$

$$K_g = -\frac{\sqrt{6}B\sin(\delta - \alpha - \mu)}{\pi T}$$

$$K_h = -\frac{\sqrt{6}BI_{dc}\sin(\alpha)\cos(\delta - \alpha - \mu/2)}{\pi T \sin(\alpha + \mu/2)}$$

$$K_i = \frac{3\sqrt{2}BV_R \cos(\alpha)}{\pi T V_l}$$

$$K_j = \frac{3\sqrt{2}BV_I \cos(\alpha)}{\pi T V_l}$$

$$K_k = -\frac{3X_c B}{\pi}$$

$$K_l = -\frac{3\sqrt{2}BV_I \sin(\alpha)}{\pi T}$$

Note that the signs of K_i, K_j, K_k and K_l should be inverted in order to represent a positive voltage pole inverter.

2.2.2 DC Transmission Line Model

As shown in Figure 2.1, the T-model is used to represent the three-terminal HVDC line. The DC side inductance and resistance are represented by a series inductor-resistor unit and the line to ground capacitance is concentrated at each side of the line.

In the steady-state, the time derivative term of the DC current is ignored. In the small-signal model, the time derivative term is included by considering the average effect of the converter transformer leakage reactance. The contribution of the transformer leakage inductance is different during normal conduction and commutation periods. Therefore, an average inductance is obtained and is added to the partial DC line inductance to obtain the effective inductance [48] given in Equation (2.5).

$$L_{eff} = L_{dc} + B(2 - \frac{3\mu}{2\pi})L_c \tag{2.5}$$

L_{dc} is the DC side inductance from the terminal to the tap point and L_c is the transformer leakage inductance. The effective inductances in the rectifier side and the inverter side are different because the transformer leakage inductances are different.

The dynamics of the DC line are modeled using ten state variables as shown in Figure 2.1, the DC voltage and current for each terminal ($\Delta V_{dc1}, \Delta V_{dc2}$, $\Delta V_{dc3}, \Delta I_{dc\_t1}, \Delta I_{dc\_t2}$ and ΔI_{dc_t3}), the MTHVDC line tap-point DC voltage (ΔV_{dcm}), and the DC current in each HVDC line section ($\Delta I_{dcbc1}, \Delta I_{dcbc2}$ and ΔI_{dcbc3}). The linearized model of the DC line is given in Equation (2.6).

$$\begin{bmatrix} \dot{\Delta I}_{dc\_t1} \\ \dot{\Delta V}_{dc1} \\ \dot{\Delta I}_{dcbc1} \\ \dot{\Delta V}_{dcm} \\ \dot{\Delta I}_{dcbc2} \\ \dot{\Delta V}_{dc2} \\ \dot{\Delta I}_{dc\_t2} \\ \dot{\Delta I}_{dcbc3} \\ \dot{\Delta V}_{dc3} \\ \dot{\Delta I}_{dc\_t3} \end{bmatrix} = \begin{bmatrix} 0 & -\frac{1}{L_{eff1}} & 0 & 0 & 0 & 0 & 0 & 0 & 0 & 0 \\ \frac{1}{C_{11}} & 0 & -\frac{1}{C_{11}} & 0 & 0 & 0 & 0 & 0 & 0 & 0 \\ 0 & \frac{1}{L_1} & -\frac{R_1}{L_1}-\frac{1}{L_1} & 0 & 0 & 0 & 0 & 0 & 0 & 0 \\ 0 & 0 & K_1 & 0 & -K_1 & 0 & 0 & -K_1 & 0 & 0 \\ 0 & 0 & 0 & \frac{1}{L_2} & -\frac{R_2}{L_2}-\frac{1}{L_2} & 0 & 0 & 0 & 0 & 0 \\ 0 & 0 & 0 & 0 & \frac{1}{C_{21}} & 0 & -\frac{1}{C_{21}} & 0 & 0 & 0 \\ 0 & 0 & 0 & 0 & 0 & \frac{1}{L_{eff2}} & 0 & 0 & 0 & 0 \\ 0 & 0 & 0 & \frac{1}{L_3} & 0 & 0 & 0 & -\frac{R_3}{L_3}-\frac{1}{L_3} & 0 & \\ 0 & 0 & 0 & 0 & 0 & 0 & 0 & \frac{1}{C_{31}} & 0 & -\frac{1}{C_{31}} \\ 0 & 0 & 0 & 0 & 0 & 0 & 0 & 0 & \frac{1}{L_{eff3}} & 0 \end{bmatrix} \begin{bmatrix} \Delta I_{dc\_t1} \\ \Delta V_{dc1} \\ \Delta I_{dcbc1} \\ \Delta V_{dcm} \\ \Delta I_{dcbc2} \\ \Delta V_{dc2} \\ \Delta I_{dc\_t2} \\ \Delta I_{dcbc3} \\ \Delta V_{dc3} \\ \Delta I_{dc\_t3} \end{bmatrix}$$

$$+ \begin{bmatrix} \frac{1}{L_{eff1}} & 0 & 0 \\ 0 & 0 & 0 \\ 0 & 0 & 0 \\ 0 & 0 & 0 \\ 0 & 0 & 0 \\ 0 & 0 & 0 \\ 0 & -\frac{1}{L_{eff2}} & 0 \\ 0 & 0 & 0 \\ 0 & 0 & 0 \\ 0 & 0 & -\frac{1}{L_{eff3}} \end{bmatrix} \begin{bmatrix} \Delta V_{dc\_t1} \\ \Delta V_{dc\_t2} \\ \Delta V_{dc\_t3} \end{bmatrix} \quad (2.6)$$

Where

$L_{t1} = L_{eff\_t1} = L_{s1} + B(2 - \frac{3\mu}{2\pi})L_{c\_t1}$

$L_{t2} = L_{eff\_t2} = L_{s2} + B(2 - \frac{3\mu}{2\pi})L_{c\_t2}$

$L_{t3} = L_{eff\_t3} = L_{s3} + B(2 - \frac{3\mu}{2\pi})L_{c\_t3}$

L_{s1}, L_{s2} and L_{s3} are the smoothing reactor for each HVDC line terminal. L_{c_t1}, L_{c_t2} and L_{c_t3} are the transformer leakage inductance for each converter transformer. R_1, R_2 and R_3 are the sectional DC line resistance for each terminal section, where $C_{11}, C_{12}, C_{21}, C_{22}$ and C_{31}, C_{32} are the distributed DC line capacitance for each line section. V_{dc_t1}, V_{dc_t2} and V_{dc_t3} are the DC voltage for rectifier terminal one, inverter terminal two, and inverter terminal three respectively.

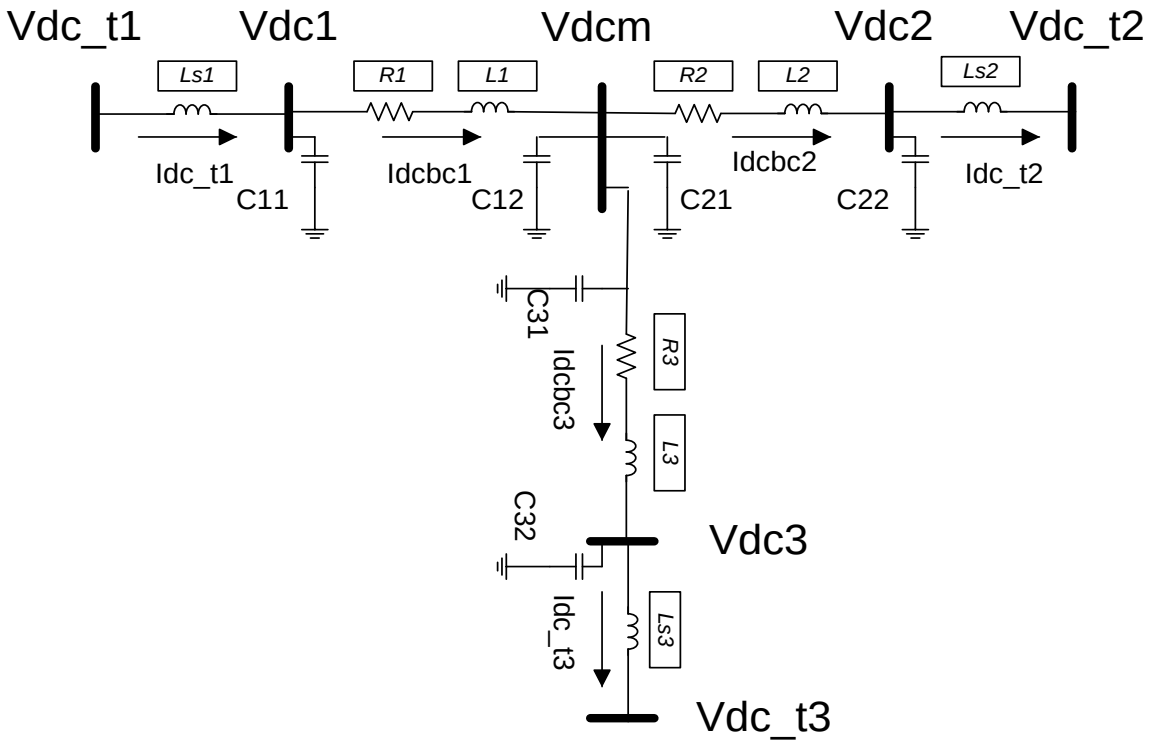

Figure 2.1 Three Terminal HVDC Transmission Line

2.2.3 HVDC Control

An HVDC transmission scheme is a complex system, consisting of a large number of components that need to operate continuously. This is achieved through several closed-loop controllers. Therefore, it is very important to have a robust controller to ensure the

HVDC system operates reliably. In this research, only active controllers under normal operating conditions are considered. Other auxiliary controllers, such as the HVDC damping controller, are not modeled.

In MTHVDC systems, one station controls the DC voltage, and all other terminals, whether rectifier or inverter, usually are in the current control mode. For example, assume a three-terminal HVDC system with the rectifier (a) and one inverter (c) in current control. The other inverter (b) controls the DC voltage. The loss (blocking) of inverter c would result in inverter b being forced to take all of the current supplied by the rectifier unless a rapid and reliable telecommunications system is available to coordinate the power and current orders between the converter stations. Therefore, the inference is that both inverters must be rated for the full power rating of the DC system. Furthermore, this dramatic change in power flow into the inverter b side AC system would not only be undesirable for the AC system at converter b, but perhaps impossible to sustain, resulting in a collapse of the DC transmission system. Therefore, it is very important to operate the MTHVDC system at a reasonable operating point. In this research, two control schemes with reliable communication systems will be assumed as shown in Table 2.1. In the MTHVDC systems, terminal one converter is operated as the rectifier and the other two terminals are operated as inverters. In control scheme one, the terminal three converter controls the DC voltage and the other two converters are controlled by the current controller. In control scheme two, the rectifier controls the MTHVDC system DC voltage, and the other two converters for terminal two and terminal three controllers control DC current.

Table 2.1 MTHVDC System Controller Arrangement

	Terminal 1 Controller	Terminal 2 Controller	Terminal 3 Controller
Converter Operation Mode	Rectifier	Inverter	Inverter
Control Scheme 1	Current	Current	Voltage
Control Scheme 2	Voltage	Current	Current

2.2.3.1 Inverter Voltage Control

In the HVDC system, the DC voltage is usually controlled by the inverter. The PI controller shown in Figure 2.2 is used to control the firing angle of the inverter to maintain the inverter DC voltage. The voltage difference between the measured inverter DC voltage and the desired DC voltage is used as the input. The inverter side DC voltage is a function of the AC side voltages, the inverter side DC current, and the firing angle as given by the linearized converter model in Equation (2.4). The V_{dci} terms in the controller equation can be replaced by the corresponding terms of Equation (2.4). The resultant linearized model for the voltage control at the inverter is given in Equations (2.7) and (2.8).

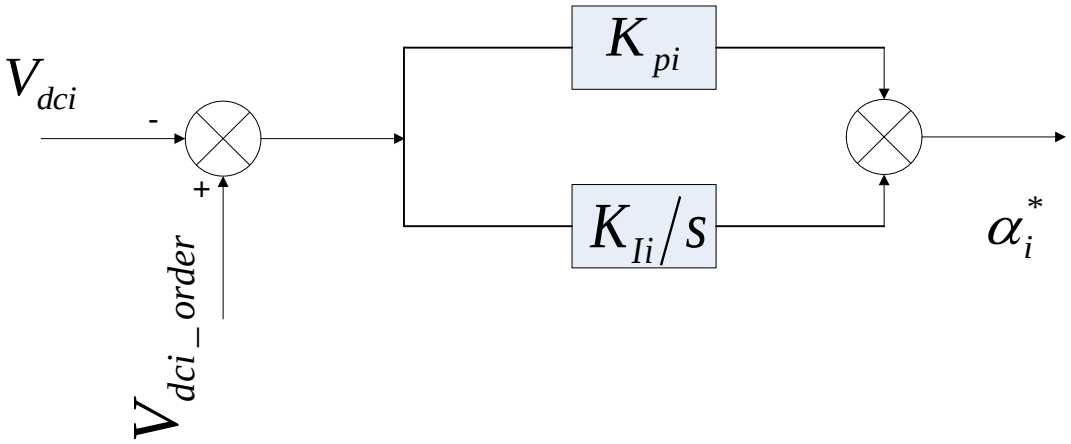

Figure 2.2 Inverter Voltage Control

$$\Delta \dot{X}_{\alpha i} = \Delta V_{dci\_order} - \Delta V_{dci} \tag{2.7}$$

$$\Delta\alpha_r^* = \frac{K_{Ii}}{1+K_{pi}\Delta V_{dc4i}}\Delta X_{\alpha i} - \frac{K_{pi}\Delta V_{dc1i}}{1+K_{pi}\Delta V_{dc4r}}\Delta V_R + \frac{K_{pi}\Delta V_{dci\_order}}{1+K_{pi}\Delta V_{dc4i}} \tag{2.8}$$

$$-\frac{K_{pi}\Delta V_{dc2i}}{1+K_{pi}\Delta V_{dc4i}}\Delta V_I - \frac{K_{pi}\Delta V_{dc3i}}{1-K_{pi}\Delta V_{dc4i}}\Delta I_{dci}$$

2.2.3.2 Current Control

Since only one of the inverters controls the DC voltage, the loading of the HVDC system depends on the DC current. Therefore, maintaining DC current close to its ordered level is important. The current controller operates on the principle of comparing the DC current order to the measured DC current. The error in this comparison is used to determine the firing angle order α of the converter. In the control scheme in Figure 2.3, one state variable $X_{\alpha i\_t2}$ is used to represent the integral portion of the controller. The state-space equation and the change in required firing angle $\Delta\alpha_{i\_t2}$ are given by Equations (2.9) and (2.10), respectively. The phase-locked loop (PLL) determines the instantaneous phase angle of the converter terminal voltages (primary side of the converter transformer) in the form of ramp signals. The trigger device then receives both the firing angle order and the phase ramp signals and produces the firing pulses for all converter valves.

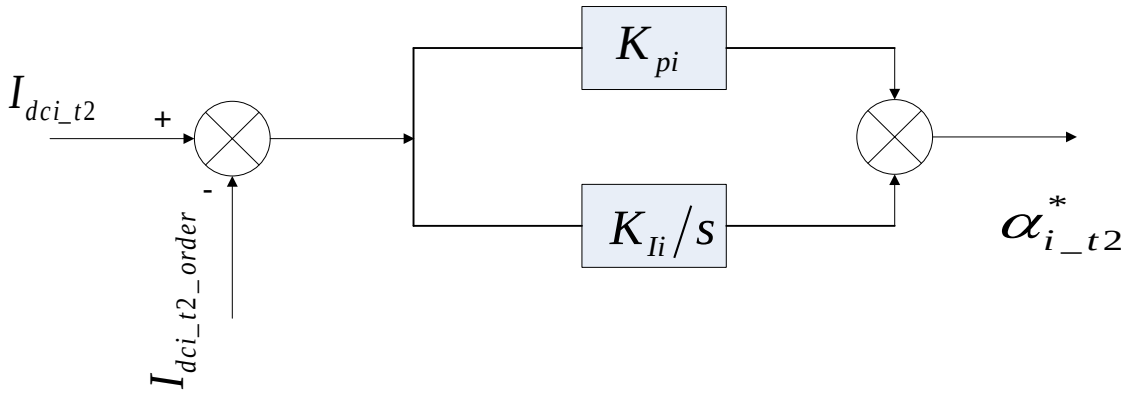

Figure 2.3 Block Diagram of Current Controller

$$\Delta \dot{X}_{\alpha i\_t2} = \Delta I_{dci\_t2} - \Delta I_{dc\_order\_t2} \tag{2.9}$$

$$\Delta \alpha^*_{i\_t2} = K_{I\_t2i} X_{\alpha i\_t2} + K_{pi\_t2} \Delta I_{dci\_t2} - K_{pi} \Delta I_{dc\_order\_t2} \tag{2.10}$$

K_{pi_t2}, K_{Ii_t2} are the proportional and integral gains of the controller and $I_{dc\_order\_t2}$ is the inverter current reference. The above equation is for the current controller at inverter terminal two. These equations can also be used for the rectifier side current controller design. In reality, each thyristor within a valve group requires a minimum forward bias voltage between its anode and cathode to be able to reliably turn on when a trigger pulse arrives. Therefore, a minimum firing angle is required. Usually, the minimum firing angle α is limited to αmin (typically 5 degrees).

2.2.3.3 Rectifier Voltage Control

In the HVDC system, it is possible to use DC voltage control at the rectifier side and DC current control at the inverter. The DC voltage control is a very fast controller, especially when the DC voltage measurement is taken directly from the converter terminal, i.e., between the converter and the smoothing reactor. Fast DC voltage control helps improve system stability. As shown in Figure 2.4, the voltage difference between the rectifier side

DC voltage and the desired DC voltage is used as the controller input. The linearized model of the voltage controller is given in Equation (2.11) and (2.12).

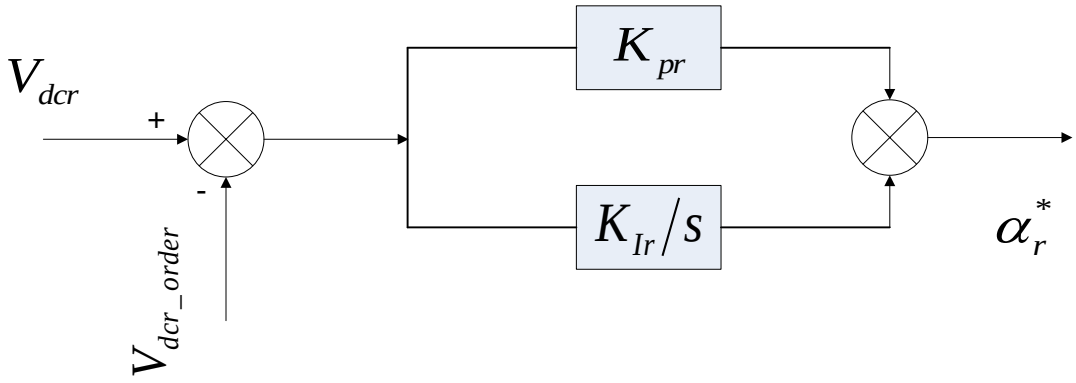

Figure 2.4 Rectifier Voltage Control

$$\Delta \dot{X}_{\alpha r} = \Delta V_{dcr} - \Delta V_{dc\_order} \tag{2.11}$$

$$\Delta\alpha_r^* = \frac{K_{Ir}}{1-K_{pr}\Delta V_{dc4r}} X_{\alpha r} + \frac{K_{pr}\Delta V_{dc1r}}{1-K_{pr}\Delta V_{dc4r}} \Delta V_R - \frac{K_{pr}\Delta V_{dc\_order}}{1-K_{pr}\Delta V_{dc4r}} + \frac{K_{pr}\Delta V_{dc2r}}{1-K_{pr}\Delta V_{dc4r}} \Delta V_I + \frac{K_{pr}\Delta V_{dc3r}}{1-K_{pr}\Delta V_{dc4r}} \Delta I_{dcr} \tag{2.12}$$

2.3.3.4 Phase-Locked Loop

It is essential for the HVDC converter operation to fire the valve at the right instant. Therefore, maintaining synchronism between the converter output voltage and the AC system voltage is very important. Phase-Locked-Loop (PLL) is the control device used to help achieve this task. As shown in Figure 2.5, a simplified PLL based on the assumption of a balanced three-phase system is used in the study.

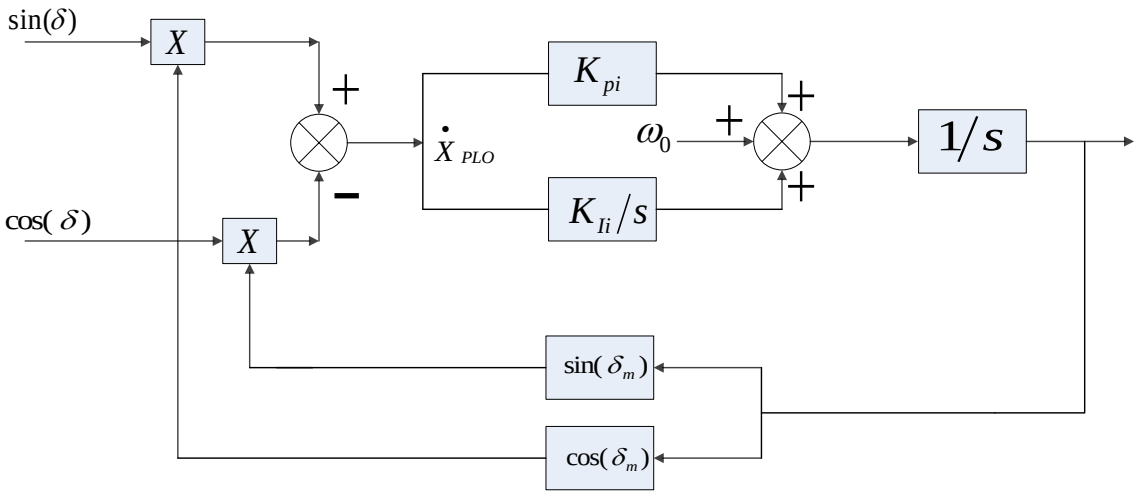

Figure 2.5 Phase-Locked Loop

An error signal $\sin(\delta - \delta_m)$ of the actual phase angle δ and the calculated phase angle δ_m is given to the PI controller to obtain the angular frequency error. The frequency error is added to the nominal frequency ω_0 and the resultant frequency is integrated to get the phase angle.

The actual phase angle can be obtained in terms of V_R and V_I. Two state variables: X_{PLO} and δ_m are used to represent the PI controller and the integrator, respectively. The linearized small-signal PLL model is given in Equation 2.13.

$$\begin{bmatrix} \Delta\dot{X}_{PLO} \\ \Delta\dot{\delta}_m \end{bmatrix} = \begin{bmatrix} 0 & -1 \\ K_{IP} & -K_{PP} \end{bmatrix} \begin{bmatrix} \Delta X_{PLO} \\ \Delta\delta_m \end{bmatrix} + \begin{bmatrix} -\frac{V_I}{V_l^2} & \frac{V_R}{V_l^2} \\ -\frac{K_{PP}V_I}{V_l^2} & \frac{K_{PP}V_R}{V_l^2} \end{bmatrix} \begin{bmatrix} \Delta V_R \\ \Delta V_I \end{bmatrix} \qquad (2.13)$$

The output of the PLL, the phase angle δ_m, is added to the desired firing angle α to get the exact firing instant to fire the converter.

State Space Model of MTHVDC System

The linearized models for the rectifier, inverter, and controller are combined to obtain the state-space model of the MTHVDC system. For the rectifier, the change in desired firing angle $\Delta\alpha r^*$ given by either the rectifier current controller (Equation (2.10)) or the rectifier voltage controller (Equation (2.12)) is added to the change in phase angle $\Delta\delta_{mr}$ obtained from the PLL model (Equation (2.13)) to obtain the rectifier side-firing angle change $\Delta\alpha r$ as shown in Equation (2.14). Similarly, for the other two inverters, the change in desired firing angle $\Delta\alpha i^*$ given by the current controller (Equation (2.12)) is added to the change in phase angle $\Delta\delta_{mi}$ to obtain the change in firing instant $\Delta\alpha i$ as shown in Equation (2.15).

$$\Delta\alpha_r = \Delta\alpha_r^* + \Delta\delta_{mr} \tag{2.14}$$

$$\Delta\alpha_i = \Delta\alpha_i^* + \Delta\delta_{mi} \tag{2.15}$$

The firing instants are substituted into the rectifier and inverter models obtained using Equation (2.9). The changes in DC voltages given by the rectifier and inverter models are substituted in the DC transmission system (Equation (2.6)). This procedure results in the state-space model of the MTHVDC system given in Equation (2.16). The overall system consists of nineteen state variables and three control inputs. The real and imaginary components of the rectifier and inverter output currents are obtained from Equation (2.17).

$$\Delta\dot{X}_H = A_H(\Delta X_H) + B_H(\Delta U_H) + E_H(\Delta V_H) \tag{2.16}$$

$$\Delta I_H = C_H(\Delta X_H) + D_H(\Delta U_H) + Y_H(\Delta V_H) \tag{2.17}$$

Where

$\Delta X_H = [\Delta X_{\alpha\_t1} \quad \Delta X_{\alpha\_t2} \quad \Delta I_{dc\_t1} \quad \Delta I_{dc\_t2} \quad \Delta V_{dcm} \quad \Delta X_{PLO\_t1} \quad \Delta\delta_{m\_t1} \quad \Delta X_{PLO\_t2}$

$$\ldots \Delta\delta_{m\_t2} \quad \Delta X_{\alpha\_t3} \quad \Delta I_{dc\_t3} \quad \Delta X_{PLO\_t3} \quad \Delta\delta_{m\_t3} \quad \Delta V_{dc1} \quad \Delta V_{dc2} \quad \Delta V_{dc3}$$

$$\ldots \Delta I_{dcbc1} \quad \Delta I_{dcbc2} \quad \Delta I_{dcbc3}]^T$$

$$\Delta V_H = \begin{bmatrix} \Delta V_{Rr\_t1} \\ \Delta V_{Ir\_t1} \\ \Delta V_{Ri\_t2} \\ \Delta V_{Ii\_t2} \\ \Delta V_{Ri\_t3} \\ \Delta V_{Ii\_t3} \end{bmatrix}, \; \Delta I_H = \begin{bmatrix} \Delta I_{Rr\_t1} \\ \Delta I_{Ir\_t1} \\ \Delta I_{Ri\_t2} \\ \Delta I_{Ii\_t2} \\ \Delta I_{Ri\_t3} \\ \Delta I_{Ii\_t3} \end{bmatrix}$$

$$\Delta U_H = \begin{bmatrix} \Delta I_{dc\_order} \\ \Delta I_{dc\_order\_t2} \\ \Delta V_{dc\_order\_t3} \end{bmatrix}$$ (DC voltage control at terminal three)

Depending on which converter terminal controls the DC voltage, the sequence in the ΔU_H term can be changed to:

$$\Delta U_H = \begin{bmatrix} \Delta V_{dc\_order\_t1} \\ \Delta I_{dc\_order\_t2} \\ \Delta I_{dc\_order\_t3} \end{bmatrix}$$ (DC voltage control at terminal one)

A_H, B_H, E_H, C_H, D_H and Y_H matrices are obtained using the procedure described above.

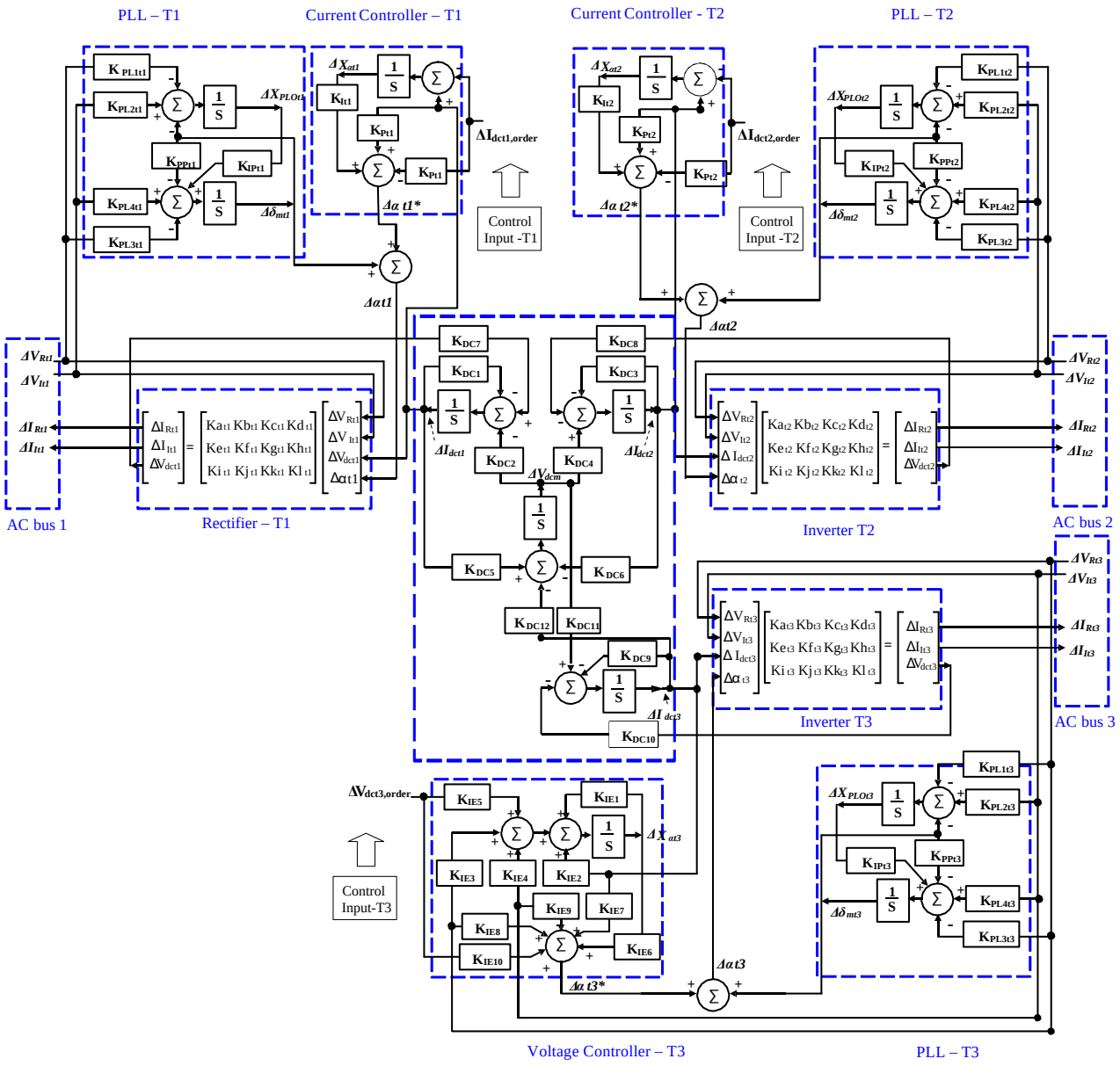

Figure 2.6 Linearized model of MTHVDC system

2.3 AC System Modeling

All the transmission lines, transformers, static loads, and AC filters are included in the AC network model. The conventional small-signal stability assessment tools are designed for electromechanical oscillation studies. The AC network dynamics are ignored, and the network is represented using the fundamental frequency admittance matrix. Therefore, this method is accurate only for low frequency (<5Hz) oscillations. In HVDC and sub-synchronous oscillation (SSO) interaction studies, the oscillation frequency is much higher (in the range of 0-60Hz) [49, 50, 51]. Therefore, a more accurate way to represent the AC network is required. Dynamic phasor is a suitable candidate for this purpose. In the following section, the dynamic phasor representations of the AC network will be briefly discussed.

The dynamic behaviors of the power system are often studied by transient stability programs, such as PSS/E and TSAT software. With the development of the technology, particularly the introduction of power electronic-based equipment e.g. HVDC and FACT devices, there is a shortage in analysis methods with fundamental frequency phasor models. For such components, a full-time domain simulation may be required. Due to the limitation of computer storage and computation time, a complete representation of a large power system in an electromagnetic transients program such as EMTDC/PSCAD is very difficult. To overcome this issue, the concept of dynamic phasors is successfully introduced to model power system electrical machines [43], flexible AC transmission Systems (FACTS) devices [52, 53], and DC-DC converters [54]. In comparison to quasi-stationary phasor analysis, dynamic phasor has a wider bandwidth in the frequency domain. Dynamic phasor modeling retains the low-frequency dynamic characteristics of a power system without

having to model the high-frequency transients introduced by the converter switching and power-electronic operation. In addition, it can be used to compute fast electromagnetic transients with larger time steps, so the simulation time is significantly reduced in comparison to the conventional time-domain EMTP type simulation [44].

2.3.1 Concept of Dynamic Phasor

A dynamic phasor is a phasor where the magnitude and phase angle are allowed to change over time. It allows electromechanical transient simulations to retain most of the dynamics associated with the electrical network without significantly increasing the computational burden. The research works in [32] demonstrated that dynamic phasors significantly improve the accuracy of electromechanical simulations, especially for power electronic converter simulations.

In this research, the dynamic phasor based on the Shifted Frequency Analysis (SFA) [42] technique is used. The basic idea is to shift the fundamental frequency by 60Hz to 0Hz so that a much larger simulation step can be used for the simulation. Similar to the communication systems, the information signal is modulated to a high-frequency carrier and transmitted to the receiving end. It is then recovered by subtracting the carrier frequency by the receiver. The SFA is similar to the demodulated process. It uses a constant shifting frequency (60 Hz or 50 Hz) to first transfer the system from the original time domain into the SFA domain and then bring the solution back into the real-time domain. By doing so, the signal retains the main characteristics of the original signal while also saving solution time. The following sections detail the mathematical background.

In power systems, transient phenomena are characterized by spectra containing high-frequency components. As the system returns to steady-state, the spectrum of the signals

becomes centered around the nominal system frequency ω_0. In general, its half-bandwidths are less than ω_0. Such signals are called bandpass signals, which can be represented as:

$$s(t) = s_R(t)\cos(\omega_0 t) - s_I(t)\sin(\omega_0 t) \tag{2.18}$$

Where $s_R(t)$ is the real component of the bandpass signal $s(t)$ and $s_I(t)$ is the imaginary component of the bandpass signal $s(t)$.

Assuming $z(t)$ is the analytic signal of $s(t)$, then

$$z(t)e^{-j\omega_0 t} = \{s(t) + jH[s(t)]\}e^{-j\omega_0 t}$$

$$=\{s_R(t)\cos(\omega_0 t) - s_I(t)\sin(\omega_0 t) + j[s_R(t)\sin(\omega_0 t) - s_I(t)\cos(\omega_0 t)]\}e^{-j\omega_0 t}$$

$$=s_R(t) + js_I(t) \tag{2.19}$$

Where $H[s(t)]$ represents of the Hilbert transform for the signal $s(t)$.

Therefore

$$S(t) = z(t)e^{-j\omega_s t} \tag{2.20}$$

Equation (2.20) shows that the spectrum of $S(t)$ is the spectrum of the analytic signal of $s(t)$ shifted by the synchronous frequency $-\omega_0$. This is the so-called "frequency shifting." By applying SFA in the simulation, a time-varying phasor solution can be obtained. The original waveform can also be traced back from the SFA results using the inverse transformation

$$s(t) = Re[S(t)e^{j\omega_0 t}] \tag{2.21}$$

The transferred magnitude and phase are embedded in the phasor quantity.

Dynamic phasor has been used in a broad area to demonstrate its capability in power system simulations. It has been primarily focused on the modeling and simulation of power electronics switching devices, HVDC, and FACTs as well as for power system sub-

synchronous resonance (SSR) analysis [55]. The results demonstrate that dynamic phasor can improve simulation accuracy.

When applied to power electronic devices, the dynamic phasors approach transforms the periodically switched system into a continuous system in order to gain more analytical insight (e.g., eigenvalue analysis). In this research, the models are derived based on the power systems elements dynamic phasor representation. The benchmarked results show the accuracy of the models. The linearized models of the AC network components are obtained using equation (2.21). It is assumed that the fundamental frequency of the system is constant. In reality, most AC network components can be represented by combinations of series R-L components and parallel R-C components. Therefore, the linearized models of series R-L components and parallel R-C components are provided in the following section.

2.3.2 AC System Dynamic Phasor Modeling

Series R-L Component

The instantaneous voltage across node 1 and node 2 or a series R-L circuit between node 1 and node 2 as shown in Figure 2.7 is:

$$V_{12} = L\frac{di_{12}}{dt} + Ri_{12} \tag{2.22}$$

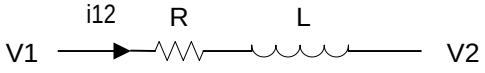

Figure 2.7 Basic series R-L Circuit

Equation (2.22) can be re-written as (2.23) in Phasor format

$$(V_R + jV_I)e^{j\omega_0 t} = L\frac{d(I_R+jI_I)e^{j\omega_0 t}}{dt} + R(I_R + jI_I)e^{j\omega_0 t} \tag{2.23}$$

The time-varying dynamic phasor representation depends on the fundamental frequency ω_0. Phasors are not instantaneous current and voltage quantities but rather are time-varying RMS quantities of the fundamental frequency. After differentiation, equation (2.23) can be written as:

$$V_R + jV_I = L\frac{d(I_R+jI_I)}{dt} + (R + j\omega_0)(I_R + jI_I)\,. \qquad .(2.24)$$

The linearized model of equation (2.24) is given in equation (2.25)

$$\begin{bmatrix} \dot{\Delta I}_R \\ \dot{\Delta I}_I \end{bmatrix} = \begin{bmatrix} \frac{-R\omega_0}{L} & \omega_0 \\ -\omega_0 & \frac{-R\omega_0}{L} \end{bmatrix} \begin{bmatrix} \Delta I_R \\ \Delta I_I \end{bmatrix} + \begin{bmatrix} \frac{\omega_0}{L} & 0 & \frac{-\omega_0}{L} & 0 \\ 0 & \frac{\omega_0}{L} & 0 & \frac{-\omega_0}{L} \end{bmatrix} \begin{bmatrix} \Delta V_{1R} \\ \Delta V_{1I} \\ \Delta V_{2R} \\ \Delta V_{2I} \end{bmatrix} \qquad (2.25)$$

Note: V_R and V_I are the real and imaginary parts of the phasor voltage between node 1 and node 2.

Parallel R-C Component

For a parallel R-C circuit between node 1 and ground as shown in Figure 2.8. The instantaneous current flowing in the circuit is:

$$i = C\frac{dv_1}{dt} + \frac{1}{R}v_1 \qquad (2.26)$$

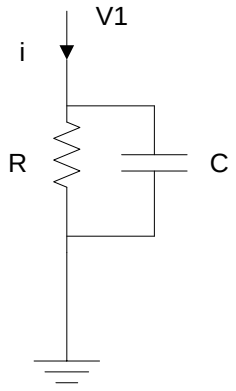

Figure 2.8 Basic parallel R-C Circuit

Equation (2.26) can be re-written as (2.27) in Phasor format

$$(I_R + jI_I)e^{j\omega_0 t} = C\frac{d(V_{1R}+jV_{1I})e^{j\omega_0 t}}{dt} + R(V_{1R} + jV_{1I})e^{j\omega_0 t} \qquad (2.27)$$

Similar to equation (2.23), the phasor relationship given in equation (2.26) can be obtained.

$$I_R + jI_I = L\frac{d(V_{1R}+jV_{1I})}{dt} + (\frac{1}{R} + j\omega_0 C)(V_{1R} + jV_{1I}) \qquad (2.28)$$

The linearized model of equation (2.28) is given in equation (2.29)

$$\begin{bmatrix} \Delta\dot{V}_{1R} \\ \Delta\dot{V}_{1I} \end{bmatrix} = \begin{bmatrix} \frac{-\omega_0}{RC} & \omega_0 \\ -\omega_0 & \frac{-\omega_0}{RC} \end{bmatrix} \begin{bmatrix} \Delta V_{1R} \\ \Delta V_{1I} \end{bmatrix} + \begin{bmatrix} \frac{\omega_0}{C} & 0 \\ 0 & \frac{\omega_0}{C} \end{bmatrix} \begin{bmatrix} \Delta I_R \\ \Delta I_I \end{bmatrix} \qquad (2.29)$$

Note: I_R and I_I are the real and imaginary parts of the phasor current flowing into the node.

By using a series R-L circuit and a parallel R-C circuit, the overall AC network model can be derived by combining the currents and voltages using Kirchhoff's law.

2.3.3 Generator Model

In conventional transient studies, generator stator flux is modeled by differential equations, and the stator transients are neglected. There are two reasons to make these assumptions. One is to have a consistent number of equations in the representation of various power system elements. For transient stability studies, it involves system slow variation which has frequencies below 5Hz. Network transients do not need to be modeled because they are rapidly decaying. Since the network transients are neglected, it is not necessary to model generator stator winding transients. In addition, the stator transients in the dq frame are represented by the $\frac{d\varphi_d}{dt}$ and $\frac{d\varphi_q}{dt}$ terms in the transformer voltage equations

as shown in (2.30) and (2.31). The $\frac{d\varphi_d}{dt}$ and $\frac{d\varphi_q}{dt}$ terms prevent φ_d and φ_q from changing instantaneously, resulting in DC offset in the phase current. The analysis with both fundamental frequency and DC components of phase currents included would be more complex and would require more computational resources. By eliminating these terms, the DC offset components and its associated dynamic performance can be removed. As a result, the φ_d and φ_q terms are assumed to change instantly following a disturbance. The speed variation ω_r is assumed to be constant to counterbalance the effect of neglecting stator transients [30].

$$e_d = \frac{d\varphi_d}{dt} - \omega_r \varphi_q - R_a i_d e \tag{2.30}$$

$$e_q = \frac{d\varphi_q}{dt} - \omega_r \varphi_d - R_a i_q e \tag{2.31}$$

As a result, the 5th and 6t^{h} order machine models are used to represent the salient pole machine and the round rotor machine in conventional small signal stability analysis tools. The detailed derivation of the generator equations can be found in [30].

If the AC network is represented by using a dynamic phasor model, two additional differential equations for the generator stator flux components in the d-q axes should be included in the synchronous machine model. As a result, both an 8th order generator model and a 7th order generator model are used for the round rotor type machine and the salient pole machine, respectively. To capture the fast dynamics in the higher frequency range (between 5Hz and 60Hz), the stator fluxes of the d and q axis are included in the generator model. The generator can be represented by equation (2.32) to (2.37). The d and q axis stator fluxes are represented by equations (2.38) and (2.39).

$$\frac{d\varphi_{fd}}{dt} = \omega_0[e_{fd} - \frac{R_{fd}}{L_{fd}} + \frac{R_{fd}}{L_{fd}} L''_{ads}(-i_d + \frac{\varphi_{fd}}{L_{fd}} + \frac{\varphi_{1d}}{L_{1d}})] \tag{2.32}$$

$$\frac{d\varphi_{1d}}{dt} = \omega_0[-\frac{R_{1d}}{L_{1d}}\varphi_{1d} + \frac{R_{1d}}{L_{1d}}L''_{ads}(-i_d + \frac{\varphi_{fd}}{L_{fd}} + \frac{\varphi_{1d}}{L_{1d}})] \quad (2.33)$$

$$\frac{d\varphi_{1q}}{dt} = \omega_0[-\frac{R_{1q}}{L_{1q}}\varphi_{1q} + \frac{R_{1q}}{L_{1q}}L''_{aqs}(-i_q + \frac{\varphi_{1q}}{L_{1q}} + \frac{\varphi_{1q}}{L_{1q}})] \quad (2.34)$$

$$\frac{d\varphi_{2q}}{dt} = \omega_0[-\frac{R_{2q}}{L_{2q}}\varphi_{2q} + \frac{R_{2q}}{L_{2q}}L''_{aqs}(-i_q + \frac{\varphi_{2q}}{L_{2q}} + \frac{\varphi_{2q}}{L_{2q}})] \quad (2.35)$$

$$\frac{d\Delta\omega_r}{dt} = \frac{1}{2H}(T_m - \varphi_d i_q + \varphi_q i_d - k_D\Delta\omega_r) \quad (2.36)$$

$$\frac{d\delta}{dt} = \Delta\omega_r * \omega_0 \quad (2.37)$$

$$\frac{d\varphi_d}{dt} = e_d + \varphi_q(1 + \Delta\omega_r) + R_a i_d \quad (2.38)$$

$$\frac{d\varphi_q}{dt} = e_q - \varphi_d(1 + \Delta\omega_r) + R_a i_q \quad (2.39)$$

In this research, the 8th order generator model will be used in conjunction with the dynamic Phasor AC network model to capture fast transients of the power system. The linearized models of the AC4A exciter and governor model are combined with the generator model [56, 57, 58, 59]. The details of the linearized generators, exciters, and governor models are provided in Appendix B.

2.4 Overall State Space Model

The linearized models of the dynamic devices are combined with the AC network to obtain the state-space model of the entire power system as shown in equation (2.41). Therefore, the dynamics of the entire network are included in the state space model. The steps to formalize the overall state-space model for the small-signal stability analysis are:

1. Combine the state variable equation (2.25) for the R-L circuit and (2.26) for the R-C circuit together to obtain the state-space model of the entire network as indicated in Equation (2.40).

$$\Delta \dot{X}_{net} = A_{net}(\Delta X_{net}) + M_{net}(\Delta V_L) + N_{net}(\Delta I_H) \qquad (2.40)$$

2. The linear state-space model of the MTHVDC system as represented in Equations (2.16) and (2.17) are also listed as (2.41) and (2.42). Equation (2.42) is substituted in the network equation (2.40) to eliminate ΔI_H terms. The modified equation (2.40) and the MTHVDC state equation (2.41) are combined to obtain the resultant state-space model.

$$\Delta \dot{X}_H = A_H(\Delta X_H) + B_H(\Delta U_H) + E_H(\Delta V_H) \qquad (2.41)$$

$$\Delta I_H = C_H(\Delta X_H) + D_H(\Delta U_H) + Y_H(\Delta V_H) \qquad (2.42)$$

3. The generator model including stator dynamics is represented by Equations (2.43) and (2.44). The output current of the generator is a function of the state variables.

$$\Delta \dot{X}_g = A_g \Delta X_g + B_g \Delta U_g + E_g \Delta \mathrm{V}_g \quad (2.43)$$

$$\Delta I_g = C_g \Delta X_g \quad (2.44)$$

The generator output current ΔI_g is equal to the generator-transformer current, which is a state variable of the network model. The network equation is rewritten in terms of the generator current.

$$\Delta \dot{I}_g = A_{tf} \Delta I_g + E_{tf1} \Delta \mathrm{V}_L + E_{tf2} \Delta \mathrm{V}_H \qquad (2.45)$$

Equation (2.49) is combined with Equations (2.43) and (2.45) to find the $\Delta \mathrm{V}_L$ in terms of the state variables, inputs, and $\Delta \mathrm{V}_H$ (a state variable of the network model). $\Delta \mathrm{V}_L$ is then substituted in Equation (2.40) and (2.43) to obtain the overall state-space model as represented by equation (2.46).

$$\Delta \dot{X} = A\Delta X + B\Delta U \qquad (2.46)$$

ΔU includes all the control inputs of the system. The system matrix (A) is analyzed in the frequency domain, to identify the dynamic behavior of the system.

2.5 Chapter Summary

In this chapter, the modeling of power system components for small signal stability analysis has been analyzed. The linearized models of the three-terminal HVDC system, including the HVDC converters, three-terminal HVDC line, DC current controller, and DC voltage controller, as well as the PLLs, have been analyzed and presented. For the entire AC power systems, generator stator dynamics have been included in the linearized models. The AC network is represented by dynamic phasor representation. By doing so, more accurate results can be obtained in the studied frequency range. In addition, the general process to obtain the overall state-space model of the entire power system is provided.

Chapter 3: Model Validation

3.1 Introduction

In order to eliminate the error caused by different modeling techniques, it is very important to validate the models. Since Electromagnetic transient (EMT) simulation programs give very accurate system responses, they are used to validate the small-signal models derived in this research. The linearized state-space models of the power systems are formulated in MATLAB using the method discussed in Chapter 2. For a small disturbance in the control inputs, the system responses obtained using the linearized models are compared with the responses of the detailed PSCAD/EMTDC models.

3.2 Validation of Linearized HVDC Model

In order to analyze the HVDC system, the modified CIGRE benchmark HVDC test system [60, 61] was used for the validation. To test the MTHVDC model, the AC buses in the test systems were replaced by infinite AC buses at each of the HVDC terminals as shown in Figure 3.1. The rectifier voltage controller, inverter constant current controller, and the PLLs are all included in the model. The linearized system has 19 state variables (10 from the DC line, 3 from the controllers, and 6 from the PLLs) and three inputs (one rectifier voltage reference, two inverter current order references).

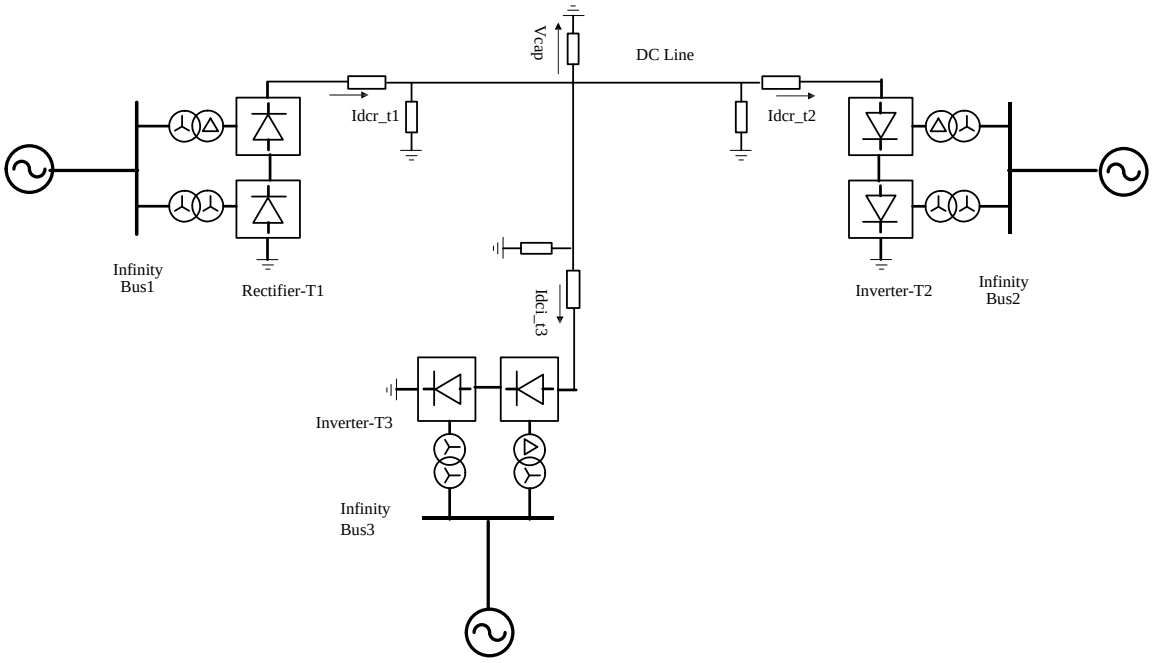

Figure 3.1 MTHVDC test system with infinite AC buses

A pulse of magnitude +2% and a duration of 0.01s was applied to the terminal-three current controller. The responses of the controller and DC line state variables obtained with the small-signal model were compared with those of PSCAD/EMTDC in Figure 3.2 to Figure 3.5. All the responses showed a very good match with the PSCAD/EMTDC results. It should be noted that the red curve represents the change of either DC voltage/ DC current of the developed small-signal model and the blue curve represents the change of either DC voltage or DC current) of the PSCAD simulation model.

A pulse of magnitude +5% and a duration of 0.01s was also applied to the rectifier voltage controller and terminal-two inverter current controller input. All the responses showed a very good correlation with the PSCAD/EMTDC results. Therefore, it was concluded that the model was accurate in representing the converter and the HVDC line.

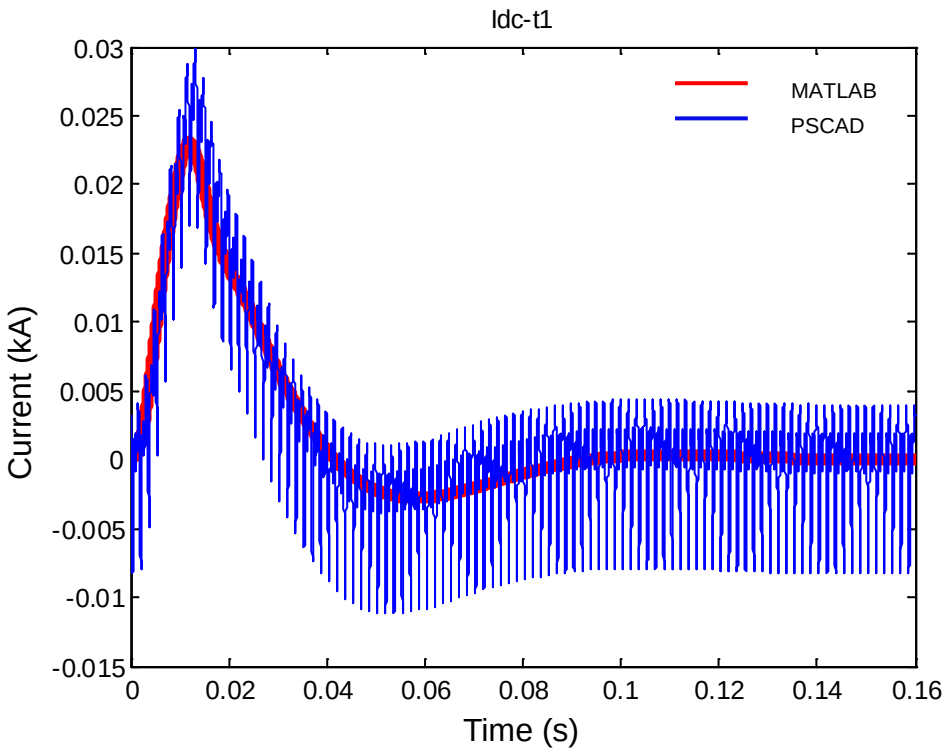

Figure 3.2 Terminal one current response

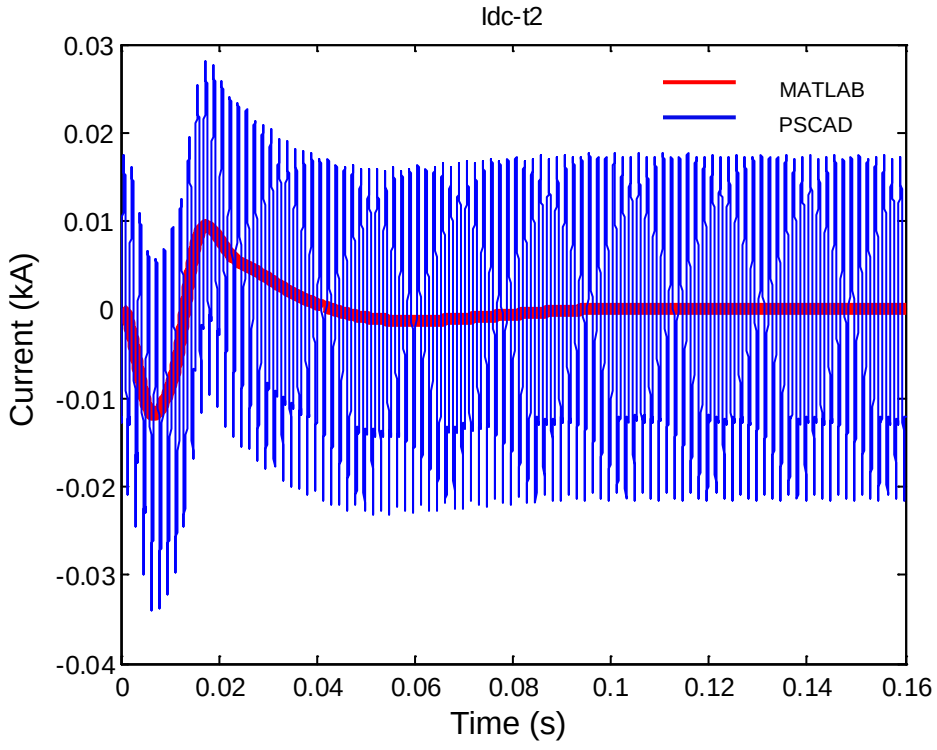

Figure 3.3 Terminal two current response

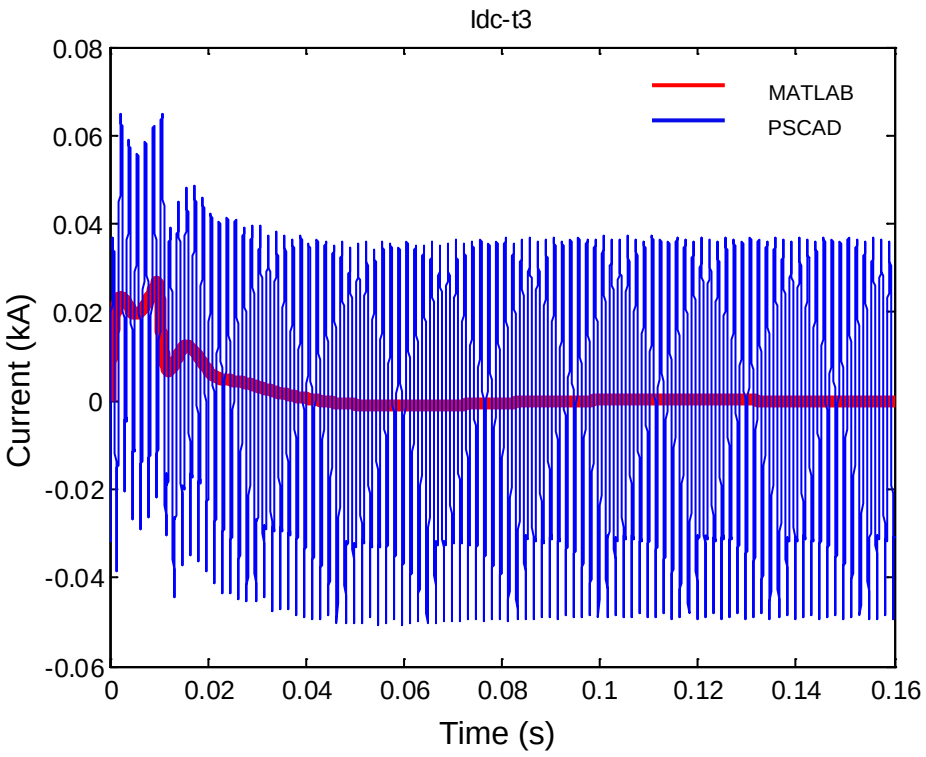

Figure 3.4 Terminal three current response

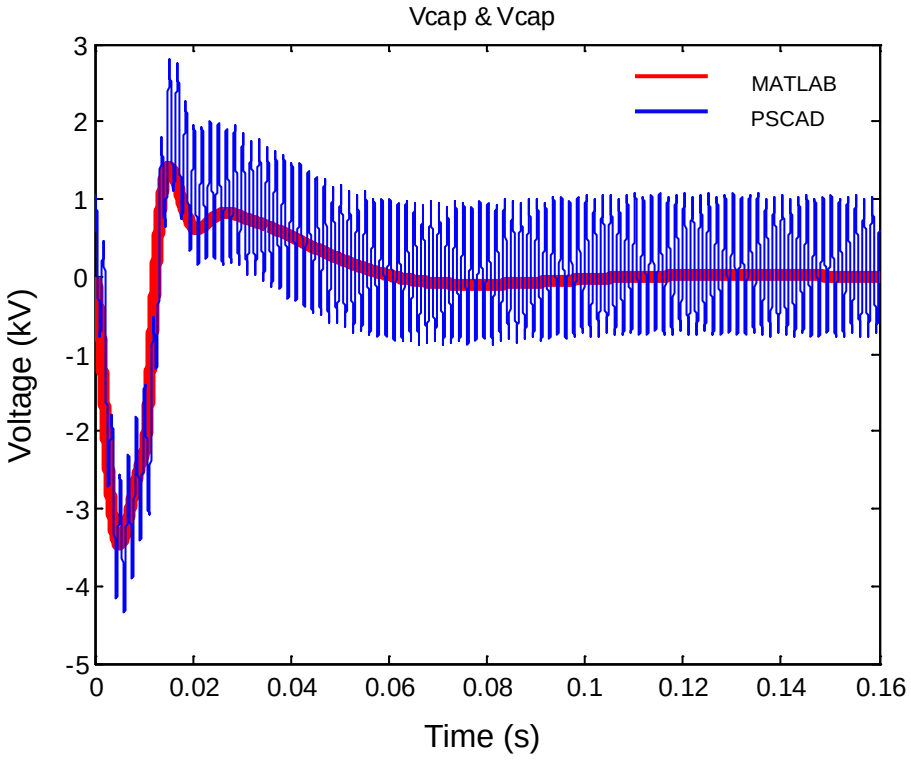

Figure 3.5 HVDC line tap point DC voltage response

To further test the three-terminal HVDC system small-signal model, the New England 39 bus test system with some modifications as shown in Figure 3.6 was used. Two MTHVDC inverter terminals are connected to buses 22 and 23 to replace the original generators 35 and 36. These two MTHVDC inverters along with two capacitor banks (representing AC filter banks), provided the same amount of real and reactive power provided by the replaced generators in the original system. Bus 40 was created to represent the rectifier converter bus. In addition, bus 38 was kept as an infinite bus and therefore, generator 38 was modeled as a voltage source. The details of the test system are given in Appendix A.

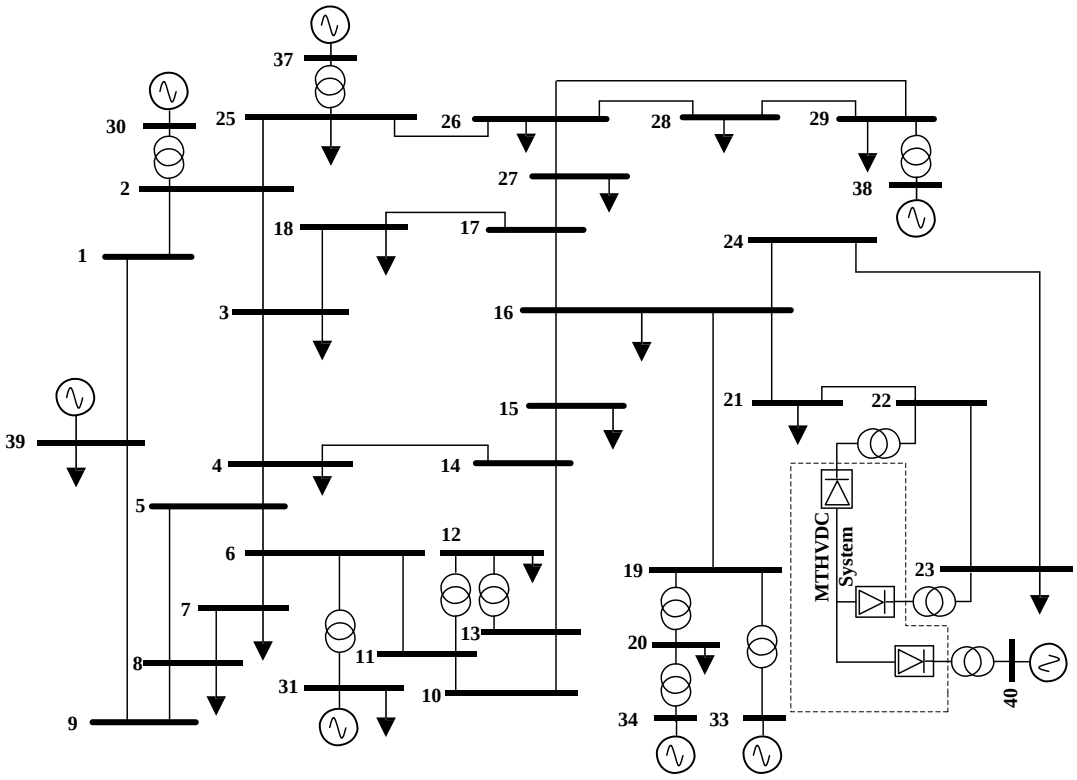

Figure 3.6 Modified IEEE New England 39 Bus System

A pulse of magnitude +2% and a duration of 0.05s were also applied to the terminal one rectifier voltage controller input. The responses were very similar to the PSCAD/EMTDC

results as shown in figure 3.7-3.14. In addition, the rotor speed of the generator confirmed that the models were also effective for low-frequency electromechanical oscillation studies. Therefore, it was concluded that the developed MTHVDC model was accurate in representing the entire studied systems. The same disturbance was also applied to other terminals, and the results showed a good agreement with the PSCAD results.

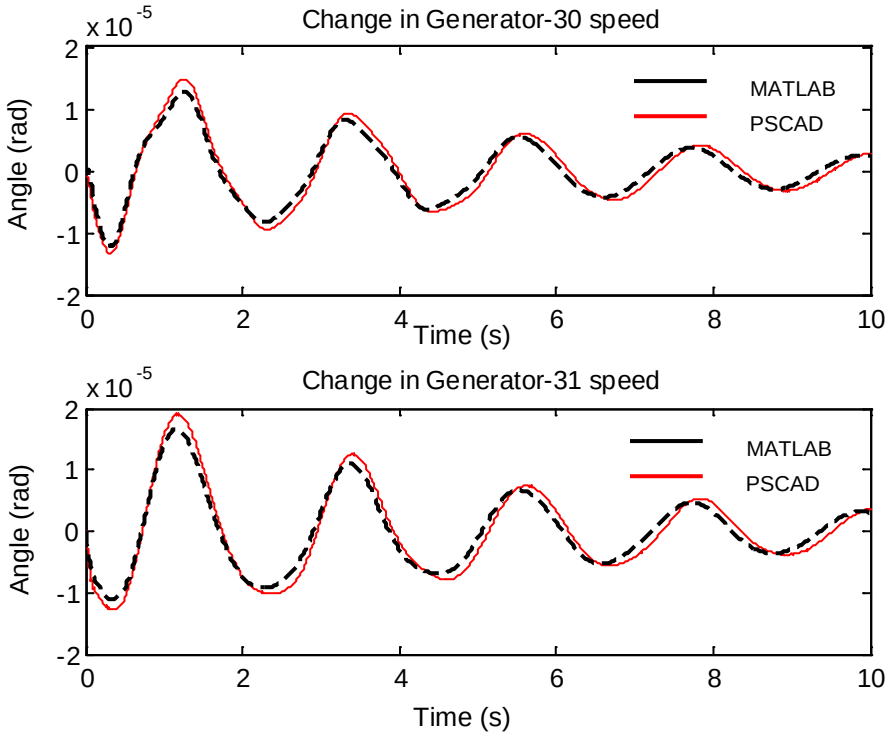

Figure 3.7 Generator 30, 31 rotor speed for a 2%, 0.05s step change on terminal two

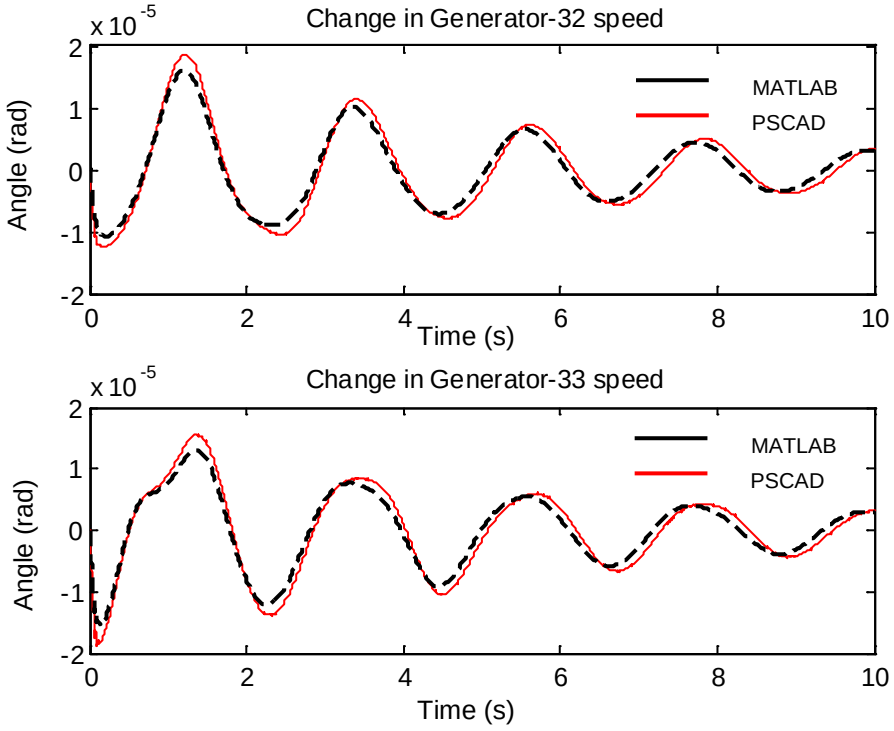

Figure 3.8 Generator 32, 33 rotor speed for a 2%, 0.05s step change on terminal two

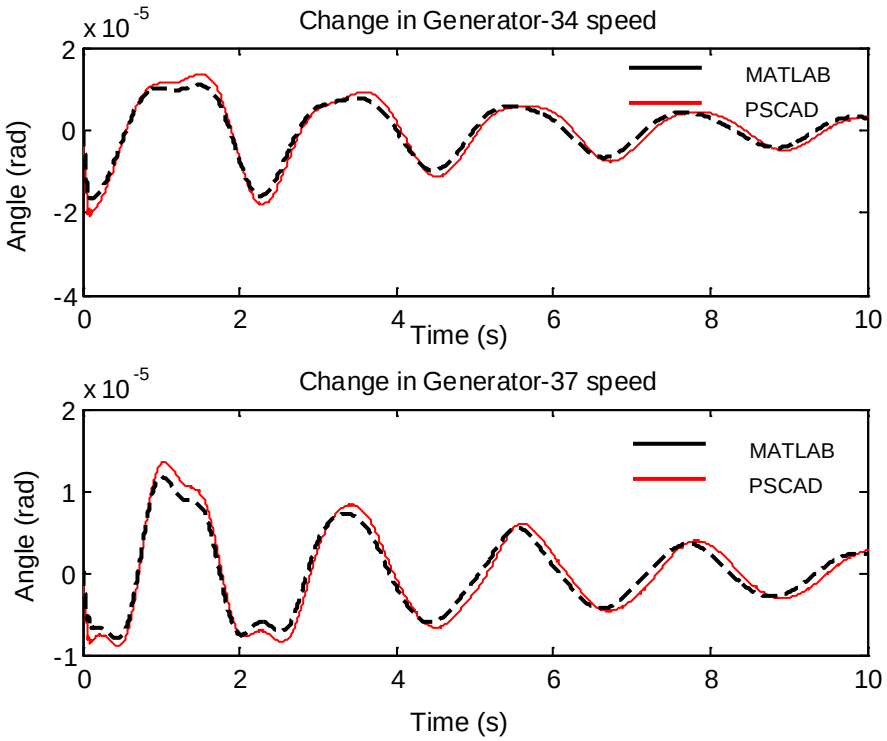

Figure 3.9 Generator 34, 37 rotor speed for a 2%, 0.05s step change on terminal two

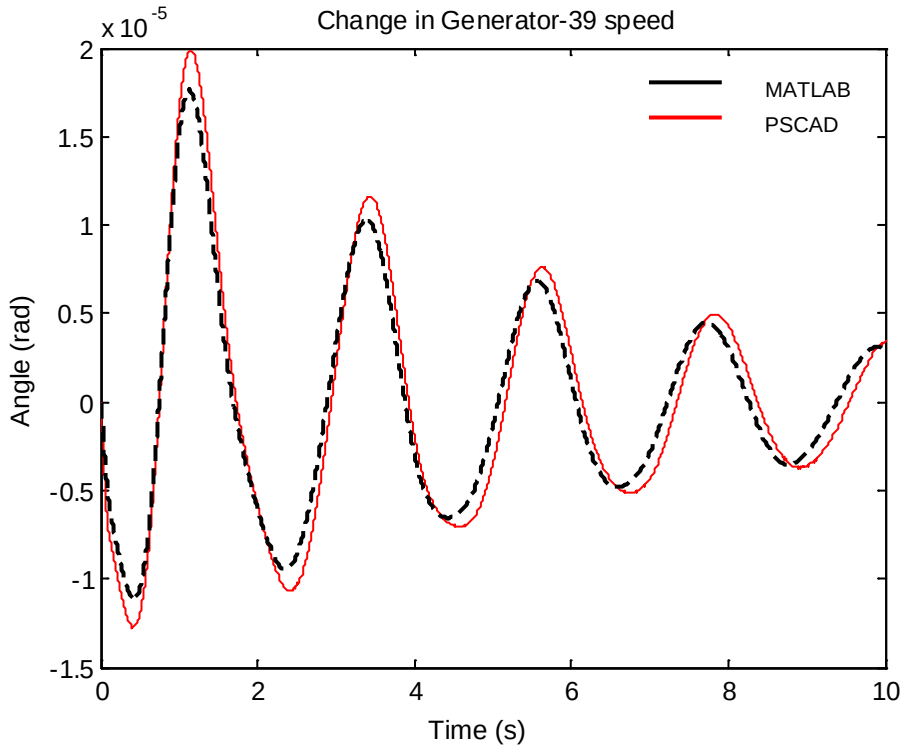

Figure 3.10 Generator 39 rotor speed for a 2%, 0.05s step change on terminal two

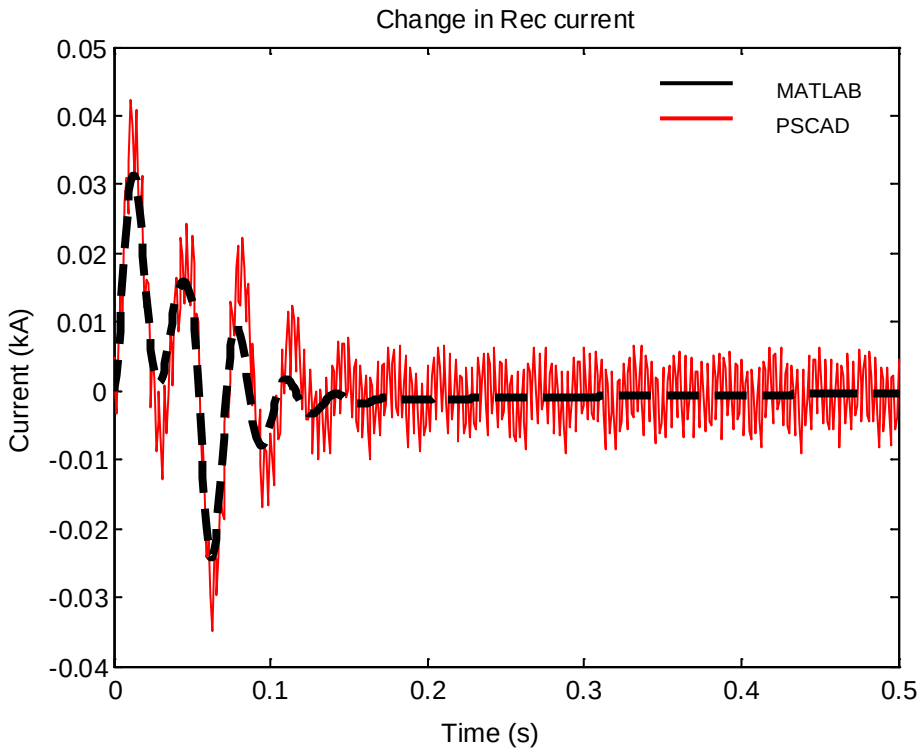

Figure 3.11 MTHVDC T1 current change for a 2%, 0.05s step change on terminal two

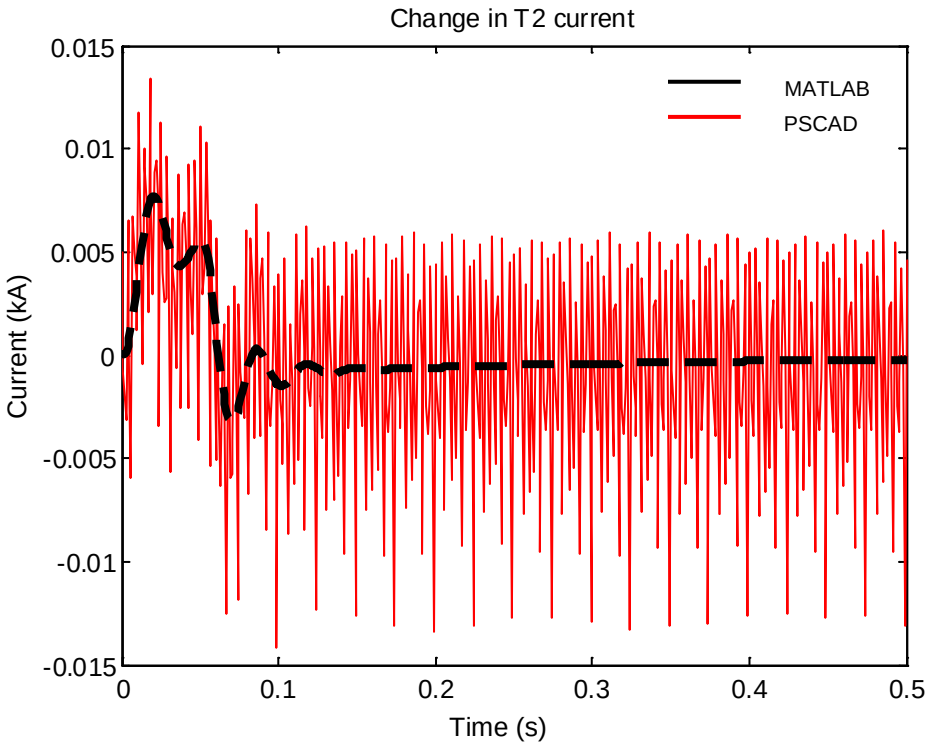

Figure 3.12 MTHVDC T2 current change for a 2%, 0.05s step change on terminal two

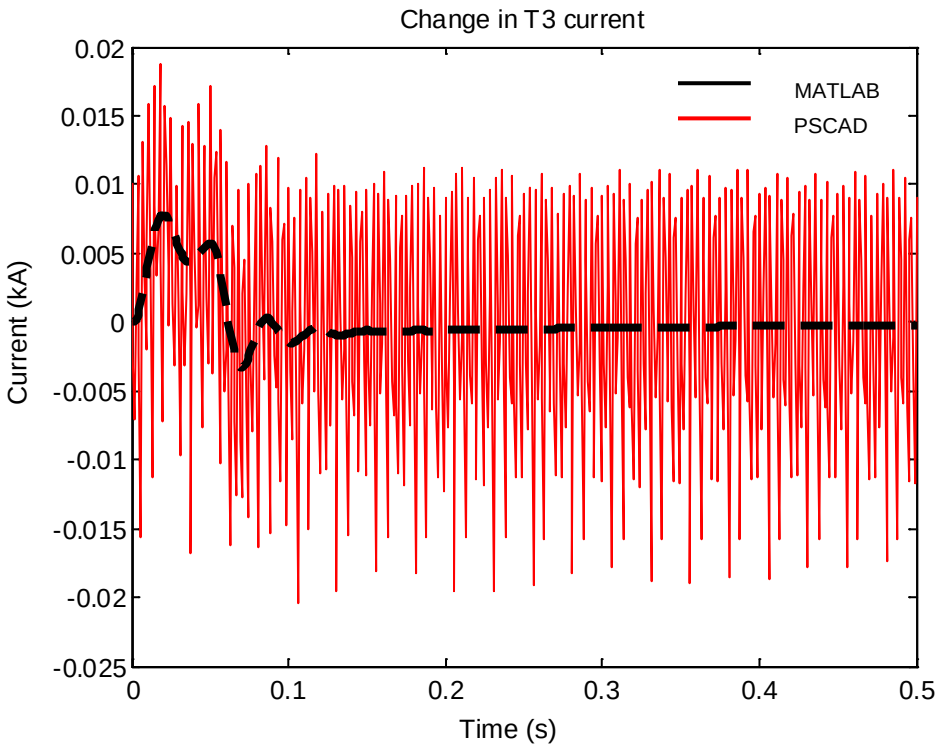

Figure 3.13 MTHVDC T3 current change for a 2%, 0.05s step change on terminal two

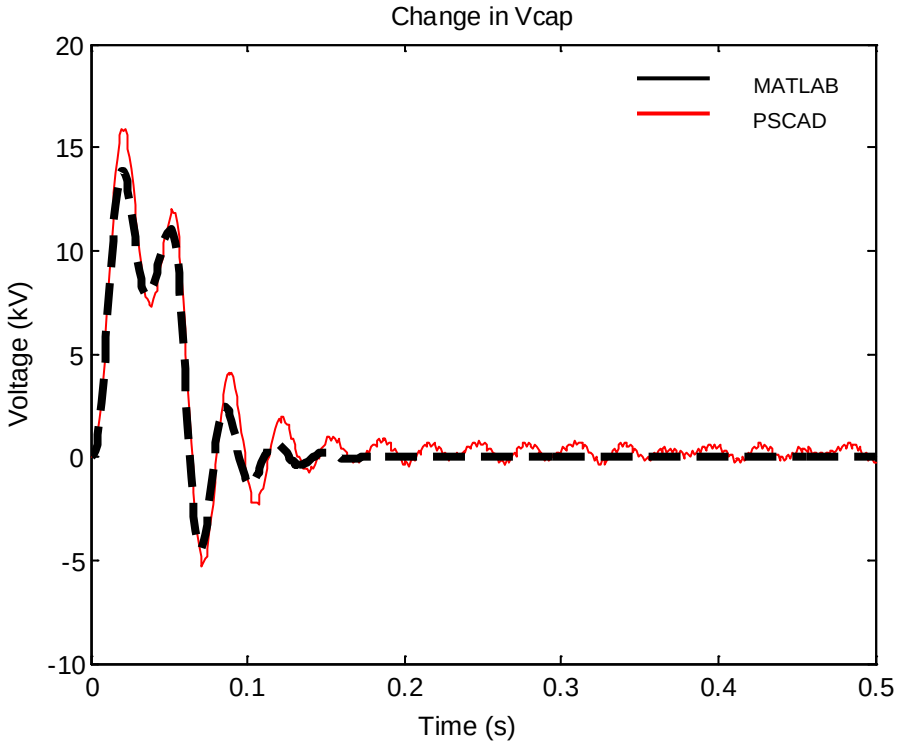

Figure 3.14 Line tap point voltage change for a 2%, 0.05s step change on terminal two

3.3 Chapter Summary

In summary, the time domain simulation provided in this section confirmed that the developed small-signal study package had a good agreement with the PSCAD/EMTDC simulation results. This confirmed that the developed MTHVDC interaction assessment tool was accurate enough to analyze the MTHVDC system interactions.

Chapter 4:Small Signal Stability Assessment of Power Systems

4.1 Introduction

Small signal stability is the ability of power systems to maintain synchronism after small disturbances. To the small-signal stability problem, the power system is first linearized at a particular operating point. The stability around the operating point is analyzed using the eigenvalue analysis of the system matrix of the linearized state-space model. This chapter briefly describes the small-signal stability and eigenvalue (modal) analysis of power systems. More details can be found in [30] (power system aspects) and in [56] (linear control theory).

4.2 Stability of Linearized Systems

The linearized state-space model of a dynamical system is given in Equation (4.1).

$$\Delta \dot{X} = A\Delta X + B\Delta U \tag{4.1}$$

Where ΔX is the vector of state variables and ΔU is the vector of system inputs. By solving Equation (4.2), we can get the eigenvalues of the system matrix (A).

$$\Delta(A - \lambda I) = 0 \tag{4.2}$$

If the system has 'n' state variables, Equation 4.2 has 'n' independent solutions $(\lambda_1, \lambda_2, ..., \lambda_n)$, which are the eigenvalues of the system.

The local stability (stability in the small) of the system at the operating point is determined using Lyapunov's first theorem [34].

The criterion is summarized in [30] as follows.

• “When the eigenvalues have negative real parts, the original system is asymptotically stable.”

• “When at least one of the eigenvalues has a positive real part, the original system is unstable.”

• “When the eigenvalues have real parts equal to zero, it is not possible on the basis of the first approximation to say anything in general.”

4.3 Modes and Modal Characteristics

The modes of the system are identified using eigenvalues, while the modal characteristics are analyzed using eigenvectors. Some important concepts are summarized in the following sections.

4.3.1 Modes

If there are no changes in the system inputs, the state-space model of the system can be written as Equation (4.3).

$$\Delta \dot{X} = A\Delta X \tag{4.3}$$

The rate of change of each state variable is a linear combination of all the state variables of the system. These cross-couplings of the state variables can be eliminated by using Equation 4.4,

$$\Delta \dot{X} = \Phi Z \tag{4.4}$$

Where, Φ is the right eigenvector matrix of the system matrix (A). After the transformation, the state-space model becomes

$$\dot{Z} = \Lambda Z \tag{4.5}$$

Where Λ is a diagonal matrix with the eigenvalues as the diagonal elements.

The rate of change of i^{th} variable is given by Equation 4.6.

$$\dot{z}_i = \lambda_i z_i \tag{4.6}$$

The transformation produces 'n' independent variables, which are called the modes of the dynamical system. The modes describe the dynamic behavior of the system. The time response of the i^{th} mode is given by Equation (4.7).

$$z_i(t) = z_i(0)e^{\lambda_i t} \tag{4.7}$$

The time-dependent characteristic of the i^{th} mode is given by $e^{\lambda_i t}$. Therefore, the modes and their stability are described by the eigenvalues as follows.

• A real eigenvalue corresponds to an aperiodic (non-oscillatory) mode. If the eigenvalue is negative, the mode is decaying, and if it is positive, the mode is unstable (aperiodic instability).

• A complex conjugate pair of eigenvalues corresponds to an oscillatory mode. If the eigenvalue pair is, $\lambda = \sigma \pm j\omega$, The frequency of oscillation is given by,

$$f = \frac{\omega}{2\pi} \tag{4.8}$$

The damping ratio is given by,

$$\xi = -\frac{\sigma}{\sqrt{\sigma^2+\omega^2}} \tag{4.9}$$

If the real part of the eigenvalues is negative (i.e. damping ratio is positive), the mode is stable. The damping ratio ζ determines the rate of decay of the amplitude of the oscillation. The time constant of amplitude decay is $1/|\sigma|$. It means that the amplitude decays to 1/e or

37% of the initial amplitude in 1/|σ| seconds. In reality, decay time is also used to define the damping of the oscillation.

4.3.2 Right Eigenvectors(Mode Shapes)

The right eigenvector of a mode gives the mode shape, which shows the relative phasors of the state variables when that mode is excited. The right eigenvector (Φ_i) of the i^{th} mode is given by,

$$A\Phi_i = \lambda_i \Phi_i \tag{4.10}$$

Assume only the i^{th} mode of the system is excited. Then, the state variables are given by,

$$\begin{pmatrix} \Delta X_1 \\ \Delta X_2 \\ \vdots \\ \Delta X_n \end{pmatrix} = \begin{pmatrix} \phi_{i1} \\ \phi_{i2} \\ \vdots \\ \phi_{in} \end{pmatrix} z_i \tag{4.11}$$

$\phi_{i1}, \phi_{i2}, \text{L}\ , \phi_{in}$ are the elements of the i^{th} right eigenvector (Φ_i).

The magnitudes of the elements of (Φ_i) give the relative activities of the state variables in the i^{th} mode and the phase angles give the phase displacement of the state variables with regards to the mode. Since the units and scaling of the state variables are different, the magnitudes of the elements cannot be compared against each other. Therefore, only the phase angles of the mode shapes are considered in this thesis while analyzing HVDC interactions. The length of the line does not represent the magnitude of the mode shape in all mode shape plot. The right eigenvectors in this research are all normalized to have a unit length.

4.3.3 Left Eigenvectors

The left eigenvector (Ψ_i) of the i^{th} mode is given by,

$$\Psi_i A = \lambda_i \Psi_i \tag{4.12}$$

Assume only the i^{th} mode of the system is excited. The mode is given by,

$$z_i = \psi_{i1}\Delta X_1 + \psi_{i2}\Delta X_2 + \text{L} + \psi_{in}\Delta X_n \tag{4.13}$$

$\psi_{i1}, \psi_{i2}, \text{L}, \psi_{in}$ are the elements of the i^{th} right eigenvector (Ψ_i).

The elements of (Ψ_i) are the weights of the state variable to the i^{th} mode.

The left eigenvectors in this research are all normalized to have a unit length.

4.3.4 Participation Factors

The participation factors [61, 62, 63] are nondimensional scalars used to measure the relative participation (magnitude) of the state variables in a mode.

The participation factor (p_{ki}) is given by,

$$p_{ki} = \phi_{ki}\psi_{ik} \tag{4.14}$$

Where ϕ_{ki} is the k^{th} element of the i^{th} right eigenvector (a column vector) and ψ_{ik} is the k^{th} element of the i^{th} left eigenvector (a raw vector).

p_{ki} is the relative participation of the k^{th} state variable in the i^{th} mode. All the participation factors of the i^{th} mode are arranged in a vector to obtain the participation vector as given in Equation (4.15).

$$p_i = \begin{pmatrix} p_{1i} \\ p_{2i} \\ \vdots \\ p_{ni} \end{pmatrix} \tag{4.15}$$

The elements of p_i are dimensionless and the sum of the elements is 1. Therefore, the participation factors (elements) can be used as an index to compare the relative participation of the state variables in that mode. Since the participation factors of an oscillatory mode are complex numbers, the magnitudes of the participation factors are used for the comparisons. In this thesis, the magnitude of the highest participant is considered as 100% and other participants are scaled accordingly.

4.4 Chapter Summary

In the chapter, the techniques needed to perform modal analysis are introduced. They are:

1. The oscillation modes are identified using eigenvalues. The frequency and damping ratio of the oscillatory modes are obtained using Equations (4.8) and (4.9).
2. Participation factors are used to evaluate the relative participation of each state variable in the modes. The interactions of the state variables of different dynamical systems are identified using the participations.
3. The phase angles of the mode shapes are used to identify the relation between the state variables in the oscillation mode.

   If two state variables have the same phase angle (the angle difference between these two state variables is zero or very small) in the mode shapes of the oscillation mode, these two state variables are called “Oscillating together” in this mode. On the other hand, if the angle difference between these two state variables is 180 degrees (or very close to 180 degrees) in the mode shapes of the oscillation mode, these two state variables are called “Oscillating against each other” in this mode.

Chapter 5:HVDC Interactions in MTHVDC Systems

5.1 Introduction

In Manitoba, there are three point-to-point HVDC transmission lines with a total capacity of 5854 MW. They transmit over 70% of the province's total hydroelectric power to the load center in southern Manitoba. The newly completed Bipole III was constructed between the Keewatinohk converter station in northern Manitoba and the Riel converter station on the east side of Winnipeg. It has a 1350km overhead transmission line with a corridor located on the west side of Manitoba. It is terminated at the Riel converter station. The west route of Bipole III offers many opportunities for future DC taps that could meet load growth in western Manitoba and import/export with our west neighboring utilities. This tapping option is valuable since generation development in western Manitoba is limited due to resource constraints. Also, with load growth in western Manitoba, voltage stability becomes a concern. Taps on the existing HVDC line will relieve the southern-western AC system loading and, therefore, may eliminate the voltage stability concerns without adding new voltage support devices. Therefore, tapping on the existing HVDC lines is a practical option.

In this research, the proposed three-terminal HVDC line consists of three sections. Section one is from the rectifier station to the HVDC line tap point with a length of 960 km. Section two has a length of 400km, which starts from the line tap point to the terminal two inverter station. Section three has a length of 100km and it starts from the line tap point to terminal three inverter station. This arrangement, as shown in Figure 5.1, mimics

a potential HVDC line tap on the future Manitoba Hydro HVDC system approximately 400km away from Winnipeg. The rectifier station delivers about 1300MW to the inverters, and the terminal-two inverter receives about 650MW and terminal three receives about 560MW. A smoothing reactor is also required for each HVDC terminal to limit the fault current and smooth the DC current. Therefore, a 500mH smoothing reactor is modeled for each terminal of the three-terminal HVDC systems. Detailed line parameters as well as different operating points are provided in Appendix A.

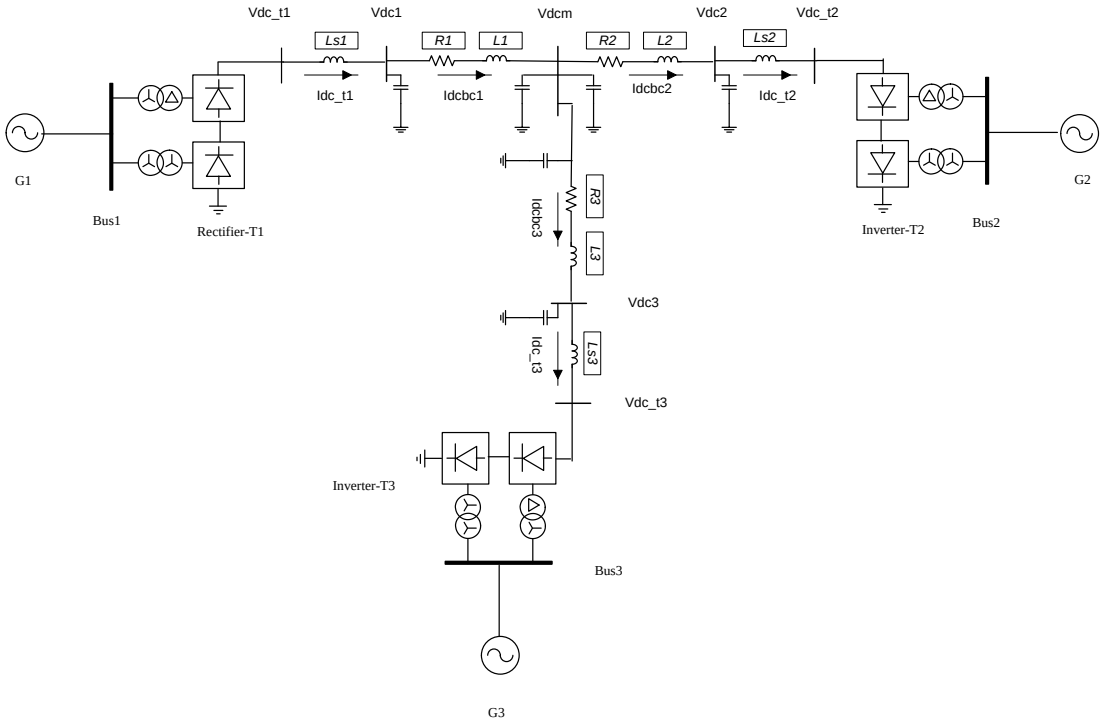

Figure 5.1 MTHVDC test systems

5.2 Multi-terminal HVDC System Configurations

To study the MTHVDC system controller interactions, small-signal stability assessment as described in Chapter 4 is used. The single-line-diagram of the three-terminal HVDC

test system as shown in Figure 5.2 is used. In the test system, three generators are connected to each terminal of the three-terminal HVDC system through their dedicated step-up transformers and transmission lines. Each generator represents the AC system of the converter terminal. Loads at each terminal have been modeled at the high side of the step-up transformers. At each converter bus, a capacitor bank is modeled to represent the AC filters for the converter, which also provides reactive power to the system. Generators are operating at their own scheduled real and reactive power outputs. The HVDC loading is adjusted to respect the transmission line and transformer limits to avoid overloading under steady-state conditions. The parameters of generators, exciters, and governors are given in Appendix A.

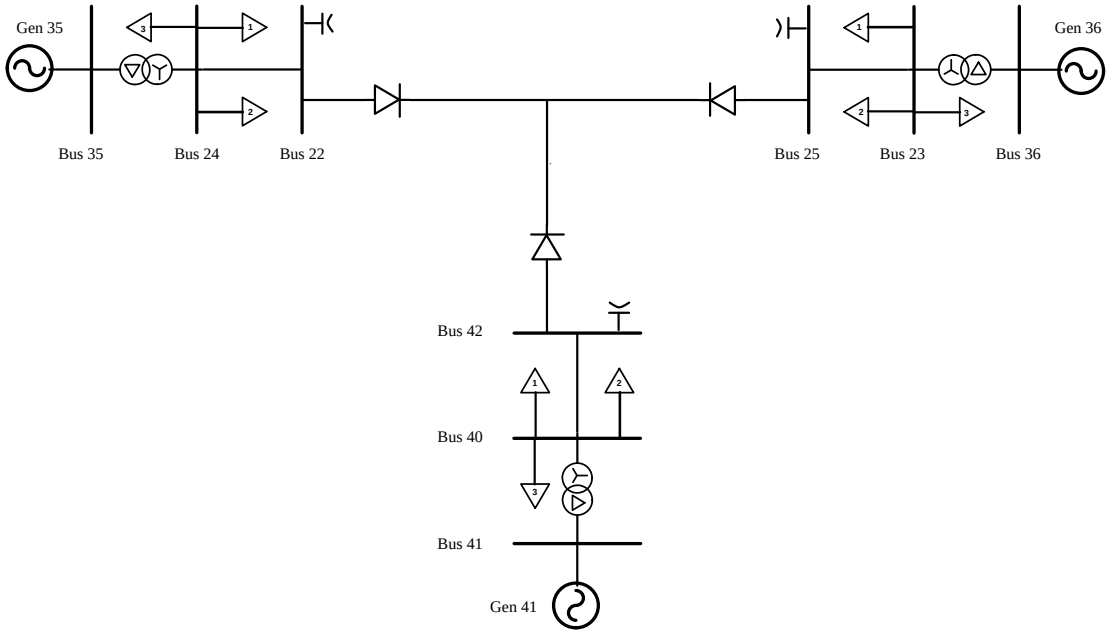

Figure 5.2 Single-line-diagram for the test system

For the controller arrangement, there are only two possible controller schemes for three-terminal HVDC systems. One is the DC voltage control at the inverter terminal, and the other is the DC voltage control at the rectifier terminal. Each scheme has a total of three

installed DC controllers. In control scheme one, a voltage controller is installed at the terminal-three inverter controlling the DC voltage, while the other two terminals are controlled by the DC current controllers, one at the rectifier terminal and the other at the terminal-two inverter as shown in Figure 5.3. Three PLLs, one at each HVDC terminal, are also modeled in the test system.

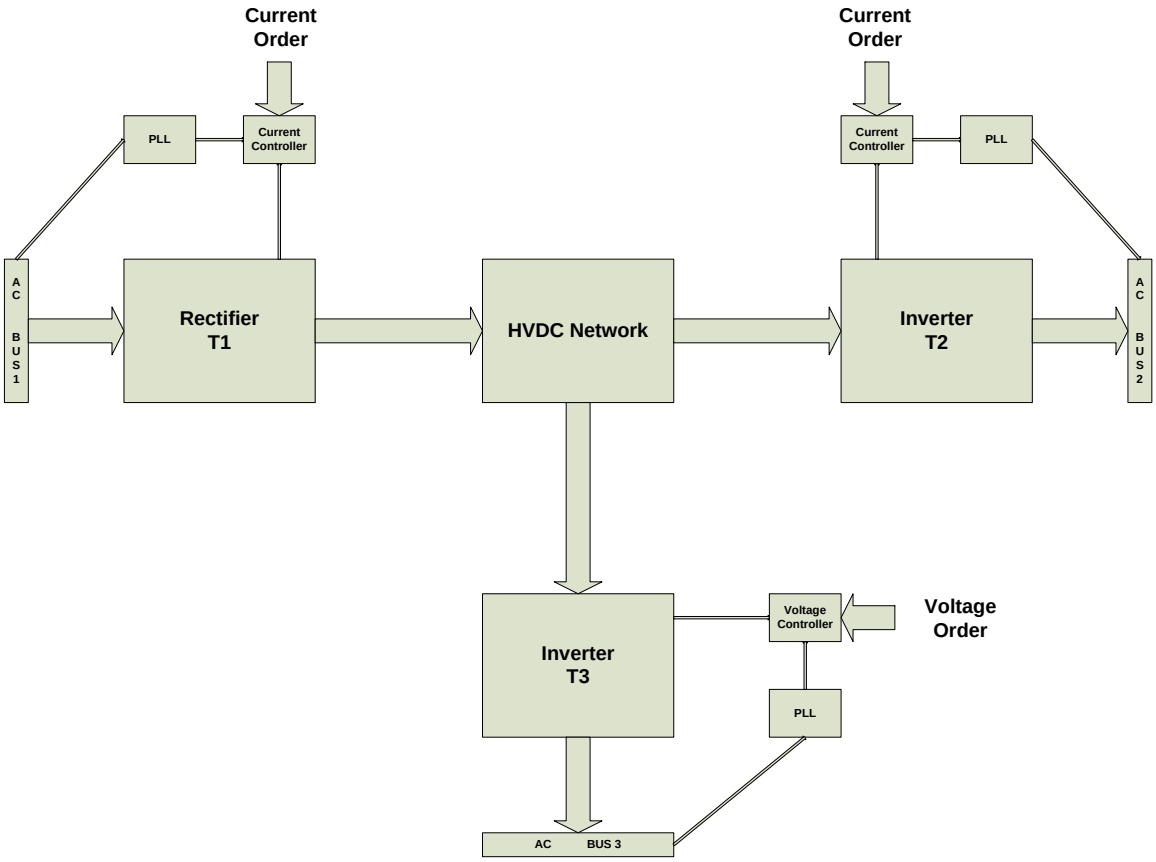

Figure 5.3 Three-terminal HVDC system – scheme one

For control scheme two, the voltage controller is installed at the rectifier side controlling the DC voltage, and another two inverters are both equipped with a current controller as shown in Figure 5.4. Similarly, three PLLs, one at each HVDC terminal, are also being modeled in the test systems. Table 5.1 summarized these two control schemes for the three-terminal HVDC systems.

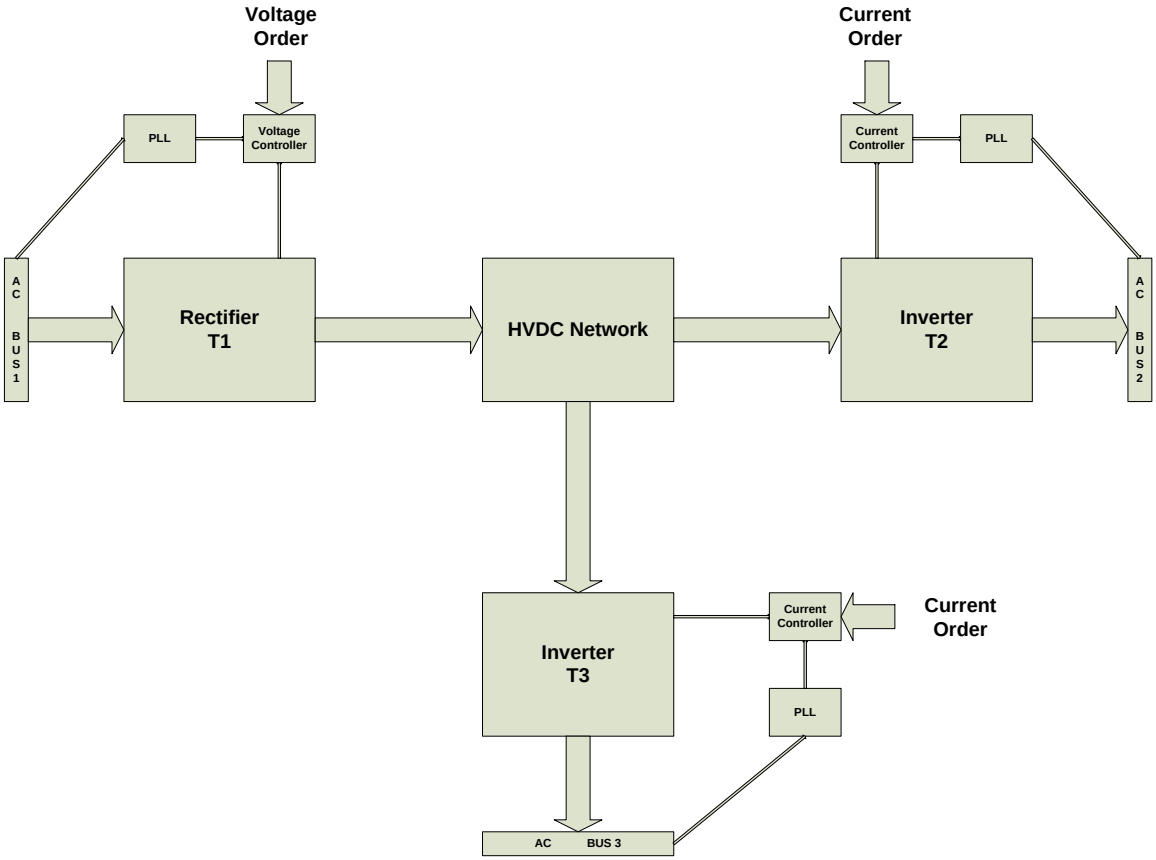

Figure 5.4 Three-terminal HVDC system – scheme two

	Rectifier (Terminal 1)	Inverter (Terminal 2)	Inverter (Terminal 3)
Control Scheme 1	Current	Current	Voltage
Control Scheme 2	Voltage	Current	Current

Table 5.1 Three-terminal HVDC system controller arrangement

For the controller parameter selection, the gain of the controller can be obtained by trial and error. In general, if the proportional gain is increased, the system response will be faster. If the proportional gain is too high, the system may become unstable. On the other hand, increasing the integral gain will eliminate steady-state error faster. However, this will also increase the overshoot. Therefore, the controller gain is optimized so that both

fast control and minimal overshoot can be achieved. In the meantime, the controller parameters are selected to ensure the oscillation modes can be easily identified and any unstable oscillation mode (or positive eigenvalue) should also be avoided. To do so, the proportional gains for all DC controllers are set to small values and the integral gains are set to ensure that the oscillation mode has a good damping ratio. The detailed control parameters are provided in Appendix A

In MTHVDC systems, several possible oscillation modes exist. According to the mode shapes and participation factors, the oscillation modes are categorized into a) DC network resonance, b) AC-DC network interactions, c) HVDC controller interactions, and d) electromechanical oscillations. Followings are some of the main characteristics of these oscillation modes.

For the DC network resonance mode, it has the highest oscillation frequency. The DC voltage, DC current and smoothing reactor state variables are the major participants of this mode. For the AC-DC oscillation mode, both DC quantities (such as DC voltage, DC current) and AC quantiles (such as AC voltage, equivalent machine state variable) participate in this mode. This oscillation mode has a relatively high oscillation frequency. For the MTHVDC controller mode, it has an oscillation frequency in the sub-synchronous range. In the MTHVDC systems, several controllers control either DC voltage or DC current. These controller state variables interacted with each other create the controller interaction mode. The controller mode is usually dominated by either one or several controller state variables. For the electromechanical oscillation mode, it has the lowest oscillation frequency. In the test system, there are three equivalent machines, one at each HVDC terminal. These machines may interact with each other and create the

electromechanical oscillation mode. Improper system configuration and control parameter selection may raise small-signal system concerns for the MTHVDC. The main focus of this chapter is categorizing each oscillation mode, identifying the problemistic oscillation mode and eliminate the potential controller interaction which may raise small-signal stability concerns in the three-terminal HVDC system.

5.2 Study Procedure for Controller Interaction Analysis

To analyze MTHVDC system controller interactions, a certain procedure must be followed to evaluate the performance of MTHVDC systems. In the following section, a general study procedure involving data preparation, case studies, criteria set up, and result analysis is proposed and will be explained in detail. It includes 1) Power system load flow data preparation, 2) Power system dynamic data preparation. 3) Eigenvalue analysis. 4) Evaluation criteria and 5) Oscillation analysis and mode identification.

Step 1—Power System Load Flow Data Preparation

The three-terminal HVDC system consists of three LCC type converters (one for rectifier operation and two for inverter operations) and three sections of HVDC transmission lines. In the PSS/E load flow data format, four converter buses are required to represent the three-terminal HVDC system: one for each of the three converter terminals and one for the HVDC line tap point. The HVDC line resistance and inductance for each section need to be specified. In terms of the converter setting, the set value is the converter nominal operating voltage [65] for the voltage-controlled converter. For current-controlled converters, a positive set value or negative set value is used to distinguish whether the converter is in rectifier operation or inverter operation. A positive DC current set value represents rectifier operation, and a negative DC current set value represents inverter

operation. The converter bus AC voltage, number of valve groups per converter, converter transformer leakage reactance, as well as transformer tap range and tap ratio are also modeled in the converter model. The nominal firing angle ranges for all converters are specified to ensure proper HVDC operation and reactive power consumption. During the solution process, if the firing angle is outside the operating range, the converter transformer tap will be adjusted accordingly and bring the firing angle into the specified operating range.

For AC systems, generator real and reactive power limiter, generator step-up transformer impedance, transmission line impedance, switching capacitor steps and size, shunt reactors size, as well as load information are required. The load flow case should be solved, and tolerance should be respected. The voltage at each bus should be maintained in the nominal operating range of 0.95p.u. to 1.05p.u. All generator dispatch and transmission line loading should be in their operating range. No equipment in the study case should exceed its specified limit.

Since the load flow case was solved, both the equipment information (line impedance, transformer impedance, and generator sub- transient impedance, etc.) and the solved load flow information (bus voltage, bus angle, generator dispatch, and firing angle, etc.) can be directly used. The developed small-signal study package directly read the PSS/E raw file information and linearized the system at the operating point (PSS/E solution point).

Step 2—Power System Dynamic Data Preparation

To perform the frequency domain eigenvalue analysis, dynamic data for the test system is also required for both the AC system dynamic device and the three-terminal HVDC

system. In this research, the IEEE standard GENROU model, EXAC4 model, and HYGOV models are used for the generator, exciter, and governor models.

For the developed MTHVDC system, the converter transformer size, the DC line charging capacitance, and the HVDC line tap point voltage are required and are summarized in Appendix A. In the test systems, six PI controllers have been modeled for HVDC control purposes, three for the Phase-Lock-Loop (PLL) control circuits and three for converter control (one for voltage controller and two for current controllers) circuits. For the PLL controller, set values of 10 and 50 were used for K_p and K_i respectively. For the converter voltage controller and current controllers, the proportional gains are set to a very small value so that the oscillation mode can be easily identified. To mimic the DC quantity measurement delay, a low pass filter with a 1ms time delay is used for the current measurement circuit and a 5ms time delay for the voltage measurement circuit. The detailed control parameter settings for the test system are attached in Appendix A.

Similar to the load flow data, both machine and its control system parameters, MTHVDC system parameters are provided in the PSS/E raw data file. The developed small-signal study package directly read the PSS/E dynamic file and linearized the system at the operating point (PSS/E load flow solution point).

Step 3—Eigenvalue Analysis

It is proposed in this thesis that a detailed eigenvalue analysis can be performed to obtain information about the oscillatory modes, such as frequency, damping ratio, and participation factors. The power flow and dynamic data of the test system obtained in previous steps are input to the developed small-signal stability assessment tool. The program creates the linearized models of all the dynamic devices around the steady-state

operating point (given by the power flow result). As illustrated in chapter 2.4, the program reads in both the AC system and MTHVDC system load flow data and dynamic data prepared in the previous steps and generates the overall state space small signal stability model for the entire power systems. The state-space model is then analyzed using eigenvalue analysis to determine the oscillatory modes and the damping ratio for each mode.

Step 4—Evaluation Criteria

To evaluate the performance of each oscillation mode, certain criteria are required. In this research, both the damping ratio and the decay time are used to evaluate the performance of each oscillation mode.

In general, the damping ratio of 5% is sufficient for the electromechanical oscillation modes (<3Hz). However, for higher frequency modes, a lower damping ratio would be sufficient based on the decay time. Table 5.2 and Table 5.3 show the relationship between the oscillation damping ratio and the decay time. For example, the amplitude of a 2Hz oscillation with a 5% damping ratio takes about 1.59s to drop below 36.7% (1/e) of its initial value. The amplitude of a 60Hz oscillation mode with a 5% damping ratio drops below 36.7% of its initial value within only 0.05s. Table 5.2 clearly shows that the same damping ratio for different oscillation frequency has different decay times.

On the other hand, a 7.6% damping ratio is required for the amplitude of a 1Hz oscillation drops to 37% of its initial value with 2s decay time. However, a 23.9% damping ratio is required for the 0.1Hz oscillation to have the same amount of decay time. Table 5.3 clearly shows that the same decay time for different oscillation frequency has different damping ratios.

Frequency	Damping Ratio	Time required for magnitude decay to its 1/e
Hz	%	(s)
0.1	5.0%	31.79
0.5	5.0%	6.36
1	5.0%	3.18
2	5.0%	1.59
3	5.0%	1.06
5	5.0%	0.64
10	5.0%	0.32
20	5.0%	0.16
30	5.0%	0.11
40	5.0%	0.08
50	5.0%	0.06
60	5.0%	0.05
120	5.0%	0.03

Table 5.2 Relation between damping ratio and decay time (constant damping)

Frequency	Damping Ratio	Time required for magnitude decay to its 1/e
Hz	%	(s)
0.1	23.9%	2.00
0.5	13.4%	2.00
1	7.6%	2.00
2	3.9%	2.00
3	2.6%	2.00
5	1.6%	2.00
10	0.8%	2.00
20	0.4%	2.00
30	0.3%	2.00
40	0.2%	2.00
50	0.2%	2.00
60	0.1%	2.00
120	0.1%	2.00

Table 5.3 Relation between damping ratio and decay time (constant decay time)

In general, the higher the oscillation frequency is, the lower the damping ratio required to meet the damping requirement based on the decay time. One advantage of using the

time constant of amplitude decay is that it can be measured directly from time-domain simulation results for transient stability analysis. For a specific oscillation frequency, the damping ratio can be easily quantified in terms of the decay time.

Step 5—Oscillation Analysis and Mode Identification

The characteristics of the modes are analyzed using the properties of the eigenvectors. The right eigenvector of a particular mode gives the mode shape, which shows the relative phasors of the state variables when that mode is excited. Since the units and scaling of the state variables are different, the magnitudes of the elements cannot be compared against each other. Therefore, only the phase angles of the mode shapes are used to determine the relative phases of the state variables in a particular mode. For example, the angles of mode shapes can be used to determine whether two state variables oscillate together or against each other in an oscillatory mode. For the same oscillation mode, the oscillation frequency and damping ratio vary depending on the system condition. However, the mode shape for the key participants remains the same for the same oscillation mode and is the key indicator to identify the oscillation mode.

The participation factors are obtained by multiplying the relevant elements of the right eigenvector and the left eigenvector [equation 4.14]. The elements of a participation factor vector are dimensionless, and the sum of all elements is equal to 1. Therefore, the participation factor (elements) can be used as an index to compare the relative participation of the state variables in a mode. Since the participation factor of an oscillatory mode is a complex number, the magnitude of the participation factor is used for the comparisons. Based on the above analysis, it is recommended to analyze power system oscillation and identify mode in the following steps.

1. *Examine the oscillation frequency and damping ratio*

   For any oscillation mode, the oscillation frequency and damping ratio are the main concerns. In general, the higher the oscillation frequency, the smaller the wave-length and the shorter the distance the oscillation propagates. Hence fewer dynamic devices are involved. As indicated in Table 5.2 and Table 5.3, the time required for the oscillation amplitude reduces to 37% of its original value is different for different oscillation frequencies with the same damping ratio. Therefore, the damping ratio requirements for different oscillation frequencies are different to meet the performance requirement. In general, the higher the oscillation frequency, the lower the required damping ratio to meet the performance requirement. In this thesis, the decay time of 1Hz oscillation with a 5% damping ratio is used as a reference (the oscillation magnitude reduces to 37% of its original value in 3.18s). The result is compared with the reference decay time to evaluate the oscillation performance.

2. *Participation Analysis*

   As defined in 4.3.4, the participation factor is used as an index to compare the relative participation of the state variables in the oscillation mode. Depending on the value of the participant factor, major participants can be identified which dominates the oscillation mode and have the greatest contribution to the oscillation. The participation factor provides detailed inside information regarding the oscillation. The oscillation frequency, damping ratio, and the relative participation factors of the state variables can be changed by adjusting the relative control parameters. In order to gain a better understanding of each oscillation mode and

identify undamped oscillation modes, the related control parameters can be changed, and the results analyzed. Thus, proper control parameters can be selected to ensure all oscillation modes are stable and the system has no small signal stability concern.

3. *Mode shape Analysis*

   As defined in 4.3.2, the mode shape shows the relative phasor angle of the state variables in the oscillation mode. It is clearly shown in Figure 5.6 that the angle between the terminal two DC voltage and the HVDC line tap point DC voltage is about 180 degrees apart. Therefore, these two state variables oscillate against each other. Similarly, Figure 5.8 shows that terminal one DC voltage oscillates against terminal two, terminal three, and HVDC line tap point DC voltages in Mode-2. Figure 5.8 also shows that all three-terminal HVDC currents oscillate together. The mode shape helps us understand the relationship between each state variable in the oscillation mode and helps to select the proper controller to improve the damping ratio for the undamped oscillation. In general, more attention should be paid to the state variables oscillates against each other since they are the root cause of the oscillation mode.

4. *Additional Considerations*

   As shown in Table 5.5, the DC network resonance modes have the oscillation frequencies of 224.0 Hz and 118.0Hz. If the interconnected AC system has the harmonic resonance at or close to these DC network resonance frequencies, it will interact with the DC network resonance, creating problems for the overall power

system. Under this situation, detailed studies need to be performed to investigate the problem and eliminate the issue.

The above proposed general study procedure can be used to analyze any power system oscillation. In flowing sections, MTHVDC system interactions will be assessed using the above-proposed study procedure.

5.3 MTHVDC Systems Interaction Analysis – Control Scheme One

In scheme one, terminal three inverter controls the DC voltage and the other two terminals are controlled by the DC current controllers. The overall state-space model of the three-terminal HVDC test system consists of 89 state variables, including 24 for generators, 9 for exciters, 6 for governors, 22 for MTHVDC systems, and 28 for AC networks (including transformers, transmission lines, loads and capacitors). The state variables index for the three-terminal HVDC systems is also provided in Table 5.4. In this table, X_{idc_t1}, X_{idc_t2}, X_{vdc_t3} are the state variables of terminal one DC current controller, terminal two DC current controller and terminal three DC voltage controller.

MTHVDC system state variable index									
1	I_{dc_t1}	2	I_{dc_t2}	3	I_{dc_t3}	4	V_{dc_t1}	5	V_{dc_t2}
6	V_{dc_t3}	7	V_{dc_t4}	8	I_{dcl_t14}	9	I_{dcl_t24}	10	I_{dcl_t34}
11	PLL_{1_t1}	12	PLL_{2_t1}	13	PLL_{1_t2}	14	PLL_{2_t2}	15	PLL_{1_t3}
16	PLL_{2_t3}	17	I_{dcm_t1}	18	X_{idc_t1}	19	I_{dcm_t2}	20	X_{idc_t2}
21	V_{dcm_t3}	22	X_{vdc_t3}						

Table 5.4 MTHVDC system state variable index-scheme one

Table 5.5 tabulated the major oscillatory modes of the test system. The participations are based on the magnitudes of the participation factors. The phase displacements of the state

variables in a particular mode are given by phase angles of the relevant mode shapes. All these oscillation modes will be discussed in detail in the following sections.

Mode	Frequency	Damping Ratio	Major Participants	Mode Description
	(Hz)	(%)		
1	224.00	3.31%	Vdc_t2 (100%),Idcl_t2(77%), Idc_t2(39%),Vdc_t4(13.9%)	DC Network Resonance
2	118.00	5.34%	Vdc_t1(100%), Idcl_t1(63.6%), Idc_t1(35.3%), Idc_t4(21.9%)	DC Network Resonance
3	76.59	19.63%	Vdc_t4(100%), G41_Fsq(68.8%), Idc_t1(55.2%), Vl_bus42(47%), Idc_t3(37.1%),VR_bus42(33.9%)	AC-DC Network Interaction
4	13.00	33.94%	Xidc_t1(100%), Idcl_t1(49.8%), PLLx1_t3(40.6%), Idc_t1(30.3%)	DC controller interaction
5	10.33	33.80%	PLLx1_t3(100%), Xvdc_t3(44.8%), Idc_t2(36.9%), Xidc_t1(35.4%)	DC controller interaction
6	3.59	40.97%	Xvdc_t3(100%),Xidc_t2(65.7%), PLLx1_t2(50.8%),Xidc_t1(19.7%	DC controller interaction
7	1.29	2.70%	G36_wr(100%), G36_Ang(96.5%), G35_wr(25.0%), G35_Ang(24.4%), Xvdc_t3(12.4%),Xidc_t2(5.5%)	Electrical-Mechnical Oscillation
8	1.26	24.13%	G35_wr(100%), G35_Ang(94.9%), Xidc_t2(51.6%), G36_wr(16.7%), G36_Ang(15.6%), Xvdc_t3(6.2%)	Electrical-Mechnical Oscillation
9	0.16	29.80%	G41_wr(100%), G41_Ang(95.0%), Xidc_t1(53.6%), Xvdc_t3(1.0%)	Electrical-Mechnical Oscillation

Table 5.5 Major participation of selected modes in scheme one test system

5.3.1 DC Network Resonance Modes

Mode-1 and Mode-2 in Table 5.5 are the DC network resonance modes. HVDC quantities mainly participate in these two modes. Mode-1 has an oscillation frequency of 224.0Hz and a damping ratio of 3.31%. The participation factors for all 89 state variables in Mode-1 are provided in Figure 5.5. Terminal two DC voltage, V_{dc_t2} (100%), terminal two smoothing reactor, I_{dcl_t2}, (77%), terminal two DC current, I_{dc_t2} (39%), and the

HVDC line tap point DC voltage, V_{dc_t4} (13.9%), participate in this mode. As shown in Figure 5.6, the angle between the terminal two DC voltage, V_{dc_t2}, and HVDC line tap point DC voltage, V_{dc_t4}, is almost 180 degrees. Therefore, the terminal two DC voltage in this mode oscillates against the HVDC line tap point DC voltage. Similarly, the angle difference between the terminal two DC current, I_{dc_t2}, and terminal three DC current, I_{dc_t3}, is about 180 degrees. Thus, terminal two DC current I_{dc_t2} in this mode oscillates against terminal three DC current I_{dc_t3} .

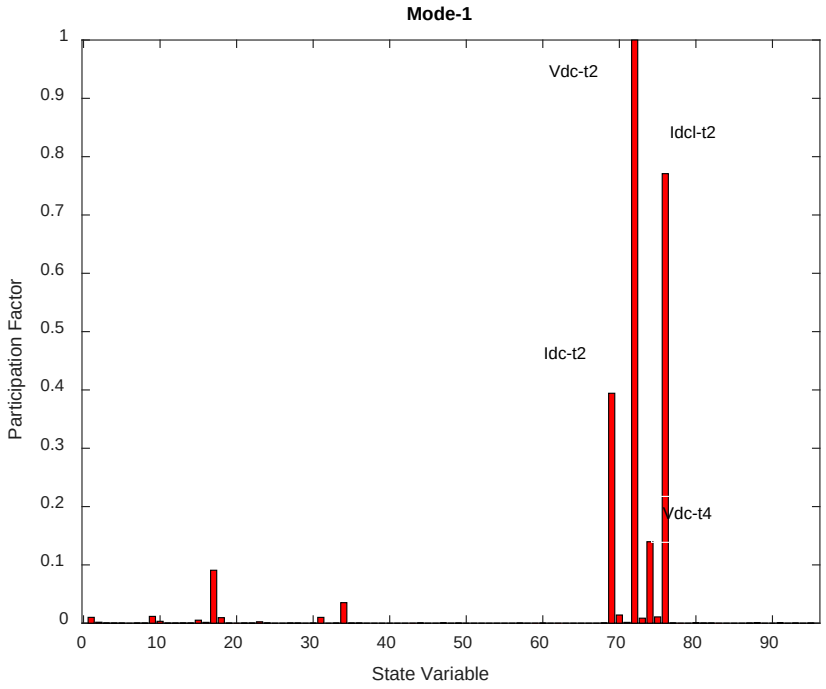

Figure 5.5 Participation of state variables in Mode-1

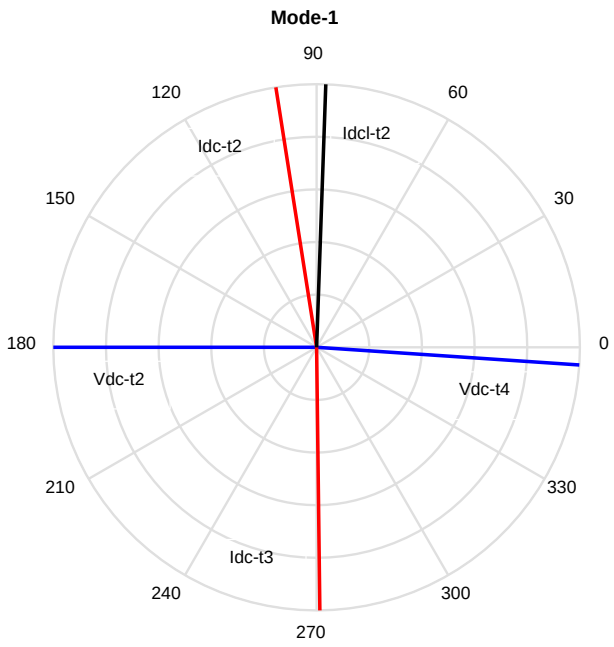

Figure 5.6 Mode shape of the major participant for Mode-1

(Note: The length of the line if Figure 5.6 does not represent the magnitude of the mode shape in all mode shape plot.)

Similar to oscillation Mode-1, Mode-2 has an oscillation frequency of 118.0Hz with a damping ratio of 5.34%. As indicated in Figure 5.7, the MTHVDC system terminal one DC voltage, V_{dc_t1} (100%), terminal one smoothing reactor, I_{dcl_t1} (63.6%), terminal one DC current, I_{dc_t1} (35.3%), and the HVDC line tap point DC voltage, V_{dc_t4} (21.9%), participate in this mode. The mode shape in Figure 5.8 clearly shows that terminal one DC voltage V_{dc_t1}, is 180 degrees apart from terminal two DC voltage V_{dc_t2}, terminal three DC voltage V_{dc_t3}, and HVDC line tap point DC voltage V_{dc_t4}. Therefore, we say that in this mode terminal one DC voltage oscillates against terminal two, terminal three, and HVDC line tap point DC voltages. The angle difference between DC currents I_{dc_t1}, I_{dc_t2}

and I_{dc_t3}, is very small. For this reason, we say that in this mode all three-terminal DC currents, I_{dc_t1}, I_{dc_t2} and I_{dc_t3} oscillate together.

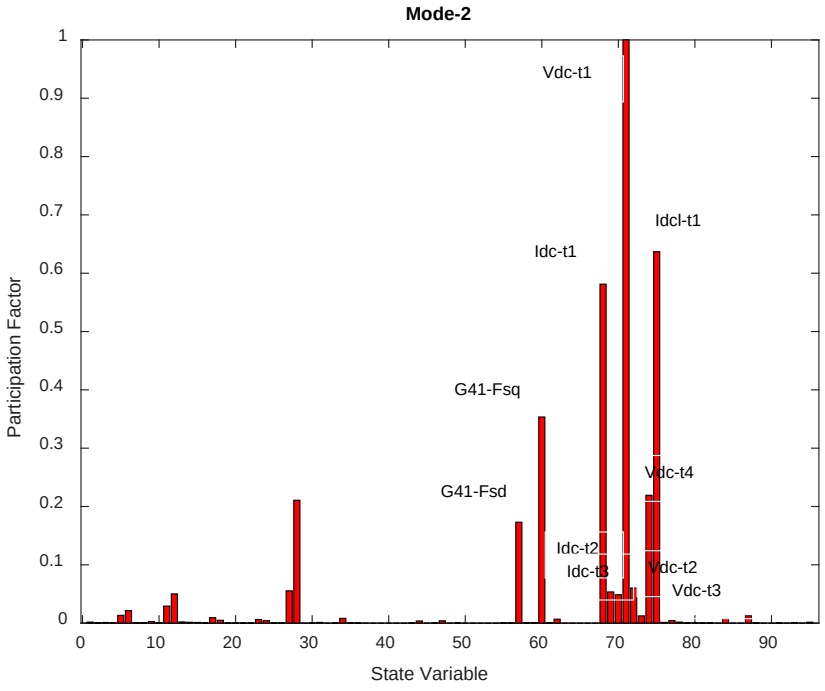

Figure 5.7 Participation of state variables in Mode-2

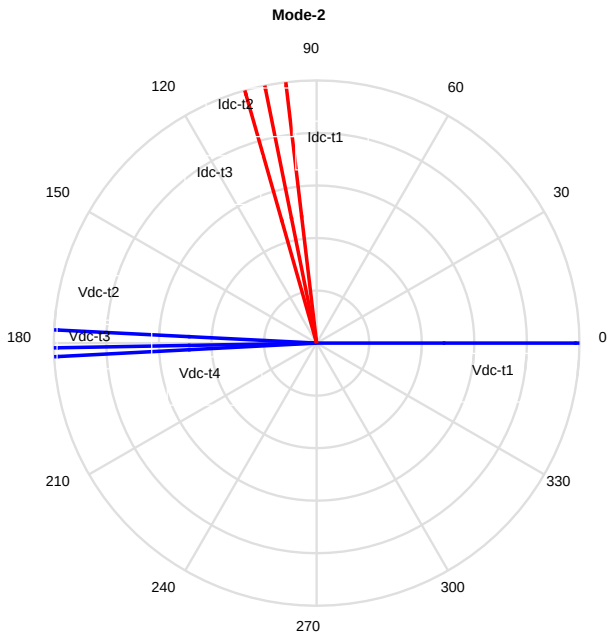

Figure 5.8 Mode shape of the major participant for Mode-2

The above analysis shows that the DC network resonance modes in the proposed three-terminal HVDC systems have higher oscillation frequencies. These two DC network resonance oscillation modes damped out quickly and the damping ratio is enough to meet the performance requirement [see Table 5.2 and 5.3]. These two oscillation modes are dominated by the DC quantities, such as the DC terminal voltages, DC currents, and DC smoothing reactors. As a result, any change of the DC terminal voltage, DC current, and DC smoothing reactor will impact the oscillation frequency and damping ratio. In particular, the size of the smoothing reactor impacts the oscillation frequency and damping ratio for these two modes significantly. Sensitivity study results in Table 5.6 show that the larger the smoothing reactor, the lower the oscillation frequency and the damping ratio.

In addition, the AC system state variables (equivalent machine state variable) also participate these two oscillation models (<1% for Mode-1 and around 10% for Mode-2).

Therefore, any change of the AC system strength will also impact the oscillation frequencies and damping ratios of these two modes even though the AC system state variables have very small participation.

Table 5.6 Impact of the smoothing reactor on Mode-1 and Mode-2

Smoothing Reactor (H)	Mode	Frequency (Hz)	Damping Ratio (%)	Mode	Frequency (Hz)	Damping Ratio (%)
1	1	206.77	1.54	2	104.35	3.23
0.75	1	212.79	2.13	2	109.69	4.01
0.5	1	224.00	3.30	2	118.05	5.34
0.25	1	251.77	5.63	2	130.89	8.25
0.125	1	286.24	7.13	2	137.72	10.71

Since the DC network resonance oscillation modes have higher oscillation frequency, they may interact with the AC system harmonics. If this occurs, a detailed study is required to investigate the interaction and mitigate the problem. Based on the above analysis, we can conclude that both DC network oscillation modes are dominated by the DC quantities. They have a sufficient damping ratio and do not have small signal stability concerns in the proposed control scheme.

5.3.2 AC-DC Interaction Modes

As shown in Table 5.5, both the HVDC quantities and AC system components participate in Mode-3 and have relatively high participation factors. Therefore, this mode is classified as the AC-DC network interaction mode. It is the only AC-DC related mode in this configuration with an oscillation frequency of 76.59Hz and a damping ratio of 19.63%. By examining the participation factor of each state variable, it is found that HVDC line tap point DC voltage V_{dc_t4} (100%) dominates this mode. Additionally, generator stator flux components Gen41-Fsq (68.8%), terminal one DC current I_{dc_t1} (55.2%),

terminal three DC current I_{dc_t3} (37.1%) and terminal one rectifier side AC system bus voltage VI_{bus42} (47%) and VR_{bus42} (33.9%) also contribute to this mode. In addition, terminal one current controller X_{idc_t1} (7.2%) and terminal three voltage controller X_{vdc_t3}(5.3%) also participate in this mode. Figure 5.9 shows the participation of all state variables in Mode-3. Figure 5.10 clearly shows that terminal one DC voltage V_{dc_t1}, terminal two DC voltage V_{dc_t2}, terminal three DC voltage V_{dc_t3}, and HVDC line tap point DC voltage V_{dc_t4}, oscillate together. It also shows that terminal one DC current I_{dc_t1} oscillates against terminal two DC current I_{dc_t2} and terminal three DC current I_{dc_t3}.

In summary, the DC voltage, generator state variables, AC system voltage, and HVDC controller state variables all participate in this mode and have relatively high participation factors. Mode -3 has a relatively high oscillation frequency and damping ratio. It does not have a small signal stability concern.

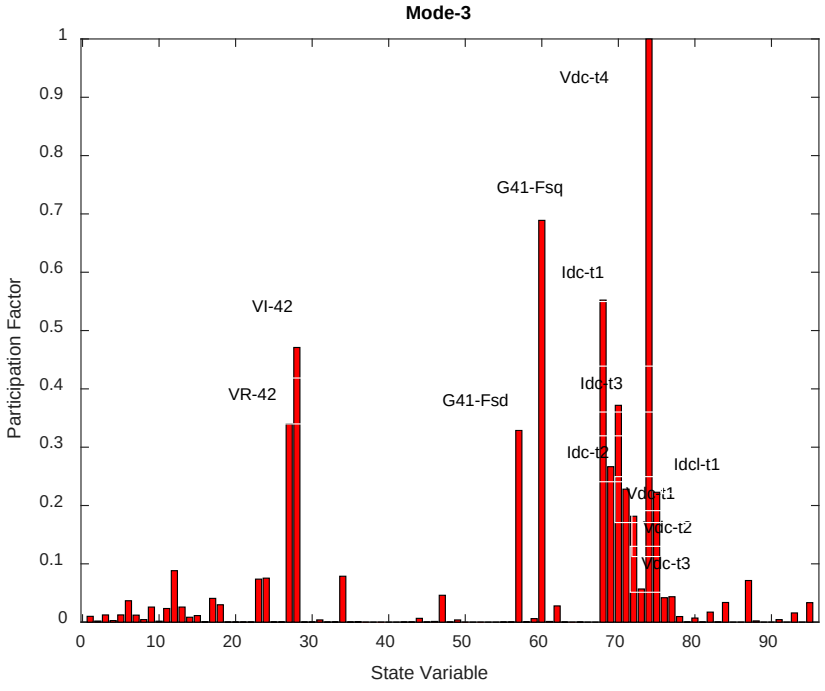

Figure 5.9 Participation of state variables in Mode-3

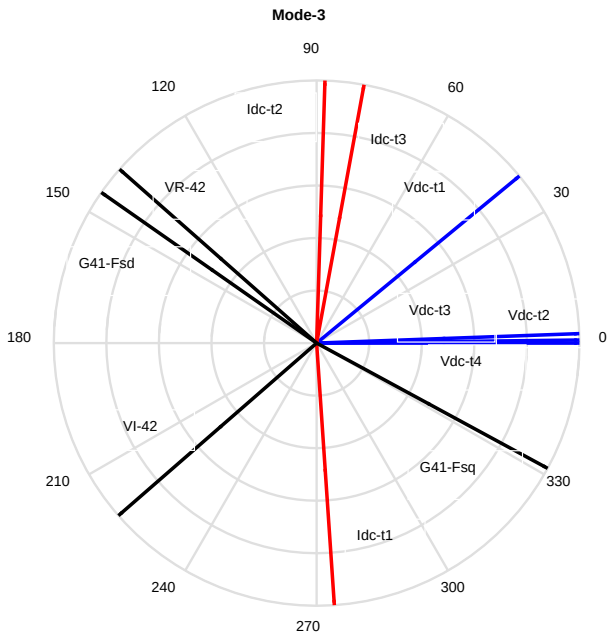

Figure 5.10 Mode shape of the major participant for Mode-3

5.3.3 HVDC Controller Interaction Modes

The HVDC controller state variables X_{idc_t1}, X_{idc_t2} and X_{vdc_t3} participate in and dominate the oscillation modes Mode-4, Mode-5, and Mode-6 in Table 5.5. As a result, these modes are classified as controller interaction modes.

Mode-4:

Mode-4 has an oscillation frequency of 13.0Hz with a damping ratio of 33.94%. Figure 5.11 shows the participation factors of each state variable for this mode. Terminal one DC current controller state variable X_{idc_t1} (100%), terminal one DC current I_{dc_t1}(30.3%), terminal one HVDC line smoothing reactor I_{dcl_t1} (49.8%), and terminal three PLL $PLL1_{t3}$ (40.67%) participate in this mode. In addition, both terminal three DC voltage controller state variable X_{vdc_t3} (10.6%) and terminal two DC current controller state

variable X_{idc_t2} (1.7%) also participate in this mode. In Figure 5.12, terminal one DC current controller state variable X_{idc_t1} and terminal two DC current controller variable X_{idc_t2} oscillate against terminal three DC voltage controller state variable X_{vdc_t3} . It also shows that all three terminal DC currents I_{dc_t1}, I_{dc_t2} and I_{dc_t3} oscillate together. The results clearly show that all three controller state variables participate in this mode and interact with each other.

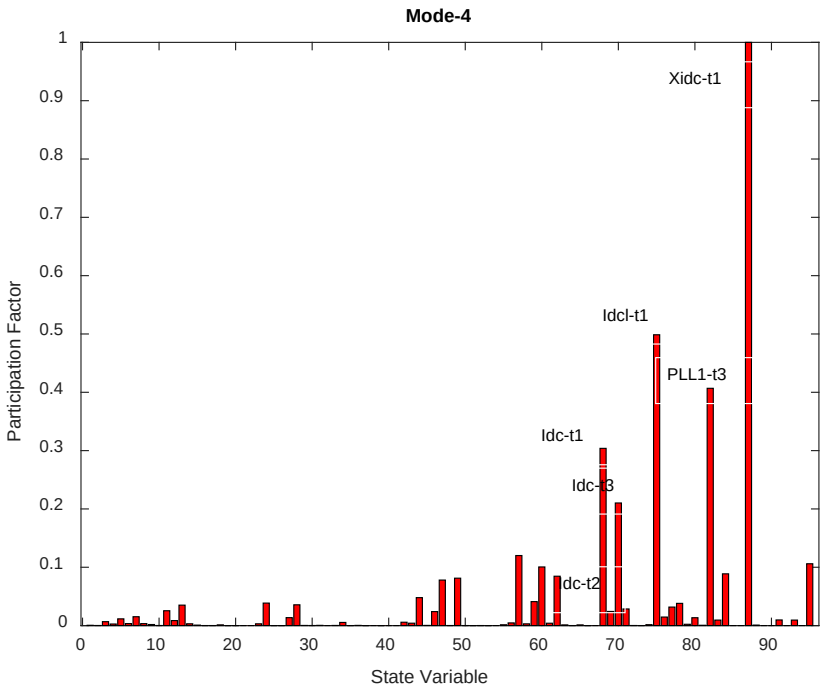

Figure 5.11 Participation of state variables in Mode-4

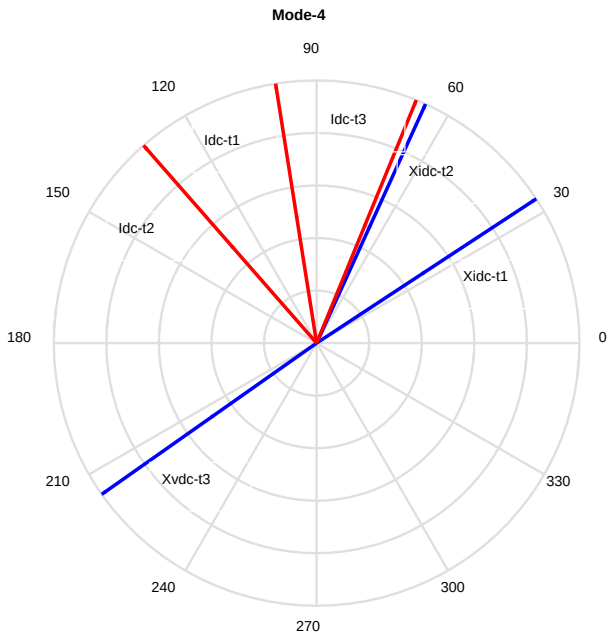

Figure 5.12 Mode shape of the major participant for Mode-4

Mode-5:

Mode-5 has an oscillation frequency of 10.33Hz with a damping ratio of 33.80%. As shown in Figure 5.13, the PLL for terminal three DC voltage controller $PLL1_{t3}$ (100%) dominates this mode. Terminal three DC voltage controller state variable X_{vdc_t3}(44.8%), terminal one DC current controller state variable X_{idc_t1}(35.4%), and terminal two DC current controller state variable X_{idc_t2} (23.5%) also participate in this mode. Mode shapes in Figure 5.14 indicate that terminal two DC current I_{dc_t2} oscillates against terminal one DC current I_{dc_t1} and terminal three DC current I_{dc_t3}. Terminal one DC current controller state variable X_{idc_t1} oscillates against terminal two DC current controller state variable X_{idc_t2} and terminal three DC voltage controller state variable X_{vdc_t3}.

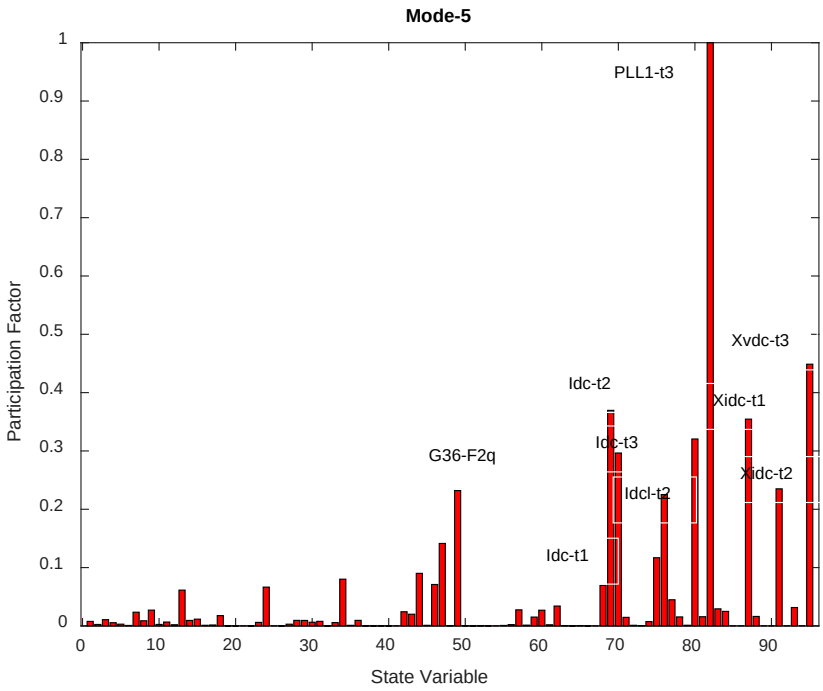

Figure 5.13 Participation of state variables in Mode-5

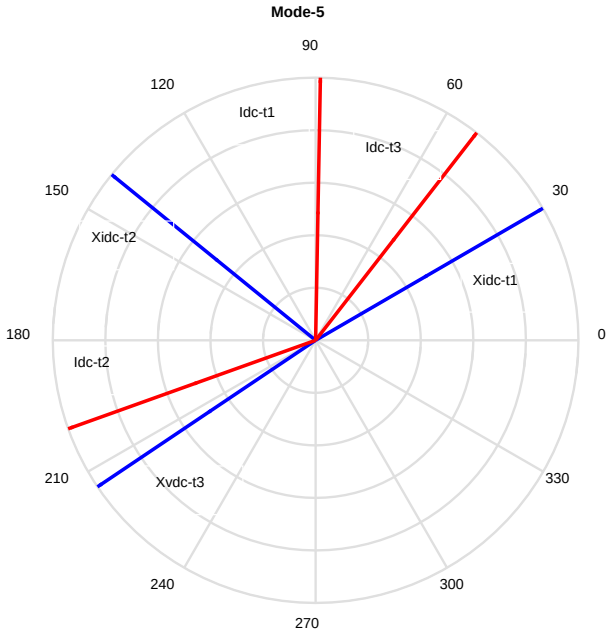

Figure 5.14 Mode shape of the major participant for Mode-5

Mode-6:

Mode-6 has an oscillation frequency of 3.59Hz and a damping ratio of 40.97%. As shown in Figure 5.15, terminal three DC voltage controller state variable X_{vdc_t3} (100%) dominates this mode. The other major contributors are the terminal two DC current controller state variable X_{idc_t2}(65.7%), terminal one DC current controller state variable X_{idc_t1}(19.7%), and terminal two PLL $PLL1_{t2}$(50.8%). In this mode, terminal one DC current controller state variable X_{idc_t1} oscillates against both terminal two DC current controller state variable X_{idc_t2} and terminal three DC voltage controller state variables X_{vdc_t3} as shown in Figure 5.16. Terminal two DC current I_{dc_t2} oscillates against terminal three DC current I_{dc_t3}.

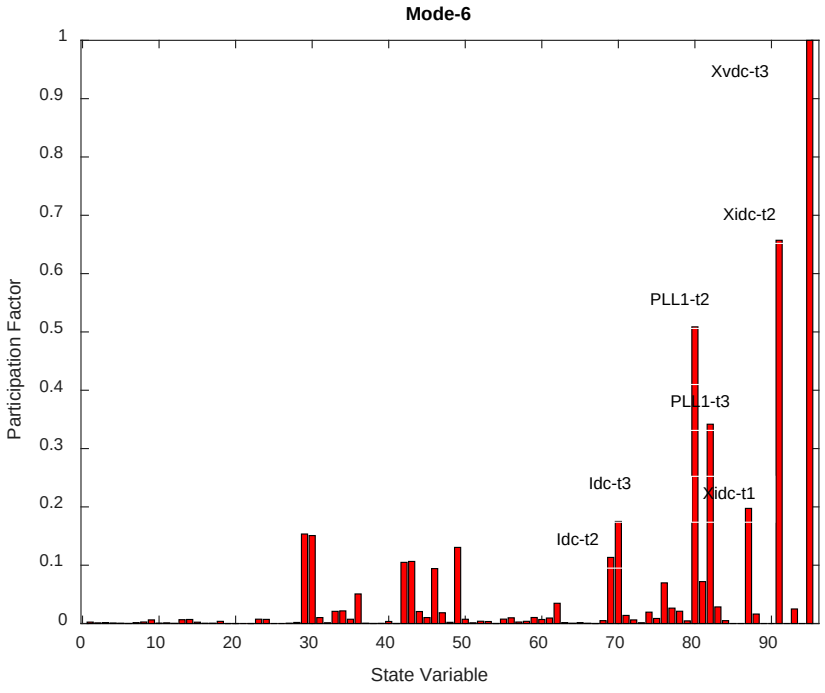

Figure 5.15 Participation of state variables in Mode-6

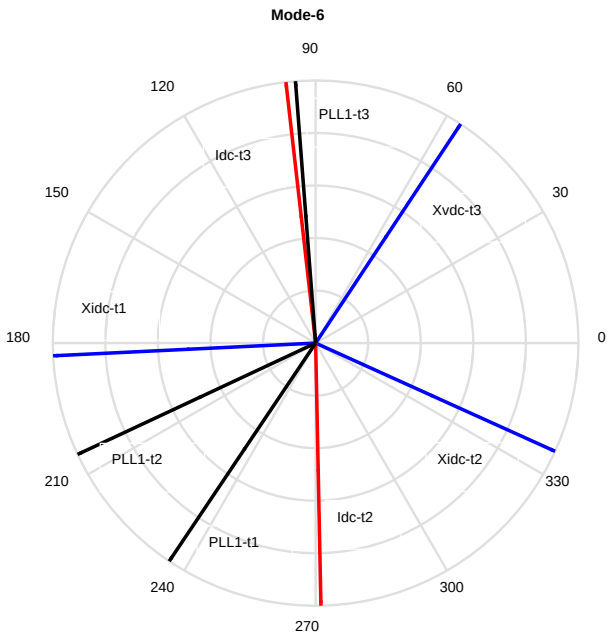

Figure 5.16 Mode shape of the major participant for Mode-6

In this section, three controller interaction modes, Mode-4, Mode-5, and Mode-6 are introduced. With the selected controller parameters, all three controller interaction modes have enough damping ratios. All controller interaction oscillation damped out quickly and have no small signal stability concern. However, if one of the controller interaction modes in the three-terminal HVDC system has a very low or negative damping ratio, the whole MTHVDC system may become unstable. In addition, these controllers may interact with other dynamic devices in the power system, such as the series compensated lines and FACTs in the power systems and raise small signal stability concerns. Therefore, it is recommended to perform eigenvalue analysis to ensure that control parameters are properly selected, and the system has no small signal stability concern in the whole operating range.

5.3.4 Electromechanical Oscillation Modes

Generator speed and generator rotor angle state variables $G35_{wr}$, $G35_{ang,}$ $G36_{wr}$, $G36_{ang}$, $G41_{wr}$ and $G41_{ang}$ as well as the HVDC controller state variables X_{idc_t1}, X_{idc_t2} and X_{vdc_t3} participate in and dominate the oscillation modes Mode-7, Mode-8, and Mode-9 in Table 5.5. Therefore, these modes are classified as electromechanical oscillation mode [58]. Mode-7 has an oscillation frequency of 1.29Hz with a damping ratio of 2.7%. Figure 5.17 clearly shows the participation of each state variable for this mode. The state variables are the terminal three generator rotor speed $G36_{wr}$ (100%), the generator rotor angle $G36_{ang}$ (96.5%), the terminal two generator rotor speed $G35_{wr}$(25%), the terminal two generator rotor angle $G35_{ang}$(16.7%), the terminal three DC voltage controller state variable X_{vdc_t3} (12.4%) and the terminal two DC current controller state variable X_{idc_t2} (5.5%). As shown in Figure 5.18, generator 35 rotor speed $G35_{wr}$ and generator 36 rotor speed $G36_{wr}$ oscillates together, and generator 35 rotor angle $G35_{ang}$ and generator 36 rotor angle $G36_{ang}$ oscillates together. Similarly, terminal two DC current controller state variable X_{idc_t2} oscillates together with terminal three voltage controller state variable X_{vdc_t3}.

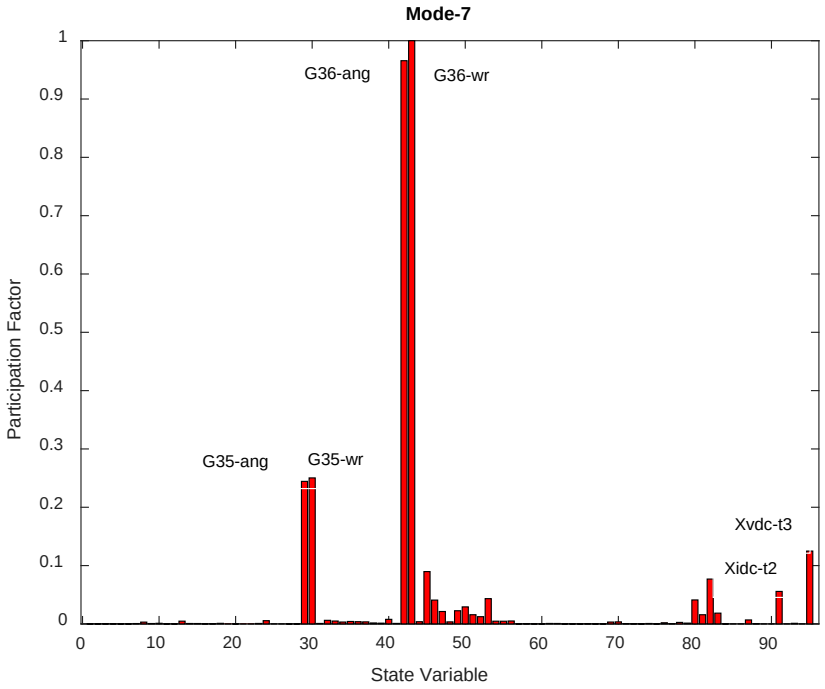

Figure 5.17 Participation of state variables in Mode-7

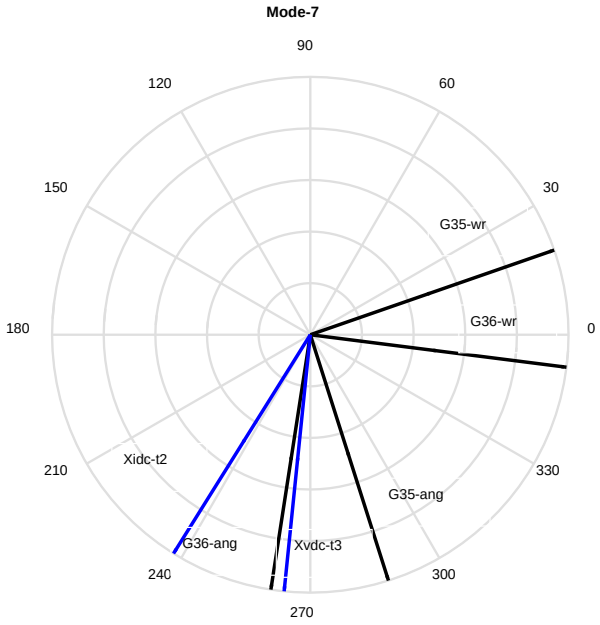

Figure 5.18 Mode shape of the major participant for Mode-7

Mode-8 has an oscillation frequency of 1.26Hz with a damping ratio of 24.13%. Figure 5.19 shows the detailed participation for this mode. The main participants in this mode are the terminal two generator rotor speed $G35_{wr}$ (100%), generator rotor angle $G35_{ang}$ (94.9%), terminal three generator rotor speed $G36_{wr}$(16.7%), terminal two generator rotor angle $G36_{ang}$(15.6%), terminal two DC current controller state variable X_{idc_t2} (51.6%) and terminal three DC voltage controller state variable X_{vdc_t3} (6.2%). Figure 5.20 shows the angle difference between generator 36 rotor speed $G36_{wr}$ and generator 35 rotor speed $G35_{wr}$ is about 180 degrees. Therefore, the $G35$ generator speed state variable oscillates against the $G36$ generator speed state variable. Similarly, the terminal two generator rotor angle $G35_{ang}$ oscillates against the terminal three generator rotor angle $G36_{ang}$, and the terminal two DC current controller state variable X_{idc_t2} oscillates against terminal three DC voltage controller state variable X_{vdc_t3}.

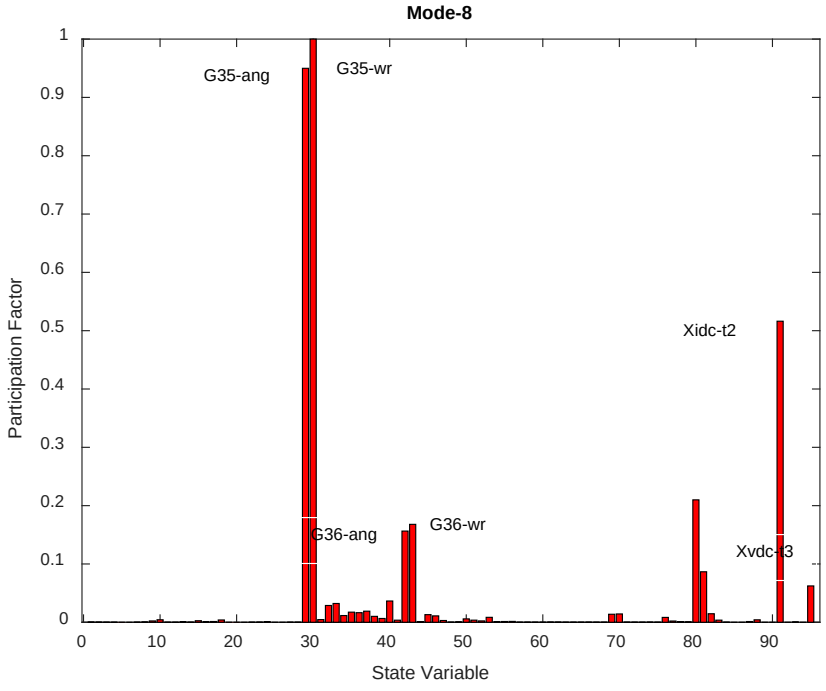

Figure 5.19 Participation of state variables in Mode-8

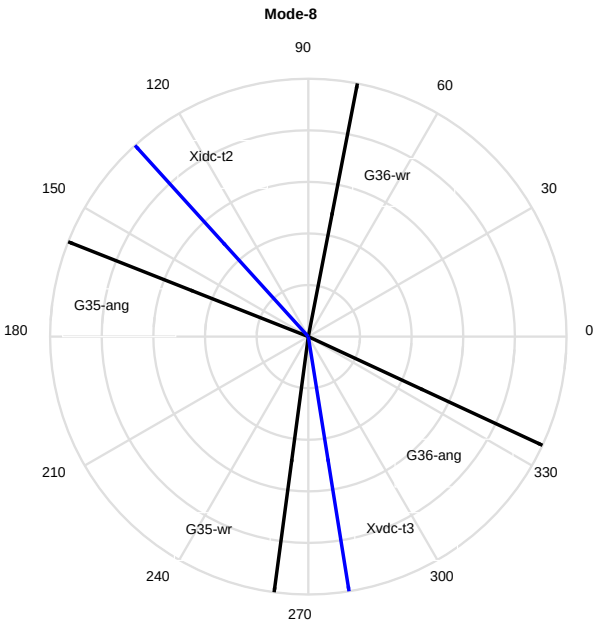

Figure 5.20 Mode shape of the major participant for Mode-8

Mode-9 in Table 5.5 has an oscillation frequency of 0.16Hz with a damping ratio of 29.8%. As shown in Figure 5.21, generator rotor speed $G41_{wr}$(100%), generator rotor angle $G41_{ang}$(94.9%) and the HVDC system terminal one DC current controller state variable X_{Idc_t1}(53.6%) participate in this mode. Terminal one generator speed dominates this mode. In addition, the terminal three DC voltage controller state variable X_{vdc_t3} (1.0%) also participates in this mode with very small participation. Figure 5.22 shows the mode shape of Mode-9.

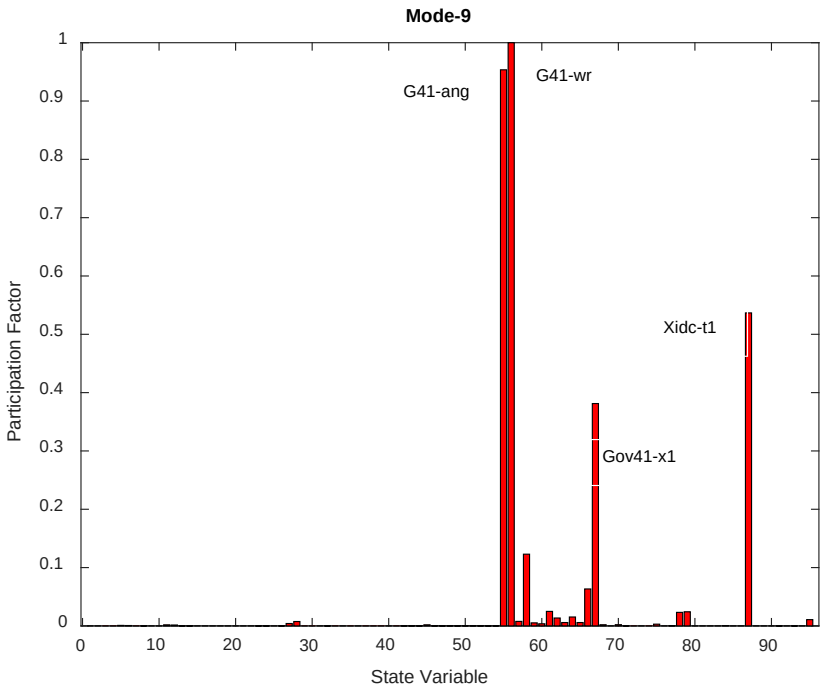

Figure 5.21 Participation of state variables in Mode-9

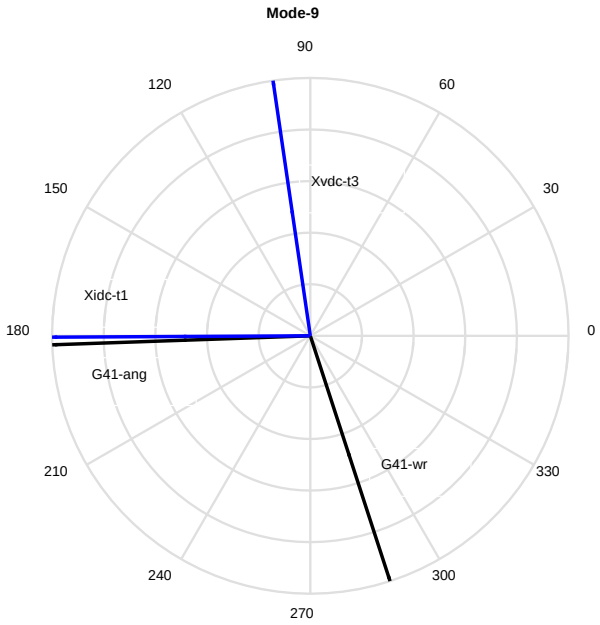

Figure 5.22 Mode shape of the major participant for Mode-9

In this section, three electromechanical oscillation modes, Mode-7, Mode-8, and Mode-9 are briefly discussed. Using a 1Hz oscillation with a 5% damping ratio as a reference (the oscillation amplitude reduces to 37% of its original value in 3.18s), Mode-8 has enough damping ratio and no small signal stability concern. Mode-9 barely meets the damping requirement and has no small signal stability concern. However, the damping ratio for Mode-7 is small and its oscillation amplitude taking 4.57s reduces to 37% of its original value. According to the current Manitoba Hydro damping guideline [21], this mode must be carefully monitored to ensure that the damping ratio can be maintained.

Upon further investigation of the participants of all electromechanical oscillation modes, it was observed that DC controller state variables also participate in all three modes. This implies that the damping ratio of electromechanical oscillation can be changed (depend on the participation factor) by changing DC controller parameters. Depending on the participation factor, the DC controller has a different impact on these oscillation modes. Increasing controller gain can either increase or decrease damping ratios for these modes. Unfavorable control parameter change may reduce the damping ratio, therefore raising the stability concern.

The results also clearly show that machines at DC terminal two and DC terminal three interact with each other through the MTHVDC systems. Like the synchronized AC system, oscillations can pass through the HVDC systems from one terminal to another.

5.3.5 Time Domain Simulation

A power system consists of a complex interconnection of nonlinear components. In the small-signal stability analysis, the nonlinear behavior of the dynamic devices is linearized at a particular steady-state operating point. Frequency domain eigenvalue analysis is then

performed based on the linearized model. The nonlinearities of the power systems are ignored in the eigenvalue analysis. To evaluate the controller performance, confirm suspected oscillations, and ensure robust controller design with no stability concerns, a time-domain simulation must be performed. To do so, an electromagnetic transient simulation was performed for the MTHVDC test case shown in Figure 5.2. The PSCAD study case has been created with a rectifier in current control, a terminal-two inverter in current control, and a terminal-three inverter in voltage control. The control parameters are the same as in the small-signal study cases provided in Appendix A. A 5% 100ms step change is applied to each controller reference and the results are provided in the following section. Figure 5.23 and 5.24 show the DC voltage and DC current with a 5% 100ms step change on the terminal one DC current reference. Figure 5.24 clearly shows that the terminal one DC current controller response is fast and the system has enough damping ratio. This further proves that the system is stable with no stability issues. Similarly, Figure 5.25 and 5.26 show the DC voltage and DC current with a 5% 100ms step change on the terminal two current reference. Figure 5.27 and 5.28 show the DC voltage and DC current with a 5% 100ms step change on the terminal three voltage reference. All results demonstrate that the HVDC controller is well designed with fast response and is stable for operation. The HVDC system has no stability concerns. Based on both the small signal study results and the time domain study results, it is concluded that the three-terminal HVDC system with the proposed control scheme is stable and has no stability concern. ((Note: T1, T2 and T3 in Figures 5.23-5..28 represent terminal one, terminal two and terminal three, respectively)

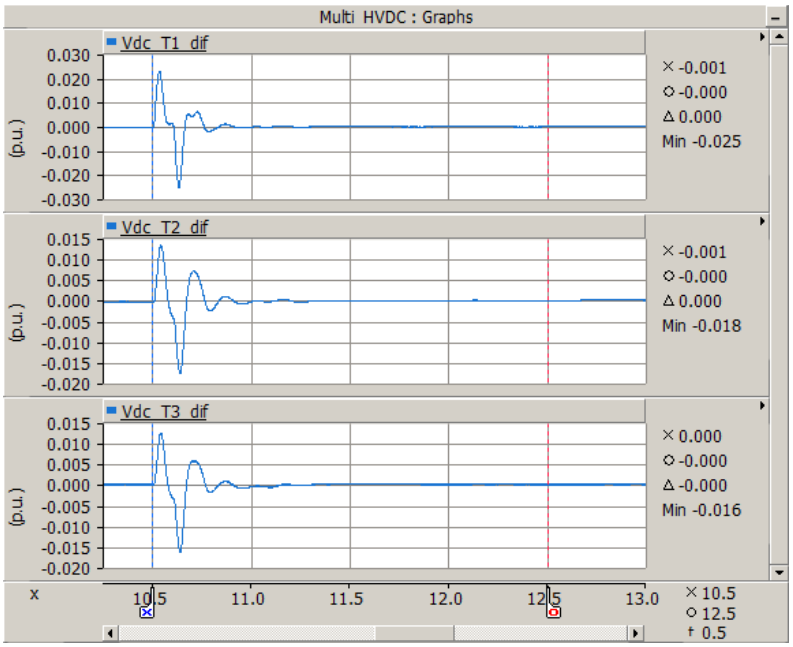

Figure 5.23 DC voltage responses - 5% 100ms step change on T1 DC current reference

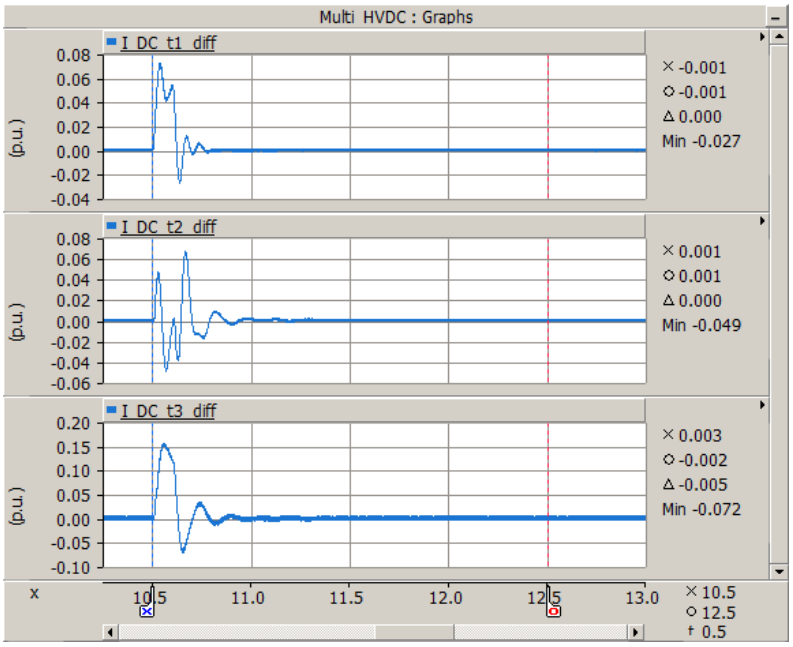

Figure 5.24 DC current response s- 5% 100ms step change on T1 DC current reference

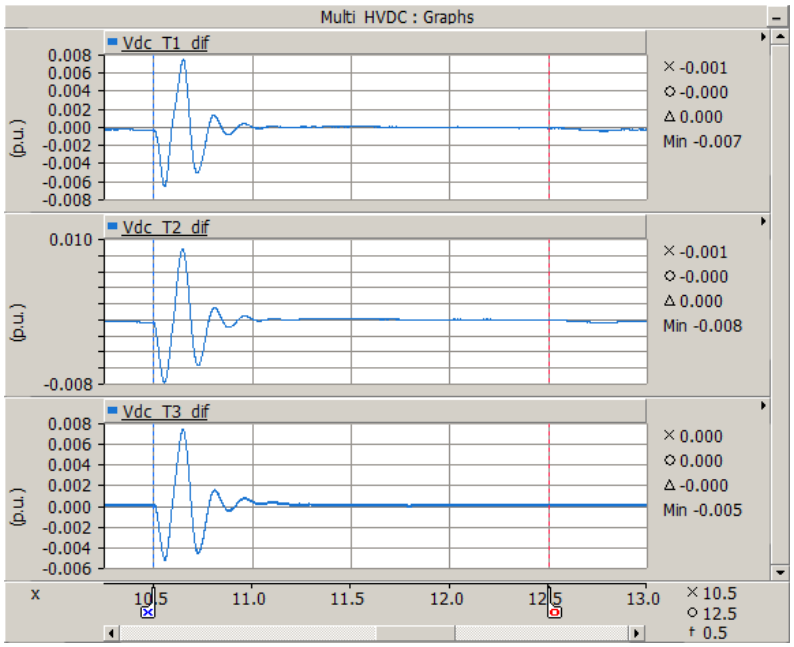

Figure 5.25 DC voltage responses - 5% 100ms step change on T2 DC current reference

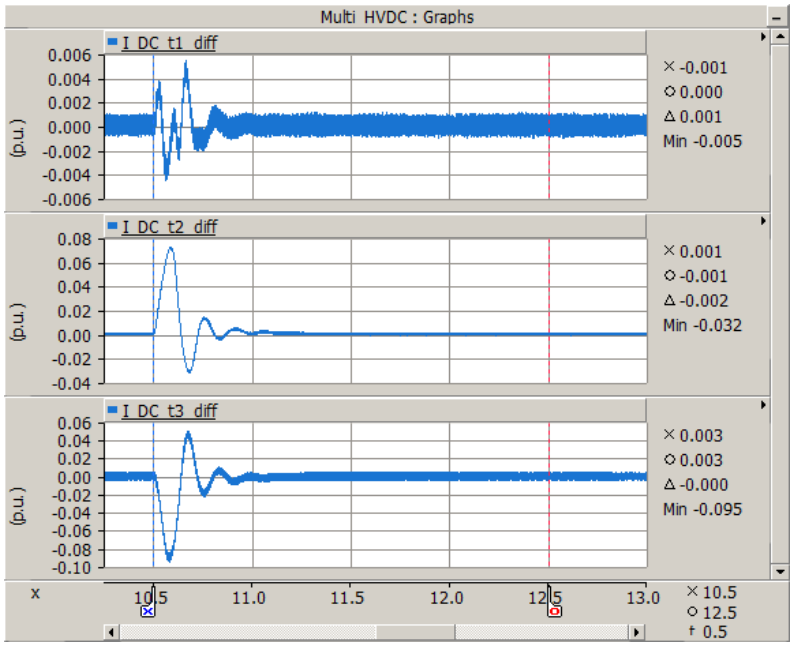

Figure 5.26 DC current responses- 5% 100ms step change on T2 DC current reference

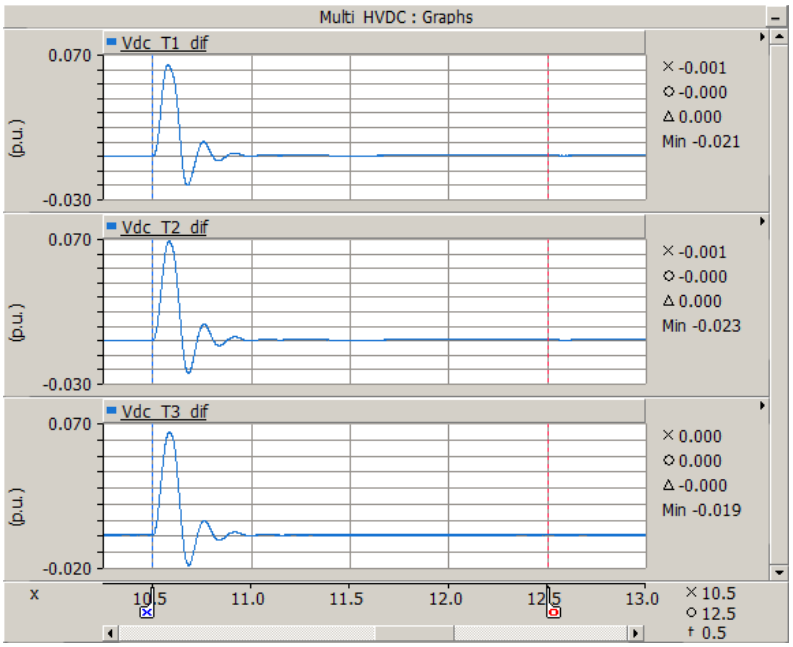

Figure 5.27 DC voltage responses - 5% 100ms step change on T3 DC voltage reference

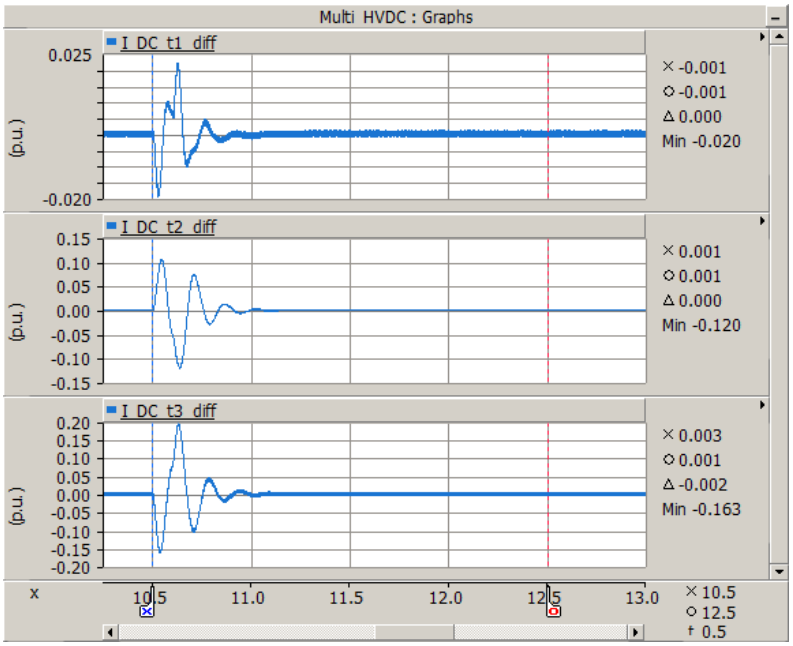

Figure 5.28 DC current responses - 5% 100ms step change on T3 DC voltage reference

5.4 MTHVDC Interaction Analysis – Control Scheme Two

Similar to control scheme one, the same developed MTHVDC system with a different controller arrangement has been studied. In scheme two, the rectifier is in DC voltage control mode and the other two inverters are in DC current control mode. The rest of the three-terminal HVDC test systems remain the same as in scheme one. Additionally, scheme two HVDC systems are operated at the same operating point as in the control scheme one. The same amount of power is generated at the rectifier side and delivered to inverter stations. The controller parameters are selected to ensure the oscillation modes can be easily identified. In the meantime, the unstable oscillation mode (or positive eigenvalue) should also be avoided. Similar study processes have been applied as in control scheme one. The detailed control parameters are provided in Appendix A. The overall state-space model of the test system consists of 89 state variables, including 24 for the generators, 9 for exciters, 6 for governors, 22 for MTHVDC systems and 28 for AC networks (including transformers, transmission lines, loads and capacitors). The state variables index for the MTHVDC systems is also provided in Table 5.7. In this table, X_{vdc_t1}, X_{idc_t2}, X_{idc_t3} are the state variables of terminal one DC voltage controller, terminal two DC current controller and terminal three DC current controller.

MTHVDC System State Variables Index									
1	I_{dc_t1}	2	I_{dc_t2}	3	I_{dc_t3}	4	V_{dc_t1}	5	V_{dc_t2}
6	V_{dc_t3}	7	V_{dc_t4}	8	I_{dcl_t14}	9	I_{dcl_t24}	10	I_{dcl_t34}
11	PLL_{1_t1}	12	PLL_{2_t1}	13	PLL_{1_t2}	14	PLL_{2_t2}	15	PLL_{1_t3}
16	PLL_{2_t3}	17	V_{dcm_t1}	18	X_{vdc_t1}	19	I_{dcm_t2}	20	X_{idc_t2}
21	I_{dcm_t3}	22	X_{idc_t3}	23		24		25	

Table 5.7 MTHVDC system state variable index-scheme two

Table 5.8 tabulated the major oscillatory mode for the three-terminal HVDC system. The participations are based on the magnitudes of the participation factors. The phase displacements of the state variables in a particular mode are given by phase angles of the relevant mode shapes.

Mode	Frequency (Hz)	Damping Ratio (%)	Major Participants	Mode Description
1N	224.11	3.33%	Vdc_t2 (100%),Idcl_t2(77%), Idc_t2(39.3%), Vdc_t4(13.9%)	DC Network Resonance
2N	118.95	5.19%	Vdc_t1(100%), Idcl_t1(62.8%), Idc_t1(60.6%), Vdc_t4(22.1%)	DC Network Resonance
3N	82.64	16.26%	Vdc_t4(100%), G41_Fsq(55.7%), Idc_t3(43.4%), Idc_t1(41.2%),VI_bus42(35.7%),VR_bus42(29.5%)	AC-DC Network Interaction
4N	51.30	31.06%	Xvdc_t1(100%), G41_Fsq(98.6%), Vdc_t1(70.4%), VI_bus42(63.6%), G41_Fsd(60.2%),Vdc_t4(38.3%)	DC controller Interaction
5N	7.64	12.34%	Xidc_t3(100%), Xidc_t2(95.4%), PLLx1_t3(80.3%), Idc_t3(78.0%), Idc_t2(72.6%), Idcl_t2(44.5%)	DC controller Interaction
6N	3.34	7.03%	Xidc_t2(100%), Xvdc_t1(92.3%), Idcl_t1(66.2%), PLLx1_t2(58.7%), PLLx1_t3(58.1%), Xidc_t3(49.1%)	DC controller Interaction
7N	1.41	4.61%	G35_ang(100%), G35_wr(99.3%), G36_wr(76.9%), G36_ang(74.4%), Xidc_t2(29.1%),Xidc_t3(9.5%), Xvdc_t1(7.5%)	Electro-Mechnical Oscillation
8N	1.37	6.48%	G35_ang(100%), G35_wr(99.4%), G36_wr(79.4%), G36_ang(76.4%), Xidc_t2(26.7%),Xidc_t3(11.6%), Xvdc_t1(2.8%)	Electro-Mechnical Oscillation
9N	0.19	36.33%	G41_wr(100%), G41_ang(82.4%), Xvdc_t1(24.4%)	Electro-Mechnical Oscillation

Table 5.8 Major participation of selected modes in scheme two test system

5.4.1 DC Network Resonance Modes

Similar to control scheme one, Mode-1N and Mode-2N in Table 5.8 are classified as the DC network interaction mode. The participation factors for all 89 state variables in Mode-1N are provided in Figure 5.29. This mode has an oscillation frequency of 224.11Hz and a damping ratio of 3.33%. Terminal two DC voltage, V_{dc_t2} (100%), terminal two smoothing reactor, I_{dcl_t2}, (77%), terminal two DC current, I_{dc_t2} (39.3%), and the HVDC line tap point DC voltage, V_{dc_t4} (13.9%), all participate in this mode. The mode shape of

Mode-1N shown in Figure 5.30 indicates that terminal two DC voltage V_{dc_t2} and HVDC line tap point DC voltage V_{dc_t4} oscillate against each other. The angle between these two state variables is about 180 degrees. Similarly, the angle between the terminal two DC current I_{dc_t2} and the terminal three DC current I_{dc_t3} is about 180 degrees. These two terminal DC currents I_{dc_t2} and I_{dc_t3} oscillate against each other.

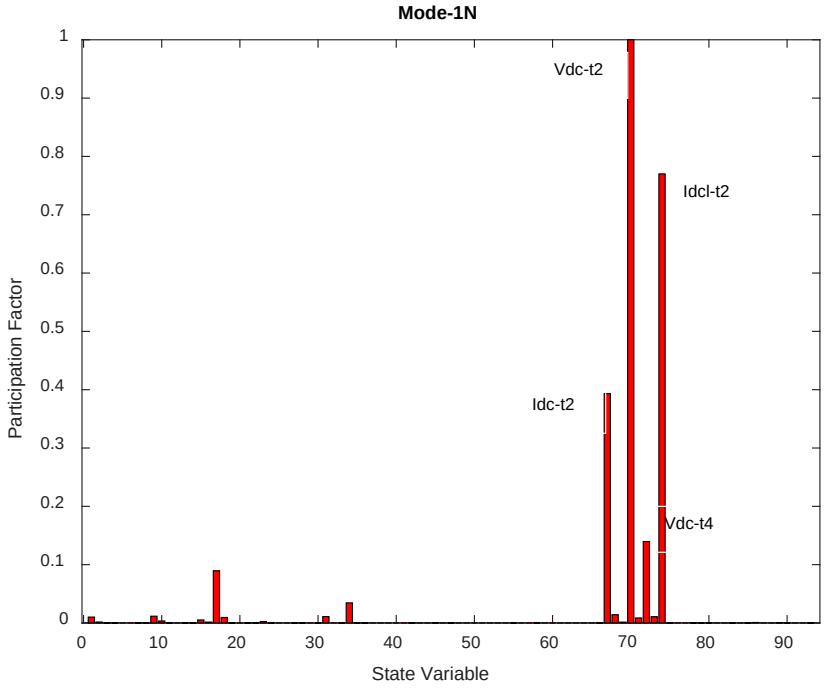

Figure 5.29 Participation of state variables in Mode-1N

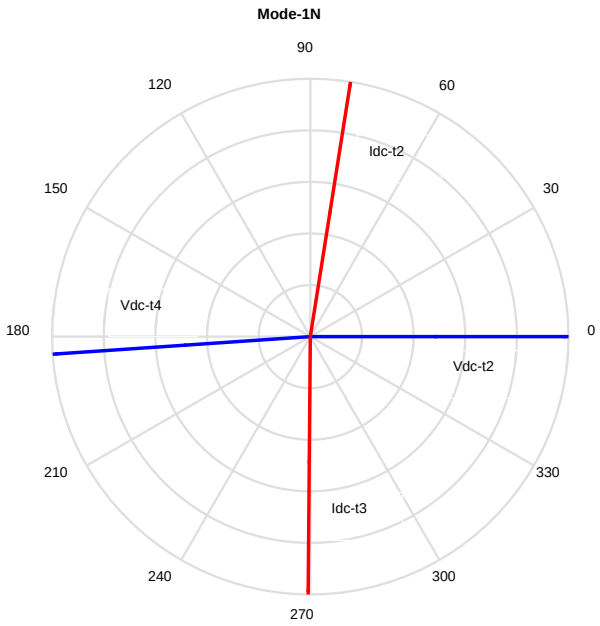

Figure 5.30 Mode shape of the major participant for Mode-1N

Similarly, Mode-2N has an oscillation frequency of 118.95Hz and a damping ratio of 5.19%. As shown in Figure 5.31, terminal one DC voltage, V_{dc_t1} (100%), terminal one smoothing reactor, I_{dcl_t1} (62.8%), terminal one DC current, I_{dc_t1} (60.6%), and the HVDC line tap point DC voltage, V_{dc_t4} (22.1%), participate in this mode. Terminal one DC voltage controller X_{vdc_t1} (1.1%) also participates in this mode with a very small participation factor. The mode shape of Mode-2N in Figure 5.32 clearly shows that terminal one DC voltage V_{dc_t1} is 180 degrees apart from terminal two DC voltage V_{dc_t2}, terminal three DC voltage V_{dc_t3}, and HVDC line tap point DC voltage V_{dc_t4}. Therefore, terminal one DC voltage in this mode oscillates against terminal two, terminal three, and HVDC line tap point DC voltages. The angle difference between DC currents I_{dc_t1}, I_{dc_t2}

and I_{dc_t3}, is very small. For this reason, we say that all three terminal DC currents, I_{dc_t1}, I_{dc_t2} and I_{dc_t3} oscillate together in this mode.

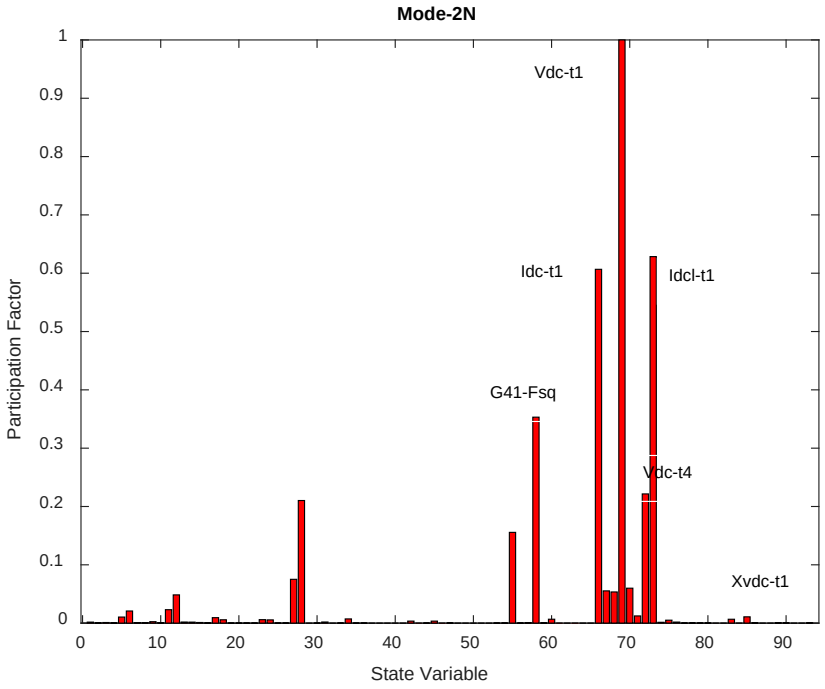

Figure 5.31 Participation of state variables in Mode-2N

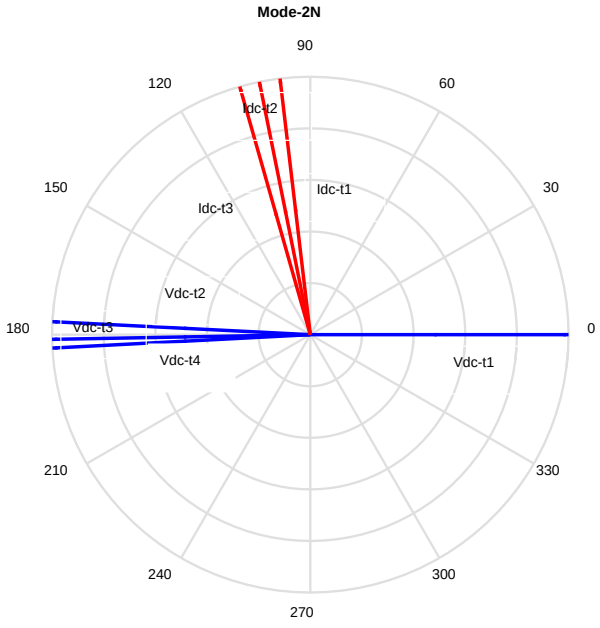

Figure 5.32 Mode shape of the major participant for Mode-2N

The above analysis shows that DC network resonance modes in the proposed three-terminal HVDC systems have higher oscillation frequencies. These two oscillation modes damped out quickly and the damping ratios are enough to meet the performance requirement [see Table 5.2 and 5.3]. And these two modes do not have small signal stability concerns in the proposed control scheme.

These two oscillation modes are dominated by the DC quantities, such as the DC terminal voltages, DC currents, and DC smoothing reactors. As a result, any change of the DC terminal voltage, DC current, and DC smoothing reactor will impact the oscillation frequency and damping ratio. In particular, the size of the smoothing reactor significantly impacts the oscillation frequency and damping ratio for these two modes.

In addition, the AC system state variables (equivalent machine state variable) also participate these two oscillation modes (<1% for Mode-1N and around 10% for Mode-2N). Therefore, any change of the AC system strength will impact the oscillation frequency and damping ratio for these two modes.

5.4.2 AC-DC Interaction Modes

Mode-3N in Table 5.7 is the AC-DC network interaction mode. Both the HVDC quantities and AC system components participate in and have relatively high participation factors in Mode-3N. It is the only AC-DC network interaction mode that has an oscillation frequency of 82.64Hz and a damping ratio of 16.23%. As shown in Figure 5.33, the HVDC line tap point DC voltage V_{dc_t4} (100%) dominates this mode. Terminal one generator stator flux components Gen41-Fsq (55.7%), terminal three DC current, I_{dc_t3} (43.4%),

terminal one DC current, I_{dc_t1} (41.2%), terminal one AC side bus voltage VI_{bus42} (35.7%), VR_{bus42} (29.4%), and terminal one DC voltage controller state variable X_{vdc_t1} (10.7%) also largely contribute to this mode. The mode shape in Figure 5.34 shows that terminal one DC voltage V_{dc_t1}, terminal two DC voltage V_{dc_t2}, terminal three DC voltage V_{dc_t3}, and HVDC line tap point DC voltages V_{dc_t4}, all oscillate together. it also shows that terminal one DC current I_{dc_t1} oscillates against both terminal two DC current I_{dc_t2} and terminal three DC current I_{dc_t3}.

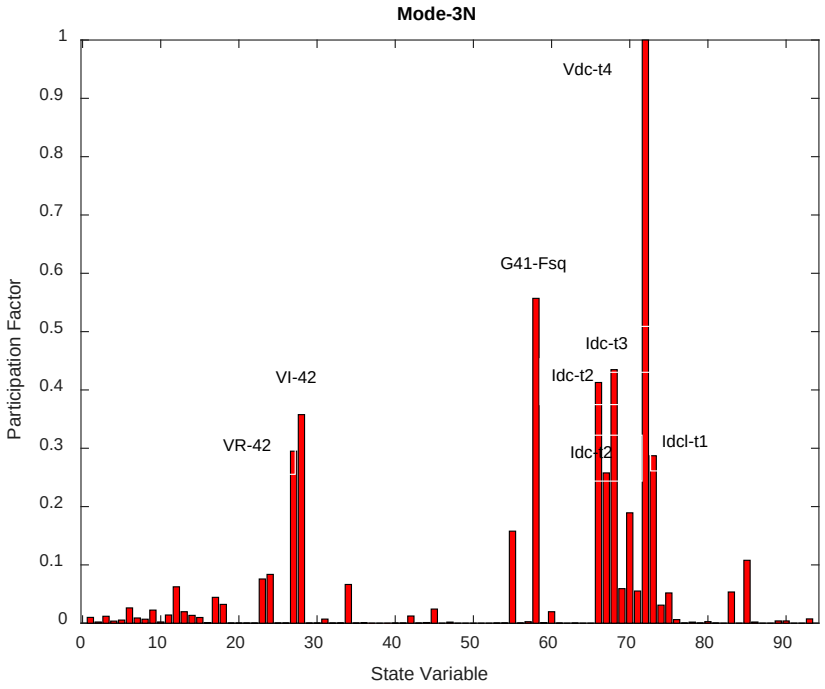

Figure 5.33 Participation of state variables in Mode-3N

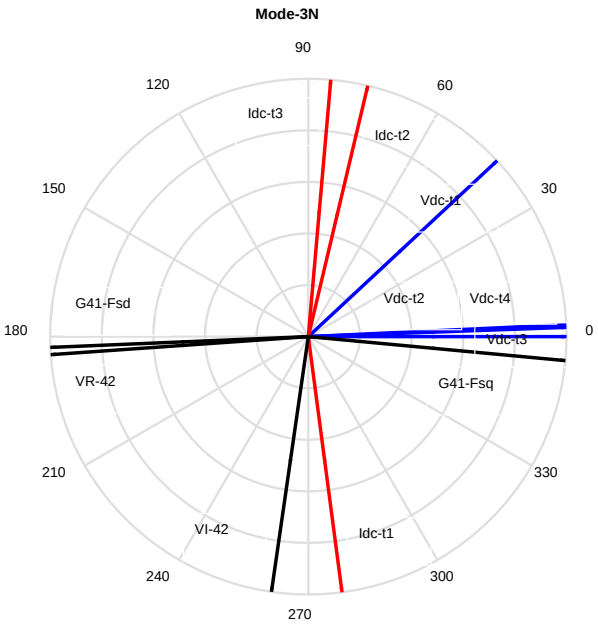

Figure 5.34 Mode shape of the major participant for Mode-3N

In summary, Mode-3N has a relatively high oscillation frequency. This mode is a highly damped oscillation mode with no small signal stability concern. The DC voltage, AC system voltage, generator state variable, and HVDC controller state variables all participate in. Therefore, the oscillation frequency and damping ratio of this mode will potentially be influenced by the AC system strength, HVDC loading, and parameter settings.

5.4.3 HVDC Controller Interaction Modes

The controller state variables X_{vdc_t1}, X_{idc_t2} and X_{idc_t3} participate in and dominate the oscillation modes Mode-4N, Mode-5N, and Mode-6N in Table 5.7. Therefore, these modes are classified as controller interaction modes.

Mode-4N:

Mode-4N has an oscillation frequency of 51.30Hz with a damping ratio of 31.06%. The major participants are terminal one DC voltage controller X_{vdc_t1} (100%), terminal one generator stator flux component Gen41-Fsq (98.6%) and terminal one DC voltage V_{dc_t1} (70.4%). The other contributors are HVDC line tap point DC voltage V_{dc_t4}(38.3%), terminal three DC current I_{dc_t3} (25.1%), terminal two DC current I_{dc_t2} (17.2%), and terminal one DC current I_{dc_t1} (13.9%). Figure 5.35 shows the participation for each state variable of this mode. As shown in Figure 5.36, the angle between terminal one DC voltage, terminal two DC voltage, terminal three DC voltage, and HVDC line tap point DC voltage is very small. All DC terminal voltages oscillate together in this mode. For DC current, terminal two DC current I_{dc_t2} and terminal three DC current I_{dc_t3} oscillate together against terminal one DC current I_{dc_t1}.

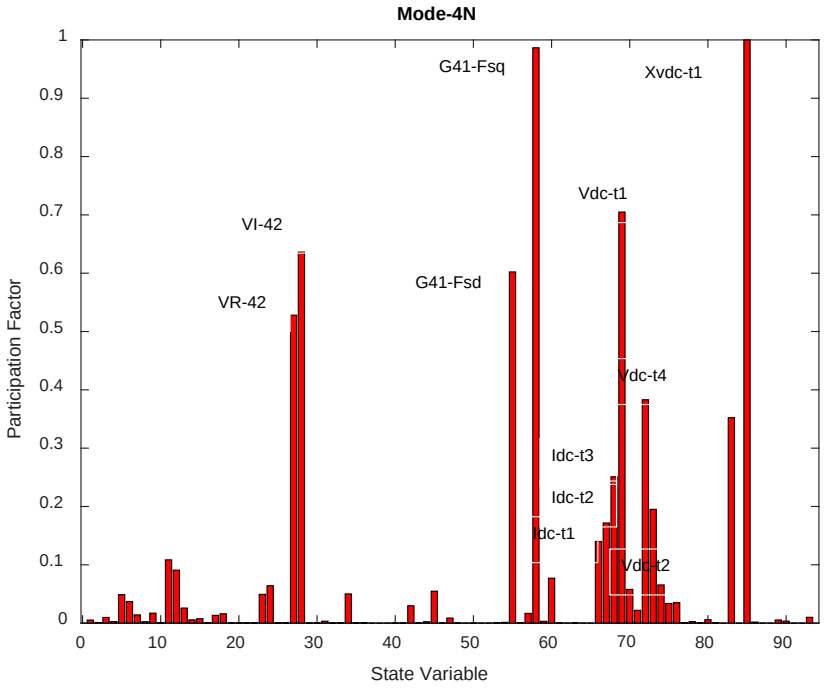

Figure 5.35 Participation of state variables in Mode-4N

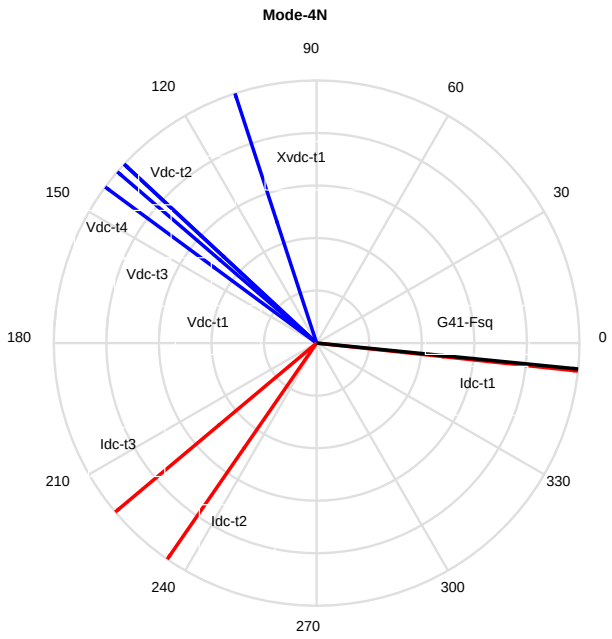

Figure 5.36 Mode shape of the major participant for Mode-4N

Mode-5N:

Mode-5N has an oscillation frequency of 7.64Hz with a damping ratio of 12.34%. The inverter side DC current controller state variables X_{idc_t3}(100%), X_{idc_t2} (95.4%), inverter side DC current I_{dc_t3}(78%) and I_{dc_t2}(72.6%) participate in this mode. Additionally, both terminal three PLL $PLL1_{t3}$ (80.37%) and terminal two PLL $PLL1_{t2}$ (40.4%) also participate in this mode. Figure 5.37 shows the participation for each state variable of this mode. In Figure 5.38, terminal two DC current controller state variable X_{idc_t2} and terminal three DC current controller state variable X_{idc_t3} oscillate against each other. Terminal two DC current I_{dc_t2} and terminal three DC current I_{dc_t3} oscillate against each other.

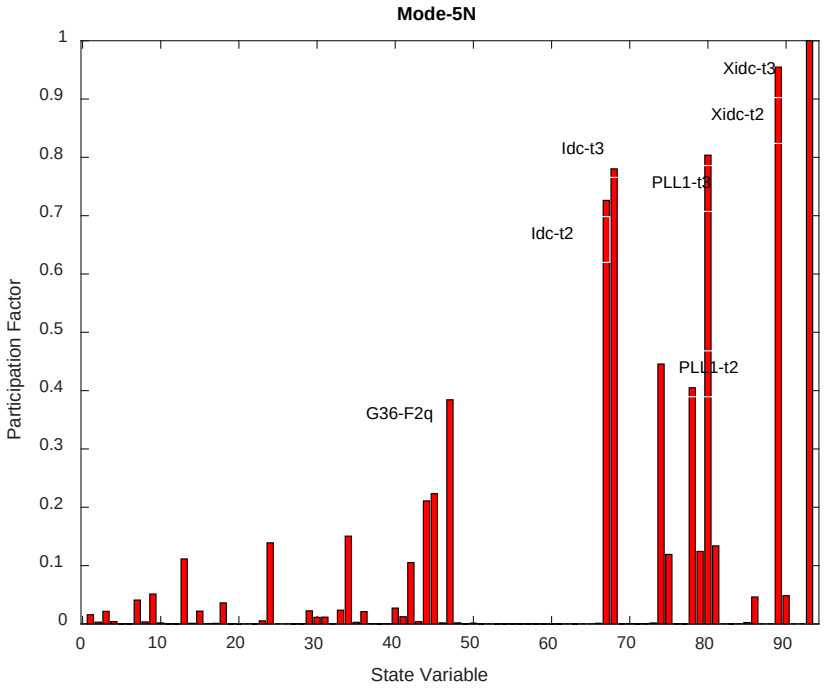

Figure 5.37 Participation of state variables in Mode-5N

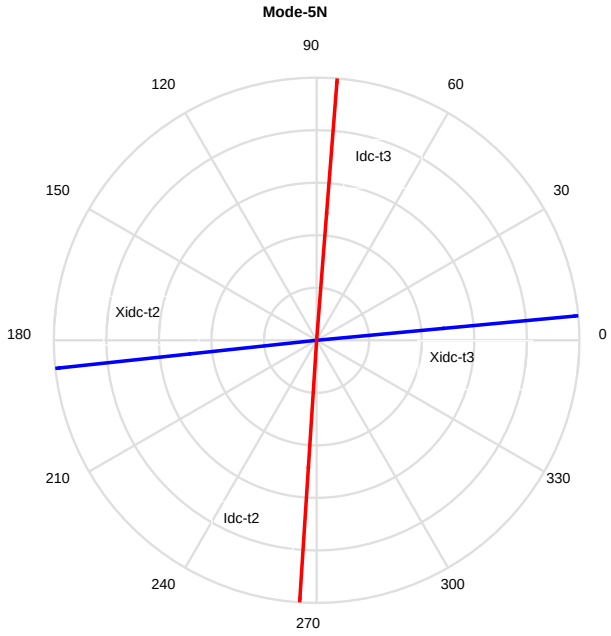

Figure 5.38 Mode shape of the major participant for Mode-5N

Mode-6N:

The controller interaction mode, Mode-6N, has an oscillation frequency of 3.34Hz with a damping ratio of 7.03%. As shown in Figure 5.39, terminal two DC current controller state variable X_{idc_t2} (100%) and terminal one DC voltage controller state variable X_{vdc_t1} (92.3%) dominate this mode. The other major contributors are terminal three DC current controller state variable X_{idc_t3} (49.1%), terminal one smoothing reactor I_{dcl_t1} (66.2%), terminal two PLL PLL_{1_t2} (58.7%), and terminal three PLL PLL_{1_t3} (58.1%). In Figure 5.40, terminal two DC current controller state variable X_{idc_t2} oscillates together with terminal three DC current controller state variable X_{idc_t3}. All three terminal DC currents I_{dc_t1}, I_{dc_t2} and I_{dc_t3} oscillate together.

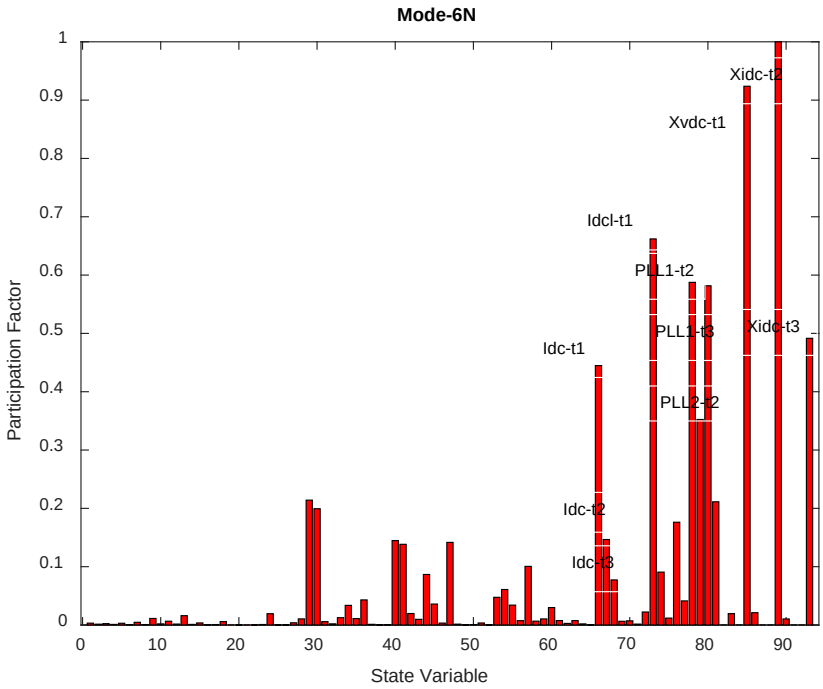

Figure 5.39 Participation of state variables in Mode-6N

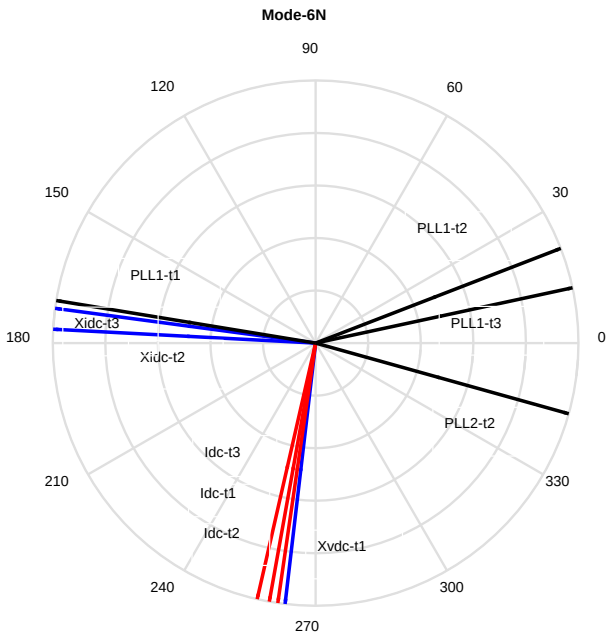

Figure 5.40 Mode shape of the major participant for Mode-6N

In this section, three controller interaction modes, Mode-4N, Mode-5N, and Mode-6N are introduced. With the selected controller parameters, all three controller interaction modes have enough damping ratios and have no small signal stability concern. However, if one of the controller interaction modes in the three-terminal HVDC system has a very low or negative damping ratio, the whole MTHVDC system may become unstable. In addition, these controllers may interact with other dynamic devices in the power system, such as the series compensated lines and FACTs in the power systems and raise small signal stability concerns. Therefore, it is recommended to perform eigenvalue analysis to ensure that control parameters are properly selected, and the system has no small signal stability concern in the whole operating range.

5.4.4 Electromechanical Oscillation Modes

Generator speed and generator rotor angle state variables $G35_{wr}$, $G35_{ang,}$ $G36_{wr}$, $G36_{ang}$, $G41_{wr}$ and $G41_{ang}$ as well as the HVDC controller state variables X_{idc_t1}, X_{idc_t2} and X_{vdc_t3} participate in and dominate the oscillation mode Mode-7N, Mode-8N, and Mode-9N in Table 5.7. These oscillation modes have a lower oscillation frequency (<5Hz). Therefore, they are classified as an electromechanical oscillation mode. Mode-7N has an oscillation frequency of 1.41Hz with a damping ratio of 4.61%. Figure 5.41 shows the participation of each state variable for this mode. They are terminal two generator rotor angle $G35_{ang}$ (100%), generator rotor speed $G35_{wr}$ (99.3%), terminal three generator rotor speed $G36_{wr}$ (76.9%), terminal three generator rotor angle $G36_{ang}$(74.4%), terminal two current controller state variable X_{idc_t2} (29.1%), terminal three current controller state variable X_{idc_t3} (9.5%), and terminal one voltage controller state variable X_{vdc_t1} (7.5%). In Figure 5.42, generator 35 rotor speeds $G35_{wr}$ and generator 36 rotor speed $G36_{wr}$ oscillate together, and generator 35 rotor angle $G35_{ang}$ and generator 36 rotor angel $G36_{ang}$ oscillate together. Similarly, terminal two current controller state variable X_{idc_t2} oscillates together with terminal three current controller state variable X_{idc_t3}.

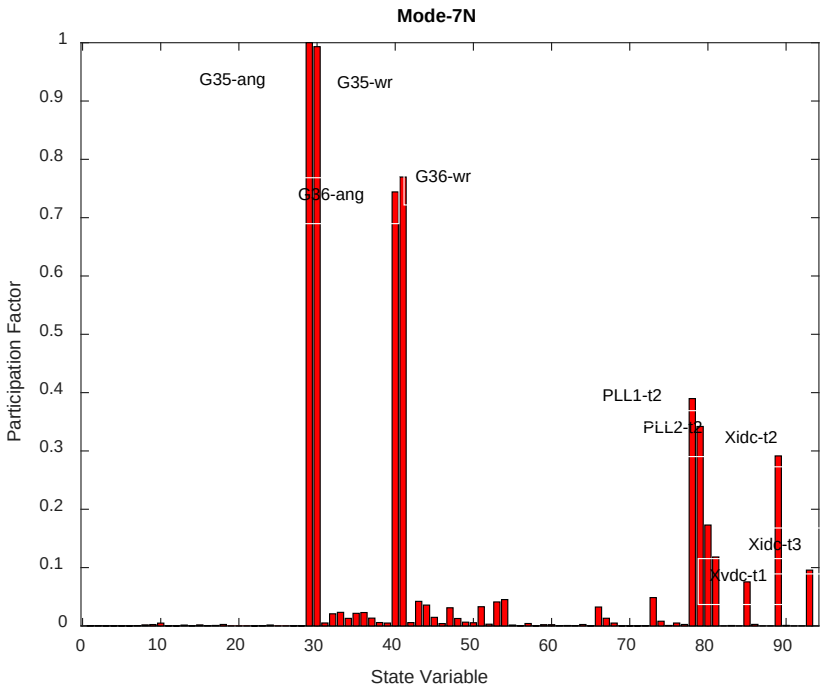

Figure 5.41 Participation of state variables in Mode-7N

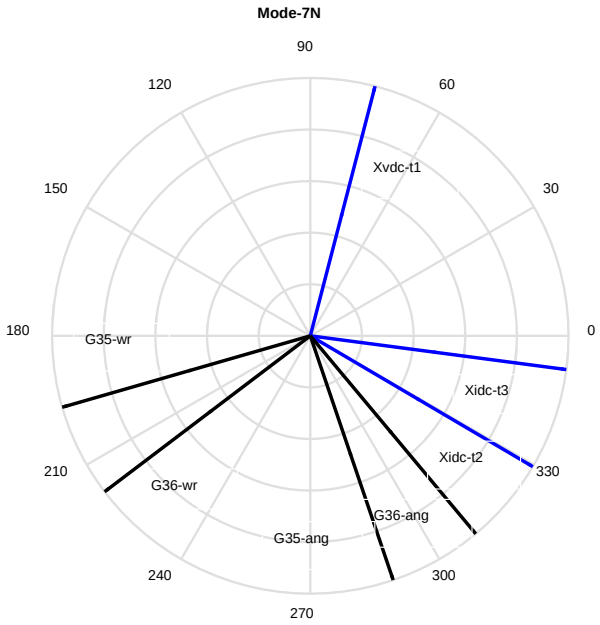

Figure 5.42 Mode shape of the major participant for Mode-7N

Mode-8N has an oscillation frequency of 1.37Hz with a damping ratio of 6.48%. Figure 5.43 shows the participation of each state variable in this mode. They are terminal two generator rotor angle $G35_{ang}$(100%), terminal two generator rotor speed $G35_{wr}$(99.4%), terminal three generator rotor speed $G36_{wr}$ (79.4%), generator rotor angle $G36_{ang}$ (76.4%), terminal two DC current controller state variable X_{idc_t2} (26.7%), terminal three DC current controller state variable X_{idc_t3} (11.6%), and terminal one DC voltage controller state variable X_{vdc_t1} (2.8%). In Figure 5.44, terminal two DC current controller state variable X_{idc_t2} oscillates against terminal three DC current controller state variable X_{idc_t3} and terminal one DC voltage controller state variable X_{vdc_t1}.

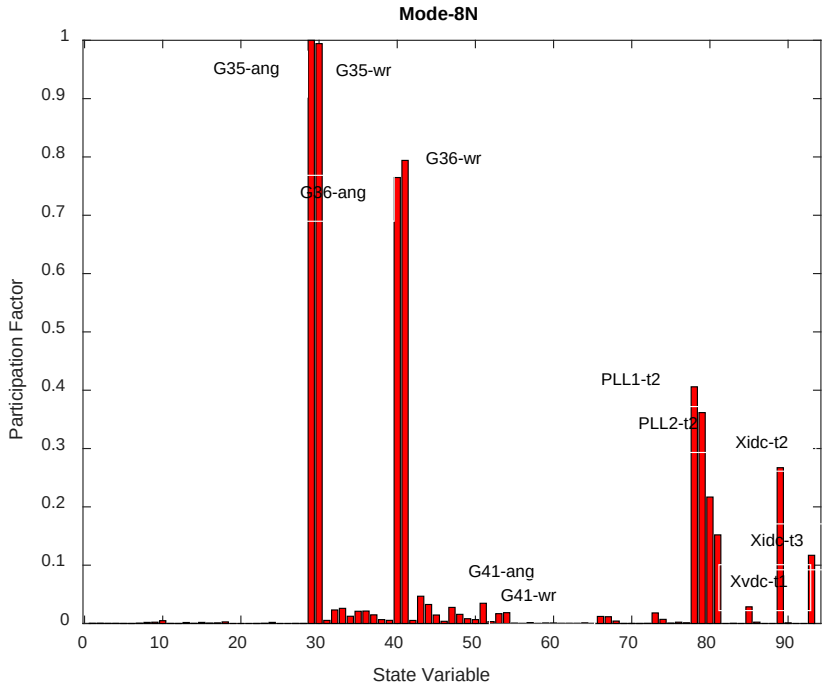

Figure 5.43 Participation of state variables in Mode-8N

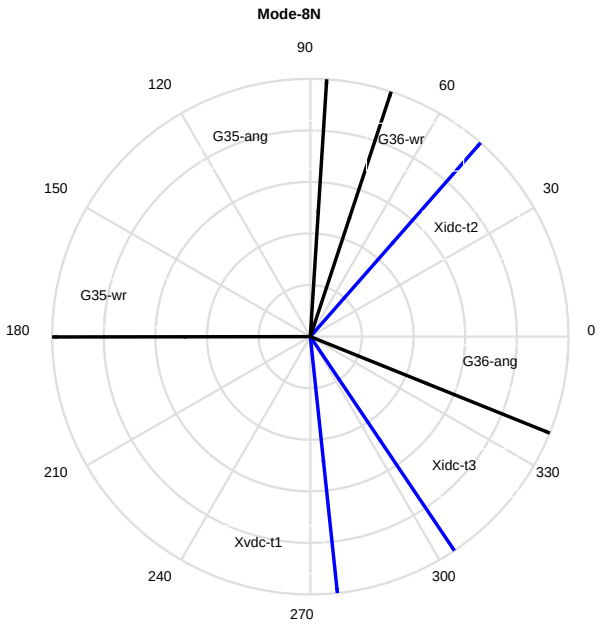

Figure 5.44 Mode shape of the major participant for Mode-8N

Mode-9N has an oscillation frequency of 0.19Hz with a damping ratio of 36.33%. As shown in Figure 5.45, terminal one generator rotor speed $G41_{wr}$ (100%), generator rotor angle $G41_{ang}$ (82.4%), and terminal one DC voltage controller state variable X_{vdc_t1} (24.4%) are the main participants for this mode. Additionally, terminal three DC current controller state variable X_{idc_t3} (1.10%) also participates in this mode. The mode shape of Mode-9N is shown in Figure 5.46.

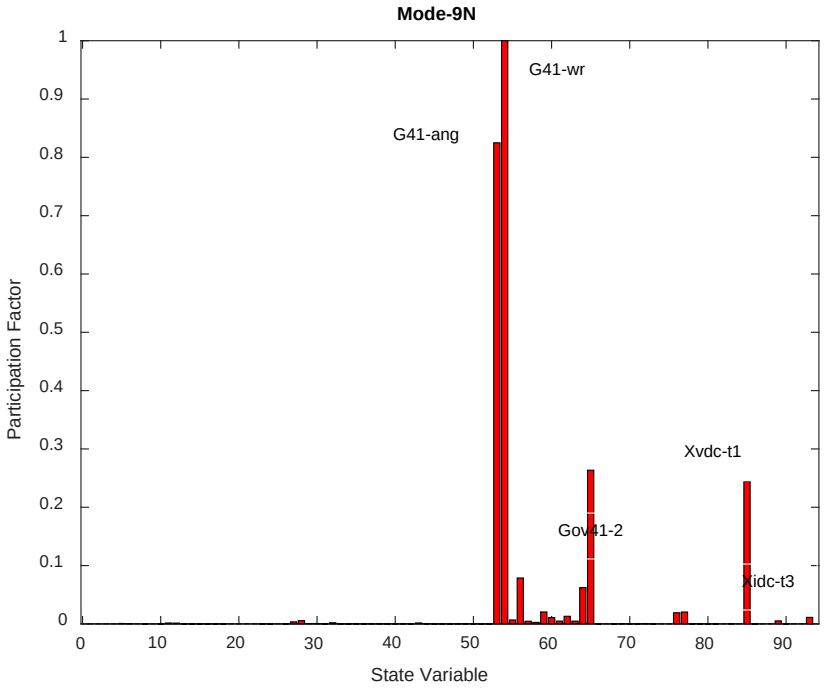

Figure 5.45 Participation of state variables in Mode-9N

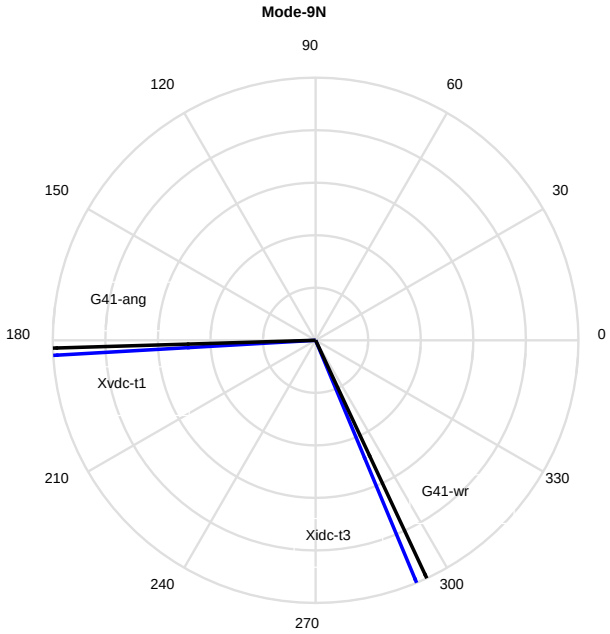

Figure 5.46 Mode shape of the major participant for Mode-9N

In this section, three electromechanical oscillation modes, Mode-7N, Mode-8N, and Mode-9N are briefly discussed. Using 1Hz oscillation with a 5% damping ratio as a reference (it requires 3.18s for the oscillation amplitude to reduce to 37% of its original value), Mode-7N, Mode-8N and Mode-9N have enough damping ratio and no small signal stability concern in the study case.

Upon further investigation of the participants of all electromechanical oscillation modes, it was observed that DC controller state variables also participate in all these modes. This implies that the damping ratio of electromechanical oscillation can be changed (depend on the participation factor) by changing DC controller parameters. Depending on the participation factor, different DC controllers have a different impact on these oscillation modes. Increasing controller gain can either increase or decrease the damping ratios for these modes. Unfavorable control parameter change may reduce the damping ratio, therefore raising the stability concern.

The results clearly show that machines at DC terminal two and DC terminal three interact with each other through the MTHVDC systems. This proves that MTHVDC systems cannot isolate the oscillations and prevent oscillation prorogation from one side of the HVDC system to another. Like the synchronized AC system, oscillation can pass through the HVDC systems from one terminal to another.

5.4.5 Time Domain Simulation

To evaluate the controller performance, confirm suspected oscillations, and ensure the robust controller design, time-domain simulation must be performed to ensure that the controller performance meets the requirement and there is no stability concern. To do so, the electromagnetic transient simulation was performed for the MTHVDC test case shown

in Figure 5.2. The PSCAD study case, which is the same as in the MTHVDC interaction study, has been created with a rectifier in DC voltage controller, terminal-two inverter in DC current control, and terminal-three inverter in DC current control. The control parameters are also attached in Appendix A, which is the same as in the small-signal study cases. A 5% 100ms step change is applied to each controller reference. The results are as follows. Figure 5.47 and 5.48 show the DC voltage and DC current with a 5% 100ms step change on the terminal one DC voltage reference. The results indicate that the controller response quickly and the system is stable with no stability issues. Similarly, Figure 5.49 and 5.50 show the DC voltage and DC current with a 5% 100ms step change on the terminal two DC current reference. Figure 5.51 and 5.52 show the DC voltage and DC current with a 5% 100ms step change on the terminal three current reference. With the selected controller parameters, both small-signal study and time-domain study results demonstrate that the scheme two MTHVDC systems with the proposed control parameters is stable and no stability concern. (Note: T1, T2 and T3 in Figures 5.47-5..52 represent terminal one, terminal two and terminal three, respectively)

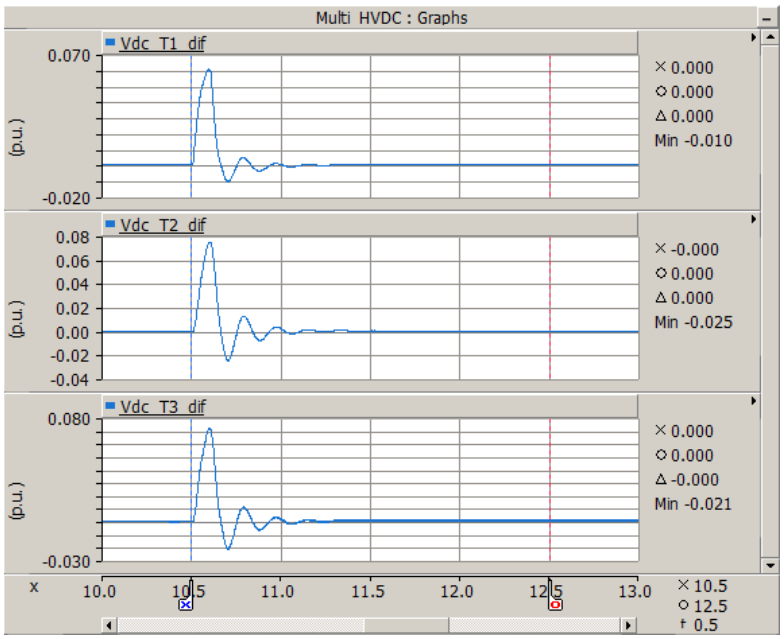

Figure 5.47 DC voltage responses – 5% 100ms step change on T1 DC voltage reference

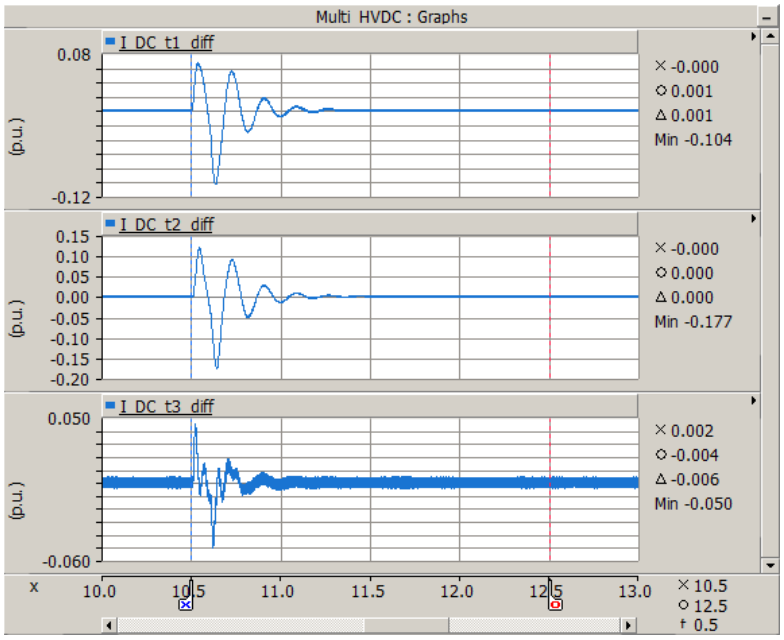

Figure 5.48 DC current responses - 5% 100ms step change on T1 DC voltage reference

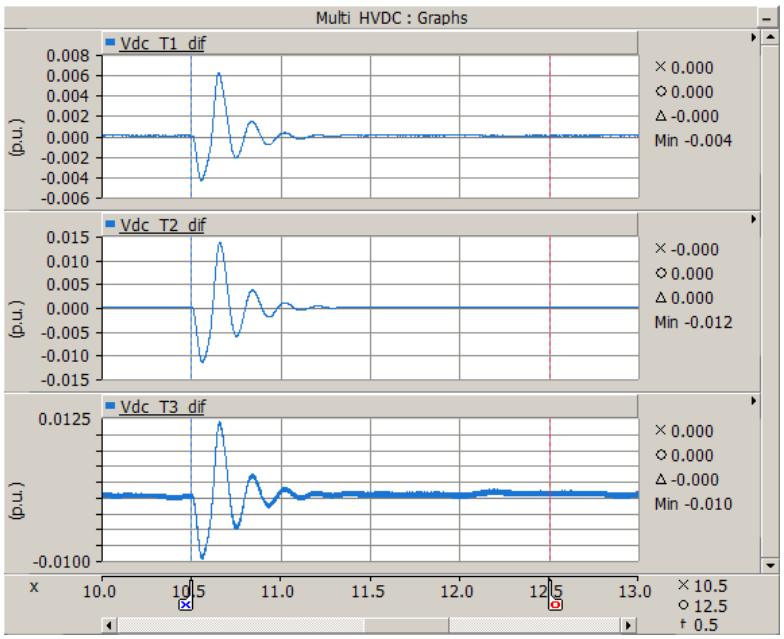

Figure 5.49 DC voltage responses - 5% 100ms step change on T2 DC current reference

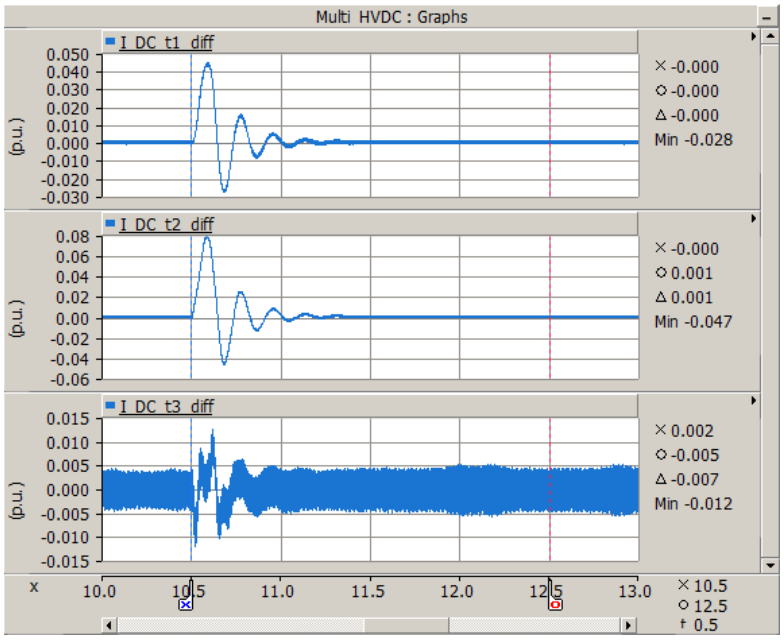

Figure 5.50 DC current responses - 5% 100ms step change on T2 DC current reference

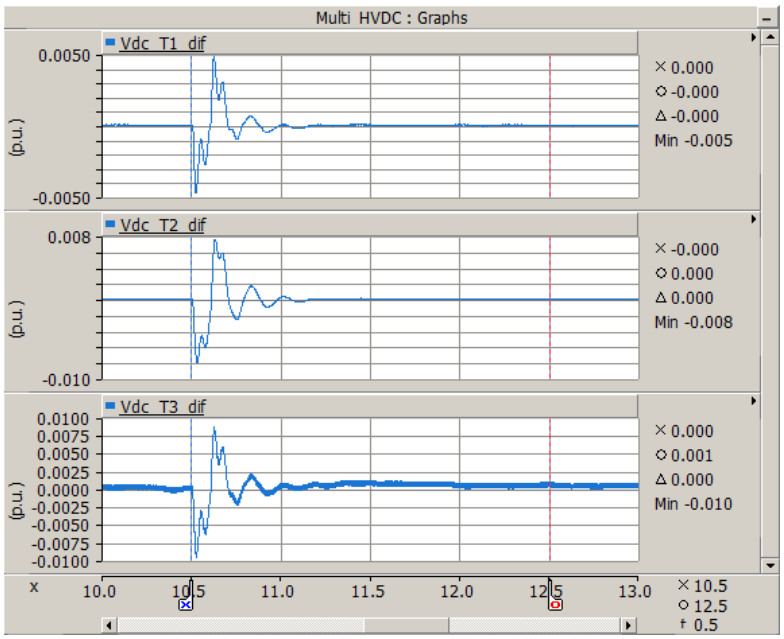

Figure 5.51 DC voltage responses - 5% 100ms step change on T3 DC current reference

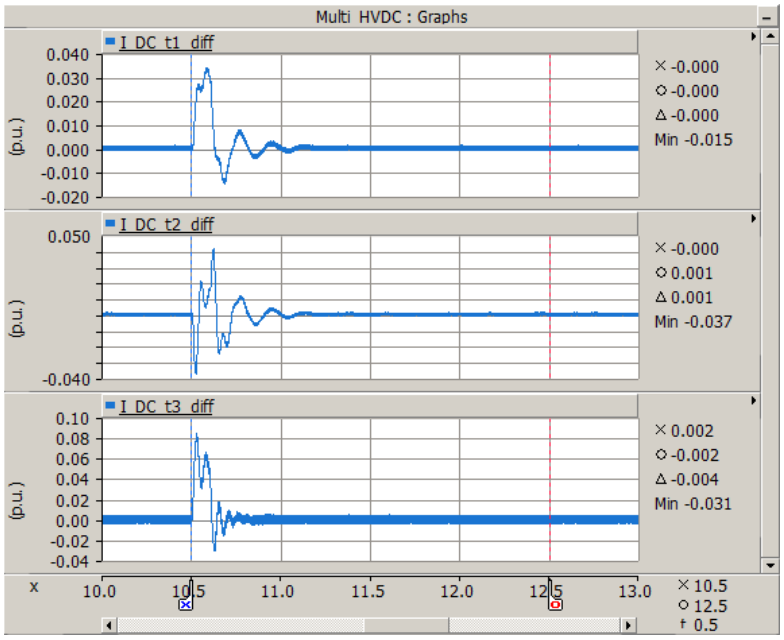

Figure 5.52 DC current responses - 5% 100ms step change on T3 DC current reference

5.5 Observation of MTHVDC System Interaction

In the previous section, each oscillation mode in the three-terminal HVDC system with different controller arrangements was discussed. This includes the mode shapes and participation factors for each oscillation mode. In this section, the comparison of each oscillation mode in the two control schemes will be discussed. The purpose is to identify the difference and find out which control scheme for the three-terminal HVDC system is more robust in terms of small-signal stability.

5.5.1 DC Network Resonance Modes

The oscillation frequency and the damping ratio for the three-terminal HVDC schemes are tabulated in Table 5.5 and Table 5.8. As shown in Table 5.9, both the oscillation frequencies and damping ratios for Mode-1 and Mode-1N are nearly identical. The major participation factors for both modes are also identical for all participants as shown in Figure 5.53. HVDC terminal voltages and currents, V_{dc_t1}, V_{dc_t2}, V_{dc_t3}, I_{dc_t1}, I_{dc_t2}, I_{dc_t3}, all participate in and dominate these two modes. However, the HVDC system controller state variables do not participate in these two modes. The results indicate that as long as the DC line length and DC smoothing reactor remain the same, and the HVDC system operates at the same (or very similar) operating point, the DC network interaction mode for these two schemes are almost identical. HVDC controller arrangement and controller gain have no (or very minor) impact on the DC network interaction oscillation mode.

The mode shapes in Figure 5.53 clearly show that the angle between each major participant for these two modes is very close.

Name	Mode-1	Mode-1N
Scheme	One	Two
Frequency (Hz)	224.00	224.11
Damping Ratio (%)	3.31	3.33
Major Participation	Vdc_t2(100%)	Vdc_t2(100%)
	Idcl_t2(77%)	Idcl_t2(77%)
	Idc_t2(39%)	Idc_t2(39.3%)
	Vdc_t4(13.9%)	Vdc_t4(13.9)

Table 5.9 Mode-1 and Mode-1N Network resonance modes comparison

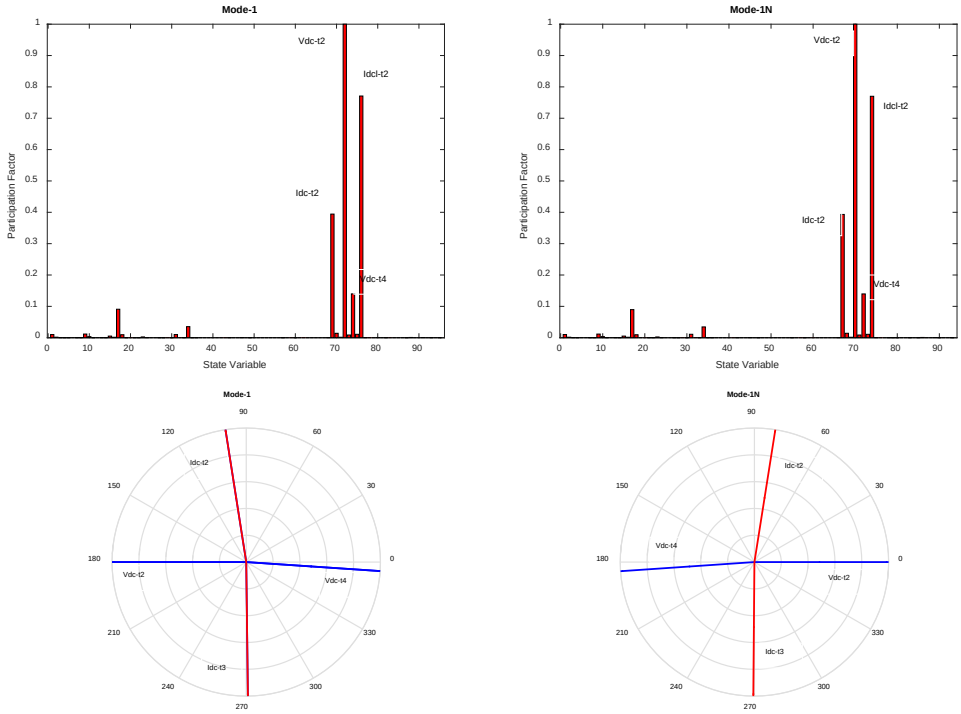

Figure 5.53 Participation factor and mode shape for Mode-1 and Mode-1N

As shown in Table 5.10, the oscillation frequencies, damping ratios and the major participation for Mode-2 and Mode-2N are nearly identical. MTHVDC system DC terminal voltage and DC current, V_{dc_t1} , V_{dc_t2} , V_{dc_t3} , I_{dc_t1} , I_{dc_t2} , I_{dc_t3} , participate in and dominate this mode. In addition, the terminal one DC controller state variable also participates in this mode. Although the relative participation factor for the DC controller

state variable is very small (1.2% for the DC current controller state variable in Mode-2, and 1.0% for the DC voltage controller state variable in Mode-2N), it influences the oscillation frequency and the damping ratio. As a result of the different controller arrangement, the oscillation frequency and damping ratio for Mode-2 and Mode-2N are slightly different. Consequently, changing the controller arrangement and controller gain will impact the oscillation frequency and damping ratio for this mode.

Mode shapes also indicate that the angles between each major participant of these two modes are the same.

Name	Mode-2	Mode-2N
Scheme	One	Two
Frequency (Hz)	118.00	118.95
Damping Ratio (%)	5.34	5.19
Major Participation	Vdc_t1(100%)	Vdc_t2(100%)
	Idcl_t1(63.6%)	Idcl_t1(62.8%)
	Idc_t1(35.3%)	Idc_t1(60.6%)
	Idc_t4(21.9%)	Vdc_t4(22.19)
	Xidc_t1(1.2%)	Xvdc_t1(1.0)

Table 5.10 Mode-2 and Mode-2N DC Network Interaction modes comparison

In conclusion, DC network resonance modes are dominated by DC quantities and have higher oscillation frequency. The DC controller arrangement, DC control parameter as well as the AC system have a very small impact on these modes due to the small participation of the corresponding state variables. On the other hand, the size of the smoothing reactor will impact the oscillation frequency and damping ratio. The larger the size of the smoothing reactor, the lower the oscillation frequency and damping ratio.

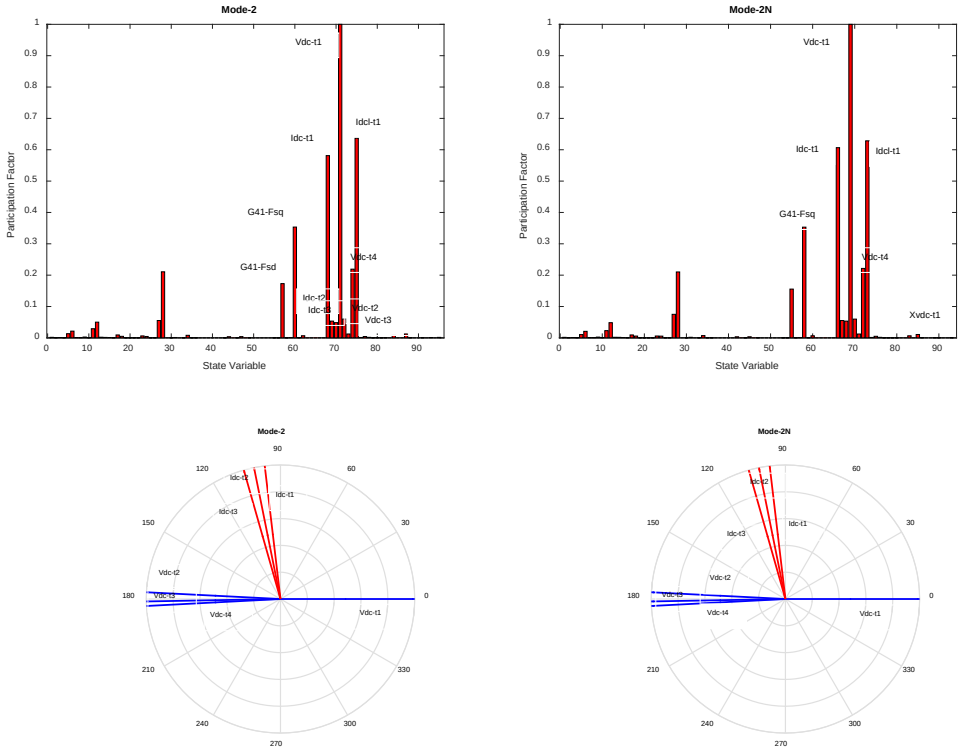

Figure 5.54 Participation factor and mode shape for Mode-2 and Mode-2N

5.5.2 AC-DC Interaction Modes

As shown in Table 5.11, similar state variables participate in Mode-3 and Mode-3N. Due to the different controller arrangements, the DC current controller state variable participates in Mode-3 and the DC voltage control state variable participates in Mode-3N. They have different participation factors in these two modes as shown in Table 5.11. A sensitivity study has been performed and the results indicate that Mode-3N is more sensitive to the control parameter change than Mode-3. In addition, the same state variables in these two modes also do not have the same participation factors. For example, the terminal one DC current state variable has a participation factor of 0.55 in Mode-3 and a participation factor of 0.41 in Mode-3N. Similarly, for terminal three DC current, the

participation factor is 0.27 in Mode-3 and 0.43 in Mode-3N. Further investigation into the participation factors reveals that the DC voltage participation and the AC system voltage participation are also different for these two modes. As a result, these two modes have a slightly different oscillation frequency and damping ratio. The mode shape shown in Figure 5.55 appears such that the relative angle differences between major participants for Mode-3 and Mode-3N are almost identical. Regardless of the difference in oscillation frequency and damping ratio, the mode shapes indicate that Mode-3 and Mode-3N are the same oscillation mode. Therefore, it is concluded that the controller arrangement does not change the oscillation mode. However, the controller arrangement does impact the AC-DC interaction oscillation frequency and the damping ratio.

Name	Mode-3	Mode-3N
Scheme	One	Two
Frequency (Hz)	76.59	82.64
Damping Ratio (%)	19.63	16.26
Major Participation	Vdc_t4(100%)	Vdc_t4(100%)
	G41_Fsq(68.8%)	G41_Fsq(55.7%)
	Idc_t1(55.2%)	Idc_t3(43.4%)
	VI_bus42(47%)	Idc_t1(41.2%)
	Idc_t3(27.1%)	VI_bus42(35.7%)
	VR_bus42(33.9%)	VR_bus42(29.5%)
	Xidc_t1(7.1%)	Xvdc_t1(6.8%)

Table 5.11 Mode-3 and Mode-3N AC-DC Network Interaction Modes Comparison

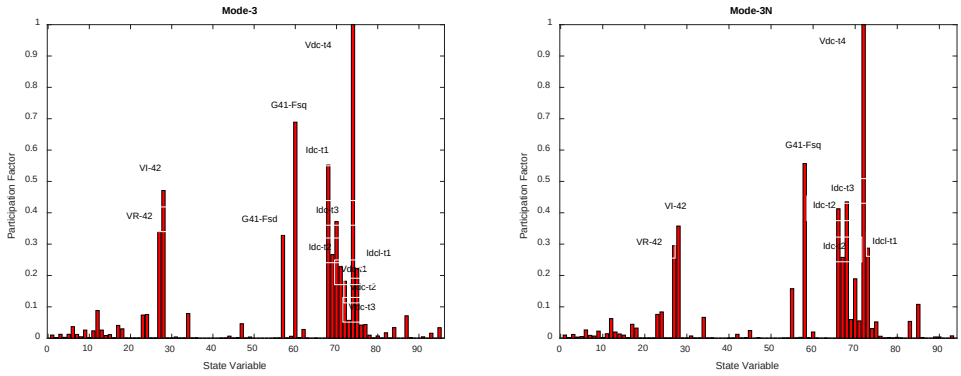

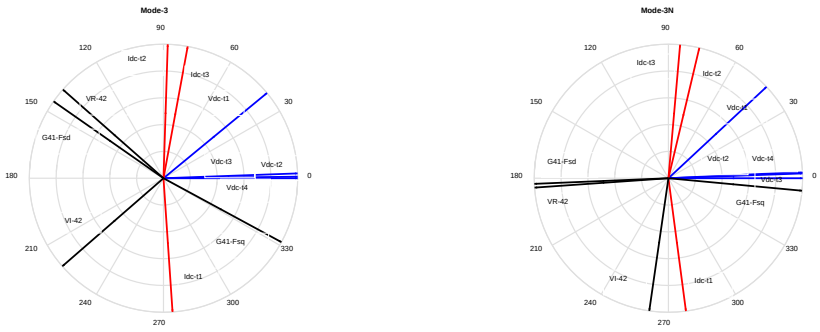

Figure 5.55 Participation factor and mode shape for Mode-3 and Mode-3N

In summary, AC voltage, DC voltage, and DC current participate and dominate the AC-DC interaction mode with the controller state variable has minor participation. As a result, this mode is largely influenced by the AC system strength and DC system loading. The controller arrangement and parameter change slightly impact the oscillation frequency and damping ratio. However, it does not change the mode shape.

5.5.3 Controller Interaction Mode

In terms of the controller interaction, there are three controller interaction modes in each control scheme. Mode-4, Mode-5, and Mode-6 in scheme one as listed in Table 5.12 and Mode-4N, Mode-5N, and Mode-6N in scheme two as listed in Table 5.13. The detailed comparison for each mode will be discussed:

Mode-4 and Mode-4N:

These two oscillation modes have similar oscillation frequency and damping ratios. They are dominated by the terminal one DC controller state variables with a small participation of the other two terminal controller state variables. In Mode-4, HVDC quantities such as DC currents and the smoothing reactor state variables also highly participate in this mode. Mode shape shows that terminal one and terminal two DC current

controller state variables oscillate together against the terminal three DC voltage controller state variable. A sensitivity study has been performed and the results indicate that this mode is sensitive to terminal one DC current controller gain. Both the oscillation frequency and damping ratio of this mode change significantly when the terminal one DC current controller gains change. Further investigation on participation factors indicates that the controller state variable participation factor changes dramatically when the controller gain changes. Therefore, an appropriately selected controller gain is required to ensure stability.

Name	Mode-4	Mode-5	Mode-6
Scheme	One	One	One
Frequency (Hz)	13.00	10.33	3.59
Damping Ratio (%)	33.94	33.80	40.97
Major Participation	Xidc_t1(100%)	PLLx1_t3(100%)	Xvdc_t3(100%)
	Idcl_t1(49.8%)	Xvdc_t3(44.8%)	Xidc_t2(65.7%)
	PLLx1_t3(40.6%)	Xidc_t1(35.4%)	PLLx1_t2(50.8%)
	Idc_t1(30.3%)	Idc_t2(36.9%)	Xidc_t1(19.7%)
	Idc_t3(21.0%)	Idc_t3(29.6%)	Idc_t3(17.5%)
	Xvdc_t3(10.6%)	Xidc_t2(23.5%)	Idc_t2(11.3%)

Table 5.12 HVDC controller interaction modes-Scheme one

Name	Mode-4N	Mode-5N	Mode-6N
Scheme	Two	Two	Two
Frequency (Hz)	51.3	7.64	3.34
Damping Ratio (%)	31.06	12.34	7.03
Major Participation	Xvdc_t1(100%)	Xidc_t3(100%)	Xidc_t2(100%)
	G41_Fsq(98.6%)	Xidc_t2(95.4%)	Xvdc_t1(92.3%)
	Vdc_t1(70.4%)	PLLx1_t3(80.3%)	PLLx1_t2(58.7%)
	VI_bus42(63.6%)	Idc_t3(78.0%)	PLLx1_t3(58.1%)
	G41_Fsd(60.2%)	Idc_t2(72.6%)	Xidc_t3(49.1%)
	Vdc_t4(38.3%)	Idcl_t2(44.5%)	Idc_t2(16.6%)

Table 5.13 HVDC controller interaction modes – Scheme two

In Mode-4N, HVDC terminal DC voltage and terminal one AC system voltage, as well as terminal one generator state variables highly participate in this mode.

Mode shape shows that the terminal one DC voltage controller state variable, the terminal two DC current controller state variable, and the terminal three controller state variable oscillate together. Upon increasing terminal one DC voltage controller proportion gain, the participation of terminal one DC voltage controller state variable drops significantly, and the oscillation frequency increases. Upon further increase of the DC voltage controller gain, the DC voltage controller state variable participation factor further reduces, and the mode becomes a DC network oscillation mode with an oscillation frequency around 70Hz. The tendency toward becoming a DC network oscillation mode is increased by increasing the voltage controller proportion gain and by increasing the AC side system strength. On the other hand, this mode is always dominated by the DC voltage controller state variable when increasing the integral gain of the DC voltage controller. However, the damping ratio will be significantly decreased due to the increase of integral gain. A sensitivity study has been conducted, and the results indicate that the oscillation frequency lies between 50-70 Hz with different controller gain combinations. The results also prove that the controller state variable participation factor changes dramatically with changes in the integral gain. This mode is very sensitive to the controller parameter setting. For an HVDC system connected to a remote generating station, a load rejection at the inverter station may cause the frequency at the rectifier end to increase to a higher level. In Manitoba Hydro, the Northern Collector System (NCS) experiences frequency excursions up to 84Hz. Under this situation, the controller interaction mode (between 50-70Hz) may interact with the power system equipment and cause oscillation/power system resonance to occur.

Based on the above analysis, it is concluded that Mode-4N is very sensitive to the controller parameter selection. It is vulnerable to interactions with the system and can cause power system resonance to occur.

Mode-5 and Mode-5N:

These two oscillation modes have similar oscillation frequency and damping ratios. They are dominated by the terminal three controller state variables. Due to different controller arrangement, Mode-5 is dominated by the terminal three DC voltage controller state variable, terminal three PLLs, and the terminal one and terminal two DC current controller state variables. Mode shape shows that terminal one DC current controller state variable always oscillates against the terminal three DC voltage controller state variable. On the other hand, Mode-5N in scheme two is dominated by the terminal three DC current controller state variable and terminal two DC current controller state variable. Mode shape shows that these two DC current controller state variables always oscillate against each other. In Mode-5N, both DC current controllers are located at inverter stations. It implies that if one inverter requires DC current increase, the other inverter DC current controller also responses to this requirement and decreases its DC current order. Improperly selected control parameters may enhance this oscillation and make the three-terminal HVDC system unstable. Based on the above analysis, it is concluded that Mode-5N is sensitive to the controller parameter selection and operating point change.

Mode-6 and Mode-6N:

These two oscillation modes have similar oscillation frequency and damping ratios. All three HVDC controller state variables participate in and dominate these modes. In Mode-6, the terminal one DC current controller state variable oscillates against the terminal two

DC current controller state variable and the terminal three DC voltage controller state variable.

In Mode-6N, the terminal two DC current controller state variable oscillates together with the terminal three DC current controller state variable. Since both DC current controllers are located at inverter stations in control scheme two. It implies that if one inverter requires DC current increase, the other inverter DC current controller also responds to this requirement and increases its DC current order. Improperly selected control parameters may enhance this oscillation mode and make the three-terminal HVDC system unstable.

Based on the above analysis, it was observed that all controller state variables and HVDC quantities participate in the controller interaction oscillation mode. Depending on the controller arrangement and parameter selection, the relative participation factor for each controller state variable is different. Each mode is dominated by a different controller state variable and hence has a different oscillation pattern, different oscillation frequency and damping ratio. The study results indicate that controller parameters significantly impacts these controller interaction modes.

5.5.4 Electromechanical Oscillation Modes

For the electromechanical oscillation modes, there are three electromechanical oscillation modes in each scheme. (Mode-7, Mode-8, and Mode-9 in scheme one and Mode-7N, Mode-8N, and Mode-9N in scheme two). The oscillation frequencies are all below 3 Hz and they have enough damping ratio. In all of these oscillation modes, the generator rotor speed and rotor angle participate in and dominate these modes. HVDC

controller state variables also participate in these modes with a relatively small participation factor.

Mode-7 and Mode-7N:

Figure 5.56 shows the participation and mode of Mode-7 and Mode-7N. In both oscillation modes, the terminal-three generator 36 rotor speed state variable and terminal two generator 35 rotor speed state variable oscillate together. Generator 35 and 36 rotor angle state variables also oscillate together. Comparing the mode shape of these two oscillation modes, it is found that similar state variables participate in these two modes and they have similar mode shapes. The participation factors comparison also indicates that each state variable has slightly different participation in these two oscillation modes. Therefore, the oscillation frequencies and damping ratios for these two modes are slightly different. However, they are the same electromechanical oscillation modes.

Name	Mode-7	Mode-7N
Scheme	One	Two
Frequency (Hz)	1.29	1.41
Damping Ratio (%)	2.70	4.61
Major Participation	G36_wr(100%)	G35_ang(100%)
	G36_ang(96.5%)	G35_wr(99.3%)
	G35_wr(25%)	G36_wr(76.9%)
	G35_ang(24.4%)	G36_ang(74.4%)
	Xvdc_t3(12.4%)	Xidc_t2(29.2%)
	Xidc_t2(5.5%)	Xidc_t3(9.5%)
		Xvdc_t1(7.5%)

Table 5.14 Mode-7 and Mode-7N comparaison

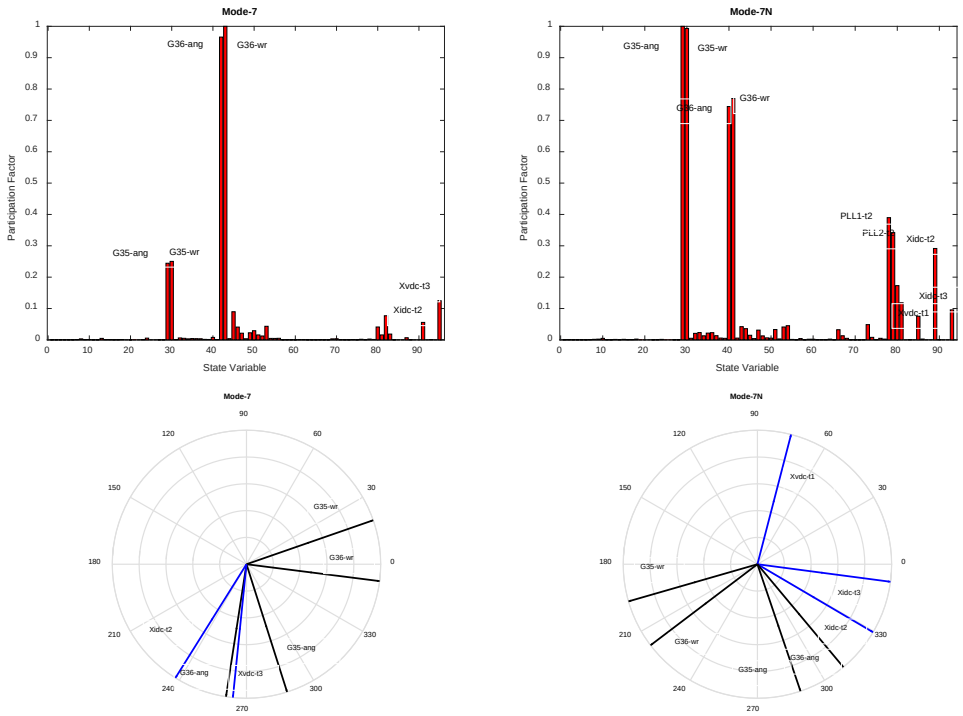

Figure 5.56 Participation factor and mode shape for Mode-7 and Mode-7N

Mode-8 and Mode-8N:

Figure 5.57 shows the participation factors and mode shapes of Mode-8 and Mode-8N. As listed in Table 5.15, similar machine state variables and HVDC controller state variables participate in these two modes. Due to different HVDC controller arrangements and control parameters, the oscillation frequencies, damping ratio, as well as mode shapes are slightly different for these two modes.

Further investigation indicates that when either DC voltage controller or DC current controller integral gain are adjusted, the damping ratio of these modes changes. Depending on the participation of the controller state variables, the influence of the controller gain on the damping ratio is different. For example, the terminal two DC current controller state variable has large participation in Mode-8 of 0.51 as shown in Table 5.14, increasing the

integral gain from 50 to 100 and decreasing participation of terminal two DC current controller state variable to 0.12. The damping ratio changes from 24.13% to 3.4%. Upon further increase of the integral gain, the damping ratio of this mode becomes negative and the MTHVDC system becomes unstable. However, with a change in the integral gain, the mode shape of this mode remains unchanged.

Mode-9 and Mode-9N:

Figure 5.58 shows the participation factors and mode shapes of Mode-9 and Mode-9N. As listed in Table 5.16, similar machine state variables and HVDC controller state variables participate in these two modes. Due to different HVDC controller arrangements and control parameters, the oscillation frequencies, damping ratio, as well as mode shapes are slightly different for these two modes. Depending on the participation of the controller state variables, the influence of the controller gain on the damping ratio is different.

A similar analysis has been conducted, and the same conclusion can be made that changing controller integral gain will change the oscillation frequency and damping ratio. Therefore, it can be concluded that the controller action does affect the performance of the electromechanical mode. The damping ratio may be improved by changing the participant controller gain.

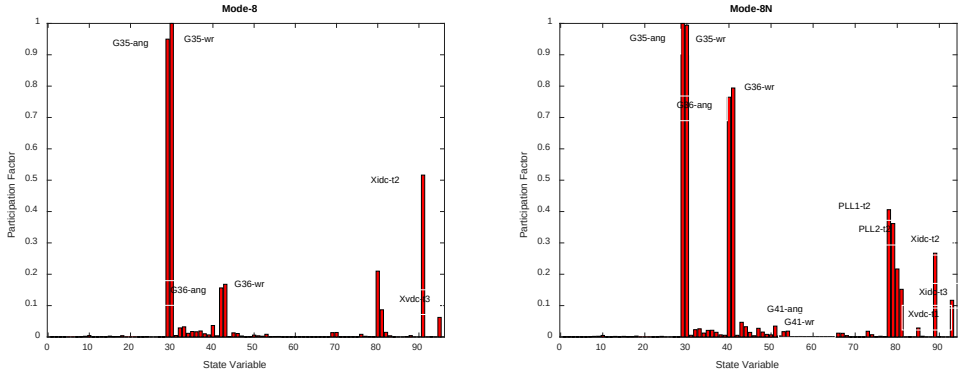

Figure 5.57 Participation factor and mode shape for Mode-8 and Mode-8N

Name	Mode-8	Mode-8N
Scheme	One	Two
Frequency (Hz)	1.26	1.37
Damping Ratio (%)	24.13	6.48
Major Participation	G35_wr(100%)	G35_ang(100%)
	G35_ang(94.9%)	G35_wr(99.4%)
	Xidc_t2(51.6%)	G36_wr(79.4%)
	G36_wr(16.7%)	G36_ang(76.4%)
	G36_ang(15.6%)	Xidc_t2(26.7%)
	Xvdc_t3(6.2%)	Xidc_t3(11.6%)
		Xvdc_t1(2.8%)

Table 5.15 Mode-8 and Mode-8N comparaison

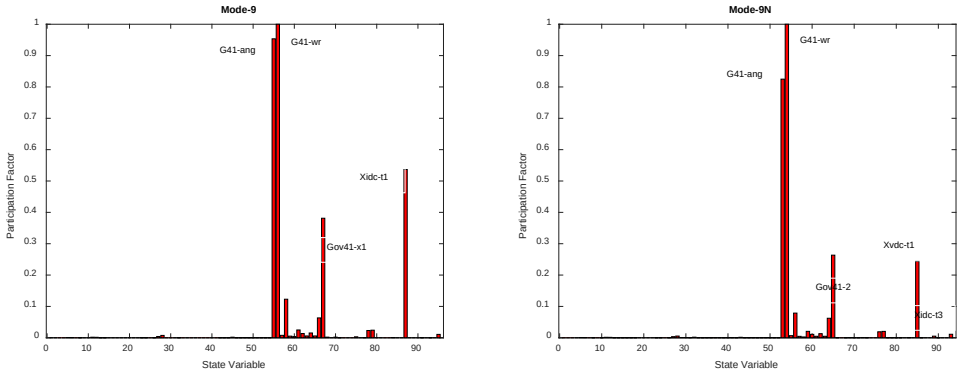

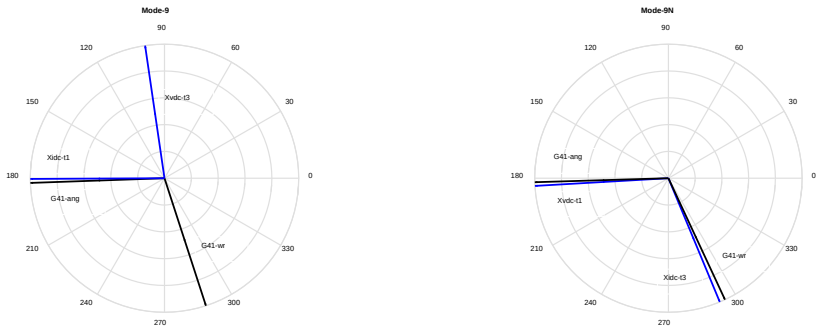

Figure 5.58 Participation factor and mode shape for Mode-9 and Mode-9N

Name	Mode-9	Mode-9N
Scheme	One	Two
Frequency (Hz)	0.16	0.19
Damping Ratio (%)	29.80	36.33
Major Participation	G41_wr(100%)	G41_wr(100%)
	G41_ang(95.0%)	G41_ang(82.4%)
	Xidc_t1(53.6%)	XVdc_t1(24.4%)
	Xvdc_t3(1.0%)	PLLx1_t1(2.0%)
	PLLx1_t1(0.5%)	PLLx2_t1(1.9%)
	PLLx2_t1(0.3%)	Xvdc_t3(1.1%)

Table 5.16 Mode-9 and Mode-9N comparison

In summary, machine rotor speed and angle state variables dominate these electromechanical oscillation modes. The HVDC controller state variables also participate in these modes. Therefore, the HVDC system controller arrangement and control parameter selection impact the electromechanical oscillation frequencies and damping ratios. Improperly selected controller parameters may cause the electromechanical oscillation to become unstable. It further demonstrates that the MTHVDC controller can be tuned to improve the electromechanical oscillation damping. The results also clearly show that machines at different terminals interact with each other through MTHVDC

systems. It proves that the MTHVDC system cannot isolate the oscillations and prevent the oscillation prorogation from one side of the HVDC system to the other.

5.6 Chapter Summary

In this chapter, the general study procedure to analyze MTHVDC system controller interactions is proposed. This procedure has five steps, they are:

1. Power System Load Flow Data Preparation
2. Power System Dynamic Data Preparation
3. Eigenvalue Analysis
4. Evaluation Criteria
5. Oscillation Analysis and Mode Identification
    a. Examing the oscillation frequency and damping ratio
    b. Participation analysis
    c. Mode shape analysis
    d. Additional consideration

Following the proposed analysis method, the MTHVDC system interactions for the three-terminal MTHVDC system with two different controller arrangements have been conducted. Detailed study results for each oscillation mode of these two three-terminal HVDC control schemes are provided.

The results show that machines at different terminals interact with each other through MTHVDC systems. It proves that HVDC systems cannot isolate the oscillations and prevent oscillation propagation from one side of the HVDC system to the other. The results also demonstrate that the damping ratio for the electromechanical oscillation can be improved by changing the HVDC controller parameter.

In addition, the results also show that different controller arrangements have a different impact on each oscillation mode, with a minor impact on the DC network resonance mode and a significant impact on the DC controller interaction mode. As a result, the oscillation frequency, damping ratio, and mode shape all change. It has a noticeable impact on both the AC-DC interaction and the electromechanical oscillation mode. By comparing control schemes one and two, it is concluded that the controller arrangement scheme one is more robust than scheme two.

Chapter 6: Impact of the System Strength to Controller Interaction

6.1 Introduction

In power systems, system strength has a major impact on system stability. In the HVDC system, AC/DC system interactions and the associated HVDC system issues are dependent upon the strength of the AC system relative to the capacity of the DC link [67]. For an AC system connected with only one single HVDC link, the effective short-circuit ratio (ESCR) is used to define the AC system strength [68]. It is defined as:

$$ESCR = \frac{S - Q_c}{P_d}$$

Where S is AC system short-circuit capacity.

Q_c is the total AC filters and shunt capacitors at the converter station.

P_d is the DC-link power.

The ESCR allows for the presence of AC filters and shunt capacitors at the converter terminals. Typically, it is classified as a weak AC system if the ESCR is less than 3. It is classified as a moderate system if the system with ESCR is between 3 and 5. Any system with ESCR greater than 5, is classified as a strong AC system. When an HVDC line is connected to weak AC systems, issues such as high dynamic voltages, voltage instability, harmonic resonance, and HVDC system interactions may occur. These oscillations will be generally affected by the network strength and topology as well as the control parameters.

In this chapter, the change in the controller interaction oscillation with different system strengths for both control schemes is studied. Both the oscillation frequency and damping

ratio of each controller mode related to system strength are investigated. As indicated in Chapter 5, both participation factor and mode shapes for each oscillation modes are examined. Scenarios with different system configurations, different controller parameters as well as different operating point have been considered. The system strength is adjusted by changing the generator MVA rating while maintaining the sub-transient impedance. For the rectifier side AC system, the generator rating is changed from 1800MVA to 7200 MVA, which corresponds to the ESCR of 1.88 to 6.89. For the terminal two side AC system, the generator rating is changed from 600MVA to 2000MVA, which corresponds to the ESCR of 2.23 to 6.23. For terminal three side AC systems, the generator rating is changed from 1000MVA to 4000MVA, which corresponds to the ESCR of 1.93 to 6.02. In each study scenario, the HVDC line configurations, controller arrangement, and controller parameters remain unchanged. The study results for each of the control schemes are summarized in the following sections. The three-terminal HVDC test systems are shown in Figure 5.2 and G1, G2 and G3 represent the equivalent AC system for each terminal of the three-terminal HVDC systems.

6.2 System Strength Impact on Controller Interaction-Scheme One

In this research, HVDC line configurations, HVDC controller parameter settings, and HVDC system operating point variations have been considered for different system strengths. The detailed analysis results of all three controller interaction modes in the original three-terminal HVDC systems are provided. In the original system, terminal one and terminal two are in DC current control mode, and terminal three controls the DC

voltage. The line length between terminal one and the line tap point is about 800km, it is about 400km between terminal two and the line tap point, and it is about 100km between terminal three and the line tap point. Table 6.1 shows the controller interaction oscillation frequencies and damping ratios for different AC system strength. Correspondingly, Table 6.2 and Table 6.3 show participation factors result and mode shape angles between controller state variables for all oscillation modes with different AC system strength. It is noted that T1 PF, T2 PF and T3 PF in all participation factor analysis tables represent the terminal one, terminal two and terminal three controller state variable participation factor, respectively.

System Strength			Mode-4		Mode-5		Mode-6	
T1 (MVA)	T2(MVA)	T3(MVA)	Frequency (Hz)	Damping (%)	Frequency (Hz)	Damping (%)	Frequency (Hz)	Damping (%)
1800	600	1000	12.71	30.62%	11.43	39.72%	4.55	50.77%
3600	600	1000	12.53	19.40%	10.90	42.75%	4.54	49.67%
5400	600	1000	12.41	17.25%	10.82	42.99%	4.52	49.40%
7200	600	1000	12.34	16.31%	10.79	43.08%	4.51	49.27%
1800	600	1000	12.71	30.62%	11.43	39.72%	4.55	50.77%
1800	1000	1000	12.66	33.33%	10.85	42.19%	4.12	45.21%
1800	1500	1000	12.67	34.07%	10.58	44.20%	3.95	40.66%
1800	2000	1000	12.68	34.35%	10.46	45.27%	3.90	38.31%
1800	600	1000	12.71	30.62%	11.43	39.72%	4.55	50.77%
1800	600	2000	13.09	29.05%	8.88	37.41%	3.28	78.61%
1800	600	3000	13.11	29.73%	8.40	33.64%	1.48	94.68%
1800	600	4000	13.11	28.60%	8.23	31.82%	0.92	97.27%

Table 6.1 Frequency and damping ratio - original system

System Strength	Mode-4			Mode-5			Mode-6		
T1 /T2/T3 (MVA)	T1 PF	T2 PF	T3 PF	T1 PF	T2 PF	T3 PF	T1 PF	T2 PF	T3 PF
1800/600/1000	1.000	0.064	0.127	0.511	0.049	0.460	0.337	0.419	1.000
3600/600/1000	1.000	0.120	0.026	0.243	0.040	0.487	0.368	0.421	1.000
5400/600/1000	1.000	0.132	0.016	0.211	0.042	0.491	0.375	0.421	1.000
7200/600/1000	1.000	0.138	0.014	0.198	0.042	0.493	0.379	0.421	1.000
1800/600/1000	1.000	0.064	0.127	0.511	0.049	0.460	0.337	0.419	1.000
1800/1000/1000	1.000	0.037	0.122	0.360	0.079	0.492	0.238	0.789	1.000
1800/1500/1000	1.000	0.031	0.117	0.307	0.091	0.502	0.192	1.000	0.965
1800/2000/1000	1.000	0.029	0.115	0.287	0.097	0.506	0.161	1.000	0.870
1800/600/1000	1.000	0.064	0.127	0.511	0.049	0.460	0.337	0.419	1.000
1800/600/2000	1.000	0.051	0.020	0.362	0.246	0.597	0.196	0.137	0.648
1800/600/3000	1.000	0.054	0.013	0.395	0.368	0.509	0.070	0.060	0.202
1800/600/4000	1.000	0.055	0.012	0.378	0.389	0.419	0.040	0.090	0.130

Table 6.2 Participation Factors for each oscillation mode- original system

System Strength	Mode-4			Mode-5			Mode-6		
T1 /T2/T3 (MVA)	T1-T2 Ang	T2-T3 Ang	T3-T1 Ang.	T1-T2 Ang	T2-T3 Ang	T3-T1 Ang.	T1-T2 Ang	T2-T3 Ang	T3-T1 Ang.
1800/600/1000	44.00	120.70	195.30	115.80	73.10	171.10	136.70	89.69	133.61
3600/600/1000	16.90	119.10	224.00	166.90	45.70	147.40	135.91	90.42	133.67
5400/600/1000	12.60	122.80	224.60	173.66	41.94	144.40	136.38	90.78	132.84
7200/600/1000	10.00	127.00	223.00	176.30	40.60	143.10	136.62	90.83	132.55
1800/600/1000	44.00	120.70	195.30	115.80	73.10	171.10	136.70	89.69	133.61
1800/1000/1000	38.52	148.00	173.48	104.30	70.20	185.50	143.40	86.76	129.84
1800/1500/1000	33.40	159.60	167.00	98.00	71.30	190.70	149.48	83.70	126.82
1800/2000/1000	31.34	164.66	164.00	96.09	70.81	193.10	152.80	81.60	125.60
1800/600/1000	44.00	120.70	195.30	115.80	73.10	171.10	136.70	89.69	133.61
1800/600/2000	21.00	152.30	186.70	164.40	16.90	178.70	111.80	87.40	160.80
1800/600/3000	18.60	137.90	203.50	174.60	0.60	184.80	62.90	117.60	179.50
1800/600/4000	18.08	125.32	216.60	178.70	10.80	170.50	43.70	125.30	191.00

Table 6.3 Mode shapes for each oscillation mode- original system

Terminal one AC system strength variation

Mode-4:

As shown in Table 6.1, the oscillation frequencies and damping ratios for all three controller interaction modes change when the terminal one AC system strength is increased. The oscillation frequency of Mode-4 decreases from 12.71Hz to 12.34Hz and the damping ratio drops from 30.62% to 16.31%. By examining the participation factor of this mode, it is revealed that the terminal one AC system strength significantly impacts the damping ratio of Mode-4. This is because this mode is dominated by the terminal one current

controller state variable, which has the highest participation factor of 1.0 for all study scenarios. On the other hand, the participation factors for the other two terminal controller state variables vary with terminal one AC system strength. As shown in Table 6.2, the terminal two current controller state variable participation factor increases from 0.064 to 0.138, and the terminal three voltage controller state variable participation factor decreases from 0.127 to 0.014. Table 6.3 provides the mode shape angles between each controller state variable. In this mode, the terminal one current controller state variable and terminal two current controller state variable oscillate together against the terminal three voltage controller state variable. When terminal one AC system strength is increased from 1800MVA to 3600MVA, the angle between terminal one and terminal two current controller state variables decreases from 44 degrees to 16.9 degrees. When the terminal one AC system strength is further increased to 7200MVA, the angle between these two controller state variables further decreases to approximately 10 degrees. On the other hand, the angle between the terminal two current controller state variable and the terminal three voltage controller state variable slightly decreases from 120.7 degrees to 119.1 degrees when the terminal one AC system strength increases from 1800MVA to 3600MVA. Further increasing terminal one AC system strength to 7200VMA, increases the angle between these two controller state variables from 119.1 degrees to 127 degrees. Similarly, the angle between the terminal three voltage controller state variable and the terminal one current state variable increases from 195.3 degrees to 224.6 degrees when AC system strength increases from 1800MVA to 5400MVA. Further increasing terminal one AC system strength causes the angle between these two controller state variables to decrease to 223.0 degrees. Even though the mode shape angle changes between each control state

variable, the oscillation mode for Mode-4 remains the same. This mode has enough damping ratio and has no small signal stability concerns for all study scenarios.

Mode-5:

The study results also show that the other two controller oscillation modes change due to the rectifier side AC system strength change. As shown in Table 6.1, the oscillation frequency for Mode-5 slightly decreases from 11.43Hz to 10.79Hz and the damping ratio slightly increases from 39.72% to 43.08%. When the terminal one AC system strength increases from 1800MVA to 7200MVA, the participation factor of the terminal one current controller state variable decreases from 0.511 to 0.198, and the terminal two current controller state variable participation factor drops from 0.049 to 0.042, and the terminal three voltage controller state variable participation factor increases from 0.46 to 0.493. Mode shape results in Table 6.3 indicate that the mode shape angle between terminal one current controller and terminal two current controller state variables increases from 115.8 degrees to 176.3 degrees and the angle between the terminal two current controller and terminal three voltage controller state variables decreases from 73.1 degrees to 40.60 degrees. Similarly, the angle between the terminal three voltage controller and the terminal one current controller state variables decreases from 171.1 degrees to 143.1 degrees. Although the angle between each controller state variable changes, the oscillation mode for Mode-5 remains unchanged as the terminal one current controller state variable oscillates against the terminal two current controller state variable and the terminal three voltage controller state variable. As a result, both the oscillation frequency and damping ratio change slightly due to the terminal one AC system strength change. The results show

that this mode has enough damping ratio and has no small signal stability concerns for all study scenarios.

Mode-6:

As shown in Table 6.1, Mode-6 oscillation frequency slightly decreases from 4.55Hz to 4.51Hz and the damping ratio decreases from 50.77% to 49.27%. The participation factor of the terminal one current controller state variable slightly increases from 0.337 to 0.379, and the terminal two current controller state variable participation factor slightly increases from 0.419 to 0.421. On the other hand, the participation factor of the terminal three voltage controller state variable remains unchanged with the highest participation of 1. Mode shape indicates that the angle between terminal one and terminal two current controller state variables slightly decreases from 136.7 degrees to 135.91 degrees when terminal one AC system strength increases to 3600MVA. Further increasing terminal one AC system strength to 7200MVA increases this angle to 136.62 degrees. On the other hand, the angle between the terminal two current controller state variable and the terminal three voltage controller state variables increases from 89.69 degrees to 90.83 degrees when terminal one AC system strength increases to 7200MVA. The angle between the terminal three voltage controller state variable and the terminal one current controller state variable increases from 133.61 degrees to 133.67 degrees when terminal one AC system strength increases to 3600MVA. Further increasing terminal one AC system strength to 7200MVA decreases the angle between these two state variables changes from 133.67 degrees to 132.55 degrees. The results indicate that the angle between each terminal controller state variable slightly changes and that terminal one AC system strength has a minor impact on this oscillation mode. Therefore, the oscillation mode remains unchanged with the terminal

one current controller state variable oscillating against both the terminal two current controller and the terminal three voltage controller state variables. These results further prove that all three controllers interact with each other and that the participation factors for each state variable as well as the mode shape are all impacted by the system strength. However, this mode has enough damping ratio and has no small signal stability concerns for all study scenarios.

Similar analysis has been performed with the terminal two AC system and terminal three AC system strength change. The results are provided in Appendix C1. In addition, the AC system strength impact on the three-terminal HVDC system with different HVDC line tap points, different control parameters, and different operation points have been conducted. The results are also provided in Appendix Table C1.4-C1.12. All the results show some similarity in response to AC system strength change. Based on the results, it is observed that:

1. Mode-4 is dominated by the terminal one current controller state variable. Regardless of which terminal AC system strength changes, the participation factor of the terminal one current controller state variable always remains at the highest value of 1.0. Mode shape results show that angles between each controller state variable changes when AC system strength changes. However, the mode shape remains the same as the terminal one current controller state variable and terminal two current controller state variable oscillate together against the terminal three voltage controller state variable. Therefore, any AC system strength change impacts both the oscillation frequency and the damping ratio.

2. In Mode-5, both the terminal one current controller state variable and the terminal three voltage controller state variable have a relatively high participation factor. Regardless of whichever terminal AC system strength changes, the participation factors of all controller state variables change. Mode shape results show that angles between each controller state variable also change when the AC system strength change. However, mode shape remains the same as the terminal one current controller state variable oscillates against the terminal two current controller state variable and terminal three voltage controller state variable. The study results indicate that both the oscillation frequency and the damping ratio of this mode change when AC system strength changes.
3. Mode-6 is dominated by the terminal three voltage controller state variable. Regardless of which terminal AC system strength changes, the participation factors of all controller state variables change. Participation analysis results indicate that the participation factor of the terminal three voltage controller state variable decreases significantly from 1.0 to 0.13 when the terminal three AC system strength increases. Mode shape results show that angles between each controller state variable also change when AC system strength changes. However, the consequences are different with different AC system strength changes. For terminal one and terminal two AC system strength change, the angle between each controller state variable slightly changes. The oscillation mode remains the same as the terminal one controller state variable oscillates against the terminal two current controller state variable and terminal three voltage controller state variable. For terminal three AC system strength change, angles between each controller state

variable change significantly. If terminal three AC system strength is strong enough, the oscillation mode will change from the terminal one controller state variable oscillating against the terminal two current controller state variable and terminal three controller state variable to the terminal one current controller state variable and terminal two current controller state variables oscillating together against the terminal three controller state variable. As explained in the analysis, the oscillation mode is completely changed. The controller state variable is no longer the major participant. The AC system equivalent machine state variable becomes the dominant participate. This mode becomes an electromechanical oscillation mode and HVDC controller state variables have minor participation. This mode has enough damping ratio and has no small signal stability concerns in all study scenarios.

6.3 System Strength Impact on Controller Interaction-Scheme Two

A similar study has been performed for control scheme two. In this scheme, terminal one is the rectifier converter terminal which is in DC voltage control mode. The other two inverter terminals are all controlled by DC current controllers. Each terminal AC system strength has been changed to examine the impact on the controller interaction mode. Similar to the study procedure in control scheme one, terminal one rectifier side AC system strength varies from 1800 MVA to 7200MVA, terminal two inverter side AC system strength varies from 600MVA to 2000 MVA, and terminal three inverter side AC system varies from 1000MVA to 4000MVA. HVDC line configurations, HVDC controller

parameter settings, and HVDC system operating point variations also have been considered. The results of the oscillation frequency and damping ratio for all three controller interaction modes in different operating scenarios are provided in the following sections.

Table 6.4 shows the controller interaction oscillation frequencies and damping ratios for different AC system strengths in the original system configuration. Correspondingly, Table 6.5 and Table 6.6 show the participation factor results and mode shape angles between each controller state variable for all oscillation modes under the same study scenario.

System Strength			Mode-4N		Mode-5N		Mode-6N	
T1 (MVA)	T2(MVA)	T3(MVA)	Frequency (Hz)	Damping (%)	Frequency (Hz)	Damping (%)	Frequency (Hz)	Damping (%)
1800	600	1000	50.42	31.33%	9.00	12.80%	3.69	13.26%
3600	600	1000	65.19	20.92%	9.01	12.71%	4.03	12.70%
5400	600	1000	67.37	18.46%	9.01	12.69%	4.13	12.83%
7200	600	1000	68.21	17.64%	9.01	12.68%	4.18	12.98%
1800	600	1000	50.42	31.33%	9.00	12.80%	3.69	13.26%
1800	1000	1000	51.26	30.45%	8.45	13.75%	3.50	14.07%
1800	1500	1000	51.68	30.31%	8.20	14.76%	3.42	14.43%
1800	2000	1000	51.87	30.32%	8.08	15.41%	3.38	14.59%
1800	600	1000	50.42	31.33%	9.00	12.80%	3.69	13.26%
1800	600	2000	51.29	28.92%	8.92	10.29%	3.46	9.40%
1800	600	3000	51.88	28.33%	9.02	10.18%	3.37	11.16%
1800	600	4000	52.21	28.17%	9.11	10.33%	3.33	12.97%

Table 6.4 Frequency and damping ratio with different system strength

System Strength	Mode-4N			Mode-5N			Mode-6N		
T1 /T2/T3 (MVA)	T1 PF	T2 PF	T3 PF	T1 PF	T2 PF	T3 PF	T1 PF	T2 PF	T3 PF
1800/600/1000	1.000	0.010	0.012	0.011	0.542	0.478	1.000	0.702	0.674
3600/600/1000	0.177	0.015	0.014	0.001	0.542	0.459	0.759	0.695	0.816
5400/600/1000	0.082	0.014	0.013	N/A	0.542	0.452	0.637	0.663	0.824
7200/600/1000	0.058	0.013	0.012	N/A	0.542	0.449	0.578	0.648	0.828
1800/600/1000	1.000	0.010	0.012	0.011	0.542	0.478	1.000	0.702	0.674
1800/1000/1000	1.000	0.002	0.010	0.001	0.932	0.823	1.000	0.973	0.570
1800/1500/1000	0.991	0.001	0.001	N/A	1.000	0.878	0.884	1.000	0.466
1800/2000/1000	0.982	N/A	N/A	N/A	1.000	0.872	0.827	1.000	0.422
1800/600/1000	1.000	0.010	0.012	0.011	0.542	0.478	1.000	0.702	0.674
1800/600/2000	1.000	0.001	0.001	0.010	0.558	0.498	0.998	0.667	1.000
1800/600/3000	0.974	N/A	N/A	0.001	0.556	0.523	0.873	0.567	1.000
1800/600/4000	0.957	N/A	N/A	N/A	0.553	0.539	0.830	0.532	1.000

Table 6.5 Participation Factors for each oscillation mode- original system

System Strength	Mode-4N			Mode-5N			Mode-6N		
T1 /T2/T3 (MVA)	T1-T2 Ang	T2-T3 Ang	T3-T1 Ang.	T1-T2 Ang	T2-T3 Ang	T3-T1 Ang.	T1-T2 Ang	T2-T3 Ang	T3-T1 Ang.
1800/600/1000	72.73	11.65	275.62	116.10	178.30	65.60	71.19	27.61	261.20
3600/600/1000	45.51	5.01	309.48	115.30	177.64	67.06	69.90	26.90	263.20
5400/600/1000	44.91	4.21	310.88	N/A	177.20	N/A	70.27	26.80	262.93
7200/600/1000	44.41	3.87	311.72	N/A	177.13	N/A	70.80	26.90	262.30
1800/600/1000	72.73	11.65	275.62	116.10	178.30	65.60	71.19	27.61	261.20
1800/1000/1000	67.28	9.60	283.12	111.60	178.78	69.62	73.10	25.50	261.40
1800/1500/1000	70.60	13.50	275.90	N/A	179.30	N/A	73.70	24.50	261.80
1800/2000/1000	N/A	N/A	N/A	N/A	179.90	N/A	74.00	24.10	261.90
1800/600/1000	72.73	11.65	275.62	116.10	178.30	65.60	71.19	27.61	261.20
1800/600/2000	82.84	2.54	274.62	98.40	179.80	81.80	68.34	32.60	259.06
1800/600/3000	62.34	N/A	N/A	98.08	179.88	82.04	68.50	29.70	261.80
1800/600/4000	N/A	N/A	N/A	N/A	179.58	N/A	68.84	27.16	264.00

Table 6.6 Mode shapes for each oscillation mode- original system

Terminal one AC system strength Variation

Mode-4N:

As shown in Table 6.13, the oscillation frequencies and damping ratios for all three controller interaction modes change with the increase of the rectifier side AC system strength. The oscillation frequency of Mode-4N increases from 50.42Hz to 68.21Hz and the damping ratio decreases from 31.33% to 17.64%. By examining the participation factor, it is revealed that the rectifier side AC system strength significantly impacts the damping ratio of Mode-4N. This mode is dominated by the terminal one rectifier side voltage controller state variable in the original study case. With the increase of terminal one AC system strength from 1800MVA (SCR=1.88) to 2100MVA (SCR=2.21), the participation factor of the terminal one equivalent machine state variable dominates this mode. Meanwhile, the participation factor of the terminal one voltage controller state variable drops from 1.0 to 0.997, and the terminal one DC voltage (participation factor of 0.97) and HVDC line tap point DC voltage (participation factor of 0.78) both have a relatively high

participation factor. Further increasing terminal one AC system strength above 2200MVA increases both terminal one DC voltage and HVDC line tap point voltage participation factors On the other hand, the participation factors of the terminal one AC system equivalent machine state variable and the terminal one voltage controller state variable keep decrease. The participation factors of these two state variables decrease even more if the rectifier side AC system strength is further increased. With the rectifier side AC system strength increased to 2400MVA, HVDC line tap point DC voltage dominates this mode with a participation factor of 1.0. In the meantime, the participation factor of terminal one DC voltage drops to 0.975 and the participation factor of the terminal one voltage controller state drops to 0.710. Further increasing rectifier AC system strength beyond 5400MVA significantly decreases the participation factor of terminal one DC voltage to 0.49 leaving only the HVDC line tap point DC voltage (PF=1.0) to dominate this oscillation mode. In the meantime, the terminal one voltage controller participation factor drops to 0.082. Further increasing rectifier side AC system strength to 7200MVA decreases the participation factor of the terminal one voltage controller state variable to 0.058.

The other two terminal controller state variables also participate in this mode and the participation factors vary with the rectifier side AC system strength change. As shown in Table 6.14, the terminal two current state variable has a minor participation factor of 0.01 in the original study case. With the increase of rectifier side AC system strength to 3600MVA, the participation of the terminal two current controller state variable slightly increases to 0.015. Further increasing terminal one AC system strength decreases the participation factor of the terminal two current controller state variable to 0.014. The participation factor continues to decrease upon further increase of rectifier side AC system

strength. The terminal three current controller state variable participation factor slightly increases from 0.012 to 0.014 when the rectifier side AC system strength increases from 1800MVA to 3600MVA. Upon further increase of rectifier side AC system strength to 7200MVA, rather than increasing, the terminal three participation factor decreases from 0.014 to 0.012.

From the above analysis results, it is observed that the participation factors for all three HVDC controller state variables are 1.0, 0.010, and 0.012 in the original case with rectifier side AC system strength of 1800MVA and 0.082, 0.013, and 0.012 when the rectifier side AC system strength is increased to 7200MVA. In this mode, all three HVDC controller state variables have decreased participation when the rectifier side AC system strength is increased. As explained in the previous section, when the rectifier side AC system strength is increased, HVDC line tap point DC voltage becomes the dominant participant. The oscillation mode changes to HVDC line resonance mode. To explore the impact of the original DC network resonance mode, further investigation was conducted. The results indicate that the original HVDC line resonance mode also changes and a different state variable dominates the oscillation mode when the rectifier side AC system strength increases. Initially, the HVDC line tap point DC voltage dominates the oscillation mode. When the rectifier side AC system strength increases to 2400MVA, the equivalent machine state variable dominates this mode. Obviously, both the oscillation frequency and the damping ratio change to different values. Upon further increase of rectifier side AC system strength to a higher value, the rectifier side AC bus voltage dominates the oscillation mode. Increasing rectifier side AC system strength to 4000MVA causes terminal one DC voltage

to eventually become the dominant participant. As a result, both the oscillation frequency and damping ratio of the original DC network interaction oscillation mode change.

The participation factor analysis indicates that the rectifier side AC system impacts the HVDC controller state variable participation and hence the controller interaction.

Table 6.14 provides the angles between each controller state variable. The angle between terminal one and terminal two controller state variables is 72.73 degrees, which is the largest angle difference between all three controller state variables. With the rectifier side AC system strength increase to 7200MVA, the angle between the terminal one voltage controller state variable and terminal two current controller state variable reduces from 72.73 degrees to 44.41 degrees. Similarly, the angle between the terminal two current controller state variable and terminal three current controller state variable slightly decreases from 11.65 degrees to 3.87 degrees. The angle between the terminal three current controller state variable and the terminal one current state variable increases from 275.62 degrees to 311.72 degrees. Even though the angle changes in between each control state variable, the oscillation mode for Mode-4N remains unchanged as all terminal controller state variables oscillate together.

Based on the above analysis, it is observed that the oscillation frequency and damping ratio change drastically due to the significant terminal one voltage controller state variable participation factor change and mode shape change. As a result, both the oscillation frequency and damping ratio for Mode-4N significantly change. The results show that this mode has enough damping ratio and has no small signal stability concern.

Mode-5N:

The study results also show the impact of the rectifier side AC system strength on the other two HVDC controller oscillation modes. In Table 6.13, the oscillation frequency for Mode-5N slightly increases from 9.00Hz to 9.01Hz and the damping ratio slightly decreases from 12.80% to 12.68%. In Table 6.14, the participation factor of the terminal one voltage controller state variable decreases from 0.011 to 0.001 when the terminal one AC system strength increases from 1800MVA to 3600MVA. If the rectifier side AC system strength is further increased, the participation of the terminal one voltage controller state variable becomes very small and disappears in the participation list. The participation factor of the terminal two current controller state variable remains unchanged with a value of 0.542 and the participation factor of the terminal three current controller state variable decreases from 0.478 to 0.449 when the rectifier side AC system strength increases to 7200MVA. Mode shape results in Table 6.15 indicate that the angle between the terminal one voltage controller state variable and terminal two current controller state variables decreases slightly from 116.10 degrees to 113.0 degrees when terminal one AC system strength increases to 3600MVA. Similarly, the angle between the terminal one voltage controller state variable and terminal three current controller state variable slightly increases from 65.6 degrees to 67.06 degrees and the angle between the terminal two current controller state variable and terminal three current controller state variable decreases from 178.30 degrees to 177.64 degrees. Further increasing terminal one AC system strength beyond 3600MVA causes the terminal one voltage controller state variable to disappear in the participation list. As a result, angles related to the terminal one voltage controller state variable become unavailable. Regardless of the angle changes between each controller state variable, the oscillation mode for Mode-5N remains unchanged as the

terminal one voltage controller state variable and terminal three current controller state variable oscillate together against the terminal two current controller state variable. With the increase of rectifier side AC system strength, the terminal one voltage controller state variable diminished from the participation list, and the mode becomes the terminal two current controller state variable oscillating against the terminal three current controller state variable. Both the oscillation frequency and damping ratio for this mode changes slightly due to the rectifier side AC system strength change. However, the results indicate that this mode has enough damping ratio and has no small signal stability concern.

Mode-6N:

In Table 6.13, the oscillation frequency for Mode-6N slightly increases from 3.69Hz to 4.18Hz and the damping ratio decreases from 13.26% to 12.70% when the AC system strength increases to 3600MVA. Upon further increase of AC system strength to 7200MVA, the damping ratio increases from 12.70% to 12.98%. The participation factor of the terminal one voltage controller state variable decreases from 1.0 to 0.578, and the participation factor of the terminal two current controller state variable slightly decreases from 0.702 to 0.648. The participation factor of the terminal three current controller state variable increases from 0.674 to 0.828. The participation analysis indicates that the rectifier side AC system impacts each HVDC controller state variable participation in this mode. As shown in Table 6.15, mode shape result indicates that the angle between the terminal one voltage controller and terminal two current controller state variables slightly decreases from 71.19 degrees to 69.90 degrees when the rectifier side AC system strength increases to 3600MVA. Upon further increase of the AC system strength from 3600MVA to 7200MVA, the angle increases from 69.90 degrees to 70.80 degrees rather than

decreasing. The angle between the terminal two current controller state variable and the terminal three current controller state variable decreases from 27.61 degrees to 26.80 degrees when the AC system strength increases to 5400MVA. Further increase of AC system strength to 7200MVA causes the angle to increase back from 26.80 degrees to 26.90 degrees. The angle between the terminal three current controller state variable and the terminal one voltage controller state variable increases from 261.20 degrees to 263.20 degrees when the rectifier side AC system strength increase to 3600MVA. If the rectifier side AC system strength is further increases from 3600MVA to 7200MVA, the angle between these two state variables decreases from 263.20 degrees to 262.30 degrees. The result shows the angle between each terminal controller state variables slightly changes due to the change of rectifier side AC system strength. However, the oscillation mode remains unchanged as the terminal one voltage controller state variable oscillates together with the terminal two current controller state variable and terminal three current controller state variables. As a result, both the oscillation frequency and damping ratio of Mode-6N change due to the change of rectifier side AC system strength. However, this mode has enough damping ratio and has no small signal stability concern.

Similar analysis has been performed with the terminal two AC system and terminal three AC system strength change. The results are provided in Appendix C2. In addition, the AC system strength impact on the three-terminal HVDC system with different HVDC line tap points, different control parameters, and different operation points have been conducted. The results are also provided in Appendix Table C2.4 to Table C2.12. All the results show some similarity in response to AC system strength change. Based on the results, it is observed that:

1. Mode-4N is dominated by the terminal one voltage controller state variable with minor participation of the terminal two current controller state variable and the terminal three current controller state variable. Terminal one AC system strength has a significant impact on this oscillation mode. Obviously, terminal two and terminal three AC system strength changes also have a limited impact on this oscillation mode. Regardless of which terminal AC system strength changes, the participation factors of all controller state variables change. In particular, the participation factor of the terminal one voltage controller state variable decreases significantly from 1.0 to 0.058 when the terminal one AC system strength increases from 1000MVA to 4000MVA. Considering the participation factors are 1.0, 0.01, and 0.011 for all three controller state variables in the original system with terminal one AC system strength of 1800MVA and are 0.058, 0.013, and 0.012 with terminal one AC system strength of 7200MVA, the oscillation mode is totally changed. The terminal one voltage controller state variable is no longer a major participant. The study results indicate that the dominating state variable keeps changing with the increase of terminal one AC system strength. Terminal one equivalent machine state variable, terminal one DC voltage, and HVDC line tap point DC voltage all, in turn, become the dominant participant with terminal one AC system strength increase. Depending on the dominant participant, this mode switches in between electromechanical oscillation mode (terminal one equivalent machine state variable dominated), HVDC network resonance mode (terminal one DC voltage dominated), or HVDC network resonance mode (HVDC line tap point DC voltage dominated). With the increase of terminal one AC system strength, the controller state variable

participation are significantly reduced. On the other hand, both terminal two and terminal three AC system strength also affect the participation of the terminal one controller state variable. For the other two terminal AC system strength changes, the terminal one voltage controller state variable always dominates the oscillation mode. Mode shape results show that angles between each controller state variable also change when AC system strength changes. However, the oscillation mode remains the same as the terminal one voltage controller state variable oscillates together with the terminal two current controller state variable and the terminal three current controller state variable. The angle between each controller state variable changes significantly with the terminal one AC system strength change. However, the angle changes very insignificantly when the strength of the other two terminal AC systems changes. Therefore, AC system strength impacts both the oscillation frequency and the damping ratio of this mode. However, this mode has enough damping ratio and has no small signal stability concern under all study scenarios.

The study results show that this mode has an oscillation frequency between 50Hz and 70Hz. Both the HVDC network quantities, machine state variables, and the AC system voltage participate in this mode. Depending on the system configuration and application, it may interact with other equipment in both AC systems and DC systems, such as the AC system filter, DC system smoothing rector, series compensated AC transmission line and multi-mass turbine generators. Extra tension must be taken to avoid SSR type oscillation to occur.

2. In Mode-5N, both the terminal two current controller state variable and the terminal three current controller state variable have higher participation. The terminal one voltage controller state variable also participates in this mode with a relatively low participation factor. The results show that the participation factors for all controller state variables change regardless of which terminal AC system strength changes. However, terminal one AC system strength changes have a minor impact on this mode due to the relatively low participation of the terminal one controller state variable. Mode shape results show that the angles between each controller state variable also change when the AC system strength changes. However, the mode shape remains the same as the terminal one voltage controller state variable and the terminal three current controller state variable oscillate together against the terminal two current controller state variable. The study results indicate that both the oscillation frequency and damping ratio change when AC system strength changes.
3. Mode-6N is dominated by the terminal one voltage controller state variable with both terminal two and terminal three current controller state variables having relatively high participation. The participation factors for all controller state variables change regardless of which terminal AC system strength changes. However, terminal one AC system strength changes have a very significant impact on the participation of its own terminal controller state variable. Similar conclusions can be drawn for the other two controller state variables. Mode shape results show that angles between each controller state variable also change when the AC system strength changes. However, the mode shape remains the same as the terminal one voltage controller state variable, terminal two current controller

state variable, and the terminal three current controller state variable oscillate together. The results indicate that both the oscillation frequency and damping ratio of this mode change when AC system strength changes.

In the above sections, two MTHVDC control schemes have been discussed. Each one of the schemes has its own characteristics. For scheme one, terminal three acts as the inverter which is in DC voltage control. The other two converters are in DC current control with one acting as the rectifier and the other acting as the inverter. Changing the terminal three AC system strength causes the participation of the terminal three controller state variable to decreases significantly. If the AC system is strong enough, the AC system equivalent machine state variable will dominate this mode and the controller state variable has minor participation. In the meantime, mode shape angles between each controller state variable also change which may lead to an entire change in the oscillation mode. As a result, this mode becomes an electromechanical oscillation mode with HVDC controller state variables having minor participation.

For scheme two, terminal one acts as the rectifier which is in DC voltage control while the other two converters act as inverters in DC current control. There is an oscillation mode with an oscillation frequency in the range of 40Hz to 70Hz. The equivalent machine state variable, terminal one DC voltage, HVDC line tap point DC voltage, and terminal one DC voltage controller all participate in this mode. Changing the terminal one AC system strength causes the participation of the terminal one DC voltage controller state variable to drop significantly. Depending on the strength of the terminal one AC system, the above-mentioned state variables, in turn, dominate this mode. Under certain system conditions, this oscillation mode may interact with other equipment in both the AC and DC system,

such as AC system filter, DC system smoothing rector, series compensated AC transmission line, and multi-mass turbine generators which may cause sub-synchronous resonance. Therefore, extra tension must be taken to avoid this type of oscillation to occur. In the meantime, mode shape angles between each controller state variable also change which may lead to a complete change in the oscillation mode. As a result, this mode may become either an HVDC network resonance mode or an electromechanical oscillation mode with HVDC controller state variables having minor participation.

Based on these analysis results, we can conclude that:

1. There are controller interactions in the MTHVDC systems. The participation analysis shows that almost all controller state variables participate in every oscillation mode with different participation factors. Any terminal AC system strength change impacts all controller state variable participation factor.
2. Different AC system strengths have different impacts on each oscillation mode. In general, AC system strengths has a significant impact on oscillation modes dominated by its own terminal controller state variable, and has an insignificant impact on oscillation modes dominated by other terminal controller state variables.
3. Mode shape analysis results prove that angles between each controller state variable also change due to AC system strength change. However, the mode shape pattern remains unchanged.
4. The voltage control terminal AC system strength has a significant impact on the voltage controller state variable dominated oscillation mode. Significant AC system strength variation changes the mode shape angle significantly, which may cause the oscillation mode change.

5. In comparing these two control schemes, scheme one is more stable and has a lower chance of sub-synchronous resonance.
6. A Three-terminal HVDC system can not isolate oscillations. Instead, oscillations can propagate from one AC system to the other through the HVDC line due to the interaction between each terminal.
7. The changes in participation factor and mode shape angle are complicated because the controller parameter, system configuration, MTHVDC operating point, and the AC system strength all affect the final output. Higher system strength does not always positively improve the oscillation damping ratio. Therefore, it is very important to perform a system small signal type study to cover all possible operating scenarios to ensure that the proposed system has no small signal stability issues.

6.4 System Topologies Change Impact on Controller Interaction

To examine the impact of system topology changes on controller interaction, the proposed two MTHVDC schemes with different HVDC line configurations, different controller parameters, and different operating points have been studied. The results are summarized in Tables 6.7 for scheme one MTHVDC system – terminal three in DC voltage control.

The oscillation frequency and damping ratios for Mode-4, Mode-5, and Mode-6 vary with system topologies. For example, when the HVDC lines tap point changes, the Mode-4 oscillation frequency changes from 12.71Hz to 14.85Hz, and the damping ratio changes

from 33.64% to 36.69%. In addition, controller parameter changes also impact the oscillation frequency and damping ratio. The Mode-4 oscillation frequency changes from 12.71Hz to 10.96Hz and the damping ratio changes from 30.62% to 76.10% when the control parameter changes. Furthermore, the operating point changes also impact the oscillation frequency and the damping ratio. The Mode-4 oscillation frequency changes from 12.71Hz to 13.04Hz and the damping ratio changes from 30.62% to 35.65% when the operating point changes. Similarly, the same trend also applies to the other two oscillation modes. The study results demonstrate that the HVDC line configurations, the control parameter, as well as the operating point all impact the oscillation frequency and damping ratio.

Similar studies have been performed for scheme two MTHVDC systems – terminal one on DC voltage control. The results are summarized in Table 6.8. The results show that both the oscillation frequency and the damping ratio for Mode-4N, Mode-5N, and Mode-6N change when the system configuration changes. For example, the oscillation frequency for Mode-4N changes from 50.42Hz to 53.18Hz, and the damping ratio changes from 31.33% to 31.60% when the HVDC lines tap point changes. The oscillation frequency for Mode-4N changes from 50.42Hz to 52.86Hz, and the damping ratio changes from 31.33% to 38.59% when the HVDC system controller parameter changes. Moreover, the oscillation frequency for Mode-4N also changes from 50.42Hz to 50.13Hz, and the damping ratio changes from 31.33% to 30.50% when the operating point changes. The other two oscillation modes have similar performance.

The above observations further prove that the HVDC line configuration, control parameter selection, and the operating point, all impact the oscillation frequency and

damping ratio. However, with properly selected control parameters for different system configurations, all HVDC controller interaction oscillation modes have enough damping ratio and the system has no small signal stable concern.

System Configuration	Mode-4		Mode-5		Mode-6	
	Frequency(Hz)	Damping(%)	Frequency(Hz)	Damping(%)	Frequency(Hz)	Damping(%)
Original Scheme	12.71	30.62%	11.43	39.72%	4.55	50.77%
HVDC line Impedance	14.85	34.87%	10.19	40.25%	4.38	50.92%
Control Parameter	10.96	76.10%	13.63	32.67%	4.97	57.31%
Operating Point	13.04	35.65%	12.04	30.02%	4.63	45.62%

Table 6.7 Frequency and damping ratio for different system configuration-scheme one

System Configuration	Mode-4N		Mode-5N		Mode-6N	
	Frequency(Hz)	Damping(%)	Frequency(Hz)	Damping(%)	Frequency(Hz)	Damping(%)
Original Scheme	50.42	31.33%	9.00	12.80%	3.69	13.26%
HVDC line Impedance	53.18	31.60%	7.96	19.01%	3.94	14.48%
Control Parameter	52.86	38.59%	10.05	10.06%	3.58	8.59%
Operating Point	50.13	30.50%	9.09	4.74%	3.91	5.87%

Table 6.8 Frequency and damping ratio for different system configuration-scheme two

As shown in Table 6.8, the damping ratios for Mode-5N and Mode-6N in scheme two decrease significantly when the operating point changes. The damping ratios decrease from 12.80% to 4.74% for Mode-5N and from 13.26% to 5.87% for Mode-6N. To investigate the impact of the operating point changes on the oscillation frequency and the damping ratio, further study has been conducted. Initially, both MTHVDC systems are operated at the same operating point: when terminal one has an operating voltage of 500kV and delivers approximately 1305MW power to the inverter sides. In the meantime, terminal two and terminal three receive approximately 650MW and 560MW of power respectively. Subsequently, the operating point changes and terminal two receives about 510MW power and terminal three receives about 700MVA, which is a 50MW power shift from the terminal two inverter to the terminal three inverter side. All other controller

parameters remain the same for both test cases. The results in Table 6.9 shows both the oscillation frequency and damping ratio for the operating point changes.

System Configuration	Mode-4/4N		Mode-5/5N		Mode-6/6N	
	Frequency(Hz)	Damping(%)	Frequency(Hz)	Damping(%)	Frequency(Hz)	Damping(%)
Scheme One OP1	12.71	30.62%	11.43	39.72%	4.55	50.77%
Scheme One OP2	13.04	35.65%	12.04	30.02%	4.63	45.62%
Scheme Two OP1	50.42	31.33%	9.00	12.80%	3.69	13.26%
Scheme Two OP2	50.13	30.50%	9.09	4.74%	3.91	5.87%

Table 6.9 Frequency and damping ratio for different schemes at the same operating point

Clearly, the maximum damping ratio change in scheme one is in Mode-5 where the damping ratio changes from 39.72% to 30.02% (24.4% damping ratio change due to the operating point change). However, the maximum damping ratio change in scheme two in Mode-5N is from 12.80% to 4.74% which is a 63% damping ratio drop due to the operating point change. The study results demonstrate that control scheme two of the MTHVDC system is more sensitive to the operating point change. MTHVDC system control scheme one is more robust than control scheme two and has a lower chance of small-signal stability issues upon system operating point change. Therefore, it is suggested to perform a small signal type study for the MTHVDC system to cover all operating scenarios to ensure that the HVDC system is operated safely.

6.6 Chapter Summary

This chapter discussed the impact of AC system strength on MTHVDC controller interactions. Two MTHVDC control schemes with various system configurations, including different HVDC line tap points, different control parameters, and different operating points, have been studied with various AC system strength conditions. The

results indicate that the participation factor and mode shape angle of the oscillation mode change due to AC system strength change. As a result, both the oscillation frequency and damping ratio are impacted by AC system strength. The results also indicate that AC system strength has a significant impact on its own terminal controller state variable dominated oscillation mode. Most importantly, the AC system strength has a significant impact on voltage controller state variable dominated oscillation mode. Higher system strength does not always positively improve the oscillation damping ratio. Furthermore, The MTHVDC system cannot isolate oscillation. Instead, oscillation can propagate from one side of the AC system to the other through the MTHVDC system. Other parameters, such as system configuration, controller parameter selection as well as the system operating also impact the controller interaction oscillation. The participation factor analysis and mode shape angel analysis results prove that the proposed Multi-terminal HVDC (MTHVDC) system scheme one, with current control at rectifier, current control at one inverter and voltage control at the other inverter, is more robust than control scheme two and has a lower chance of having small signal stability concern. This scheme is less impacted by the operating point change.

Therefore, it is very important to perform a system small signal study to cover all possible operating scenarios to ensure that the system has no small signal stability issues.

Chapter 7:Conclusions, Contributions and Future Work

7.1 Conclusions and Contributions

High-voltage direct current power transmission systems are becoming increasingly integrated into modern power networks. The majority of HVDC transmission systems in the world are based upon line-commutated converters and point to point DC links. Due to the development of technology, tapping on the exiting LCC HVDC transmission line with LCC technology raises industry interests. In the multi-terminal HVDC systems, three or more converter stations tied together allow power to be transferred to different locations. Multi-terminal HVDC systems can be used to enhance system stability, increase system operation flexibility, and interconnect multiple power plants and load centers into the same power grid. On the other hand, due to the existence of multiple controllers in the MTHVDC system, the controller interactions become a concern in the planning, design, and installation of the MTHVDC systems. Therefore, it is necessary to develop a small signal assessment tool to analyze the controller interactions in the multi-terminal HVDC systems. In this thesis, three-terminal HVDC systems with different controller arrangement is the main research area. To perform eigenvalue analysis for the multi-terminal HVDC systems, a traditional small signal stability analysis tool does not have the capability due to the constant-admittance matrix models for the AC system. To overcome this issue, a dynamic phasor technique is used to model the entire AC system. In addition, the generator stator dynamic has also been included in the model. The model has been developed and benchmarked with the PSCAD/EMTDC results. The results indicate that the developed

small-signal assessment tool is accurate in analyzing the controller interactions in multi-terminal HVDC systems. The conclusions and contributions of the thesis are described as below:

1. *Developed the three-terminal LCC HVDC system*

To analyze MTHVDC system controller interaction, a current injection model of the linearized three-terminal LCC HVDC system has been developed. It has been combined with the dynamic phasor model of the entire AC systems to analyze the high-frequency controller interactions in the three-terminal HVDC system. The benchmarked results prove that this model is accurate, and it facilitates the analysis of the three-terminal HVDC system controller interactions.

2. *Proposed a general study procedure to analyze controller interactions*

A general study procedure to analyze MTHVDC system controller interaction was proposed. This five-step study procedure includes power system power flow data preparation, power system dynamic data preparation, eigenvalue analysis, evaluation criteria, and oscillation analysis and mode identification. This study procedure can be used to perform HVDC system interaction oscillation analysis.

3. *Analysis interactions modes in three-terminal LCC-HVDC systems*

In the thesis, an analysis of the three-terminal HVDC system with two different controller arrangements has been performed using the proposed study procedure. The results show that the size of the smoothing reactor does impact the oscillation frequency. The damping ratio for the electromechanical oscillation can be improved by changing the HVDC controller parameter. Machines at different terminals interact with each other through the MTHVDC systems. The results also indicate that different

controller arrangements impact the oscillation mode shape, oscillation frequency, and damping ratio. Control scheme one is more robust than control scheme two.

4. *Analysis of the impact of the system strength on three-terminal HVDC system controller interactions*

In the thesis, an investigation is done on the impact of the system strength on the controller interactions. The results indicate that there are controller interactions in the MTHVDC systems. AC system strength has a significant impact on oscillation modes dominated by its own terminal controller state variables but has an insignificant impact on oscillation modes dominated by other terminal controller state variables. For oscillation modes dominated by voltage controller state variables, AC system strength change may change the oscillation mode. However, higher system strength does not always positively improve the oscillation damping ratio.

5. *Analysis of the system configuration impact on the MTHVDC system controller interactions*

The impacts of a system configuration change, controller parameter change, and system operating point change have been analyzed. The results indicate that all of these quantities impact the oscillation frequency and damping ratio. It is concluded that the control scheme one arrangement is a better solution for the three-terminal HVDC system. It is more robust than control scheme two with no small signal stability concerns. These contributions have led to the following publications

- K. Ma, U.D. Annakkage and C. Karawita, "Development of a Small-Signal Assessment Tool for Multi-terminal LCC Schemes," AC/DC 2019

7.2 Recommendations for Studying MTHVDC Systems Controller Interactions in Integrated Power Systems

Based on the findings of this research, the following recommendations will be proposed for studies related to controller interactions in integrated power systems.

- If the MTHVDC system is connected to the integrated power systems, a detailed controller interaction study needs to be performed. A linearized model of MTHVDC systems including the converter model, HVDC line model, and basic controller model should be developed. The entire AC network should be modeled using dynamic phasor. Generators should be modeled to include the stator dynamic. By doing so, accurate results can be obtained in the studied frequency range. The general process to obtain the overall state-space model of the entire power system is provided in Chapter 2.
- To validate the results of the developed linearized systems and eliminate the error caused by different simulation techniques, the same studied case should be created using commercial software such as PSCAD/EMTDC. The system responses obtained using the linearized models are compared with the responses of the commercial software to ensure model accuracy.
- It is recommended to use the proposed procedure involving power system load flow and dynamic data preparation, eigenvalue analysis, evaluation criteria set up and oscillation analysis, and mode identification to perform controller interaction study. As indicated in the procedure, mode shape and major participation factor for each individual oscillation modes should all be carefully examined. By doing so, the correct oscillation mode can be identified. As

shown in Chapter 5, machines at different terminals of the MTHVDC system interact with each other through the MTHVDC systems. The damping of the electromechanical oscillation mode can be improved by changing the controller gain. By comparing the mode shape and major participation factor for each individual oscillation modes in the MTHVDC systems, it is concluded that different controller arrangement has a significant impact on MTHVDC system small signal stability.

- It is recommended to perform a system small signal study to cover all possible operating scenarios. As shown in Chapter 6, system strength change significantly impacts the participation factor and mode shape angle for the same oscillation mode. As a result, the oscillation frequency and damping ratio change dramatically. The results in Chapter 6 clearly show that certain controller interaction mode is highly sensitive to the controller parameters. Therefore, it is very important to perform eigenvalue analysis to cover system configuration change, entire controller parameter setting range, possible operating range as well as various system strength condition to ensure that the system has no small signal stability concern.
- It is recommended to perform time-domain analysis using the selected controller parameters in the small-signal analysis to ensure these parameters are also suitable for time-domain analysis. As illustrated in this thesis, all controller interaction oscillation modes are effectively identified. This study procedure can be used to perform any type of controller interaction study.

7.3 Direction for Future Work

The focus of this research is the analysis of MTHVDC controller interactions using small-signal stability assessment. To analyze these high-frequency interactions accurately, small-signal models for the MTHVDC system have been developed, and the AC network dynamics, as well as the generator stator dynamics, have been modeled and validated against PSCAD/EMTDC simulations. Ultimately, a small signal model for testing MTHVDC power systems has been proposed. The interactions in the MTHVDC system, including HVDC network resonance oscillation, AC-DC network interaction, and controller interactions as well as electromechanical oscillations in the MTHVDC system have been analyzed using the developed small-signal models.

The proposed small-signal model can be used to analyze the interactions of the other dynamic devices in power systems. It includes:

- The scope of research has been limited to three-terminal HVDC systems. However, there are LCC HVDC systems with four and more terminals in power systems. There are possible interactions between HVDC controllers and other dynamic devices in power systems that need to be investigated.
- In this research, the AC systems for the three-terminal HVDC systems are independent. In reality, the AC systems between inverter terminals as well as the AC systems between the rectifier and inverter AC system may integrate. As a result, controller interaction may become even more complicated. Further investigation can be carried out to investigate the impact on controller interactions in the meshed AC network.
- Voltage source converter (VSC) type HVDC links have been proposed and are widely used in modern power systems. The interactions between the controllers in VSC/hybrid

MTHVDC systems can be investigated using the proposed methodology. However, the linearized model of the VSC converter is required.

References

[1] G. Asplund, L. Carlsson, and O. Tollerz, “50 Years HVDC”, ABB Review 4/2003, pp. 6–13.

[2] N.G. Hingorani, “High-voltage DC transmission: a power electronics workhorse,” IEEE Spectrum, vol. 33, no. 4, pp. 63–72, April 1996.

[3] ABB Library and references for HVDC: www.abb.com/hvdc

[4] L.Carlsson, “Classical HVDC: Still continuing to evolve,” Modern Power Systems, V22,n6, June 2002, p. 19-21

[5] J. Varley, “HVDC: fifty years on,” Modern Power Systems, October 2004, V24, n 10, p. 18-20

[6] A. Persson and L. Carlsson, “New technologies in HVDC converter design,” IEE Conf. Publication AC and DC Power Transmission, April 1996, P. 387-392

[7] http://www.cepri.com.cn/products/details_84_545.html

[8] N. G. Hingorani, “FAXTS-flexible AC transmission system,” IEE Conference Publication, 1991, p. 1-7

[9] L. Gyugyi, “Unified power-flow control concept for flexible AC transmission systems,” IEE Proceedings, Part C: Generation, Transmission and Distribution. 1992, p 323-331.

[10] D. Povh, “Use of HVDC and FACTS,” Proceedings of the IEEE.

[11] E. Acha, V.G., Demetriades, G.D.; Flourentzou, N.: Recent Advances in High-Voltage Direct-current Power Transmission Systems”, IEEE International Conference, 2006, p. 206-213.

[12] T.J. Hammons, M. Willingham, K.N. Mak, M. Da Silva, M. Morozowski, and B.K. Blyden, “Generation and transmission improvements in developing countries,” IEEE Trans. on Energy Conversion, V 14, n 3, Sept. 1999, p. 760-765.

[13] A.M.H.A. Karim, N.H.A. Maskati and S. Sud, “status of Gulf co-operation council (GCC) electricity grid system interconnection,” Proc. of IEEE Power Engineering Society General Meeting 2004, Pt. 2, Vol 2, P. 1385-1388

[14] T. J. Hammons, D. Woodford, J. Loughtan, M. Chamia, J. Donahoe, D. Povh, B. Bisewski, W. Long, “Role of HVDC transmission in future energy development,” IEEE Power Engineering Review, v20, n 2, 2000, p. 10-25.

[15]L. Weimers, “AC or DC: which way should China go ?”, Modern Power Systems, v25, n 8, Sept. 2005, p. 11-17

[16] C. Ashmore, “Transmit the light fantastic,” IET, Power Engineer, April 2006, v20, n2, p. 24-27

[17] G. Buigues, V.Valverde, A Etxegarai, P. Eguia, E. Torres, “Present and Future Multiterminal HVDC Systems: Current Status and Forthcoming Developments,” International Conference on Renewable Energies and Power Quality (ICREPQ ’17), Renewable Energy and Power Quality Journal, Vol 1, No. 15, pp. 83-88, April 2017.

[18] K. Tharani, A. Gupta and A. Gupta, “An Overview to HVDC links in India,” International Journal of Electrical, Electronics and Computer Engineering 2(1), pp. 94–98,2013.

[19] C.V.Thio, “ Nelson River HVDC Bipole-two part I- System Aspects,” IEEE Transactions on Power Apparatus and Systems, vol. PAS-98, No.1, pp. 165–173, Jan/Feb 1979.

[20] C. Bartzsch et al., “Manitoba Hydro’s Bipole III transmission Project – Design Aspects and Major Technical Features” Cigre, Paper B4-051, Winnipeg Colloquium 2017.

[21] Manitoba Hydro, “Transmission System Interconnection Requirements,” Version 4, July 2016

[22] W. Wang and M. Anderson, “Development in UHVDC Multi-terminal and VSC DC Grid,” 2016 international High Voltage Direct Current Conference, Shanghai, Oct. 25-27 2016

[23] A. Ardito, L. Camilli, C. D. Mario, A. Giorgi, G. Pazienza, C. Pincella, M. Rebolini, R. Rendina, G. Simioli, G. P. Stigliano, and Tagliatesta, “Feasibility of a new long distance submarine HVDC link between Sardinia and the Italian Mainland,” in Cigre General Session, Paris (France), 2004

[24]N. Kumar, R. Kumar, M. S. Rao, M. M. Goswami, B. B. Mukherjee, and O. Chandy, "Commissioning Experience and Challenges of World’s First 800 kV, 6000 MW NER – Agra Multi-terminal HVDC System",

[25] S. Arabi, G.J. Rogers, D.Y. Wong, P. Kundur, and M.G. Lauby, “Small Signal Stability Program Analysis of SVC and HVDC in AC Power Systems,” IEEE Transactions on Power Systems, vol. 6, no. 3, pp. 1147–1153, August 1991.

[26] T. Smed and G. Andersson, “Utilizing HVDC to Damp Power Oscillations,” IEEE Transactions on Power Delivery, vol. 8, no. 2, pp. 620–627, April 1993.
[27] M. Bahrman, E.V. Larsen, R.W. Piwko, and H.S. Patel, “Experience with HVDC-turbine-generator torsional interaction at Square Butte,” IEEE Transactions on Power Apparatus and Systems, vol. PAS-99, no. 5, pp. 966–976, July-August 1980.
[28] M. Bahrman, E.V. Larsen, R.W. Piwko, and H.S. Patel, “Field Tests and Analysis of Torsional Interaction Between the Coal Creek Turbine-Generators and the CU HVDC System,” IEEE Transactions on Power Apparatus and Systems, vol. PAS-100, no. 1, pp. 336–344, January 1981.
[29] R.M. Hamouda, M.R. Iravani, and R. Hackam, “Torsional Oscillations of Series Capacitor Compensated AC/DC Systems,” IEEE Transactions on Power Systems, vol. 4, no. 3, pp. 889–896, August 1989.
[30] P. Kundur, Power System Stability and Control, McGrew-Hill, Inc, 1994.
[31] D.Y. Wong, G.J. Rogers, B. Porretta, and P. Kundur, “Eigenvalue Analysis of Very Large Power Systems,” IEEE Transactions on Power Systems, vol. 3, no.2, pp. 472–480, May 1988.
[32] P. Kundur, G.J. Rogers, D.Y. Wong, L. Wang, and M.G. Lauby, “A comprehensive computer program package for small signal stability analysis of power systems,” IEEE Transactions on Power Systems, vol. 5, no. 2, pp. 1076–1083, November 1990.
[33] IEEE/CIGRE Joint TF on Stability Terms and Definitions, “Definition and Classification of Power System Stability,” IEEE Transactions on Power Systems, vol. 19, no. 2, pp. 1387–1401, May 2004.
[34] A.M. Lyapunov, Stability of Motion-English Translation, Academic Press Inc.,1967.
[35] C. Osauskas and A.Wood, “Small-Signal Dynamic Modeling of HVDC Systems,” IEEE Transactions on Power Delivery, vol. 18, no. 1, pp. 220–225, January 2003.
[36] M. Parniani and M.R. Iravani, “Computer analysis of small-signal stability of power systems including network dynamics,” IEE Proceedings of Generation, Transmission and distribution, vol. 142, no. 6, pp. 613–617, November 1995.
[37] K.R. Padiyar and M.K. Geetha, “Study of torsional interactions in multiterminal DC systems through small signal stability analysis,” International Conference on AC and DC Power Transmission, September 1991, pp. 411–413.

[38] J.M. Undrill and T.E. Kostyniak, “Subsynchronous Oscillations Part1 - Comprehensive System Stability Analysis”, IEEE Transactions on Power Apparatus and Systems, vol. PAS-95, no. 4, pp. 1446–1455, February 1976.

[39] C. Karawita, “HVDC Interaction Studies Using Small Signal Stability Assessment,” Ph.D. thesis, University of Manitoba, Canada, 2009.

[40] Chandana Karawita, U. D. Annakkage, “A Hybrid Network Model for Small Signal Stability Analysis of Power Systems,” IEEE Transactions on Power Systems, Vol.25, No. 1, Feb. 2010.

[41] Chandana Karawita, U. D. Annakkage, “Multi-In-Feed HVDC Interaction Studies Using Small Signal Stability Assessment,” IEEE Transactions on Power Delivery, Vol.24, No. 2, April 2009

[42] Peng Zhang, et al., “Multi-In-Feed HVDC Interaction Studies Using Small Signal Stability Assessment,” IEEE Transactions on Power Delivery, Vol.24, No. 2, April 2009

[43] A. Stankovic, B. Lesieutre, and T. Aydin, “Modeling and analysis of single-phase induction machines with dynamic phasors,” *IEEE Trans. Power Syst.*, vol. 14, no. 1, pp. 9–14, Feb. 1999

[44] PSCAD/EMTDC Users Manual, Manitoba HVDC Research Centre, Winnipeg, Canada, 2002.

[45] C. Osauskas, D.J. Hume, and A. Wood, “A small-signal frequency domain model of an HVDC converter,” IEE Proceedings-Generation, Transmission and Distribution, vol. 148, no. 6, pp. 573–578, April 2001.

[46] D.J. Hume, Harmonic and Interharmonic Cross Modulation in HVDC Links, Ph.D. thesis, University of Canterbury, New Zealand, 2002.

[47] M. Szechtman, T. Wess, and C.V. Thio, “First Benchmark Model for HVDC Control Studies,” Electra, no. 135, pp. 55–75, April 1991.

[48] W. Hammer, Dynamic Modeling of Line and Capacitor Commutated Converters for HVDC Power Transmission, Ph.D. thesis, Swiss Federal Institute of Technology, Zurich, 2003.

[49] R.W. Piwko and E.V. Larsen, “HVDC System For Damping of Subsynchrnous Oscillations,” IEEE Transactions on Power Apparatus and Systems, vol. PAS-101, no. 7, pp. 2203–2211, July 1982.

[50] Y.Y. Hsu and L. Wang, “Modal Control of An HVDC System For The Damping of Subsynchronous Oscillations,” IEE Proceedings, vol. 136-C, no. 2, pp. 78–86, March 1989.
[51] D.J. Kim, H.K. Nam, and Y.H. Moon, “A Practical Approach to HVDC System Control for Damping Subsynchronous Oscillation Using the Novel Eigenvalue Analysis Program,” IEEE Transactions on Power Systems, vol. 22, no. 4, pp. 1926–1934, November 2007.
[52] P. Mattavelli, G. C. e. Verghese, and A. M. Stankovic, “Phasor dynamics of thyristor-controlled series capacitor systems,” *IEEE Trans.Power Syst.*, vol. 12, no. 3, pp. 1259–1267, Aug. 1997.
[53] P. C. Stefanov and A. M. Stankovic, “Modeling of UPFC operation under unbalanced conditions with dynamic phasors,” *IEEE Trans. Power Syst.*, vol. 17, no. 2, pp. 395–403, May 2002.
[54] P. Mattavelli, A. M. Stankovic, and G. C. Verghese, “SSR analysis with dynamic phasor model of the thyristor-controlled series capacitor,” *IEEE Trans. Power Syst.*, vol. 14, no. 1, pp. 200–208, Feb. 1999.
[55] IEEE Subsynchronous Resonance TF, “First Benchmark Model For Computer Simulation Of Subsynchronous Resonance,” IEEE Transactions on Power Apparatus and Systems, vol. PAS-96, no. 5, pp. 1565–1572, September/October 1977.
[56] N. Martins, S. Gomes Jr., P. E. M. Quinto, J.C.R. Ferraz, S.L. Varricchio, and A. De Castro, “Some recent developments in small-signal stability and control,” Proc. Of Power EngineeringSociety Winter Meeting 2002, New York, 2002, pp. 1171-1177
[57] Chi-Tsong Chen, Linear System Theory and Design, Oxford University Press, 1999.
[58] IEEE Std. 421.5-1992, IEEE Recommended Practice for Excitation System Models for Power System Stability Studies, IEEE, 1992.
[59] W.G. on Prime Mover and Energy Supply Models for System Dynamic Performance Studies, “Hydraulic Turbine And Turbine Control Models For System Dynamic Studies,” IEEE Transactions on Power Systems, vol. 7, no. 1, pp.167–179, February 1992.
[60] B. Gemmell and J. Laughran, “HVDC Offers the Key to Untapped Hydro Potential,” IEEE Power Engineering Review, vol. 22, no. 5, pp. 8–11, May 2002.
[61] M. Szechtman, T. Wess, and C.V. Thio, “First Benchmark Model for HVDC Control Studies,” Electra, no. 135, pp. 55–75, April 1991.

[62] I.J. Perez-Arriaga, G.C. Verghese, and F.C. Schweppe, “Selective Modal Analysis with Applications to Electric Power Systems, PART I: Heuristic Introduction,” IEEE Transactions on Power Apparatus and Systems, vol. PAS-101, no. 9, pp. 3117–3125, September 1982.

[63] G.C. Verghese, I.J. Perez-Arriaga, and F.C. Schweppe, “Selective Modal Analysis With Applications to Electric Power Systems, Part II: The Dynamic Stability Problem,” IEEE Transactions on Power Apparatus and Systems, vol. PAS-101, no. 9, pp. 3126–3134, September 1982.

[64] G. Rogers, Power System Oscillations, Kluwer Academic Publishers, Norwell, Massachusetts, USA, 2000.

[65] PSS/E User’s Manual, Siemens Power Technologies International, Schenectady, NY, USA.

[66] P. Kundur, M. Klein, G.J. Rogers, and M.S. Zywno, “Application of Power System Stabilizers for Enhancement of Overall System Stability,” IEEE Transactions on Power Systems, vol. 4, no. 2, pp. 614–626, May 1989.

[67] CIGRE WG 14.07, ‘Guide for planning DC lines terminating at AC system Locations having low short-circuit capacitors, Part I: AC-DC interaction phenomena’ 1992

[68] J. Arrillage, “High Voltage Direct Current Transmission,” 2nd Edition, The Institution of Electrical Engineers, London, United Kingdom

[69] L.A.S. Pilotto, M. Szechtman, A. Wey, W.F. Long, and S.L. Nilsson, “Synchronizing and Damping Torque Modulation Controllers for Multi-infeed HVDC Systems,” IEEE Transactions on Power Delivery, vol. 10, no. 3, pp. 1505–1513, July 1995

[70] L.E. Jones and G. Andersson, “Selecting Robust Input Signals For HVDC Damping Controllers,” Conference on AC and DC Power Transmission-IEE, April-May 1996, pp. 152–156.

Appendix A
MTHVDC System Parameters

A.1 Three Terminal HVDC System Data

Converter Data

Converter Data	Terminal One	Terminal Two	Terminal Three
Number of Valve Group in Series	2	2	2
AC system Voltage (kV)	345	345	345
DC current Order (kA)	2.61	1.41	1.2
DC Voltage (kV)	500.00	462.87	468.22
Firing Angle (degree)	18	139.07	140.763
Transformer (MVA)	1500	1183.6	1183.6
Transformer Impedance (p.u.)	0.18	0.18	0.18
Transformer Ratio	1.5938	1.7314	1.7228

HVDC Line Data

HVDC parameter	Section1(T1-T4)	Section 2(T2-T4)	Section 3(T3-T4)
Distance (km)	960	400	100
Resistance (ohm)	11.6215	4.8222	1.2055
Inductance (H)	0.9089	0.3771	0.09431
Capacitance (uf)	5.97375 x 2	2.47875 x 2	0.61975 x 2
Smoothing Reactor (H)	0.5	0.5	0.5

Phase Lock Loop

PLL Setting	Terminal One	Terminal Two	Terminal Three
KP(scheme one)	10	50	50
KI(scheme one)	50	100	100
KP(scheme two)	10	10	10
KI(scheme two)	50	150	80

HVDC Controller Data

Control Parameter	Terminal One	Terminal Two	Terminal Three
Control Mode (Scheme One)	Current	Current	Voltage
KP(scheme one)	0.01	0.01	0.01
KI(scheme one)	50	10	80
Control Mode (Scheme Two)	Voltage	Curent	Current
KP(scheme Two)	0.01	0.01	0.01
KI(scheme Two)	80	10	10

A.2 Generator, Exciter and Governor Data

Generator Data

Machine Parameter	Terminal One	Terminal Two	Terminal Three
	G41	G35	G36
Td0' (s)	6.700	10.200	6.560
Td0"(s)	0.050	0.050	0.050
Tq0'(s)	0.410	1.500	1.500
Tq0"(s)	0.060	0.060	0.060
H(MW.s/MVA)	2.430	4.200	3.030
D	0.000	0.000	0.000
Xd (p.u.)	2.900	1.000	2.950
Xq(p.u.)	2.800	0.690	2.820
Xd'(p.u.)	0.570	0.310	0.697
Xq'(p.p.)	0.911	0.310	1.700
Xd"=Xq"(p.u.)	0.450	0.250	0.500
Xl(p.u.)	0.280	0.125	0.350
S(1.0)	0.080	0.150	0.070
S(1.2)	0.268	0.425	0.391
Rating (MVA)	1800.000	1000.000	1000.000
Terminal Voltage (kV)	13.800	13.800	13.800

Exciter Data

Exciter Parameter	Terminal One	Terminal Two	Terminal Three
	G41	G35	G36
Tr	0.020	0.020	0.020
Vimax	1.000	1.000	1.000
Vimin	-1.000	-1.000	-1.000
Tc	0.150	0.150	0.150
Tb	0.100	0.100	0.100
Ka	5.000	5.000	6.200
Ta	0.020	0.060	0.050
Vrmax	12.000	12.000	12.000
Vrmin	-12.000	-12.000	-12.000
Kc	0.000	0.000	0.000

Governor Data

Governor Parameter	Terminal One	Terminal Two	Terminal Three
	G41	G35	G36
R	0.050	0.050	0.050
T1	0.050	0.050	0.050
Vmax	1.000	1.000	1.000
Vmin	0.000	0.000	0.000
T2	2.100	2.100	2.100
T3	7.000	7.000	7.000

Dt	0.000	0.000	0.000

A.3 Test System Power Flow Data

Power Flow – AC Bus Data

Bus Number	Base kV	Type	Voltage Magnitude	Angle
22	345	Load	1.0092	-2.99
23	345	Load	1.0049	-4.22
24	345	Load	1.0064	-3.72
25	345	Load	1.0108	-3.61
35	13.8	Gen	1.03	0
36	13.8	Gen	1.03	-0.23
40	345	Load	1.0271	-6.69
41	13.8	Gen	1.03	-3.24
42	345	Load	1.0246	-8.12

Power Flow – Generator Data

Generator Bus	MW	Mvar
42	1408.128	107.535
35	840.778	331.373
36	900.75	354.656

Power Flow – Load Data

Load Bus	MW	Mvar	Id
23	456.3	245.700	1
23	205.6	78.100	2
23	800	200.000	3
24	610.7	139.500	1
24	800	200.000	2
24	81.9	6.500	3
40	100	0.000	1

Power Flow – Transformer Data

From Bus	To Bus	Resistance	Reactance	MVA
23	36	0	0.008	100
24	35	0	0.008	100
40	41	0	0.00452	100

Power Flow – Transmission Line Data

From Bus	To Bus	Resistance	Reactance	Susceptance
22	24	0.000193	0.002015	0.008390
23	25	0.000193	0.002015	0.008390

40	42	0.000193	0.002015	0.008390

Power Flow – Shunt Capacitor Data

Bus	Mvar
22	500
25	600
42	750

Appendix B
Linearized HVDC Converter, PLL Models, Generator, Exciter and Governor Models

B.1 Linearized HVDC Converter Model

The 6-pulse bridge is the basic building block of HVDC converters. Three valves (1, 3, and 5) connected together form the upper limb and other three valves (4, 6, and 2) form lower limb as shown in Figure 2.1. The 6-pulse bridge is connected to the AC system through a three-phase converter transformer. The DC voltage can be changed by changing the firing angle. Ideally, when the next valve on the same limb is fired, the conducting valve will stop if there is no inductance in the circuit. However, due to the presence of converter transformer leakage inductance (Lc), there is a period in which both of the valves are conducting. This period is called the "commutation period" and the corresponding phase angle is referred to as "commutation angle" (μ). Each valve in the bridge has a normal conduction period of 120 degrees and two commutation periods (2 × μ) in each cycle.

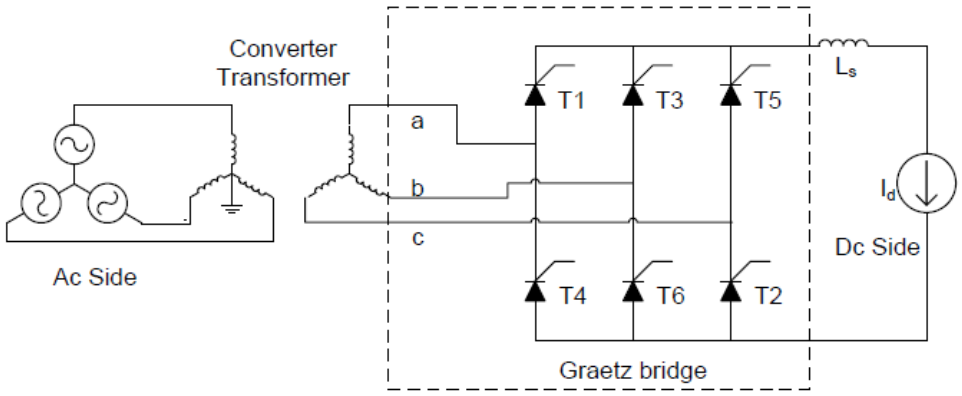

Figure B1.1 Three Phase Graetz Bridge

The DC side voltage is given by equation (B1.1)

$$V_{dc} = \frac{3\sqrt{2}B}{\pi T} V_l \cos(\alpha) - \frac{3X_c B}{\pi} I_{dc} \tag{B1.1}$$

Where B is the number of 6 pulse bridges

T is the converter transformer turn ratio (ac/dc)

α is firing angle

X_c is transformer reactance referred to DC side

V_l is AC side line-line voltage magnitude

The fundamental frequency component of the converter AC current can be obtained from the current waveform shown in Figure B1.2 using Fourier series expansion.

The fundamental component of the phase-a current is given by Equation (B1.2).

$$i_{a1} = A_{a1}\cos(\omega_0 t) + C_{a1}\sin(\omega_0 t) \tag{B1.2}$$

Where,

$$A_{a1} = \frac{\sqrt{2}BV_l}{\pi X_c T^2}\int_{\frac{\pi}{6}+\alpha}^{\frac{\pi}{6}+\alpha+\mu}[\cos(\alpha)-\cos(\theta-\frac{\pi}{6})]\cos(\theta)d\theta + \frac{2B}{\pi T}\int_{\frac{\pi}{6}+\alpha}^{\frac{5\pi}{6}+\alpha+\mu} I_{dc}\cos(\theta)d\theta$$

$$-\frac{\sqrt{2}BV_l}{\pi X_c T^2}\int_{\frac{5\pi}{6}+\alpha}^{\frac{5\pi}{6}+\alpha+\mu}[\cos(\alpha)-\cos(\theta-\frac{5\pi}{6})]\cos(\theta)d\theta$$

$$C_{a1} = \frac{\sqrt{2}BV_l}{\pi X_c T^2}\int_{\frac{\pi}{6}+\alpha}^{\frac{\pi}{6}+\alpha+\mu}[\cos(\alpha)-\cos(\theta-\frac{\pi}{6})]\sin(\theta)d\theta + \frac{2B}{\pi T}\int_{\frac{\pi}{6}+\alpha}^{\frac{5\pi}{6}+\alpha+\mu} I_{dc}\sin(\theta)d\theta$$

$$-\frac{\sqrt{2}BV_l}{\pi X_c T^2}\int_{\frac{5\pi}{6}+\alpha}^{\frac{5\pi}{6}+\alpha+\mu}[\cos(\alpha)-\cos(\theta-\frac{5\pi}{6})]\sin(\theta)d\theta$$

The real and the imaginary components of the AC current can be simplified as given in Equations (B1.3) and (B1.4) respectively.

$$I_R = -\frac{\sqrt{3}BX_c I_{dc}^2 V_R}{\pi V_l^2} + \frac{\sqrt{3}BM_1 V_I}{2\pi X_c T^2} - \frac{\sqrt{6}BI_{dc}}{\pi T}\cos(\delta - \alpha - \mu) \quad \text{(B1.3)}$$

$$I_I = -\frac{\sqrt{3}BX_c I_{dc}^2 V_I}{\pi V_l^2} - \frac{\sqrt{3}BM_1 V_R}{2\pi X_c T^2} - \frac{\sqrt{6}BI_{dc}}{\pi T}\sin(\delta - \alpha - \mu) \quad \text{(B1.4)}$$

In steady-state, the DC side voltage and the real and imaginary components of the AC current depend on the commutation angle (μ). In reality, the DC current cannot be changed instantaneously due to both the DC line inductance and the smoothing reactor and the fact that the commutation period is usually small (<30 degrees) in normal HVDC operation. Therefore, we can assume the change in the DC current during the commutation period is negligible. As a result, the commutation angle can be expressed as a function of DC side current, AC side voltage, and firing angle as given in Equation (B1.5).

$$\mu = \cos^{-1}(\cos\alpha - \frac{\sqrt{2}X_c T I_{dc}}{V_l}) - \alpha \quad \text{(B1.5)}$$

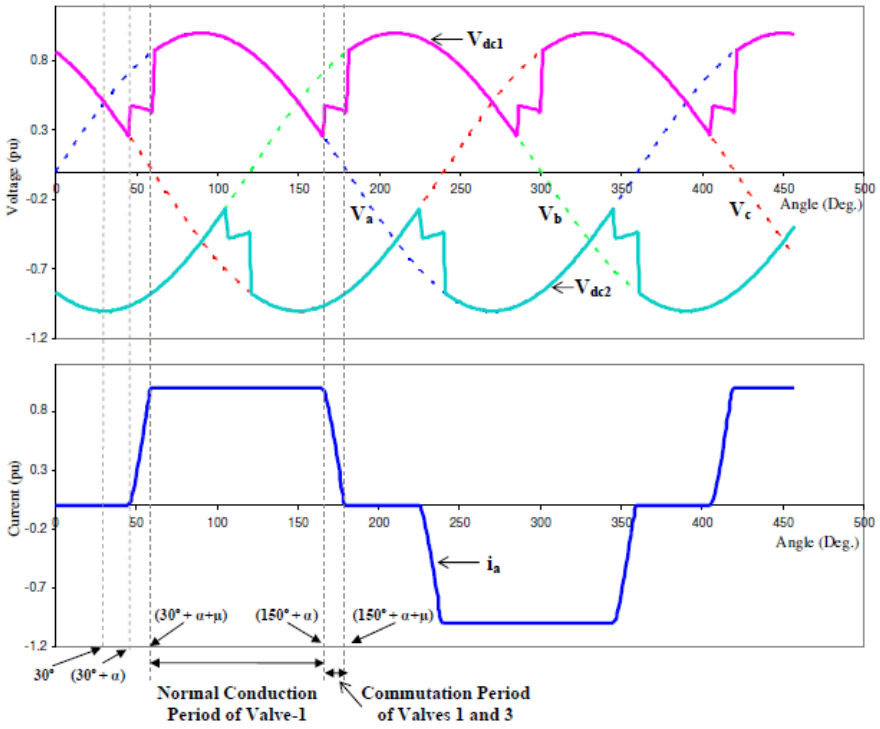

Figure B1.2 DC side Voltage and AC side phase a current of a Graetz Bridge

The fundamental frequency relationships (Equations B1.1, B1.3, and B1.4) derived from the converter switching waveforms are used to obtain the linearized model. The commutation angle in these relationships is replaced by Equation (2.8).

The converter linearized relationships can be defined using four inputs (real component and imaginary component of AC side voltage, DC side current, and firing angle) and three outputs (real component and imaginary component of AC side current and DC side voltage). The changes in the outputs for small changes in the inputs are given by Equation (B1.6).

$$\begin{bmatrix} \Delta I_R \\ \Delta I_I \\ \Delta V_{dc} \end{bmatrix} = \begin{bmatrix} K_a & K_b & K_c & K_d \\ K_e & K_f & K_g & K_h \\ K_i & K_j & K_k & K_l \end{bmatrix} \begin{bmatrix} \Delta V_R \\ \Delta V_I \\ \Delta I_{dc} \\ \Delta \alpha \end{bmatrix} \tag{B1.6}$$

Where

$$K_a = -\frac{\sqrt{3}BX_c I_{dc}^2}{\pi V_l^2} - \frac{\sqrt{6}BI_{dc}V_I \sin(\delta - \alpha - \mu)}{\pi T V_l^2}$$

$$K_b = -\frac{\sqrt{3}BM_1}{2\pi X_c T^2} + \frac{\sqrt{6}BI_{dc}V_R \sin(\delta - \alpha - \mu)}{\pi T V_l^2}$$

$$K_c = -\frac{\sqrt{6}B\cos(\delta - \alpha - \mu)}{\pi T}$$

$$K_d = -\frac{\sqrt{6}BI_{dc}\sin(\alpha)\sin(\delta - \alpha - \mu/2)}{\pi T \sin(\alpha + \mu/2)}$$

$$K_e = -\frac{\sqrt{3}BM_1}{2\pi X_c T^2} + \frac{\sqrt{6}BI_{dc}V_I \cos(\delta - \alpha - \mu)}{\pi T V_l^2}$$

$$K_f = -\frac{\sqrt{3}BX_c I_{dc}^2}{\pi V_l^2} - \frac{\sqrt{6}BI_{dc}V_R \cos(\delta - \alpha - \mu)}{\pi T V_l^2}$$

$$K_g = -\frac{\sqrt{6}B\sin(\delta - \alpha - \mu)}{\pi T}$$

$$K_h = -\frac{\sqrt{6}BI_{dc}\sin(\alpha)\cos(\delta - \alpha - \mu/2)}{\pi T \sin(\alpha + \mu/2)}$$

$$K_i = \frac{3\sqrt{2}BV_R \cos(\alpha)}{\pi T V_l}$$

$$K_j = \frac{3\sqrt{2}BV_I \cos(\alpha)}{\pi T V_l}$$

$$K_k = -\frac{3X_c B}{\pi}$$

$$K_l = -\frac{3\sqrt{2}BV_I \sin(\alpha)}{\pi T}$$

This model is similar to the one given in [30], except, the real and imaginary components rather than positive and negative sequences are used as the variables to be consistent with the common approach of linearized power systems. The detailed derivation can be found in [32]. Note that the signs of K_i, K_j, K_k and K_l should be inverted in order to represent a positive voltage pole inverter.

B.1 Linearized Generator Model

In tradition small signal analysis, generators are represented either by round rotor (6^{th} order) or salient pole (5^{th} order) machine models. To include the stator flux components, two additional differential equations representing the stator flux in d-q

axes are added to the synchronous machine model. Therefore, an 8^{th}order machine model is used for the round rotor machine and a 7^{th}order machine model is used for salient pole machine. In this research, the ac network is represented using dynamic phasor, therefore, an 8^{th}order round rotor machine is used to represent generator. The linearized model for the machine, exciter and governor are provided in the following sections. The standard notations and the d-q axes selection are according to [15].

The changes in the d-q axes current are:

$$\Delta i_d = K_{id3}\Delta\Phi_d + K_{id4}\Delta\Phi_{fd} + K_{id5}\Delta\Phi_{1d}$$

Where

$$K_{id3} = -\frac{L_{ad}L_{pd}(L_{fd}+L_{1d})}{L_l L_d L_{fd} L_{1d}} - \frac{1}{L_d}$$

$$K_{id4} = \frac{L_{pd}}{L_l L_{fd}}$$

$$K_{id5} = \frac{L_{pd}}{L_l L_{1d}}$$

$$L_{pd} = \frac{1}{(\frac{1}{L_l} + \frac{1}{L_{ad}} + \frac{1}{L_{fd}} + \frac{1}{L_{1d}})}$$

$$\Delta i_q = K_{iq6}\Delta\Phi_q + K_{iq7}\Delta\Phi_{1q} + K_{iq8}\Delta\Phi_{2q}$$

Where

$$K_{iq6} = -\frac{L_{aq}L_{pq}(L_{1q}+L_{2q})}{L_l L_q L_{1q} L_{2q}} - \frac{1}{L_q}$$

$$K_{iq7} = \frac{L_{pq}}{L_l L_{1q}}$$

$$K_{iq8} = \frac{L_{pq}}{L_l L_{2q}}$$

$$L_{pq} = \frac{1}{(\frac{1}{L_l} + \frac{1}{L_{aq}} + \frac{1}{L_{1q}} + \frac{1}{L_{2q}})}$$

The generator state space model is also provided in the form of $\Delta\dot{X}_g = A_g\Delta X_g + B_g\Delta U_g + E_g\Delta \mathrm{V}_g$. There are total eight state variables: generator rotor angle (δ), rotor speed (ω_r), d-axis stator winding flux (Φ_d), d-axis field winding flux (Φ_{fd}), d-axis damper winding flux (Φ_{1d}), q-axis stator winding flux (Φ_q), q-axis first damper winding flux (Φ_{1q}) and q-axis second damper winding flux (Φ_{2q}). There are two inputs, one is the mechanical torque (T_m) and the other one is the field voltage (E_{fd}).

$$\begin{bmatrix} \Delta\dot{\delta} \\ \Delta\dot{\omega}_r \\ \Delta\dot{\Phi}_d \\ \Delta\dot{\Phi}_{fd} \\ \Delta\dot{\Phi}_{1d} \\ \Delta\dot{\Phi}_q \\ \Delta\dot{\Phi}_{1q} \\ \Delta\dot{\Phi}_{2q} \end{bmatrix} = \begin{bmatrix} 0 & ag_{12} & 0 & 0 & 0 & 0 & 0 & 0 \\ 0 & ag_{22} & ag_{23} & ag_{24} & ag_{25} & ag_{26} & ag_{27} & ag_{28} \\ ag_{31} & ag_{32} & ag_{33} & ag_{34} & ag_{35} & ag_{36} & 0 & 0 \\ 0 & 0 & ag_{43} & ag_{44} & ag_{45} & 0 & 0 & 0 \\ 0 & 0 & ag_{53} & ag_{54} & ag_{55} & 0 & 0 & 0 \\ ag_{61} & ag_{62} & ag_{63} & 0 & 0 & ag_{66} & ag_{67} & ag_{68} \\ 0 & 0 & 0 & 0 & 0 & ag_{76} & ag_{77} & ag_{78} \\ 0 & 0 & 0 & 0 & 0 & ag_{86} & ag_{87} & ag_{88} \end{bmatrix} \begin{bmatrix} \Delta\delta \\ \Delta\omega_r \\ \Delta\Phi_d \\ \Delta\Phi_{fd} \\ \Delta\Phi_{1d} \\ \Delta\Phi_q \\ \Delta\Phi_{1q} \\ \Delta\Phi_{2q} \end{bmatrix}$$

$$+ \begin{bmatrix} 0 & 0 \\ bg_{21} & 0 \\ 0 & 0 \\ 0 & bg_{42} \\ 0 & 0 \\ 0 & 0 \\ 0 & 0 \\ 0 & 0 \end{bmatrix} \begin{bmatrix} \Delta T_m \\ \Delta E_{fd} \end{bmatrix} + \begin{bmatrix} 0 & 0 \\ 0 & 0 \\ eg_{31} & eg_{32} \\ 0 & 0 \\ 0 & 0 \\ eg_{61} & eg_{62} \\ 0 & 0 \\ 0 & 0 \end{bmatrix} \begin{bmatrix} \Delta V_R \\ \Delta V_I \end{bmatrix}$$

The parameters in the equation are:

$$ag_{12} = \omega_0 \qquad\qquad ag_{22} = -\frac{K_d}{M}$$

$$ag_{23} = \frac{1}{M}[-i_q + \Phi_q K_{id3}] \qquad ag_{24} = -\frac{1}{M}[\Phi_q K_{id4}]$$

$$ag_{25} = \frac{1}{M}[\Phi_q K_{id5}] \qquad ag_{26} = -\frac{1}{M}[-i_d + \Phi_d K_{iq6}]$$

$$ag_{27} = -\frac{1}{M}[\Phi_d K_{iq7}] \qquad ag_{28} = -\frac{1}{M}[\Phi_d K_{iq8}]$$

$$ag_{31} = \omega_0 e_q \qquad ag_{32} = \omega_0 \Phi_q$$

$$ag_{33} = \omega_0 R_a K_{id3} \qquad ag_{34} = \omega_0 R_a K_{id4}$$

$$ag_{35} = \omega_0 R_a K_{id5} \qquad ag_{36} = \omega_0$$

$$ag_{43} = \frac{\omega_0 R_{fd} L_{pd}}{L_l L_{fd}} \qquad ag_{44} = -\frac{\omega_0 R_{fd} L_{pd}}{L_{fd}}\left(\frac{1}{L_l} + \frac{1}{L_{ad}} + \frac{1}{L_{1d}}\right)$$

$$ag_{45} = \frac{\omega_0 R_{fd} L_{pd}}{L_{1d} L_{fd}} \qquad ag_{53} = \frac{\omega_0 R_{1d} L_{pd}}{L_{1d} L_l}$$

$$ag_{54} = \frac{\omega_0 R_{1d} L_{pd}}{L_{1d} L_{fd}} \qquad ag_{55} = -\frac{\omega_0 R_{1d} L_{pd}}{L_{1d}}\left(\frac{1}{L_l} + \frac{1}{L_{ad}} + \frac{1}{L_{fd}}\right)$$

$$ag_{61} = -\omega_0 e_d \qquad ag_{62} = -\omega_0 \Phi_d$$

$$ag_{63} = -\omega_0 \qquad ag_{66} = \omega_0 R_a K_{iq6}$$

$$ag_{67} = \omega_0 R_a K_{iq7} \qquad ag_{68} = \omega_0 R_a K_{iq8}$$

$$ag_{76} = \frac{\omega_0 R_{1q} L_{pq}}{L_{1q} L_l} \qquad ag_{77} = -\frac{\omega_0 R_{1q} L_{pq}}{L_{1q}}\left(\frac{1}{L_l} + \frac{1}{L_{aq}} + \frac{1}{L_{2q}}\right)$$

$$ag_{78} = \frac{\omega_0 R_{1q} L_{pq}}{L_{1q} L_{2q}} \qquad ag_{86} = \frac{\omega_0 R_{2q} L_{pq}}{L_{1q} L_l}$$

$$ag_{87} = \frac{\omega_0 R_{2q} L_{pq}}{L_{1q} L_{2q}} \qquad ag_{88} = -\frac{\omega_0 R_{2q} L_{pq}}{L_{2q}}\left(\frac{1}{L_l} + \frac{1}{L_{aq}} + \frac{1}{L_{1q}}\right)$$

$$bg_{21} = \frac{1}{M} \qquad bg_{42} = \frac{\omega_0 R_{fd}}{L_{ad}}$$

$eg_{31} = \omega_0 \sin(\delta)$ $eg_{32} = -\omega_0 \cos(\delta)$

$eg_{61} = \omega_0 \cos(\delta)$ $eg_{62} = \omega_0 \sin(\delta)$

The R-I components of the generator output current in terms of the state variables are given as follows. It is in the form of ($\Delta I_g = C_g \Delta X_g$).

$$\begin{bmatrix} \Delta I_R \\ \Delta I_I \end{bmatrix} = \begin{bmatrix} cg_{11} & 0 & cg_{13} & cg_{14} & cg_{15} & cg_{16} & cg_{17} & cg_{18} \\ cg_{21} & 0 & cg_{23} & cg_{24} & cg_{25} & cg_{26} & cg_{27} & cg_{28} \end{bmatrix} \begin{bmatrix} \Delta\delta \\ \Delta\omega_r \\ \Delta\Phi_d \\ \Delta\Phi_{fd} \\ \Delta\Phi_{1d} \\ \Delta\Phi_q \\ \Delta\Phi_{1q} \\ \Delta\Phi_{2q} \end{bmatrix}$$

The parameters in the above equation are:

$cg_{11} = -I_I$ $cg_{13} = K_{id3} \sin(\delta)$

$cg_{14} = K_{id4} \sin(\delta)$ $cg_{15} = K_{id5} \sin(\delta)$

$cg_{16} = K_{id6} \cos(\delta)$ $cg_{17} = K_{id7} \cos(\delta)$

$cg_{18} = K_{id8} \cos(\delta)$

$cg_{21} = I_R$ $cg_{23} = -K_{id3} \cos(\delta)$

$cg_{24} = -K_{id4} \cos(\delta)$ $cg_{25} = -K_{id5} \cos(\delta)$

$cg_{26} = K_{id6} \sin(\delta)$ $cg_{27} = K_{id7} \sin(\delta)$

$cg_{28} = K_{id8} \sin(\delta)$

B.2 Linearized Exciter Model

The IEEE standard AC4A exciter model is used in this research. The linearized model is given in Equation (B.1) in the form of ($\Delta\dot{X}_e = A_e\Delta X_e + B_e\Delta U_e + E_e\Delta V_g$). It consists of three state variables, Field voltage (E_{fd}), X_{E1} and X_{E2}.

$$\begin{bmatrix}\Delta\dot{E}_{fd}\\ \Delta\dot{X}_{E1}\\ \Delta\dot{X}_{E2}\end{bmatrix} = \begin{bmatrix}ae_{11} & ae_{12} & ae_{13}\\ 0 & ae_{22} & ae_{23}\\ 0 & 0 & ae_{33}\end{bmatrix}\begin{bmatrix}\Delta E_{fd}\\ \Delta X_{E1}\\ \Delta X_{E2}\end{bmatrix} + \begin{bmatrix}be_1\\ be_2\\ 0\end{bmatrix}\left[\Delta V_{ref}\right] + \begin{bmatrix}0 & 0\\ 0 & 0\\ ee_{31} & ee_{32}\end{bmatrix}\begin{bmatrix}\Delta V_R\\ \Delta V_I\end{bmatrix}$$

The parameters in the equation are:

$$ae_{11} = -\frac{1}{T_A} \qquad ae_{12} = \frac{K_A}{T_A}\left(1 - \frac{T_C}{T_B}\right)$$

$$ae_{13} = -\frac{K_A T_C}{T_A T_B} \qquad ae_{22} = -\frac{1}{T_B}$$

$$ae_{23} = -\frac{1}{T_B} \qquad ae_{33} = -\frac{1}{T_r}$$

$$be_1 = \frac{K_A T_C}{T_A T_B} \qquad be_2 = \frac{1}{T_B}$$

$$ee_{31} = \frac{V_R}{T_r V_l} \qquad ee_{32} = \frac{V_I}{T_r V_l}$$

Where V_l is the magnitude of the machine terminal voltage.

B.3 Linearized Governor Model

As shown in Figure B.1, the mechanical-hydraulic governor and hydro turbine are used in the research. The linearized governor model consists of five state variables, X_1, X_2, X_3 , X_4 and q. The linearized model is given in equation (B.10) in the form of ($\Delta\dot{X}_T = A_T\Delta X_T + C_T\Delta\omega_r + B_T\Delta U_T$).

$$\begin{bmatrix}\dot{\Delta X_1}\\ \dot{\Delta X_2}\\ \dot{\Delta X_3}\\ \dot{\Delta X_4}\\ q\end{bmatrix}=\begin{bmatrix}at_{11} & at_{12} & 0 & at_{14} & 0\\ at_{21} & 0 & 0 & 0 & 0\\ 0 & at_{32} & at_{33} & 0 & 0\\ 0 & at_{42} & 0 & at_{44} & 0\\ 0 & 0 & at_{53} & 0 & at_{55}\end{bmatrix}\begin{bmatrix}\Delta X_1\\ \Delta X_2\\ \Delta X_3\\ \Delta X_4\\ q\end{bmatrix}+\begin{bmatrix}ct_1\\ 0\\ 0\\ 0\\ 0\end{bmatrix}[\Delta\omega_r]+\begin{bmatrix}bt_1\\ 0\\ 0\\ 0\\ 0\end{bmatrix}[\Delta\omega_{ref}]$$

The parameters in the equation are:

$at_{11}=-\frac{1}{T_p}$ $\quad$ $at_{12}=-\frac{R_t+R_p}{T_p}$

$at_{14}=\frac{1}{T_p}$ $\quad$ $at_{21}=q$

$at_{32}=\frac{1}{T_g}$ $\quad$ $at_{33}=-\frac{1}{T_g}$

$at_{42}=\frac{R_t}{T_R}$ $\quad$ $at_{44}=-\frac{1}{T_R}$

$at_{53}=\frac{2q^2}{T_w G^3}$ $\quad$ $at_{55}=-\frac{2q}{T_w}(\frac{1}{G^2}-f_p)$

$ct_1=-\frac{1}{T_p}$

$bt_1=\frac{1}{T_p}$

Where q is the flow rate and G is is the gate position.

The mechanical torque produced by the turbine is:

$$[\Delta T_m]=[0 \quad 0 \quad dt_3 \quad 0 \quad dt_5]\begin{bmatrix}\Delta X_1\\ \Delta X_2\\ \Delta X_2\\ \Delta X_4\\ \Delta q\end{bmatrix}+\left[-DG-\frac{A_t q^2}{G^2}(q-q_{NL})\right][\Delta\omega_r]$$

$dt_3=-\frac{2A_t q^2}{G^3}(q-q_{NL})$

$dt_5=\frac{A_t}{G^3}(3q^2-2qq_{NL})$

Where $q_{NL}$is the turbine no load-flow.

B.4 State Space Generator Model with Exciter and Governor

The linearized generator model is:

$$\Delta\dot{X}_g = A_g\Delta X_g + B_g\Delta U_g + E_g\Delta \mathrm{V}_g$$

$$\Delta I_g = C_g\Delta X_g$$

The linearized exciter model is:

$$\Delta\dot{X}_e = A_e\Delta X_e + B_e\Delta U_e + E_e\Delta V_g$$

ΔE_{fd} is the state variable of the exciter model, which is the input to the generator model. The generator and exciter are combined together through ΔE_{fd}.

The linearized governor model is:

$$\Delta\dot{X}_T = A_T\Delta X_T + AA_T\Delta\omega_r + B_T\Delta\omega_{ref}$$

$$\Delta T_m = C_T\Delta X_T + CC_T\Delta\omega_r$$

ΔT_m is the output of the governor model, which is the input to the generator model. The generator and the governor model are combined together to eliminate the ΔT_mterm.

Appendix C
Linearized HVDC Converter, PLL Models, Generator, Exciter and Governor Models

C.1 AC system strength on Controller interaction- Scheme one

Table C1.1 shows the controller interaction oscillation frequencies and damping ratios for different AC system strength. Correspondingly, Table C1.2 and Table C1.3 show participation factors result and mode shape angles between controller state variables for all oscillation modes with different AC system strength. It is noted that T1 PF, T2 PF and T3 PF in all participatioin factor analysis table represent the terminal one, terminal two and terminal three controller state variable participation factor repectively.

Table C1.4 to Table C1.6 show that the study results with different AC system strength for the three-terminal HVDC system have a different HVDC line tap point. In this case, line sections between terminal one and the HVDC line tap point are swapped with the section between terminal two and the HVDC line tap point. All control parameters as well as the operating point remain the same as in the original study case. Table C1.7 to Table C1.9 show that the study results with a system strength increase for the three-terminal HVDC system with different control parameters. In this case, the proportional gain for all HVDC voltage and current controllers change from 0.01 to 0.5. The integral gain as well as the PLL gains changed slightly to ensure that there is no negative damping mode in the study. Table C1.10 to Table C1.12 show that the study results with system strength change for the three-terminal HVDC system operated at different operating points. In this case,

terminal one (rectifier) DC power remains constant, terminal two DC power slightly decreases from 653MW to 639MW, and terminal three DC power increases from 560MW to 570MW. All other conditions such as the system configuration, controller arrangement, and control parameters remain the same as in the original cases.

C.1.1 Terminal Two AC system strength variation:

Mode-4:

A similar analysis has been conducted for the terminal two AC system strength change. As shown in Table C1.1, when terminal two (current control terminal) AC system strength is increased, Mode-4 oscillation frequency slightly decreases from 12.71Hz to 12.68Hz and the damping ratio slightly increases from 30.62% to 34.35%. The results indicate that the terminal one current controller state variable retains the highest participation of 1.0 in this mode as shown in Table C1.2. The participation factor of the terminal two current controller state variable decreases from 0.064 to 0.029 and the terminal three voltage controller state variable participation factor decreases from 0.127 to 0.115. Mode shape shows that the terminal one current controller and the terminal two current controller state variables oscillate together against the terminal three voltage controller state variable in this mode. With an increase in terminal two AC system strength, the angle between terminal one and terminal two current controller state variables decreases from 44 degrees to 31.34 degrees and the angle between the terminal two current controller state variable and the terminal three voltage controller state variable increases from 120.7 degrees to 164.66 degrees. The angle between the terminal three voltage controller state variable and the terminal one current controller state variable decreases from 195.3 degrees to 164.0 degrees. Although the angles change, the mode shape remains the same as the terminal

one current controller and the terminal two current controller state variables oscillate together against the terminal three voltage controller state variable. As a result, both the oscillation frequency and the damping ratio slightly changes. However, this mode has enough damping ratio and has no small signal stability concerns for all study scenarios.

Mode-5:

In Mode-5, the oscillation frequency of this mode slightly decreases from 11.43Hz to 10.46Hz and the damping ratio increases from 39.72% to 45.27% when terminal two AC system strength increases from 600MVA to 2000MVA. The participation factor for the terminal one current controller state variable decreases from 0.511 to 0.287, and the terminal two current controller state variable participation factor increases from 0.049 to 0.097. The terminal three voltage controller state variable participation factor increases from 0.460 to 0.506. Mode shape indicates that the angle between the terminal one current controller and the terminal two current controller state variables decreases from 115.80 degrees to 96.09 degrees. The angle between the terminal two current controller state variable and the terminal three voltage controller state variable decreases from 73.10 degrees to 70.20 degrees when terminal two AC system strength increases from 600MVA to 1000MVA. Further increasing terminal two AC system strength to 1500MVA increases the angle from 70.20 degrees to 71.30 degrees. This angle decreases again to 70.81 degrees if terminal two AC system strength is further increased to 2000MVA. The mode shape angle can either be increased or decreased with increasing terminal two AC system strength. The angle between the terminal three voltage controller state variable and the terminal one current controller state variable increases from 171.10 degrees to 193.10 degrees. The mode shape angles between each controller state variables slightly change due to the

terminal two AC system strength change. However, the study results prove that the oscillation mode remains unchanged as the terminal one current controller state variable oscillates against both the terminal two current controller state variable and the terminal three voltage controller state variable. As a result, the oscillation frequency and the damping ratio change due to terminal AC system strength change However, this mode has enough damping ratio and has no small signal stability concerns for all study scenarios.

Mode-6:

In Mode-6, the oscillation frequency decreases from 4.55Hz to 3.90Hz and the damping ratio decreases from 50.77% to 38.31% when the terminal two AC system strength increases from 600MVA to 2000MVA. The results in Table 6.2 show that the participation factor of the terminal one current controller state variable decreases from 0.337 to 0.161, the participation factor of the terminal two current controller state variable increases from 0.419 to 1.0 and the participation factor of the terminal three voltage controller state variable drops from 1.0 to 0.87. Mode shape angles indicate that the angle between the terminal one current controller state variable and terminal two current controller state variable increases from 136.7 degrees to 152.8 degrees and the angle between the terminal two current controller state variable and terminal three voltage controller state variable slightly decreases from 89.69 degrees to 81.6 degrees. The angle between the terminal three voltage controller state variable and terminal one current controller state variable decreases from 133.61 degrees to 125.60 degrees. Although mode shape angles change, the oscillation mode with terminal one current controller state variable oscillates against terminal two current controller state variable and terminal three voltage controller state variable remains unchanged. The oscillation frequency and damping ratio of this mode

change due to terminal AC system strength change. However, This mode has enough damping ratio and has no small signal stability concerns for all study scenarios.

C1.2Terminal Three AC system strength variation

Mode-4:

The same analysis process has been conducted for the terminal three AC system strength increase. Increasing terminal three (voltage control terminal) AC system strength from 1000MVA to 4000MVA causes the Mode-4 oscillation frequency to increase slightly from 12.71Hz to 13.11Hz. As shown in Table C1.1, the damping ratio slightly decreases from 30.62% to 29.05% when the terminal three AC system strength increases from 1000MVA to 2000MVA. Further increasing terminal three AC system strength to 3000MVA, increases the damping ratio from 29.05% to 29.73%. If the terminal three AC system strength is further increased to 4000MVA, the damping ratio drops again to 28.60%. The participation factor analysis results indicate that the terminal one DC current controller state variable remains at the highest participation of 1.0 in all study cases. The participation factor of the terminal two current controller state variable decreases from 0.064 to 0.051 when the terminal three AC system strength increases to 2000MVA. Increasing the AC system strength to 4000MVA increases the participation factor for the terminal two current controller state variable from 0.051 to 0.055 and decreases the participation factor of the terminal three voltage controller state variable from 0.127 to 0.012. Mode shape indicates that the angle between the terminal one current controller state variable and the terminal two current controller state variable reduces from 44.00 degrees to 18.08 degrees. The angle between terminal two current controller state variable and terminal three voltage controller state variable increases from 120.70 degrees to 152.30 degrees when terminal

three AC system strength increases from 1000MVA to 2000MVA. Increasing the terminal three AC system strength to 4000MVA decreases the angle between these two controller state variables from 152.30 degrees to 125.32 degrees. Similarly, the angle between the terminal three voltage controller state variable and the terminal one current controller state variable decreases from 195.3 degrees to 186.7 degrees when the terminal three AC system strength increases from 1000MVA to 2000MVA. Further increasing terminal three AC system strength to 4000MVA, increases this angle from 186.7 degrees to 216.60 degrees. Although mode shape angles change, the oscillation mode of Mode-4 with the terminal one current controller state variable and terminal two current controller state variable oscillating together against the terminal three voltage controller state variable remains unchanged. Both the oscillation frequency and damping change due to therminal three AC system strength change. However, this mode has enough damping ratio and has no small signal stability concerns for all study scenarios.

Mode-5:

In Mode-5, the oscillation frequency changes dramatically from 11.43Hz to 8.23Hz, and the damping ratio decreases from 39.72% to 31.82% when the terminal three AC system strength increases from 1000MVA to 4000MVA as shown in Table 6.1. The study results shown in Table C1.2 indicate that the participation factor of the terminal one current controller state variable drops from 0.511 to 0.362 when the terminal three AC system strength increases from 1000MVA to 2000MVA. The participation factor of the terminal one current controller state variable increases to 0.395 when the terminal three AC system strength increases to 3000MVA. However, it decreases again from 0.395 to 0.378 when the terminal three AC system strength further increases to 4000MVA. The participation

factor of the terminal two current controller state variable increases from 0.049 to 0.389. The participation factor of the terminal three voltage controller state variable increases from 0.460 to 0.597 when the terminal three AC system strength increases to 2000MVA. Further increase of terminal three AC system strength to 4000MVA causes the participation factor to decrease from 0.597 to 0.419. Mode shape indicates that the angle between terminal one and terminal two current controller state variables increases from 115.8 degrees to 178.7 degrees. The angle between the terminal two current controller state variable and the terminal three voltage controller state variable decreases from 73.1 degrees to 0.6 degrees when system strength increases from 1000 MVA to 3000 MVA. Further increasing terminal three AC system strength to 4000MVA increases the angle between these two state variables from 0.6 degrees to 10.80 degrees. The angle between the terminal three voltage controller state variable and the terminal one current controller state variables increases from 171.1 degrees to 184.8 degrees when the terminal three AC system strength increases from 1000MVA to 3000MVA. The angle decreases from 184.8 degrees to 170.5 degrees if the terminal three AC system strength is further increased to 4000MVA. Mode shape analysis results indicate that the oscillation mode with the terminal one current controller state variable oscillating against the terminal two current controller state variable and the terminal three voltage controller state variables remains unchanged. As a result, when the terminal three AC system strength is increased, the oscillation frequency of Mode-5 decreases dramatically from 11.43Hz to 8.23Hz, and the damping ratio decreases from 39.72% to 31.82%. However, this mode has enough damping ratio and has no small signal stability concerns for all study scenarios.

Mode-6:

For Mode-6, the oscillation frequency significantly changes from 4.55Hz to 0.92Hz and the damping ratio dramatically increases from 50.77% to 97.27% when terminal three AC system strength increases from 1000MVA to 4000MVA. The study results in Table C1.2 indicate that the participation factor of terminal one current controller state variable decreases from 0.337 to 0.04 and the participation factor of terminal two current controller state variable decreases from 0.419 to 0.06 when terminal three AC system strength increases from 1000MVA to 3000MVA. Further increasing the AC system strength to 4000MVA increases this participation factor to 0.09. Most importantly, the participation factor of the terminal three voltage controller state variable decreases drastically from 1.0 to 0.13 when the terminal three AC system strength increases from 1000MVA to 4000MVA. This significant participation factor change impacts the oscillation frequency. By examining the participation factor, it is revealed that the terminal three AC system strength significantly impacts the damping ratio of Mode-6. This mode is dominated by the terminal three voltage controller state variable in the original study case. With the increase of terminal three AC system strength from 1000MVA (SCR=1.93) to 2000MVA (SCR=2.42), the participation factor of the terminal three PLL controller state variable dominates this mode and increases from 0.58 to 1.0. Meanwhile, the participation factor of the terminal three voltage controller state variable decreases from 1.0 to 0.640, and the terminal one equivalent machine state variable increases from 0.26 to 0.899. When the terminal three AC system strength is further increased to 3000MVA, the participation factor of the terminal three equivalent machine state variable dominates the mode and increases from 0.899 to 1.0. On the other hand, the participation factor of the terminal three PLL controller state variable drops from 1.0 to 0.572. The participation factor of the

terminal three voltage controller state variable drops even further to 0.20. When the terminal three AC system strength is further increased to 4000MVA, the terminal three equivalent machine state variable still dominates this mode with the highest participation factor of 1.0. However, the participation factor of the terminal three voltage controller state variable significantly decreases to 0.13.

From the above analysis results, it is observed that the participation factors for all three HVDC controller state variables are 0.337, 0.419, and 1.0 in the original case with terminal three AC system strength of 1000MVA and 0.04, 0.09, and 0.13 when terminal three AC system strength increases to 4000MVA. In this mode, the participation of all three HVDC controller state variables decreases with the increase of terminal three AC system strength. As explained in the previous section, with the increase of terminal three AC system strength, the terminal three PLL controller state variable becomes the dominant participant. Subsequently, the equivalent machine state variable dominates this mode when the terminal three AC system strength increases to 3000MVA. Obviously, both the oscillation frequency and damping ratio change because the mode completely changes from HVDC controller interaction oscillation mode to electromechanical oscillation mode.

The participation factor analysis indicates that the terminal three AC system impacts the HVDC controller state variable participation and hence the controller interaction mode. Mode shape analysis shows that the angle between the terminal one current controller state variable and terminal two current controller state variable significantly decreases from 136.7 degrees to 43.7 degrees when the terminal three AC system strength increases to 4000MVA. The angle between the terminal two current controller state variable and terminal three voltage controller state variable decreases from 89.69 degrees to 87.4

degrees initially when the terminal three AC system strength increases from 1000MVA to 2000MVA. Further increasing terminal three AC system strength to 4000MVA increases this angle from 87.4 degrees to 125.3 degrees. The angle between the terminal three voltage controller state variable and terminal one current controller state variable increases from 133.61 degrees to 191.00 degrees. Mode shape analysis indicates that the oscillation mode changes from terminal one current controller state variable oscillating against the terminal two current controller state variable and terminal three voltage controller state variables to the terminal one current controller state variable and terminal two current controller state variables oscillating together against the terminal three voltage controller state variable.

Table C1.4 to Table C1.6 show that the study results with different AC system strength for the three-terminal HVDC system have a different HVDC line tap point. In this case, line sections between terminal one and the HVDC line tap point are swapped with the section between terminal two and the HVDC line tap point. All control parameters as well as the operating point remain the same as in the original study case. Table C1.7 to Table C1.9 show that the study results with a system strength increase for the three-terminal HVDC system with different control parameters. In this case, the proportional gain for all HVDC voltage and current controllers change from 0.01 to 0.5. The integral gain as well as the PLL gains changed slightly to ensure that there is no negative damping mode in the study. Table C1.10 to Table C1.12 show that the study results with system strength change for the three-terminal HVDC system operated at different operating points. In this case, terminal one (rectifier) DC power remains constant, terminal two DC power slightly decreases from 653MW to 639MW, and terminal three DC power increases from 560MW

to 570MW. All other conditions such as the system configuration, controller arrangement, and control parameters remain the same as in the original cases.

System Strength			Mode-4		Mode-5		Mode-6	
T1 (MVA)	T2(MVA)	T3(MVA)	Frequency (Hz)	Damping (%)	Frequency (Hz)	Damping (%)	Frequency (Hz)	Damping (%)
1800	600	1000	12.71	30.62%	11.43	39.72%	4.55	50.77%
3600	600	1000	12.53	19.40%	10.90	42.75%	4.54	49.67%
5400	600	1000	12.41	17.25%	10.82	42.99%	4.52	49.40%
7200	600	1000	12.34	16.31%	10.79	43.08%	4.51	49.27%
1800	600	1000	12.71	30.62%	11.43	39.72%	4.55	50.77%
1800	1000	1000	12.66	33.33%	10.85	42.19%	4.12	45.21%
1800	1500	1000	12.67	34.07%	10.58	44.20%	3.95	40.66%
1800	2000	1000	12.68	34.35%	10.46	45.27%	3.90	38.31%
1800	600	1000	12.71	30.62%	11.43	39.72%	4.55	50.77%
1800	600	2000	13.09	29.05%	8.88	37.41%	3.28	78.61%
1800	600	3000	13.11	29.73%	8.40	33.64%	1.48	94.68%
1800	600	4000	13.11	28.60%	8.23	31.82%	0.92	97.27%

Table C1. 1 Frequency and damping ratio - original system

System Strength	Mode-4			Mode-5			Mode-6		
T1 /T2/T3 (MVA)	T1 PF	T2 PF	T3 PF	T1 PF	T2 PF	T3 PF	T1 PF	T2 PF	T3 PF
1800/600/1000	1.000	0.064	0.127	0.511	0.049	0.460	0.337	0.419	1.000
3600/600/1000	1.000	0.120	0.026	0.243	0.040	0.487	0.368	0.421	1.000
5400/600/1000	1.000	0.132	0.016	0.211	0.042	0.491	0.375	0.421	1.000
7200/600/1000	1.000	0.138	0.014	0.198	0.042	0.493	0.379	0.421	1.000
1800/600/1000	1.000	0.064	0.127	0.511	0.049	0.460	0.337	0.419	1.000
1800/1000/1000	1.000	0.037	0.122	0.360	0.079	0.492	0.238	0.789	1.000
1800/1500/1000	1.000	0.031	0.117	0.307	0.091	0.502	0.192	1.000	0.965
1800/2000/1000	1.000	0.029	0.115	0.287	0.097	0.506	0.161	1.000	0.870
1800/600/1000	1.000	0.064	0.127	0.511	0.049	0.460	0.337	0.419	1.000
1800/600/2000	1.000	0.051	0.020	0.362	0.246	0.597	0.196	0.137	0.648
1800/600/3000	1.000	0.054	0.013	0.395	0.368	0.509	0.070	0.060	0.202
1800/600/4000	1.000	0.055	0.012	0.378	0.389	0.419	0.040	0.090	0.130

Table C1. 2 Participation Factors for each oscillation mode -original system

System Strength	Mode-4			Mode-5			Mode-6		
T1 /T2/T3 (MVA)	T1-T2 Ang	T2-T3 Ang	T3-T1 Ang.	T1-T2 Ang	T2-T3 Ang	T3-T1 Ang.	T1-T2 Ang	T2-T3 Ang	T3-T1 Ang.
1800/600/1000	44.00	120.70	195.30	115.80	73.10	171.10	136.70	89.69	133.61
3600/600/1000	16.90	119.10	224.00	166.90	45.70	147.40	135.91	90.42	133.67
5400/600/1000	12.60	122.80	224.60	173.66	41.94	144.40	136.38	90.78	132.84
7200/600/1000	10.00	127.00	223.00	176.30	40.60	143.10	136.62	90.83	132.55
1800/600/1000	44.00	120.70	195.30	115.80	73.10	171.10	136.70	89.69	133.61
1800/1000/1000	38.52	148.00	173.48	104.30	70.20	185.50	143.40	86.76	129.84
1800/1500/1000	33.40	159.60	167.00	98.00	71.30	190.70	149.48	83.70	126.82
1800/2000/1000	31.34	164.66	164.00	96.09	70.81	193.10	152.80	81.60	125.60
1800/600/1000	44.00	120.70	195.30	115.80	73.10	171.10	136.70	89.69	133.61
1800/600/2000	21.00	152.30	186.70	164.40	16.90	178.70	111.80	87.40	160.80
1800/600/3000	18.60	137.90	203.50	174.60	0.60	184.80	62.90	117.60	179.50
1800/600/4000	18.08	125.32	216.60	178.70	10.80	170.50	43.70	125.30	191.00

Table C1. 3 Mode Shapes for each oscillation mode - original system

System Strength			Mode-4		Mode-5		Mode-6	
T1 (MVA)	T2(MVA)	T3(MVA)	Frequency (Hz)	Damping (%)	Frequency (Hz)	Damping (%)	Frequency (Hz)	Damping (%)
1800	600	1000	14.85	34.87%	10.19	40.25%	4.38	50.92%
3600	600	1000	14.00	23.94%	10.33	41.30%	4.36	50.17%
5400	600	1000	13.78	21.04%	10.35	41.72%	4.34	50.01%
7200	600	1000	13.68	19.72%	10.35	41.92%	4.33	49.93%
1800	600	1000	14.85	34.87%	10.19	40.25%	4.38	50.92%
1800	1000	1000	14.81	35.35%	9.66	45.27%	3.93	44.98%
1800	1500	1000	14.79	35.58%	9.44	47.70%	3.76	40.23%
1800	2000	1000	14.79	35.69%	9.34	48.86%	3.71	37.86%
1800	600	1000	14.85	34.87%	10.19	40.25%	4.38	50.92%
1800	600	2000	14.74	32.81%	8.09	39.23%	3.24	78.27%
1800	600	3000	14.68	32.66%	7.70	35.28%	1.48	94.50%
1800	600	4000	14.64	32.68%	7.56	33.44%	0.93	97.19%

Table C1. 4 Frequency and damping ratio – different HVDC line tap point

System Strength	Mode-4			Mode-5			Mode-6		
T1 /T2/T3 (MVA)	T1 PF	T2 PF	T3 PF	T1 PF	T2 PF	T3 PF	T1 PF	T2 PF	T3 PF
1800/600/1000	1.000	0.011	0.064	0.233	0.125	0.544	0.285	0.517	1.000
3600/600/1000	1.000	0.025	0.081	0.236	0.084	0.525	0.308	0.519	1.000
5400/600/1000	1.000	0.031	0.081	0.223	0.075	0.521	0.314	0.518	1.000
7200/600/1000	1.000	0.034	0.089	0.216	0.072	0.519	0.317	0.518	1.000
1800/600/1000	1.000	0.011	0.064	0.233	0.125	0.544	0.285	0.517	1.000
1800/1000/1000	1.000	0.011	0.065	0.221	0.123	0.553	0.196	0.973	1.000
1800/1500/1000	1.000	0.012	0.065	0.221	0.124	0.553	0.130	1.000	0.797
1800/2000/1000	1.000	0.012	0.066	0.223	0.125	0.552	0.110	1.000	0.725
1800/600/1000	1.000	0.011	0.064	0.233	0.125	0.544	0.285	0.517	1.000
1800/600/2000	1.000	0.016	0.014	0.181	0.345	0.633	0.189	0.165	0.669
1800/600/3000	1.000	0.017	0.011	0.154	0.397	0.416	0.071	0.071	0.210
1800/600/4000	1.000	0.018	0.013	0.151	0.420	0.341	0.048	0.105	0.138

Table C1. 5 Participation Factors for each oscillation mode – different HVDC line tap point

System Strength	Mode-4			Mode-5			Mode-6		
T1 /T2/T3 (MVA)	T1-T2 Ang	T2-T3 Ang	T3-T1 Ang.	T1-T2 Ang	T2-T3 Ang	T3-T1 Ang.	T1-T2 Ang	T2-T3 Ang	T3-T1 Ang.
1800/600/1000	14.50	150.50	195.00	94.38	51.13	214.49	137.30	90.51	132.19
3600/600/1000	23.00	107.90	229.10	111.67	55.27	193.06	137.00	91.26	131.75
5400/600/1000	22.18	157.02	180.80	116.90	55.27	187.83	137.61	91.50	130.89
7200/600/1000	21.54	155.25	183.21	119.23	55.14	185.63	137.87	91.75	130.38
1800/600/1000	14.50	150.50	195.00	94.38	51.13	214.49	137.30	90.51	132.19
1800/1000/1000	8.90	140.93	210.17	85.00	55.80	219.20	142.80	88.00	129.20
1800/1500/1000	6.10	136.10	217.80	79.90	58.90	221.20	148.71	84.90	126.39
1800/2000/1000	4.70	133.70	221.60	77.54	60.62	221.84	151.80	83.00	125.20
1800/600/1000	14.50	150.50	195.00	94.38	51.13	214.49	137.30	90.51	132.19
1800/600/2000	9.00	155.20	195.80	156.87	11.10	192.03	116.10	85.20	158.70
1800/600/3000	9.40	171.10	179.50	172.87	4.70	182.43	65.64	115.40	178.96
1800/600/4000	10.00	150.90	199.10	178.60	13.90	167.50	45.70	123.20	191.10

Table C1. 6 Mode Shapes for each oscillation mode- different HVDC line tap point

System Strength			Mode-4		Mode-5		Mode-6	
T1 (MVA)	T2(MVA)	T3(MVA)	Frequency (Hz)	Damping(%)	Frequency (Hz)	Damping(%)	Frequency (Hz)	Damping(%)
1800	600	1000	10.96	76.10%	13.63	32.67%	4.97	57.31%
3600	600	1000	12.00	55.84%	13.78	34.92%	4.87	56.75%
5400	600	1000	11.84	52.18%	13.97	35.32%	4.87	56.67%
7200	600	1000	11.72	50.82%	14.10	35.25%	4.80	56.65%
1800	600	1000	10.96	76.10%	13.63	32.67%	4.97	57.31%
1800	1000	1000	10.15	79.73%	13.14	36.82%	4.93	56.48%
1800	1500	1000	9.54	82.14%	12.96	39.13%	4.90	56.11%
1800	2000	1000	9.15	83.53%	12.88	40.31%	4.89	55.94%
1800	600	1000	10.96	76.10%	13.63	32.67%	4.97	57.31%
1800	600	2000	9.06	79.29%	12.89	32.71%	3.51	77.70%
1800	600	3000	8.85	80.89%	12.66	33.40%	2.05	92.46%
1800	600	4000	8.36	81.85%	12.55	33.98%	0.90	97.97%

Table C1. 7 Frequency and damping ratio with -different control parameters

System Strength	Mode-4			Mode-5			Mode-6		
T1 /T2/T3 (MVA)	T1 PF	T2 PF	T3 PF	T1 PF	T2 PF	T3 PF	T1 PF	T2 PF	T3 PF
1800/600/1000	1.000	0.052	0.077	0.231	0.969	0.224	0.609	0.261	1.000
3600/600/1000	1.000	0.066	0.108	0.490	0.936	0.171	0.619	0.255	1.000
5400/600/1000	1.000	0.054	0.148	0.542	0.925	0.125	0.640	0.253	1.000
7200/600/1000	1.000	0.045	0.175	0.536	0.922	0.102	0.644	0.252	1.000
1800/600/1000	1.000	0.052	0.077	0.231	0.969	0.224	0.609	0.261	1.000
1800/1000/1000	1.000	0.099	0.062	0.194	0.957	0.255	0.566	0.332	1.000
1800/1500/1000	1.000	0.135	0.054	0.177	0.908	0.260	0.546	0.377	1.000
1800/2000/1000	1.000	0.156	0.051	0.172	0.881	0.261	0.537	0.399	1.000
1800/600/1000	1.000	0.052	0.077	0.231	0.969	0.224	0.609	0.261	1.000
1800/600/2000	1.000	0.001	0.077	0.400	0.998	0.124	0.291	0.132	0.690
1800/600/3000	1.000	0.026	0.074	0.465	0.999	0.101	0.104	0.092	0.407
1800/600/4000	1.000	0.022	0.073	0.501	0.996	0.097	0.042	0.090	0.216

Table C1. 8 Participation Factors for each oscillation mode- different control parameters

System Strength	Mode-4			Mode-5			Mode-6		
T1 /T2/T3 (MVA)	T1-T2 Ang	T2-T3 Ang	T3-T1 Ang.	T1-T2 Ang	T2-T3 Ang	T3-T1 Ang.	T1-T2 Ang	T2-T3 Ang	T3-T1 Ang.
1800/600/1000	0.70	43.11	316.19	102.80	72.32	184.88	167.89	60.68	131.43
3600/600/1000	29.40	127.38	203.22	74.50	94.50	191.00	172.40	61.19	126.41
5400/600/1000	44.90	154.70	160.40	61.00	102.21	196.79	174.70	61.20	124.10
7200/600/1000	52.97	166.77	140.26	54.10	104.20	201.70	175.60	61.50	122.90
1800/600/1000	0.70	43.11	316.19	102.80	72.32	184.88	167.89	60.68	131.43
1800/1000/1000	2.00	37.90	320.10	114.40	76.30	169.30	167.40	61.40	131.20
1800/1500/1000	2.30	35.30	322.40	122.00	78.70	159.30	166.70	62.20	131.10
1800/2000/1000	2.24	34.00	323.76	126.50	79.95	153.55	166.50	62.46	131.04
1800/600/1000	0.70	43.11	316.19	102.80	72.32	184.88	167.89	60.68	131.43
1800/600/2000	4.80	49.89	305.31	109.60	68.10	182.30	140.25	51.50	168.25
1800/600/3000	13.70	79.10	267.20	109.80	54.44	195.76	110.00	48.61	201.39
1800/600/4000	17.70	92.40	249.90	109.28	42.83	207.89	114.10	32.30	213.60

Table C1. 9 Mode Shapes for each oscillation mode- different control parameters

System Strength			Mode-4		Mode-5		Mode-6	
T1 (MVA)	T2(MVA)	T3(MVA)	Frequency (Hz)	Damping (%)	Frequency (Hz)	Damping (%)	Frequency (Hz)	Damping (%)
1800	600	1000	13.04	35.65%	12.04	30.02%	4.63	45.62%
3600	600	1000	12.41	20.39%	11.97	37.03%	4.60	44.62%
5400	600	1000	12.31	18.16%	11.88	37.29%	4.58	44.39%
7200	600	1000	12.25	17.20%	11.84	37.38%	4.57	44.28%
1800	600	1000	13.04	35.65%	12.04	30.02%	4.63	45.62%
1800	1000	1000	13.08	35.65%	11.42	33.44%	4.17	40.37%
1800	1500	1000	13.09	35.66%	11.17	35.43%	4.01	36.11%
1800	2000	1000	13.10	35.67%	11.06	36.48%	3.95	34.05%
1800	600	1000	13.04	35.65%	12.04	30.02%	4.63	45.62%
1800	600	2000	13.04	30.04%	9.47	38.88%	3.86	67.70%
1800	600	3000	13.05	29.48%	8.53	37.79%	2.58	87.25%
1800	600	4000	13.06	29.27%	8.20	35.87%	1.11	96.71%

Table C1. 10 Frequency and damping ratio -different operating point

System Strength	Mode-4			Mode-5			Mode-6		
T1 /T2/T3 (MVA)	T1 PF	T2 PF	T3 PF	T1 PF	T2 PF	T3 PF	T1 PF	T2 PF	T3 PF
1800/600/1000	1.000	0.001	0.289	0.231	0.969	0.224	0.326	0.478	1.000
3600/600/1000	1.000	0.134	0.049	0.274	0.031	0.436	0.363	0.477	1.000
5400/600/1000	1.000	0.140	0.029	0.214	0.035	0.442	0.372	0.476	1.000
7200/600/1000	1.000	0.144	0.023	0.194	0.036	0.444	0.377	0.476	1.000
1800/600/1000	1.000	0.001	0.289	0.231	0.969	0.224	0.326	0.478	1.000
1800/1000/1000	1.000	0.001	0.250	0.640	0.204	0.494	0.229	0.870	1.000
1800/1500/1000	1.000	0.001	0.237	0.591	0.200	0.502	0.176	1.000	0.906
1800/2000/1000	1.000	N/A	0.231	0.572	0.200	0.572	0.151	1.000	0.829
1800/600/1000	1.000	0.001	0.289	0.231	0.969	0.224	0.326	0.478	1.000
1800/600/2000	1.000	0.040	0.032	0.283	0.183	0.584	0.280	0.270	0.958
1800/600/3000	1.000	0.053	0.018	0.407	0.360	0.694	0.126	0.070	0.452
1800/600/4000	1.000	0.056	0.015	0.386	0.394	0.551	0.055	0.063	0.163

Table C1. 11 Participation Factors for each oscillation mode- different operating point

System Strength	Mode-4			Mode-5			Mode-6		
T1 /T2/T3 (MVA)	T1-T2 Ang	T2-T3 Ang	T3-T1 Ang.	T1-T2 Ang	T2-T3 Ang	T3-T1 Ang.	T1-T2 Ang	T2-T3 Ang	T3-T1 Ang.
1800/600/1000	35.38	101.49	223.13	102.80	72.32	184.88	137.95	94.78	127.27
3600/600/1000	21.20	122.50	216.30	153.20	66.50	140.30	137.00	95.30	127.70
5400/600/1000	15.40	129.00	215.60	161.70	59.90	138.40	137.40	95.60	127.00
7200/600/1000	13.20	132.77	214.03	165.11	58.70	136.19	137.61	95.90	126.49
1800/600/1000	35.38	101.49	223.13	102.80	72.32	184.88	137.95	94.78	127.27
1800/1000/1000	35.50	98.44	226.06	58.50	81.50	220.00	145.53	90.20	124.27
1800/1500/1000	35.58	96.84	227.58	57.30	81.70	221.00	151.72	86.50	121.78
1800/2000/1000	35.60	N/A	228.40	56.50	82.10	221.40	154.73	84.70	120.57
1800/600/1000	35.38	101.49	223.13	102.80	72.32	184.88	137.95	94.78	127.27
1800/600/2000	22.20	169.70	168.10	151.90	34.50	173.60	121.80	87.10	151.10
1800/600/3000	18.80	154.60	186.60	172.00	9.00	179.00	96.00	94.80	169.20
1800/600/4000	17.60	140.51	201.89	179.02	4.80	176.18	0.30	123.98	235.72

Table C1. 12 Mode Shapes for each oscillation mode- different operating point

C.2 AC system strength on Controller interaction- Scheme Two

Table C2.1 shows the controller interaction oscillation frequencies and damping ratios for different AC system strengths in the original system configuration. Correspondingly, Table C2.2 and Table C2.3 show the participation factor results and mode shape angles between each controller state variable for all oscillation modes under the same study scenario.

Table C2.4 to Table C2.6 show the study results with different AC system strength for the three-terminal HVDC system with a different HVDC line tap point. In this case, line sections between terminal one and the HVDC line tap point are swapped with the section between terminal two and the HVDC line tap point. All control parameters as well as the operating point remain the same as in the original study case. Table C2.7 to Table C2.9 show study results with system strength increases for the three-terminal HVDC system with different control parameters. In this case, the integral gain for the terminal one voltage controller changes from 80 to 50, and the integral gain for the terminal two current controller changes from 10 to 20. The proportional gain as well as the PLL gain remains unchanged. Table C2.10 to Table C2.12 show study results with system strength changes for the three-terminal HVDC system operated at different operating points. In this case, terminal one (rectifier) DC power remains constant, terminal two DC power slightly decreases from 653MW to 510MW, and terminal three DC power increases from 560MW to 710MW. All other conditions such as system configuration, controller arrangement, and control parameters remain the same as in the original cases.

System Strength			Mode-4N		Mode-5N		Mode-6N	
T1 (MVA)	T2(MVA)	T3(MVA)	Frequency (Hz)	Damping (%)	Frequency (Hz)	Damping (%)	Frequency (Hz)	Damping (%)
1800	600	1000	50.42	31.33%	9.00	12.80%	3.69	13.26%
3600	600	1000	65.19	20.92%	9.01	12.71%	4.03	12.70%
5400	600	1000	67.37	18.46%	9.01	12.69%	4.13	12.83%
7200	600	1000	68.21	17.64%	9.01	12.68%	4.18	12.98%
1800	600	1000	50.42	31.33%	9.00	12.80%	3.69	13.26%
1800	1000	1000	51.26	30.45%	8.45	13.75%	3.50	14.07%
1800	1500	1000	51.68	30.31%	8.20	14.76%	3.42	14.43%
1800	2000	1000	51.87	30.32%	8.08	15.41%	3.38	14.59%
1800	600	1000	50.42	31.33%	9.00	12.80%	3.69	13.26%
1800	600	2000	51.29	28.92%	8.92	10.29%	3.46	9.40%
1800	600	3000	51.88	28.33%	9.02	10.18%	3.37	11.16%
1800	600	4000	52.21	28.17%	9.11	10.33%	3.33	12.97%

Table C2. 1. Frequency and damping ratio with different system strength-original system

System Strength	Mode-4N			Mode-5N			Mode-6N		
T1 /T2/T3 (MVA)	T1 PF	T2 PF	T3 PF	T1 PF	T2 PF	T3 PF	T1 PF	T2 PF	T3 PF
1800/600/1000	1.000	0.010	0.012	0.011	0.542	0.478	1.000	0.702	0.674
3600/600/1000	0.177	0.015	0.014	0.001	0.542	0.459	0.759	0.695	0.816
5400/600/1000	0.082	0.014	0.013	N/A	0.542	0.452	0.637	0.663	0.824
7200/600/1000	0.058	0.013	0.012	N/A	0.542	0.449	0.578	0.648	0.828
1800/600/1000	1.000	0.010	0.012	0.011	0.542	0.478	1.000	0.702	0.674
1800/1000/1000	1.000	0.002	0.010	0.001	0.932	0.823	1.000	0.973	0.570
1800/1500/1000	0.991	0.001	0.001	N/A	1.000	0.878	0.884	1.000	0.466
1800/2000/1000	0.982	N/A	N/A	N/A	1.000	0.872	0.827	1.000	0.422
1800/600/1000	1.000	0.010	0.012	0.011	0.542	0.478	1.000	0.702	0.674
1800/600/2000	1.000	0.001	0.001	0.010	0.558	0.498	0.998	0.667	1.000
1800/600/3000	0.974	N/A	N/A	0.001	0.556	0.523	0.873	0.567	1.000
1800/600/4000	0.957	N/A	N/A	N/A	0.553	0.539	0.830	0.532	1.000

Table C2. 2. Participation Factors for each oscillation mode- original system

System Strength	Mode-4N			Mode-5N			Mode-6N		
T1 /T2/T3 (MVA)	T1-T2 Ang	T2-T3 Ang	T3-T1 Ang.	T1-T2 Ang	T2-T3 Ang	T3-T1 Ang.	T1-T2 Ang	T2-T3 Ang	T3-T1 Ang.
1800/600/1000	72.73	11.65	275.62	116.10	178.30	65.60	71.19	27.61	261.20
3600/600/1000	45.51	5.01	309.48	115.30	177.64	67.06	69.90	26.90	263.20
5400/600/1000	44.91	4.21	310.88	N/A	177.20	N/A	70.27	26.80	262.93
7200/600/1000	44.41	3.87	311.72	N/A	177.13	N/A	70.80	26.90	262.30
1800/600/1000	72.73	11.65	275.62	116.10	178.30	65.60	71.19	27.61	261.20
1800/1000/1000	67.28	9.60	283.12	111.60	178.78	69.62	73.10	25.50	261.40
1800/1500/1000	70.60	13.50	275.90	N/A	179.30	N/A	73.70	24.50	261.80
1800/2000/1000	N/A	N/A	N/A	N/A	179.90	N/A	74.00	24.10	261.90
1800/600/1000	72.73	11.65	275.62	116.10	178.30	65.60	71.19	27.61	261.20
1800/600/2000	82.84	2.54	274.62	98.40	179.80	81.80	68.34	32.60	259.06
1800/600/3000	62.34	N/A	N/A	98.08	179.88	82.04	68.50	29.70	261.80
1800/600/4000	N/A	N/A	N/A	N/A	179.58	N/A	68.84	27.16	264.00

Table C2. 3. Mode shapes for each oscillation mode- original system

C2.1 Terminal two AC system strength variation

Mode-4N:

A similar analysis has been conducted for the terminal two AC system strength change. If terminal two (current control terminal) inverter side AC system strength is increased, Mode-4N oscillation frequency slightly increases from 50.42Hz to 51.87Hz and the damping ratio slightly decreases from 31.33% to 30.32% as shown in Table 6.13. The

small-signal analysis results indicate that the terminal one voltage controller state variable retains the highest participation in this mode as shown in Table 6.14. However, the participation factor slightly decreases from 1 to 0.982 when the terminal two inverter side AC system strength increases from 600MVA to 2000MVA. The participation factors for the other two terminal controller state variables vary with terminal two AC system strength change. The participation factor of the terminal two current controller state variable decreases from 0.01 to 0.002 when terminal two AC system strength increases to 1500MVA. Further increase of terminal two AC system strength causes the participation factor of the terminal two controller state variable to decrease even further. On the other hand, the terminal three current controller state variable participation factor decreases from 0.012 to 0.001 when terminal two AC side system strength increases to 1500MVA. Upon further increasing terminal two AC system strength, the participation factor of the terminal three controller state variable further drops, and it also disappears in the participation list. The participation analysis indicates that the terminal two inverter side AC system impacts all HVDC controller state variable participation in this mode.

Mode shape shows that the terminal one voltage controller state variable, terminal two current controller state variable, and terminal three voltage controller state variable oscillate together in this mode. With terminal two AC system strength increase, the angle between the terminal one voltage controller and terminal two current controller state variables initially decrease from 72.73 degrees to 67.28 degrees. Increasing the terminal two AC system strength from 1000MVA to 1500MVA increases the angle from 67.28 degrees to 70.60 degrees. Further increasing terminal two AC system strength causes the terminal two current controller state variable to disappear from the participation list and

the angle information to become unavailable. Similarly, the angle between the terminal two current controller state variable and terminal three current controller state variable decreases from 11.65 degrees to 9.60 degrees with the terminal two AC system strength increase from 600MVA to 1000MVA. The angle further increases from 9.60 degrees to 13.50 degrees when terminal two AC system strength increases to 1500MVA. The angle the between the terminal three current controller state variable and the terminal one voltage controller state variable increases from 275.62 degrees to 283.12 degrees when terminal two AC system strength increases from 600MVA to 1000MVA. Increasing terminal two AC system strength to 1500MVA causes the angle between these two controller state variables to decrease from 283.12 degrees to 275.90 degrees. Further increasing terminal two AC system strength causes the terminal three controller state variable to disappear from the participation list, making the angle information unavailable. However, the mode shape remains the same as the terminal one voltage controller state variable, terminal two current controller state variable, and terminal three current controller state variable oscillate together. The results indicate that both the oscillation frequency and damping ratio change due to the terminal two AC system strength change. However, this mode has enough damping ratio and has no small signal stability concerns.

Mode-5N:

In Mode-5N, the oscillation frequency slightly decreases from 9.00Hz to 8.08Hz and the damping ratio increases from 12.80% to 15.41%. The participation factor for the terminal one voltage controller state variable drops from 0.011 to 0.001with terminal two AC system strength increase from 600MVA to 1000MVA. Further increase of terminal two AC system strength causes the participation factor of the terminal one voltage controller state

variable further decreases below 0.001 and disappear from the participation list. The participation factor for the terminal two current controller state variable increases from 0.542 to 1.0 and the participation factor for the terminal three current controller state variable increases from 0.478 to 0.872 with terminal two AC system strength increase from 600MVA to 2000MVA. Mode shape indicates that the angle between the terminal one voltage controller state variable and the terminal two current controller state variable decreases from 116.1 degrees to 111.60 degrees with terminal two AC system strength increase to 1500MVA. Similarly, the angle between the terminal one controller state variable and the terminal three current controller state variable increases from 65.60 degrees to 69.62 degrees when terminal two AC system strength increases to 1000MVA. Further increase of terminal two AC system strength causes the participation factor of the terminal one voltage controller state variable decrease and disappear from the participation list. Therefore, the angles between terminal one and terminal two, and between terminal one and terminal three controller state variables are available. The angle between the terminal two current controller state variable and the terminal three current controller state variable increases from 178.3 degrees to 179.90 degrees with an increase of terminal two AC system strength. Although the angle between each controller state variables slightly changes due to the terminal two AC system strength change, the study results prove that the oscillation mode remains unchanged as the terminal one voltage controller state variable and the terminal three current controller state variable oscillate together against the terminal two current controller state variable. Because of the participation factor and angle change, both the oscillation frequency and the damping ratio of this mode change. However, this mode has enough damping ratio and has no small signal stability concern.

Mode-6N:

In Mode-6N, the oscillation frequency decreases from 3.69Hz to 3.38Hz and the damping ratio increases from 13.26% to 14.59%. The results in Table 6.14 show that the participation factor of the terminal one voltage controller state variable decreases from 1.0 to 0.827, the participation factor of the terminal two current controller state variable increases from 0.702 to 1.0, and the participation factor of the terminal three current controller state variable decreases from 0.674 to 0.422. Mode shape indicates that when terminal two AC system strength increase from 600MVA to 2000MVA, the angle between the terminal one voltage controller and terminal two current controller state variables increases from 71.19 degrees to 74.0 degrees, the angle between the terminal two current controller state variable and the terminal three current controller state variable slightly decreases from 27.61 degrees to 24.10 degrees, and the angle between the terminal three current controller state variable and the terminal one voltage controller state variable increases from 261.20 degrees to 261.90 degrees. However, the oscillation mode with the terminal one voltage controller state variable oscillates together with the terminal two current controller state variable and terminal three current controller state variable remains unchanged. Due to the participation factor and angle change, the oscillation frequency and the damping ratio of this mode change. However, this mode has enough damping ratio and has no small signal stability concern.

C2.2 Terminal three AC system strength variation

Mode-4N:

The same analysis process has been conducted for terminal three AC system strength increase. Increasing terminal three AC system strength causes Mode-4N oscillation

frequency to slightly increase from 50.42Hz to 52.21Hz and the damping ratio to slightly decreases from 31.33% to 28.17% as shown in Table 6.13. The participation factor analysis results indicate that, in this mode, the terminal one voltage controller state variable retains the highest participation factor for all scenarios. The terminal two controller state variable has a participation factor of 0.01 in the original study case. Increasing the terminal three AC system strength to 2000MVA decreases this value to 0.001. Further increasing terminal three AC system strength causes it to disappear from the participation list. Similar to the terminal three current controller state variable participation factor, it decreases from 0.012 to 0.001 when the terminal three AC system strength increases from 1000MVA to 2000MVA. Upon further increase in terminal three AC system strength, it decreases further and disappears from the participation list. Mode shape indicates that the angle between the terminal one voltage controller state variable and the terminal two current controller state variable slightly increases from 72.73 degrees to 82.84 degrees when the terminal three AC system strength increases to 2000MVA. Upon further increase of terminal three AC system strength to 3000MVA, it decreases from 82.84 degrees to 62.34 degrees. When the terminal three AC system strength is increased beyond 4000MVA, the angle information is not available due to the fact that the terminal two controller state variable disappears from the participation list. The angle between the terminal two current controller state variable and the terminal three current controller state variable decreases from 11.65 degrees to 2.54 degrees when the terminal three AC system strength is increased to 2000MVA. If the terminal three AC system strength is further increased, the angle information eventually becomes unavailable because the terminal three controller state variable disappears from the participation list. The angle between the terminal three

current controller state variable and the terminal one voltage controller state variable decreases from 275.62 degrees to 274.62 degrees when the terminal three AC system strength increases to 2000MVA. Further increase of terminal three AC system strength causes the terminal three controller state variable to disappear from the participation list. As a result, the angle information is no longer available. Based on the available information, it can be concluded that the oscillation mode of Mode-4N with the terminal one voltage controller state variable, terminal two current controller state variable, and terminal three current controller state variable oscillating together remains unchanged. Both the oscillation frequency and the damping ratio change due to the terminal three AC system strength change. However, this mode has enough damping ratio and has no small signal stability concern.

Mode-5N:

In Mode-5N, the oscillation frequency decreases from 9.00Hz to 8.92Hz when the terminal three AC system strength increases from 1000 MVA to 2000MVA. Further increasing the terminal three AC system strength to 4000MVA increases the oscillation frequency from 8.92Hz to 9.11Hz. Similarly, the damping ratio decreases from 12.80% to 10.18% when the terminal three AC system strength is increased from 1000MVA to 3000MVA. Further increasing terminal three AC system strength to 4000MVA increases the damping ratio of this mode from 10.18% to 10.33%. The study results shown in Table 6.14 indicate that the participation factor of the terminal one voltage controller state variable drops from 0.011 to 0.001 when the terminal three AC system strength increases to 3000MVA. Further increases in AC system strength cause the terminal one voltage controller state variable to disappear from the participation list. The participation factor of

the terminal two current controller state variable increases from 0.542 to 0.558 when the terminal three AC system strength increases from 1000MVA to 2000MVA. It decreases from 0.558 to 0.553 when the terminal three AC system strength increases to 4000MVA. The participation factor of the terminal three current controller state variable increases from 0.478 to 0.539 when the terminal three AC system strength increases form 1000MVA to 4000MVA. Mode shape indicates that the angle between the terminal one voltage controller and the terminal two current controller state variables decreases from 116.1 degrees to 98.08 degrees when the terminal three AC system strength increases from 1000MVA to 3000MVA. Upon further increase of terminal three AC system strength, the terminal one controller state variable disappears from the participation list. As a result, the angle information is no longer available. The angle between the terminal two current controller state variable and the terminal three current controller state variable increases from 178.30 degrees to 179.88 degrees when system strength increases from 1000 MVA to 3000 MVA. Further increasing AC system strength to 4000MVA decreases the angle from 179.88 degrees to 179.58 degrees. The angle between the terminal three current controller state variable and the terminal one current controller state variable increases from 65.60 degrees to 82.04 degrees when the AC system strength increases to 3000MVA. If the terminal three AC system strength is further increased, the angle information will not be available because the terminal one voltage controller state variable disappears from the participation list. The study results indicate that the oscillation mode with the terminal one voltage controller state variable and the terminal three current controller state variable oscillating together against the terminal two current controller state variable remains unchanged. Due to the participation factor and mode angle change, both the oscillation

frequency and damping ratio change. However, the results show that this mode has enough damping ratio and has no small signal stability concern.

Mode-6N:

For Mode-6N, the oscillation frequency decreases from 3.69Hz to 3.33Hz, and the damping ratio decreases from 13.26% to 9.40% when the terminal three AC system strength increases to 2000MVA. Further increase of terminal three AC system strength to 4000MVA causes the damping ratio for this mode to increase from 9.40% to 12.97%. The study results in Table 6.14 indicate that the participation factor of the terminal one voltage controller state variable decreases from 1.0 to 0.830 and the participation factor of the terminal two current controller state variable decreases from 0.702 to 0.532. Most importantly, the participation factor of the terminal three current controller state variable increases from 0.674 to 1.0 when the terminal three AC system strength increases from 1000MVA to 2000MVA. Terminal three current controller state variable dominates this mode regardless of the strength of the AC system. Mode shape results show that the angle between the terminal one voltage controller state variable and the terminal two current controller state variable slightly decreases from 71.19 degrees to 68.34 degrees when the terminal three AC system strength increases to 2000MVA. Further increasing the system strength to 3000MVA increases the angle from 68.34 degrees to 68.50 degrees. However, if the terminal three AC system strength increases to 4000MVA, the angle decreases to 68.84 degrees. The angle between the terminal two current controller state variable and the terminal three current controller state variable also increases from 27.61 degrees to 32.60 degrees when the terminal three AC system strength increases to 2000MVA. The angle decreases from 32.60 degrees to 27.16 degrees if the terminal three AC system

strength is further increased to 4000MVA. The angle between the terminal three current controller state variable and the terminal one voltage controller state variable decreases from 261.20 degrees to 259.06 degrees when the terminal three AC system strength increases to 2000MV. Increase terminal three AC system strength beyond 2000MVA does not decrease the angle, but rather increases it from 259.06 degrees to 264.00 degrees. The oscillation mode with the terminal one voltage controller state variable oscillating together with the terminal two current controller state variable and the terminal three current controller state variable remains unchanged. Due to controller state variables participation factor and mode shape angle variations with terminal three AC system change, the oscillation frequency and damping ratio of this mode change. However, the results show that this mode has enough damping ratio and has not small signal stability concern with different terminal three AC system strengths.

The same study procedure to analyze participation factor and mode shape angle has been adopted to evaluate the performance of two MTHVDC control schemes with different HVDC line tap points, different controller parameters, and different operating points. All study results are tabulated and analyzed, these results show some similarity in response to AC system strength change. Based on the results, it is observed that:

1. Mode-4N is dominated by the terminal one voltage controller state variable with minor participation of the terminal two current controller state variable and the terminal three current controller state variable. Terminal one AC system strength has a significant impact on this oscillation mode. Obviously, terminal two and terminal three AC system strength changes also have a limited impact on this oscillation mode. Regardless of which terminal AC system strength changes, the

participation factors of all controller state variables change. In particular, the participation factor of the terminal one voltage controller state variable decreases significantly from 1.0 to 0.058 when the terminal one AC system strength increases from 1000MVA to 4000MVA. Considering the participation factors are 1.0, 0.01, and 0.011 for all three controller state variables in the original system with terminal one AC system strength of 1800MVA and are 0.058, 0.013, and 0.012 with terminal one AC system strength of 7200MVA, the oscillation mode is totally changed. The terminal one voltage controller state variable is no longer a major participant. The study results indicate that the dominating state variable keeps changing with the increase of terminal one AC system strength. Terminal one equivalent machine state variable, terminal one DC voltage, and HVDC line tap point DC voltage all, in turn, become the dominant participant with terminal one AC system strength increase. Depending on the dominant participant, this mode switches in between electromechanical oscillation mode (terminal one equivalent machine state variable dominated), HVDC network resonance mode (terminal one DC voltage dominated), or HVDC network resonance mode (HVDC line tap point DC voltage dominated). With the increase of terminal one AC system strength, the controller state variable participations are significantly reduced. On the other hand, both terminal two and terminal three AC system strength also affect the participation of the terminal one controller state variable. For the other two terminal AC system strength changes, the terminal one voltage controller state variable always dominates the oscillation mode. Mode shape results show that angles between each controller state variable also change when AC system strength changes. However, the oscillation mode

remains the same as the terminal one voltage controller state variable oscillates together with the terminal two current controller state variable and the terminal three current controller state variable. The angle between each controller state variable changes significantly with the terminal one AC system strength change. However, the angle changes very insignificantly when the strength of the other two terminal AC systems changes. Therefore, AC system strength impacts both the oscillation frequency and the damping ratio of this mode. However, this mode has enough damping ratio and has no small signal stability concern under all study scenarios.

The study results show that this mode has an oscillation frequency between 50Hz and 70Hz. Both the HVDC network quantities, machine state variables, and the AC system voltage participate in this mode. Depending on the system configuration and application, it may interact with other equipment in both AC systems and DC systems, such as the AC system filter, DC system smoothing rector, series compensated AC transmission line, and multi-mass turbine generators. Extra tension must be taken to avoid SSR type oscillation to occur.

2. In Mode-5N, both the terminal two current controller state variable and the terminal three current controller state variable have higher participation. The terminal one voltage controller state variable also participates in this mode with a relatively low participation factor. The results show that the participation factors for all controller state variables change regardless of which terminal AC system strength changes. However, terminal one AC system strength changes have a minor impact on this mode due to the relatively low participation of the terminal one controller state

variable. Mode shape results show that the angles between each controller state variable also change when the AC system strength changes. However, the mode shape remains the same as the terminal one voltage controller state variable and the terminal three current controller state variable oscillate together against the terminal two current controller state variable. The study results indicate that both the oscillation frequency and damping ratio change when AC system strength changes.

3. Mode-6N is dominated by the terminal one voltage controller state variable with both terminal two and terminal three current controller state variables having relatively high participation. The participation factors for all controller state variables change regardless of which terminal AC system strength changes. However, terminal one AC system strength changes have a very significant impact on the participation of its own terminal controller state variable. Similar conclusions can be drawn for the other two controller state variables. Mode shape results show that angles between each controller state variable also change when the AC system strength changes. However, the mode shape remains the same as the terminal one voltage controller state variable, terminal two current controller state variable, and the terminal three current controller state variable oscillate together. The results indicate that both the oscillation frequency and damping ratio of this mode change when AC system strength changes.

System Strength			Mode-4N		Mode-5N		Mode-6N	
T1 (MVA)	T2(MVA)	T3(MVA)	Frequency (Hz)	Damping (%)	Frequency (Hz)	Damping (%)	Frequency (Hz)	Damping (%)
1800	600	1000	53.18	31.60%	7.96	19.01%	3.94	14.48%
3600	600	1000	64.58	22.01%	7.96	18.97%	4.35	14.12%
5400	600	1000	66.02	20.16%	7.96	18.95%	4.47	14.35%
7200	600	1000	66.58	19.52%	7.96	18.94%	4.53	14.56%
1800	600	1000	53.18	31.60%	7.96	19.01%	3.94	14.48%
1800	1000	1000	54.64	30.54%	7.45	19.52%	3.72	15.17%
1800	1500	1000	55.27	30.57%	7.22	20.09%	3.61	15.46%
1800	2000	1000	55.52	30.69%	7.12	20.46%	3.56	15.58%
1800	600	1000	53.18	31.60%	7.96	19.01%	3.94	14.48%
1800	600	2000	54.30	27.24%	7.84	16.22%	3.71	9.40%
1800	600	3000	55.25	25.90%	7.92	15.93%	3.63	10.62%
1800	600	4000	55.82	25.41%	7.99	15.94%	3.60	12.15%

Table C2. 4 Frequency and damping ratio -HVDC line tap point change

System Strength	Mode-4N			Mode-5N			Mode-6N		
T1 /T2/T3 (MVA)	T1 PF	T2 PF	T3 PF	T1 PF	T2 PF	T3 PF	T1 PF	T2 PF	T3 PF
1800/600/1000	0.957	0.011	0.019	0.001	0.525	0.505	1.000	0.751	0.567
3600/600/1000	0.135	0.011	0.015	0.001	0.526	0.496	0.903	0.698	0.797
5400/600/1000	0.072	0.012	0.014	0.001	0.526	0.492	0.766	0.668	0.811
7200/600/1000	0.053	0.012	0.014	N/A	0.526	0.490	0.699	0.653	0.816
1800/600/1000	0.957	0.011	0.019	0.001	0.525	0.505	1.000	0.751	0.567
1800/1000/1000	0.887	0.001	0.016	0.001	0.895	0.911	1.000	0.901	0.459
1800/1500/1000	0.860	0.001	0.014	0.001	0.963	1.000	0.925	1.000	0.384
1800/2000/1000	0.850	N/A	0.014	N/A	0.957	1.000	0.853	1.000	0.339
1800/600/1000	0.957	0.011	0.019	0.001	0.525	0.505	1.000	0.751	0.567
1800/600/2000	0.888	0.001	0.014	0.001	0.548	0.520	1.000	0.554	0.904
1800/600/3000	0.842	0.001	0.013	0.001	0.546	0.555	0.970	0.522	1.000
1800/600/4000	0.817	0.001	0.013	N/A	0.544	0.580	0.931	0.496	1.000

Table C2. 5 Participation Factors for each oscillation mode- HVDC line tap point change

System Strength	Mode-4N			Mode-5N			Mode-6N		
T1 /T2/T3 (MVA)	T1-T2 Ang	T2-T3 Ang	T3-T1 Ang.	T1-T2 Ang	T2-T3 Ang	T3-T1 Ang.	T1-T2 Ang	T2-T3 Ang	T3-T1 Ang.
1800/600/1000	82.40	24.20	253.40	160.30	176.67	23.03	70.75	28.10	261.15
3600/600/1000	37.40	1.50	321.10	160.40	175.70	23.90	72.80	26.70	260.50
5400/600/1000	36.50	2.50	321.00	159.80	175.26	24.94	70.70	26.00	263.30
7200/600/1000	35.40	2.73	321.87	159.70	175.18	25.12	71.40	25.90	262.70
1800/600/1000	82.40	24.20	253.40	160.30	176.67	23.03	70.75	28.10	261.15
1800/1000/1000	66.20	10.15	283.65	143.10	178.09	38.81	72.80	26.40	260.80
1800/1500/1000	66.30	10.80	282.90	136.20	179.20	44.60	73.55	25.50	260.95
1800/2000/1000	67.10	N/A	281.50	N/A	179.80	44.60	73.80	25.40	260.80
1800/600/1000	82.40	24.20	253.40	111.10	176.67	72.23	70.75	28.10	261.15
1800/600/2000	86.20	22.30	251.50	94.30	179.59	86.11	67.50	34.40	258.10
1800/600/3000	86.10	20.10	253.80	66.90	179.70	113.40	67.00	32.50	260.50
1800/600/4000	85.40	18.60	256.00	N/A	179.80	91.80	68.40	29.10	262.50

Table C2. 6 Mode shapes for each oscillation mode- HVDC line tap point change

System Strength			Mode-4N		Mode-5N		Mode-6N	
T1 (MVA)	T2(MVA)	T3(MVA)	Frequency (Hz)	Damping (%)	Frequency (Hz)	Damping (%)	Frequency (Hz)	Damping (%)
1800	600	1000	52.86	38.59%	10.05	10.06%	3.58	8.59%
3600	600	1000	66.51	21.16%	10.08	9.80%	4.01	8.80%
5400	600	1000	68.15	18.67%	10.09	9.70%	4.15	9.14%
7200	600	1000	68.82	17.83%	10.09	9.65%	4.21	9.39%
1800	600	1000	52.86	38.59%	10.05	10.06%	3.58	8.59%
1800	1000	1000	53.94	37.66%	9.67	11.25%	3.51	8.81%
1800	1500	1000	54.41	37.56%	9.52	12.41%	3.49	8.99%
1800	2000	1000	54.61	37.59%	9.46	13.15%	3.48	9.09%
1800	600	1000	52.86	38.59%	10.05	10.06%	3.58	8.59%
1800	600	2000	54.05	35.89%	10.04	7.39%	3.33	4.63%
1800	600	3000	54.77	35.33%	10.14	7.11%	3.24	6.43%
1800	600	4000	55.13	35.23%	10.22	7.17%	3.21	8.29%

Table C2. 7 Frequency and damping ratio - different control parameters

System Strength	Mode-4N			Mode-5N			Mode-6N		
T1 /T2/T3 (MVA)	T1 PF	T2 PF	T3 PF	T1 PF	T2 PF	T3 PF	T1 PF	T2 PF	T3 PF
1800/600/1000	0.558	0.012	0.017	0.033	1.000	0.430	1.000	0.500	0.629
3600/600/1000	0.080	0.015	0.013	0.026	1.000	0.398	0.882	0.550	0.850
5400/600/1000	0.042	0.014	0.012	0.023	1.000	0.387	0.740	0.526	0.864
7200/600/1000	0.030	0.014	0.012	0.021	1.000	0.382	0.671	0.512	0.867
1800/600/1000	0.558	0.012	0.017	0.033	1.000	0.430	1.000	0.500	0.629
1800/1000/1000	0.530	0.010	0.013	0.023	1.000	0.414	1.000	0.594	0.595
1800/1500/1000	0.518	N/A	0.012	0.019	1.000	0.403	1.000	0.641	0.582
1800/2000/1000	0.514	N/A	N/A	0.017	1.000	0.397	1.000	0.663	0.571
1800/600/1000	0.558	0.012	0.017	0.033	1.000	0.430	1.000	0.500	0.629
1800/600/2000	0.524	0.010	0.012	0.029	1.000	0.442	1.000	0.456	0.891
1800/600/3000	0.505	N/A	0.010	0.024	1.000	0.461	0.988	0.434	1.000
1800/600/4000	0.497	N/A	N/A	0.021	1.000	0.475	0.939	0.406	1.000

Table C2. 8 Participation Factors for each oscillation mode- different control parameters

System Strength	Mode-4N			Mode-5N			Mode-6N		
T1 /T2/T3 (MVA)	T1-T2 Ang	T2-T3 Ang	T3-T1 Ang.	T1-T2 Ang	T2-T3 Ang	T3-T1 Ang.	T1-T2 Ang	T2-T3 Ang	T3-T1 Ang.
1800/600/1000	46.55	10.20	303.25	126.00	178.64	55.36	84.70	14.00	261.30
3600/600/1000	36.67	4.70	318.63	130.40	178.00	51.60	98.10	12.70	249.20
5400/600/1000	38.20	4.20	317.60	132.30	177.64	50.06	86.90	12.20	260.90
7200/600/1000	38.10	4.00	317.90	133.60	177.46	48.94	87.72	12.19	260.09
1800/600/1000	46.55	10.20	303.25	126.00	178.64	55.36	84.70	14.00	261.30
1800/1000/1000	44.10	8.30	307.60	124.40	178.43	57.17	84.70	13.40	261.90
1800/1500/1000	43.90	9.10	307.00	122.30	179.10	58.60	85.01	12.80	262.19
1800/2000/1000	44.00	N/A	N/A	120.30	179.25	60.45	84.90	13.10	262.00
1800/600/1000	46.55	10.20	303.25	126.00	178.64	55.36	84.70	14.00	261.30
1800/600/2000	45.00	9.90	305.10	114.00	179.86	66.14	82.40	18.00	259.60
1800/600/3000	N/A	N/A	305.60	114.68	179.32	66.00	82.70	15.20	262.10
1800/600/4000	N/A	N/A	N/A	116.20	179.70	64.10	83.20	12.10	264.70

Table C2. 9 Mode shapes for each oscillation mode- different control parameters

System Strength			Mode-4N		Mode-5N		Mode-6N	
T1 (MVA)	T2(MVA)	T3(MVA)	Frequency (Hz)	Damping (%)	Frequency (Hz)	Damping (%)	Frequency (Hz)	Damping (%)
1800	600	1000	50.13	30.50%	9.09	4.74%	3.91	5.87%
3600	600	1000	64.38	20.24%	9.10	4.78%	4.26	5.12%
5400	600	1000	66.49	17.88%	9.10	4.79%	4.36	5.16%
7200	600	1000	67.31	17.10%	9.11	4.80%	4.40	5.25%
1800	600	1000	50.13	30.50%	9.09	4.74%	3.91	5.87%
1800	1000	1000	51.01	29.57%	8.59	4.34%	3.70	7.47%
1800	1500	1000	51.46	29.47%	8.36	4.91%	3.61	8.37%
1800	2000	1000	51.67	29.51%	8.25	5.44%	3.57	8.85%
1800	600	1000	50.13	30.50%	9.09	4.74%	3.91	5.87%
1800	600	2000	51.19	28.44%	9.07	4.76%	3.61	4.37%
1800	600	3000	51.78	28.00%	9.18	5.51%	3.49	7.17%
1800	600	4000	52.09	27.92%	9.26	6.08%	3.44	9.54%

Table C2. 10 Frequency and damping ratio - different operating point

System Strength	Mode-4N			Mode-5N			Mode-6N		
T1 /T2/T3 (MVA)	T1 PF	T2 PF	T3 PF	T1 PF	T2 PF	T3 PF	T1 PF	T2 PF	T3 PF
1800/600/1000	1.000	0.011	0.012	0.013	0.642	0.474	0.975	0.728	0.576
3600/600/1000	0.173	0.012	0.014	0.010	0.642	0.455	0.630	0.635	0.598
5400/600/1000	0.081	0.012	0.013	N/A	0.641	0.448	0.526	0.611	0.603
7200/600/1000	0.057	0.013	0.013	N/A	0.641	0.445	0.477	0.600	0.606
1800/600/1000	1.000	0.011	0.012	0.013	0.642	0.474	0.975	0.728	0.576
1800/1000/1000	1.000	0.010	0.010	0.012	1.000	0.761	0.952	1.000	0.465
1800/1500/1000	0.994	N/A	0.001	N/A	1.000	0.766	0.818	1.000	0.366
1800/2000/1000	0.984	N/A	N/A	N/A	1.000	0.766	0.766	1.000	0.330
1800/600/1000	1.000	0.011	0.012	0.013	0.642	0.474	0.975	0.728	0.576
1800/600/2000	1.000	0.011	0.001	0.012	0.643	0.508	1.000	0.677	0.914
1800/600/3000	1.000	0.010	0.001	N/A	0.635	0.536	0.928	0.600	1.000
1800/600/4000	0.958	N/A	N/A	N/A	0.630	0.553	0.865	0.547	1.000

Table C2. 11 Participation Factors for each oscillation mode- different operating point

System Strength	Mode-4N			Mode-5N			Mode-6N		
T1 /T2/T3 (MVA)	T1-T2 Ang	T2-T3 Ang	T3-T1 Ang.	T1-T2 Ang	T2-T3 Ang	T3-T1 Ang.	T1-T2 Ang	T2-T3 Ang	T3-T1 Ang.
1800/600/1000	55.50	9.00	313.50	123.90	178.40	57.70	88.90	19.90	251.20
3600/600/1000	32.40	5.00	322.60	130.40	179.70	49.90	90.50	18.60	250.90
5400/600/1000	38.10	4.20	317.70	N/A	179.50	50.70	91.89	18.11	250.00
7200/600/1000	38.10	4.10	317.80	N/A	179.31	51.19	93.10	18.00	248.90
1800/600/1000	55.50	9.00	313.50	123.90	178.40	57.70	88.90	19.90	251.20
1800/1000/1000	55.40	13.10	317.70	124.70	179.60	55.70	88.10	21.30	250.60
1800/1500/1000	N/A	N/A	318.40	121.80	178.96	59.24	87.70	22.00	250.30
1800/2000/1000	N/A	N/A	N/A	N/A	180.00	N/A	73.50	35.90	250.60
1800/600/1000	55.50	9.00	313.50	123.90	178.40	57.70	88.90	19.90	251.20
1800/600/2000	49.20	0.80	310.00	120.90	178.90	60.20	88.60	18.60	252.80
1800/600/3000	50.50	2.00	307.50	N/A	179.20	59.20	89.20	15.50	255.30
1800/600/4000	N/A	N/A	N/A	N/A	179.74	N/A	70.20	28.40	261.40

Table C2. 12 Mode shapes for each oscillation mode- different operating point